UNIVERSITY OF CALIFORNIA SAN DIEGO

Yeast Derlin Dfm1 is a Regulator of Endoplasmic Reticulum Homeostasis

A dissertation submitted in partial satisfaction of the
requirements for the degree Doctor of Philosophy

in

Biology

by

Rachel Kandel

Committee in charge:

Professor Sonya Neal, Chair
Professor Asa Gustaffson
Professor Randolph Hampton
Professor Maho Niwa
Professor Gentry Patrick

2022

The Dissertation of Rachel Kandel is approved, and it is acceptable in quality and form for publication on microfilm and electronically.

University of California San Diego

2022

DEDICATION

This work is dedicated to my mother, Dawn Kandel. You are the best teacher and an even better mother.

TABLE OF CONTENTS

DISSERTATION APPROVAL PAGE iii
DEDICATION iv
TABLE OF CONTENTS v
LIST OF FIGURES viii
LIST OF TABLES ix
ACKNOWLEDGEMENTS x
VITA xvi
ABSTRACT OF THE DISSERTATION xvii
Chapter 1: Introduction 1
1.1 The Role of Rhomboid Protein Family in Protein Homeostasis 2
1.2 Rhomboid pseudoproteases 3
1.2.1 Derlins 3
1.2.2 The unDERLying role in ERAD and retrotranslocation 3
1.2.3 Derlins strike first in the pre-emptive QC Pathway 7
1.2.4 Physiological role of derlins 8
1.2.5 Disease role of derlins 10
1.2.6 Dsc2 and UBAC2 11
1.2.7 Dsc2: A lever for cholesterol and sphingolipid homeostasis 11
1.2.8 UBAC2 role in energy homeostasis 13
1.2.9 Disease role of UBAC2 14
1.2.10 iRhoms 15
1.2.11 iRhoms in regulated protein degradation 15
1.3 Rhomboid Proteases 16
1.3.1 RHBDL4 16
1.3.2 RHBDL4 in ERAD 17
1.3.3 Physiological Role of RHBDL4 18
1.3.4 Disease role of RHBDL4 20
1.3.5 YqgP 20
1.4 Conclusions and Perspectives 21
1.5 Acknowledgments 23
1.6 References 24

Chapter 2: Derlin Dfm1 Employs a Chaperone-Like Function to Resolve Misfolded Membrane Protein Stress 38
2.1 Introduction 39
2.2 Results 42
2.2.1 Absence of Dfm1 and Expression of Integral Misfolded Membrane Proteins Causes Growth Stress 42
2.2.2 Disease-Associated Membrane Proteins Cause Growth Stress 44
2.2.3 Dfm1 has a Dual Role in ER Protein Stress and ERAD Retrotranslocation 44
2.2.4 Human Derlins Relieve Growth Stress 46
2.2.5 Dfm1 Solubilizes Misfolded Membrane Protein Aggregates Independent of Cdc48 Recruitment 46
2.2.6 Misfolded Membrane Proteins do not Activate the Unfolded Protein Response 49
2.2.7 Accumulation of Misfolded Membrane Proteins Upregulates Proteasome Components 50
2.2.8 The Transcription Factor Rpn4 is Involved in Misfolded Membrane Protein Stress 51
2.2.9 Misfolded Membrane Protein Stress in dfm1Δ Cells Leads to Proteasome Impairment 52
2.2.10 Misfolded Membrane Protein Stress Does Not Cause Proteasome Sequesteration 54
2.2.11 Growth Defect in dfm1Δ Cells is Ubiquitination Dependent 54
2.2.12 Ubiquitin Homeostasis is Disrupted with Misfolded Membrane Protein Accumulation 56
2.2.13 Deubiquitinases Prevent or Resolve Misfolded Membrane Protein Stress 57
2.2.14 Absence of Deubiquitinases and RPN4 in Combination with DFM1 do not Exacerbate Toxicity 57
2.2.15 Misfolded Protein Aggregation Toxicity Requires Protein Ubiquitination 58
2.2.16 Increased Expression of Dfm1 Relieves Misfolded Membrane Protein Stress in rpn4Δ and ubp6Δ Cells 59
2.3 Discussion 59
2.4 Materials and Methods 67
2.5 Acknowledgments 78
2.6 References 79
Chapter 3: An ERAD-independent role for rhomboid pseudoprotease Dfm1 in mediating sphingolipid homeostasis 140
3.1 Introduction 141
3.2 Results 145

3.2.1 Derlin Dfm1 interacts with members of the sphingolipid biosynthetic pathway ... 145
3.2.2 DFM1 genetically interacts with TSC3 ... 147
3.2.3 *dfm1Δtsc3Δ* cells have increased steady-state levels of ceramides and complex sphingolipids ... 148
3.2.4 DFM1 genetically interacts with ORM1 ... 149
3.2.5 Orm2 is targeted by Dfm1 for degradation ... 151
3.2.6 Derlin Dfm1's Cdc48 recruitment function is not required for Orm2 degradation 151
3.2.7 Orm2 degradation is dependent on EGAD, but not ERAD or INMAD ... 153
3.2.8 Dfm1 does not function at the post-ubiquitination step of Orm2 degradation pathway ... 155
3.2.9 Dfm1 does not directly function in EGAD ... 156
3.2.10 Dfm1 is required for Orm2 export from the ER to the Golgi ... 157
3.2.11 Loss of Dfm1 does not affect COPII-mediated trafficking ... 159
3.2.12 Dfm1 interacts with Ypk1-dependent phosphorylated Orm2 ... 160
3.3 Discussion ... 161
3.4 Methods ... 165
3.5 Acknowledgments ... 175
3.6 References ... 176
Chapter 4: Conclusions and Closing Remarks ... 215
4.1 Conclusions and Closing Remarks ... 216

LIST OF FIGURES

Figure 1.2.1 Cellular localization of rhomboids 34
Figure 2.2.1 Integral Membrane Protein Overexpression Causes a Growth Defect in *dfm1Δ* Cells in an ERAD Independent Manner 87
Figure 2.2.2 Dfm1 Retrotranslocation Defective Mutants Show Differing Abilities to Restore Growth 89
Figure 2.2.3 Dfm1 Reduces Misfolded Membrane Protein Toxicity Through a Chaperone-Like Activity 91
Figure 2.2.4 Dfm1 Specifically Influences Solubility of Misfolded Membrane Proteins 93
Figure 2.2.5 Misfolded Membrane Protein Stress in *dfm1Δ* Cells Does Not Activate the Unfolded Protein Response 95
Figure 2.2.6 Misfolded Membrane Protein Toxicity Results in Proteasome Impairment 97
Figure 2.2.7 Ubiquitin Stress Contributes to Misfolded Membrane Protein Toxicity 99
Figure 2.2.8 Model for misfolded membrane protein-induced toxicity 101
Supplemental Figure 2.2.1 Hmg2-GFP Microscopy Puncta are Unaffected by Dfm1 103
Supplemental Figure 2.2.2 Transcriptional Changes in Membrane Protein Stressed *dfm1Δ* Cells 105
Supplemental Figure 2.2.3 Misfolded Membrane Protein Stress in *dfm1Δ* Cells Does Not Affect Hac1 Splicing 107
Supplemental Figure 2.2.4 *Rpn4Δ* Toxicity is Specific to Misfolded Membrane Proteins ... 109
Supplemental Figure 2.2.5 *Ubp6Δ* Toxicity is Specific to Misfolded Membrane Proteins ... 111
Supplemental Figure 2.2.6 Not All Deubiquitinates Mediate Misfolded Membrane Toxicity and Toxicity is Specific to Misfolded Membrane Proteins 113
Supplemental Figure 2.2.7 Genetic Interactions Between Dfm1, Rpn4, and Ubp6 in Resolving Misfolded Membrane Protein Toxicity 115
Figure 3.2.1 BioID proximity-based labeling to identify interaction partners of Df 184
Figure 3.2.2 Dfm1 colocalizes and binds to SPOTS complex proteins 186
Figure 3.2.3 Dfm1 genetically interacts with Tsc3 188
Figure 3.2.4 Dfm1 genetically interacts with Orm1 190
Figure 3.2.5 Dfm1 targets Orm2 for degradation 192
Figure 3.2.6 Orm2 degradation requires EGAD, but not ERAD or INMAD pathway 194
Figure 3.2.7 dfm1Δ accumulates phosphorylated Orm2 exclusively in the ER 196
Figure 3.2.8 Dfm1 binds to phosphorylated Orm2 198
Supplemental Figure 3.2.1 Dfm1 does not genetically interact with Lcb1, Lcb2, and Sac1 200
Supplemental Figure 3.2.2 Orm2 is degraded in WT strains 202
Supplemental Figure 3.2.3 Dfm1 does not interact with EGAD components 204
Supplemental Figure 3.2.4 Orm2-3A accumulates exclusively in the ER 206

LIST OF TABLES

Table 1.2.1 Rhomboid Member Knockout Mice 36
Table 1.2.2 Rhomboid Member's Association with Diseases 37
Supplemental Table 2.4.1 Plasmid List 117
Supplemental Table 2.4.2 Yeast Strain Used in this Study 121
Supplemental Table 3.4.1 Plasmids used in this study 208
Supplemental Table 3.4.2 Yeast strains used in this study 209
Supplemental Table 3.4.3 Key Resources Table 214

ACKNOWLEDGEMENTS

I would like to start by thanking my advisor, Dr. Sonya Neal. Sonya, your mentorship and guidance has been instrumental in crafting me into the scientist I have become. You have taught me what can be accomplished when you treat people with empathy and compassion, and how to create a working environment that is collaborative and inclusive. Anytime I am in a leadership position, I now ask myself, “What would Sonya do?” You have pushed me to become a better scientist and a better person during my time in your lab. I feel honored to be the first doctorate student from the Neal lab and I am excited to see what the future holds for the lab. There are not very many people as amazing as you, Sonya, but the world would be a lot better off if everyone was like you.

I would like to thank all current and former Neal Lab members: Analine Aguayo, Anahita Nejatfard, Adam Conn, Narin Singh, Tiffany Kuo, Jasmine Jung, Ikran Ibrahim, Satarupa Bhaduri, Nicola Scott, Marco Proietto, Casey Horn, Isabel Wang, Rosa Chavez, Saroj Gourkanti, Yazmin Munoz, and Raghad Al Bawab. To Analine, thank you for being a true friend and the root of my support system over the last two years. I have fond memories of our long walks in graduate housing during the early months of the pandemic when we first bonded. We have laughed and cried together more times than I can even count, and I am sure we will keep it up in the future. To Jasmine, you have made me the proudest mentor in the world. I have had the privilege to work with you for close to three years and I have seen you evolve from an undergraduate who was new to lab work to a seasoned researcher. You have so much excitement and energy for everything in life. You have won every research award that UCSD has to offer and have solidified your place on nearly every project in the

lab by being our resident microscopy queen. I am so proud of your growth in the time I have worked with you, and I am excited for all the amazing opportunities you will have.

Thank you to all the people working on Tata Hall 4th floor. I remember rotating in the Neal Lab when the only other lab on the floor was the Madigan Lab and we just sat on the ground in the office because there were no desks yet. It has been amazing to see the community of scientists on this floor grow during my time here. Working in an open lab and office environment has facilitated discussions and collaborations that have made the floor a more scientifically prosperous environment. In memory of Dr. Gary Heussler, a former member of the Dutton Lab, thank you for the positivity and kindness you brought into lab every day. May your memory be a blessing.

Thank you to my committee members, Dr. Randy Hampton, Dr. Maho Niwa, Dr. Asa Gustafsson, and Dr. Gentry Patrick. I appreciate all the input into my project, and you have all done so much to strengthen the direction of this work.

I would like to thank everyone in my life that has supported me during graduate school, my friends, my family, and my partner. To my cohort mates, Alex Schieber, Robert Gallant, and Katelynn Kazane. To Alex, I have such a special bond with you that is so rare to find. I could (and have, many times) talk to you for hours and not get bored for a single second. You have pushed me outside my comfort zone, and I am so much better off for it. You are one of the most out-of-the box thinkers I know and the way you think about the world never fails to amaze me. To Robert and Katelynn, I am still convinced it is impossible to have

a conversation with either of you without you for more than 5 minutes without it turning to science. Whenever one of us has had a hard week in lab, we have always been there for each other to vent over a drink. To my friend Emily Hops, even though we have lived a plane ride away the whole time I have been in graduate school, we are just as close as we were as roommates five years ago. No matter how busy either of us gets, we have the type of friendship where we can just pick up where we left off. You have been such an incredible source of emotional support during my time in graduate school.

I would like to thank my family for all the support they have provided me. In particular, I would like to thank my mom, Dawn Kandel, my sister, Bella Kandel, my grandparents, David and Pamela Kandel, my aunt Terre Silver, and my aunt and uncle, Jeni Kandel and Ken DeJarnette. Auntie Terre, you are the person that gave me my sense of fashion and taught me there is no such thing as being too much. To my grandparents, thank you for always being supportive of me, you have both always made me feel like I am capable of anything. Grandma, I have loved over the past few years both of us developing an interest in baseball and being able to call you to chat about the latest Dodger's game. Aunt Jeni and Uncle Ken, thank you for always being the people I go to for career advice. You probably have more faith in me than I deserve, but your support means the world to me. To my sister, Bella, I am so proud of the woman you have become. I love how supportive we both are of each other and we will always be each others biggest cheerleaders. Thank you to my mama, to whom my dissertation is dedicated, for making me the person I have become. It was your never-ending support and dedication that has gotten me to where I am today. You may not have a background in biology, but that doesn't mean you haven't tried to teach yourself over the last several years. I love when you tell me you have been reading about ubiquitin to

better understand what I do or when you attend my Zoom research presentations and call me afterwards to ask questions. Growing up, your passion for teaching and dedication as a stay-at-home mom made me into a more curious and intellectual person. I have always had eccentric ideas and you always supported me in whatever way you could. I don't know how many parents would have taken it seriously if their child said they wanted to start college classes at twelve and skip the last several years of high school. But you let me do it, without ever pushing me and allowing me to make my own mistakes along the way. I appreciate the unconventional way I grew up and all you sacrificed for Bella and me. You are one of the smartest and most empathetic people I know, and I am lucky to have you as my mom.

To my love, Elliot Green, I cannot put into words how much you mean to me, but I will try. The love you have shown me is beyond anything I thought possible. Graduate school, and life, have become so much easier with you around. From making my coffee every morning, to always having dinner ready when I come home late from lab late at night, to taking me shopping when I have an off day, I am truly appreciative of everything you do for me. You have shown me what true partnership means and I will continue to strive to be the woman you deserve.

Chapter 1 is largely adapted from the material as it appears in Kandel, R.R., and Neal, S.E., The role of rhomboid superfamily members in protein homeostasis: Mechanistic insight and physiological implications, *Biochimica et Biophysica Acta – Molecular Cell Research* (2020), https://doi.org/10.1016/j.bbamcr.2020.118793. The dissertation author was the first author of this manuscript.

Chapter 2 is currently under revision for publication for the working citation: Kandel, R., Jung, J., Syau, D., Kuo, T., Songster, L., Horn, C., Chapman, C., Aguayo, A., Duttke, S., Benner, C., Neal, S., Derlin Dfm1 Employs a Chaperone-Like Function to Resolve Misfolded Membrane Protein Stress. The dissertation author was a primary investigator and the first author of this material. The authors would like to thank Tom Rapoport (Harvard Medical School), Davis Ng (National University of Singapore), Randy Schekman (University of California, Berkeley), Susan Michaelis (John Hopkins University), and Jeff Brodsky (University of Pittsburgh) for providing plasmids and antibodies. We also thank the Neal lab members for their positive reinforcement, in depth discussions and technical assistance. These studies were supported by NIH grant 1R35GM133565-01, Pew Biomedical Award, and NSF CAREER grant to S.E.N. S.H.D is supported by NIH grant R00GM135515 to S.H.D.

Chapter 3 is currently accepted for publication for the working citation: Bhaduri, S., Aguayo, A., Ohno, Y., Proietto, M., Jung, J., Wang, I., Kandel, R., Singh, N., Ibrahim, I., Fulzele, A., Bennett, E., Kihara, A., Neal, S., An ERAD-independent role for rhomboid pseudoprotease Dfm1 in mediating sphingolipid homeostasis. The dissertation author was conducted experiments for this manuscript and is a co-author of this material. The authors would like to thank Peter Espenshade (Johns Hopkins Medicine), Oliver Schmidt (Medical

University of Innsbruck), David Teis (Medical University of Innsbruck), Teresa Dunn (National Institutes of Health), Jim Wilhelm (University of California, San Diego), and Peter Novick (University of California, San Diego) for providing plasmids, yeast strains, antibodies. We thank Dr. Oswald Quehenberger from the UCSD Lipidomic Core Facility for performing lipidomic analysis. We also thank Dr. Maho Niwa, Dr. David Teis, Dr. Oliver Schmidt, and the Neal lab members for in depth discussions and technical assistance. These studies were supported by NIH grant 1R35GM133565-01, Pew Biomedical Award 34089, and NSF CAREER grant 2047391 (to S.E.N), NIH grants 5R01GM136994-02 and DP2GM119132 (to E.J.B), HHMI Gilliam Fellowship GT15096 (to S.E.N and A.A.), and KAKENHI grant JPSSH04986 (to A.K.).

VITA

2017 B.S. in General Biology, California State University Channel Islands

2022 Ph.D. in Biology, University of California San Diego

Thesis advisor: Sonya Neal

PUBLICATIONS

Kandel, R.R., and Neal, S.E., The role of rhomboid superfamily members in protein homeostasis: Mechanistic insight and physiological implications, *Biochimica et Biophysica Acta – Molecular Cell Research* (2020)

Nejatfard, A., Wauer, N., Bhaduri, S., Conn, A., Gourkanti, S., Singh, N., Kuo, T., **Kandel, R.**, Amaro, R.E. and Neal, S.E., Derlin rhomboid pseudoproteases employ substrate engagement and lipid distortion to enable the retrotranslocation of ERAD membrane substrates. *Cell reports* (2021)

Bhaduri, S., Aguayo, A., Ohno, Y., Proietto, M., Jung, J., Wang, I., **Kandel, R.**, Singh, N., Ibrahim, I., Fulzele, A., Bennett, E., Kihara, A., Neal, S., An ERAD-independent role for rhomboid pseudoprotease Dfm1 in mediating sphingolipid homeostasis. *EMBO Journal* (2022)

MANUSCRIPTS IN PRESS

Kandel, R., Jung, J., Syau, D., Kuo, T., Songster, L., Horn, C., Chapman, C., Aguayo, A., Duttke, S., Benner, C., Neal, S., Derlin Dfm1 Employs a Chaperone-Like Function to Resolve Misfolded Membrane Protein Stress. *PLOS Biology* (2022)

ABSTRACT OF THE DISSERTATION

Yeast Derlin Dfm1 is a Regulator of Endoplasmic Reticulum Homeostasis

by

Rachel Kandel

Doctor of Philosophy in Biology

University of California San Diego, 2022

Professor Sonya Neal, Chair

Protein quality control is vital for maintaining cellular health and preventing stress. Eukaryotic cells are equipped with protein quality controls pathways to identify and remove misfolded proteins. The ubiquitin proteasome system in one of the major pathways that cells use to target and degrade aberrant proteins. At the endoplasmic reticulum, a pathway called endoplasmic reticulum associated degradation utilizes the ubiquitin proteasome system for degradation of misfolded proteins. In yeast, a protein called Dfm1 is required for the degradation of misfolded membrane proteins at the endoplasmic reticulum. Dfm1 is a member of the rhomboid protein family. This is a family of integral membrane proteins including both proteases and pseudoproteases. Dfm1 is a rhomboid pseudoprotease. While

rhomboid pseudoproteases may lack a catalytic site, they are still involved in a wide array of biological processes.

Protein aggregates are a common feature of diseased and aged cells. Membrane proteins comprise a quarter of the proteome, and yet, it is not well understood how aggregation of membrane proteins is regulated and what effects these aggregates can have on cellular health. This dissertation describes our original research demonstrating Dfm1 has a chaperone-like activity that influences misfolded membrane protein aggregation. We establish that this function of Dfm1 does not require recruitment of the ATPase Cdc48 and it is distinct from Dfm1's previously identified function in dislocating misfolded membrane proteins to the cytosol for degradation. Additionally, we assess the cellular impacts of misfolded membrane proteins in the absence of Dfm1 and determine that misfolded membrane proteins are toxic to cells in the absence of Dfm1 and cause disruptions to proteasomal and ubiquitin homeostasis.

Chapter 1: Introduction

1.1 The Role of Rhomboid Protein Family in Protein Homeostasis

Proteins serve as the primary workhorses for executing a vast majority of cellular and organismal functions. Unfortunately, misfolding of proteins is a common occurrence, either due to chemical and UV damage, imbalanced subunit synthesis, or genetic mutation (Balchin et al., 2016; Hartl et al., 2011; Sontag et al., 2017). Unchecked accumulation of these aberrant proteins generates constant cellular stress and underlies many of the most pressing human maladies, including aging, cancer and neurodegenerative diseases (Eftekharzadeh et al., 2016; Hartl et al., 2011; Morimoto, 2011). To offset the catastrophic effect of unwanted proteins, organisms are equipped with quality control systems that are vital for surveillance, prevention, and rescue of protein defects (Chen et al., 2011; Jeng et al., 2015; Sicari et al., 2019; Z. Sun & Brodsky, 2019).

Recent advances have shown that the rhomboid superfamily are involved in multiple facets of protein homeostasis (Bergbold & Lemberg, 2013b; Lemberg & Adrain, 2016; Tichá et al., 2018). In general, the rhomboid protein family carries out many membrane-related processes such as development, signaling, parasitic invasion, and protein trafficking (reviewed in (Düsterhöft et al., 2017)). A prominent feature of rhomboids is their ability to cleave their membrane-anchored substrates at specific sites within the lipid bilayer; a process mediated by rhomboid proteases through their conserved serine-histidine dyad at the active site (Bondar et al., 2009; Lemieux et al., 2007; Shokhen & Albeck, 2017; Uritsky et al., 2016; Y. Zhou et al., 2012). A subclass of rhomboids has evolved from their rhomboid protease predecessors that are not proteases; they lack catalytic residues for proteolysis and are known as rhomboid pseudoproteases. Despite the absence of protease activity, rhomboid

pseudoproteases carry out similar biological processes as their rhomboid protease counterparts and function in lipid homeostasis, protein trafficking, sterol regulation, and signaling (Lemberg & Adrain, 2016; Lemberg & Freeman, 2007) . Although growing evidence suggests that both rhomboid proteases and pseudoproteases have central roles in safeguarding the proteome, little data exist regarding their systemic significance in mammals. In this review, we will discuss the mechanistic underpinnings of rhomboids in the context of protein quality control and describe current knowledge on their role in maintaining a healthy proteome in both health and disease. Overall, understanding rhomboid function within a broader organismal perspective will reveal their importance as therapeutic targets in many diseases.

1.2 Rhomboid pseudoproteases

1.2.1 Derlins

Derlins were first discovered as key mediators of ER (Endoplasmic Reticulum) protein quality control in yeast and mammals (Knop et al., 1996; Lilley & Ploegh, 2004; Mehrtash & Hochstrasser, 2019; Ye et al., 2004). Based on sequence and structural homology, derlins share structural similarities to the rhomboid-like superfamily (Greenblatt et al., 2011). Specifically, they are ER-resident integral membrane proteins and have been predicted to span the lipid bilayer 6 times (Greenblatt et al., 2011). The current knowledge and thinking of this subclass of the rhomboid family will be discussed below.

1.2.2 The unDERLying role in ERAD and retrotranslocation

Maintaining proteostasis is particularly challenging in the ER where the high demand for protein synthesis generates constant misfolding stress (Sicari et al., 2019). To off-set the catastrophic effects that accompany defective protein accumulation, misfolded ER proteins are targeted for degradation via ER-associated degradation (ERAD) (Hirsch et al., 2009; Needham & Brodsky, 2013). The span of substrates for ERAD is quite large; ranging from ER-localized misassembled proteins to misfolded membrane and luminal proteins (Bordallo et al., 1998; Foresti et al., 2014; Khmelinskii et al., 2014; Wangeline & Hampton, 2018). During ERAD, substrates destined for degradation are tagged with ubiquitin by an E3 ligase, delivered back into the cytoplasm by a dedicated export machinery and then degraded by the cytosolic 26S proteasome (Mehrtash & Hochstrasser, 2019). Perhaps one of the most intriguing features of ERAD is the requirement of removing substrates from their ER-resident to their final destination in the cytosol for proteasomal degradation; a process known as retrotranslocation (Hampton & Sommer, 2012) which is powered by Cdc48/p97 AAA-ATPase (Bodnar & Rapoport, 2017; Neal et al., 2017; Ye et al., 2003).

Retrotranslocation requires a route or channel for the removal of misfolded proteins through or from the ER membrane. The identification of an exit channel(s) has been a challenging problem that is only now yielding answers (Greenblatt et al., 2012; Neal et al., 2018; Peterson et al., 2019; Schoebel et al., 2017; Stein et al., 2014; Vasic et al., 2020). Derlins have emerged as likely candidates for transporting ERAD substrates out of the ER. For instance, human Derlin-1 was initially discovered by two independent groups for its role in assisting a viral component, US11, in degrading class 1 MHC heavy chain (MHC-1) within the infected host (Lilley & Ploegh, 2004a; Ye et al., 2004). Derlin-1 is an ER-resident multi-spanning protein with homology to the yeast Der1, which is involved in ERAD (Knop et al.,

1996). Although many studies demonstrated that derlins assist in ERAD of several substrates(Avci et al., 2014; Lemberg, 2013; Lilley & Ploegh, 2004b; Mehnert et al., 2013; Sato & Hampton, 2006; Stolz et al., 2010), their direct function in retrotranslocation remained obscure. Previous *in vitro* and structural studies by Rapoport and colleagues suggested that the multi-spanning yeast E3 ligase Hrd1 serves as a channel for luminal substrates (Peterson et al., 2019; Schoebel et al., 2017; Vasic et al., 2020). An analogous channel for ERAD membrane substrates remained to be determined until Neal and colleagues improved the understanding of membrane substrate retrotranslocation by screening a complete collection of yeast mutants via SPOCK (single plate orf compendium kit), which consists of 5,808 yeast strain array of non-essential gene deletion mutants and essential DAmP gene mutants (Jaeger et al., 2018) and identified yeast derlin Dfm1 as an independent, dedicated and specific mediator for the retrotranslocation of many ERAD membrane substrates (Fig. 1) (Neal et al., 2018). Furthermore, both human Derlin-1 and yeast Dfm1 contain a unique C-terminal SHP box for direct recruitment of Cdc48/p97 AAA-ATPase to the ER membrane and this interaction is essential for removing ERAD substrates (Greenblatt et al., 2012; Neal et al., 2018). This finding contradicted previous results in which Dfm1 had no role in ERAD (Goder et al., 2008; Sato & Hampton, 2006). This was due to *dfm1*Δ-nulls being rapidly suppressed; masking *dfm1*Δ-nulls' effect on retrotranslocation (Neal et al., 2018). Accordingly, the fast curation of the SPOCK screen has revealed Dfm1 as being one of the major mediators of ERAD.

Sequence conservation and structural homology suggest that derlins share similarities with rhomboid-like superfamily (Fleig et al., 2012). The structures of *E. coli* and *H. influenzae* rhomboid protease GlpG (Brooks & Lemieux, 2013; Lemieux et al., 2007; Y. Wang et al.,

2006), and a body of structure-function analyses, molecular modeling and mechanistic studies on the rhomboid superfamily from over a decade have elucidated some of the mechanistic principles that may be at play in derlin-mediated retrotranslocation (see recent review in (Tichá et al., 2018)). Although the structure of the bacterial rhomboid complexed with substrate is lacking, biochemical studies show that rhomboid proteases not only recognize structurally unstable single transmembrane domains (Moin & Urban, 2012; Strisovsky et al., 2009; Urban & Freeman, 2003), but they also recognize regions of extramembrane domains (Maegawa et al., 2007) and some features within polytopic transmembrane proteins (Erez & Bibi, 2009; Fleig et al., 2012; Tsai & Weissman, 2012). Furthermore, function of rhomboid proteins as surveyors of the membrane may be aided by their unusually fast diffusion in the membrane for substrate targeting (Kreutzberger et al., 2019), possibly aided by their compact fold and small hydrophobic thickness that may induce local deformation of the lipid bilayer (Bondar et al., 2009; Y. Wang et al., 2006).

Despite the absence of protease activity, derlins have retained conserved rhomboid residues (Greenblatt et al., 2012; Neal et al., 2018). This conservation implies the intriguing idea that derlins have retained the biological properties of rhomboids for use in retrotranslocation. In support of this idea, we and others previously published that human and yeast derlins utilize their conserved rhomboid motifs for removing misfolded substrates from the ER (Greenblatt et al., 2011; Neal et al., 2018). A popular working hypothesis is that derlins have retained membrane perturbing properties of its bacterial counterpart, GlpG, to facilitate the movement of substrates across the membrane (Avci & Lemberg, 2018; Neal et al., 2018). Recent work from the Rapoport lab has shown that yeast derlin and Dfm1 paralog, Der1, possesses membrane perturbation properties to assist in the retrotranslocation of ER luminal substrates.

(Wu et al., 2020). Using cryo-electron microscopy, the authors determined the structure of the Hrd1 complex, which is comprised of monomers of Hrd1, Der1, Hrd3, Yos9, and Usa1. While it had previously been reported that a Hrd1 dimer is the retrotranslocon for soluble proteins, the revised structure establishes that monomeric Hrd1 acts as a half channel and interacts with Der1, which forms the other half of the channel (Schoebel et al., 2017; Wu et al., 2020). As shown by molecular dynamic (MD) simulations, both Der1 and Hrd1 can induce distortion of the lipid bilayer. Der1 contains a lateral gate between TM2 and TM5 and TM2 contains hydrophilic residues that MD simulations predict cause lipid thinning that is proposed to aid in the retrotranslocation of substrates. Indeed, mutation of these residues to hydrophobic residues slows the degradation rate of luminal ERAD clients. This important discovery supports the hypothesis that the membrane perturbation ability of rhomboids can aid in retrotranslocation of proteins.

1.2.3 Derlins strike first in the pre-emptive QC Pathway

The ER employs various proteostatic strategies for maintaining a healthy proteome. Most notable is the ER's ability to launch a pre-emptive strike on a selection of proteins prior to their infiltration in the ER. Put less poetically, the ER's main line of defense is to prevent protein overload. This preventative system is known as the ER stress-induced pre-emptive quality control pathway (ERpQC) (Kadowaki et al., 2015, 2018). In this system, newly synthesized polypeptides are co-translationally inserted into the entry gate of the ER, which is the Sec61 channel. Studies by Noshito and colleages have shown that during acute ER stress, derlins are recruited to the Sec61 translocon pore where they reroute ER-targeted substrates to an E3 ligase to initiate ubiquitin tagging and degradation of the substrates by the cytosolic 26S proteasome (Kadowaki et al., 2015, 2018). This study implies that derlins

function at the nexus of the mechanistically distinct pathways of ERpQC and ERAD. Exactly how derlins capture incoming substrate and the extent to which rhomboid features are employed during the derlin-backed rerouting step in ERpQC remains as an open question.

1.2.4 Physiological role of derlins

The physiological role of derlin-mediated ERAD has been difficult to study due to the embryonic and perinatal lethality of mice deficient for derlin homologs: Derlin-1 and Derlin-2 respectively (Table 1) (Dougan et al., 2011; Eura et al., 2012). The recent generation of cell-type-specific derlin-deficient mice has offered a unique opportunity to delineate the significance of derlins in physiology (Table 1). Schwann-cell specific Derlin-2 KO mice results in late onset of neuropathy with myelin exhibiting severe defects in its morphology and function (Volpi et al., 2019). This defect is most likely the result of abnormal maintenance of myelin protein in the ER and consequent disruption in Schwann cellular function. Furthermore, Ren and colleagues investigated the underlying functional role of Derlin-2 in kidney-derived podocyte cells (Ren et al., 2018). Harsh environmental conditions experienced by podocytes and renal protein mutations contribute to protein misfolding in the ER of podocytes, evoking constant ER stress (Clarke et al., 2014). Furthermore, ER stress causes an onset of many kidney diseases such as diabetic nephropathy, renal fibrosis, and ischemia-reperfusion (Taniguchi & Yoshida, 2015). It is proposed that podocytes utilize Derlin-2 as a protein quality control mechanism in order to cope with persistent ER stress (Inagi et al., 2005; Ren et al., 2018). Patients with diabetic nephropathy and corresponding kidney disease mice models have upregulated Derlin-2 levels (Ren et al., 2018). Furthermore, tissue culture studies demonstrate that Derlin-2 overexpression is positively

correlated with the survival of ER-stressed podocytes (Ren et al., 2018). Overall, both studies demonstrate that Derlin-2 deficient Schwann cells and podocytes are functionally compromised when the burden of misfolded substrates becomes insurmountable.

This collection of results suggests derlins play a prominent role in safeguarding the proteome in normal physiology. If this is the case, tissues with high secretory demand should be severely affected when derlin function is compromised. Contrary to this expectation, developing Schwann, hepatocytes, podocytes and B-cells are able to cope with derlin deficiency and ER stress under normal basal conditions (Dougan et al., 2011; Eura et al., 2012; Ren et al., 2018; Volpi et al., 2019). This could be due to cellular adaptation from compensatory pathways such as functional redundancy amongst all three derlin paralogs, autophagy, or alternative ER protein quality control pathways. How cells handle the accumulation of certain substrates should be considered on a case-by-case scenario for different cell types.

Along with protecting the proteome, derlins can control abundance of specific substrates, which would modulate the activity of the substrates within the cell. For example, tissue culture studies have shown that derlins degrade a wide range of substrates including potassium channels (K_{ATP}), ENaC, ApoB, cystic fibrosis transmembrane conductance regulator (CFTR), to name a few (Greenblatt et al., 2012; F. Sun et al., 2006; Suzuki et al., 2012; You et al., 2017). This suggest derlins can regulate basic physiological processes in a substrate-specific manner. Ongoing effort of generating derlin-deficient animal models will bode well for researchers seeking to understand the physiological role of derlins. It is possible that the three mammalian derlin homologs exhibit functional redundancy. Thus,

future works in utilizing tissue-specific double or triple derlin knockout animal models would address this potential problem.

1.2.5 Disease role of derlins

Cancer cells are highly proliferative in nutrient-deprived and hypoxic conditions, making them prone to protein misfolding throughout the cell (Clarke et al., 2014). Cancer cells are susceptible to protein misfolding stress within the ER where the demand of protein folding is high (Corazzari et al., 2017). The ability of cancer cells to cope with ER stress leads to their survival and chemo-resistance (Corazzari et al., 2017). Several studies have shown that cancer cells cope with ER stress by activating ERAD. For example, derlin mRNA is overexpressed in breast cancer (Derlin-1 and Derlin-3) and colon cancer (Derlin-1) in order to mitigate ER stress (Table 2) (Bergbold & Lemberg, 2013; Dong et al., 2017; Shibata et al., 2017; Tan et al., 2015; J. Wang et al., 2008). In the contrary, another study has shown that colon cancer cells can downregulate Derlin-3 through hypermethylation of its promoter region in order to promote cancer cell survial. For example, cancer cells have an enormous demand for ATP to fuel their growth, and glycolysis, as opposed to oxidative phosphorylation, is better suited to meet this demand (Liberti & Locasale, 2016). This metabolic switch to glycolysis is accompanied by enhancement of glucose uptake through stabilization of glucose transporter, GLUT1, levels (Lopez-Serra et al., 2014). This GLUT1 stabilization is a result of transcriptional inactivation of Derlin-3, which is normally responsible for targeting the transporter for degradation (Lopez-Serra et al., 2014). Ultimately, stabilized GLUT1 leads to increased uptake in glucose which supports the high energy demand of a proliferative cancer cell. Altogether, the above studies suggest that derlin upregulation and downregulation in

different cancer cell types can support cancer cell survival and metabolism, respectively. Understanding the basic biological function of derlins during cancer progression warrants future investigation and would serve as a window into developing derlins as a therapeutic target or new biomarker for early diagnosis for cancer.

1.2.6 Dsc2 and UBAC2

Structural homology demonstrates both yeast Dsc2 and mammalian UBA Domain Containing 2 (UBAC2) belong to the rhomboid pseudoprotease class (Christianson et al., 2012; Greenblatt et al., 2012; Lloyd et al., 2013). Both proteins have significantly diverged in their primary sequence, with 20% similarity between the two proteins (Lloyd et al., 2013). Furthermore, both Dsc2 and UBAC2 contain a C-terminal motif known as the ubiquitin-associated (UBA) domain that directly interacts with ubiquitin (Christianson et al., 2011; Lloyd et al., 2013). The current knowledge on their biological function will be discussed in detail below.

1.2.7 Dsc2: A lever for cholesterol and sphingolipid homeostasis

Cell cholesterol is under constant multi-layered control. This is mainly regulated by an ER resident transcription factor, Sterol regulatory element-binding protein (SREBP), which is responsible for transcribing genes involved in sterol synthesis, low-density lipoprotein (LDL) receptor, and other lipid-related proteins (Hampton, 2008; Yang et al., 2002). SREBP itself is also controlled by feedback regulation to which the overarching concept is simple. When

cellular cholesterol is low, SREBP is activated by sequential cleavage by Golgi-resident Site-1 and Site-2 proteases, allowing SREBP-mediated sterol synthesis to occur. When cholesterol is high, SREBP is inactive, followed by less sterol synthesis (Radhakrishnan et al., 2008). Notably, the SREBP pathway is conserved in *S. pombe,* with the exception that *S. pombe* does not have Site-1 and Site-2 proteases. The detailed knowledge of SREBP regulation in fission yeast comes from an ongoing odyssey of inquiry by the Espenshade laboratory leading to a collection of basic insights (Burr et al., 2017; Hwang et al., 2016; Lloyd et al., 2013; Stewart et al., 2012). Stewart and colleagues utilized a genetic selection screen and discovered Dsc E3 ubiquitin ligase complex is required for the cleavage of fission yeast SREBP, Sre1 (Stewart et al., 2012) . This E3 ligase complex is localized in the ER and Golgi membrane and is comprised of E3 ligase Dsc1, Dsc2, Dsc3 and Dsc4 (Lloyd et al., 2013). Most noteworthy, Dsc2 is homologous to rhomboid pseudoproteases (Lloyd et al., 2013). All rhomboid proteins characterized to date specifically binds their substrates in the plane of the membrane (Tichá et al., 2018). Based on Dsc2's connection with the rhomboid superfamily, this leads to the idea that Dsc2 is an integral participant in SREBP recognition and binding. Furthermore, recent studies by Teis' laboratory has shown that in baker's yeast, the Dsc E3 ubiquitin ligase complex, which contains the rhomboid pseudoprotease Dsc2, targets a negative regulator of sphingolipid biosynthesis pathway, Orm2, for degradation in the endosome and Golgi apparatus; a pathway known as Endosome Golgi-Associated Degradation (EGAD) (Schmidt et al., 2019). This pioneering study places Dsc2 at the heart of sphingolipid homeostasis- a lipid that is critical for a plethora of cell biological processes, including growth, apoptosis, cell migration and inflammatory responses (Hannun & Obeid, 2018).

Several biochemical studies have shed light on the mechanism for rhomboid pseudoprotease Dsc2 function. For example, Dsc2 plays an important structural role in linking other members of the Dsc E3 ligase complex together (Lloyd et al., 2013). In addition, Dsc2 is able to bind to ubiquitin *in vitro*, which is mediated by its UBA domain located at the C-terminus (Lloyd et al., 2013). However, Lloyd et al., showed that the UBA domain is dispensable for cleavage of fission yeast SREBP, Sre1(Lloyd et al., 2013). Additional studies are needed to precisely understand how ubiquitin binding contributes to Dsc2 function. Overall, these biochemical studies on Dsc2 function have opened the door to a number of questions: What is the physiological role of Dsc2? To what extent are Dsc2's rhomboid features utilized in SREBP activation or Orm2 degradation? Just like its derlin counterpart, is Dsc2 directly involved in extracting Orm2 and other membrane substrates from the endosome or Golgi membrane? These questions will be interesting avenues to explore in the next few years.

1.2.8 UBAC2 role in energy homeostasis

A BLASTP search revealed that mammalian UBAC2 has significant similarity to yeast Dsc2 (Lloyd et al., 2013). Just like Dsc2, UBAC2 also has a C-terminal UBA domain, which is predicted to bind to ubiquitin. Indeed, the purified recombinant UBA tail of UBAC2 is able to bind to polyubiquitin chains, suggesting involvement of UBAC2 in the ubiquitin-proteasome protein degradation pathway (Christianson et al., 2012). Consistent with this idea, UBAC2 knockdown led to stabilization of mutant alpha1-antitrypsin, a well-known ERAD substrate (Christianson et al., 2012). Furthermore, a previous study has shown that UBAC2 contributes to energy homeostasis in mammals in a manner that is distinct from its proposed role in

ERAD as described above. UBAC2 was shown to specifically restrict trafficking of UBXD8 from the ER to lipid droplets (LDs) where it is known to regulate the rate limiting enzyme in lipid hydrolysis (Olzmann et al., 2013). Hence, UBAC2 strongly contributes to energy homeostasis by controlling cellular fat storage. It will be interesting to understand how UBAC2 mediated retention of UBXD8 in the ER is regulated.

1.2.9 Disease role of UBAC2

Genome-wide associate studies (GWAS) have strongly linked single-nucleotide polymorphisms (SNPs) of UBAC2 to Behçet disease (BD) (Table 2) (Yamazoe et al., 2017). BD is an inflammatory disease associated with development of lesions throughout the body, particularly the central nervous system (Yamazoe et al., 2017). Yamazoe et al, have shown that UBAC2 polymorphisms are elevated in BD (Yamazoe et al., 2017). Whether an elevated level of UBAC2 in BD increases the risk for BD remains to be determined. Furthermore, BD pathology is associated with other genes related to ubiquitin-related functions including ubiquitin associated and SH3 domain containing B (*UBASH3B*), small ubiquitin-like modifier 4 (*SUMO4*), and ubiquitin-conjugating enzyme E2Q family-like 1 (*UBE2QL*1) (Yamazoe et al., 2017). This suggests that the ubiquitin and protein degradation pathways may contribute to the development of BD. Future studies are warranted to confirm the general validity of these findings and to clarify the underlying mechanism of UBAC2 for this association. In this case, support from animal models will be paramount in establishing UBAC2-mediated causality in BD.

1.2.10 iRhoms

iRhoms are pseudoproteases that are evolutionarily distinct from derlins and are more closely related to rhomboid proteases. iRhoms are ER-resident integral membrane proteins with seven transmembrane helices. *Drosophila* have one iRhom while humans and mice have two, iRhom1 and iRhom2. iRhoms have diverse roles in cellular function (reviewed in (Dulloo et al., 2019)). In this review, we will focus on their role in protein stability and quality control.

1.2.11 iRhoms in regulated protein degradation

iRhoms have a broad role in controlling protein abundance via ERAD, as well as by other mechanisms. The first instance of iRhoms playing a role in protein degradation was shown by the Freeman group (Zettl et al., 2011). In *Drosophila*, iRhom is exclusively expressed in neurons and knockout flies exhibit long periods of time in a “sleep-like state”. Because the same sleep-like behavior occurs when epidermal growth factor receptor (EGFR) signaling increases, it was hypothesized that iRhom functions as a negative regulator of EGFR signaling. Indeed, the “sleep-like” phenotype is rescued by neuron-specific expression of iRhom, and, in mammalian cells, iRhoms facilitate the degradation of EGFR ligands. In human cell culture, overexpressed iRhom1 has been demonstrated to cause increased proteasome activity (Lee et al., 2015). This increase in proteasome activity was also seen with overexpression of the active rhomboids RHBDL1 and RHBDL2, and their catalytically inactive mutants, but this was not further explored. This hyperactivity was proposed to be mediated through stabilization of proteasome chaperones Pac1 and Pac2 by iRhom1,

although the exact mechanism has not been determined. The authors also showed iRhom1 protein levels are elevated under ER stress, indicating that iRhom1 may promote faster degradation of accumulating substrates during ER stress through increasing proteasome activity. iRhom1 is also involved in stabilizing the α subunit of the transcription factor hypoxia inducible factor-1 (Hif1α) by reducing its degradation by the proteasome (Z. Zhou et al., 2014). Stabilization of Hif1α in hypoxic conditions allows formation of the active transcription factor, which promotes cellular adaptation to hypoxia. Under normal conditions, Rack1 interacts with Hif1α resulting in Hif1α being degraded by the proteasome. Experimental evidence indicates iRhom1 can bind Rack1, thereby preventing its interaction with Hif1α and leading to stabilization of Hif1α. iRhom1 was also upregulated in breast cancer patients with escalated disease progression, and perhaps this allows cancer cells to adapt to hypoxia through increased Hif1α activity.

1.3 Rhomboid Proteases

1.3.1 RHBDL4

Rhomboid proteases were first discovered in Drosophila with an important role in cleaving Spitz, a membrane-bound ligand for the epidermal growth factor receptor (EGFR)(Urban et al., 2001). In mammals, there are four rhomboid proteases in the secretory pathway (RHBDL1-4) and one in the mitochondria (PARL). While many rhomboid proteases either have not been well described or are involved in cell signaling, the main described role of mammalian rhomboid RHBDL4 (also known by the gene name Rhbdd1) is in protein quality control.

1.3.2 RHBDL4 in ERAD

RHBDL4 is an ER-resident rhomboid protease that is involved in ERAD (see review (Freeman, 2014)). In contrast to derlins, which are primarily involved in retrotranslocating full-length defective proteins from the ER, RHBDL4 cleaves specific membrane substrates into fragments which are then retrotranslocated into the cytoplasm and degraded by the proteasome (Fleig et al., 2012).

Two features of RHBDL4 that are important for its role in ERAD are its ubiquitin interacting motif (UIM) and its Valosin-binding motif (VBM), which recruits the AAA-ATPase p97 (Fleig et al., 2012; Lim et al., 2016). The UIM motif on RHBDL4 indicates that substrate recognition and eventual cleavage is mediated by substrate ubiquitination. The VBM motif, which recruits p97 to RHBDL4, is highly conserved across eukaryotes, indicating an evolutionary conserved function for RHBDL4 in ERAD (Lim et al., 2016).

The Lemberg group was the first to show a role for RHBDL4 in cleaving membrane proteins and targeting them for ERAD (Fleig et al., 2012). In this seminal work, RHBDL4 was shown to cleave several membrane proteins both in their ectodomains as well as in the membrane spanning segments prior to retrotranslocation and degradation. More recent work from the Lemberg group also identified RHBDL4 as having a role in mediating the turnover of misfolded luminal proteins (Kühnle et al., 2019). RHBDL4 forms a complex with the ERAD components Erlin1 and Erlin2, which function as substrate adaptors for its targeting of luminal proteins. RHBDL4 acts in an alternative ERAD pathway for luminal aggregation-

prone proteins, whereby they are first cleaved into fragmets and subsequently removed and degraded by the proteasome, instead of being retrotranslocated in their full-length form.

1.3.3 Physiological Role of RHBDL4

Mammalian cell culture studies have elucidated that RHBDL4 can cleave a wide variety of ERAD substrates. The first identified substrate of RHBDL4 was the α subunit of the pre-T cell receptor (pTα) (Fleig et al., 2012). While there is not a strict sequence specific degron requirement, it was hypothesized that two basic amino acids in the transmembrane span of pTα triggered its degradation by RHBDL4. In support of this hypothesis, a disease variant of myelin protein zero (MPZ) that contains two basic residues in its transmembrane domain can also be cleaved by RHBDL4 and subsequently degraded. Interestingly, when the pTα degron was introduced into opsin, a multipass membrane protein, it was also cleaved by RHBDL4 (Fleig et al., 2012). This work established that RHBDL4 has loose sequence requirements for recognition and can cleave both single-pass and multi-pass membrane proteins.

The Munter group exhibited that RHBDL4 is capable of cleaving the ectodomain of amyloid precursor protein (APP) (Paschkowsky et al., 2016). Cleavage of APP by other proteases can result in amyloid β (Aβ) peptides, which are implicated in Alzheimer's disease. Secretion of Aβ peptides was reduced in cells expressing active RHBDL4 compared to cells with inactive RHBDL4 (Paschkowsky et al., 2016). However, it is unclear whether RHBDL4 mediated cleavage of APP results in degradation through ERAD. RHBDL4-mediated

processing of APP can be influenced by binding of cholesterol to specific motifs in the transmembrane domain of RHBDL4 (Recinto et al., 2018). Decreased levels of cellular cholesterol resulted in an increase in RHBDL4 mediated APP fragments, suggesting that RHBDL4 activity is influenced by the surrounding lipid environment.

Like other ERAD components, RHBDL4 transcription is increased in response to ER stress (Fleig et al., 2012). Additionally, expression of catalytically inactive RHBDL4 causes substrate trapping, which induces ER stress (Fleig et al., 2012). Recent work from the Lemberg group used proteomics to identify ERAD targets of RHBDL4 (Knopf et al., 2020). By using stable isotopic labeling in cell culture (SILAC) with wildtype RHBDL4 and RHBDL4 mutants, the authors were able to identify possible RHBDL4 substrates. Several of the proteins identified were part of the oligosacharyltransferase (OST) complex, which is responsible for glycosylating newly synthesized proteins (Knopf et al., 2020). By cleaving these subunits and targeting them for ERAD, RHBDL4 can fine tune glycosylation in the cell, which may mitigate ER stress. RHBDL4 also increases degradation of OST subunits when one component in depleted or increased.

Based on the RHBDL4 substrates identified so far, the range of proteins is very broad without universal structural requirements for cleavage. Past studies have relied on the overexpression of either RHBDL4 or its substrates; making it difficult to determine which RHBDL4 substrates are physiologically relevant. Outstanding questions which remain in terms of RHBDL4 substrates are (i) what features of a target protein determine whether it is targeted by RHBDL4 and (ii) what is the importance of ubiquitination in targeting substrates.

1.3.4 Disease role of RHBDL4

RHBDL4 is upregulated in both colorectal cancer and glioblastoma (Table 2) (Miao et al., 2017; Song et al., 2015; Wei et al., 2014; Zhang et al., 2018). However, it is not established whether this has any relation to its role in ERAD, or whether it is due solely to other functions of RHBDL4 in cell signaling pathways. Recently, the Lemberg group explored the role of RHBDL4 in regulating OST complex subunit degradation. They proposed that the upregulation of RHBDL4 seen in several cancer types could be to increase the degradation of excess OST complex subunits that could result from aneuploidy in cancer cells (Knopf et al., 2020). Alternatively, the involvement of RHBDL4 in cancer could be due to its ability to cleave the proapoptotic protein BIK (Y. Wang et al., 2008). The overexpression of RHBDL4 seen in some cancer cells could reduce apoptosis, thereby promoting cancer progression and proliferation. To date, the work associating RHBDL4 with cancer has been done using patient samples and cell culture. To better delineate the role of RHBDL4 in disease, it will be important to establish animal models to study how changes in RHBDL4 expression alter cancer progression.

1.3.5 YqgP

The close mechanistic relationship between rhomboid proteases and pseudoproteases is highlighted by recent research from the Strisovsky group showing that bacterial rhomboid YqgP of *Bacillus subtilis* regulates magnesium homeostasis and acts as a protease while also displaying functions similar to derlins (Began et al., 2020). This work elegantly established that YqgP cleaves the magnesium transporter MgtE under environmental

conditions of low magnesium and high manganese or zinc. YqgP has an additional function as a substrate adaptor for FtsH, an ATP dependent protease that works in conjunction with YqgP to degrade MgtE. Importantly, the active site of YqgP, but not its catalytic ability, is required for its interaction with FtsH and cleavage of MgtE by FtsH. This pathway has striking similarities to ERAD, with YqgP playing a similar role to derlins in recruiting other machinery for substrate degradation, while also having a direct role in degrading its substrates. This paper establishes a physiologically important process in bacteria that is regulated by a rhomboid protease, and is an example of protein homeostasis being altered in response to environmental conditions to alleviate cellular stress.

1.4 Conclusions and Perspectives

In just the past 5 years, we have learned a great deal about the rhomboid superfamily and their importance in protein homeostasis. The rhomboid superfamily is widespread and highly conserved, and it is remarkable to see how fundamental cell biological studies have paved the way to our current knowledge of rhomboid biology in health and diseases. The fundamental knowledge gained regarding the rhomboid protein family's systemic significance in animal models bodes well in providing a mechanistic and conceptual platform for understanding the broader functions of the rhomboid superfamily. Thus far, studies on cell-specific rhomboid pseudoprotease knockout mice have made a major contribution towards understanding their physiological role of rhomboid pseudoproteases. The lack of function of some rhomboid pseudoproteases has been demonstrated to activate ER stress responses in cells with large secretory demand. Moreover, biochemical studies in mammalian cell culture show that the rhomboid superfamily target a plethora of substrates and may affect downstream pathways in a substrate-specific manner. Future studies in rhomboid-deficient

animal knockouts will shed light on their biological significance. We predict that many fundamental questions about rhomboids under normal and pathophysiological conditions will be addressed in the next few years, including their specific biological role in cancer cells. Accordingly, these studies will provide fundamental knowledge in exploiting the rhomboid superfamily for potential therapeutics and will be an incredibly exciting area of research in the years to come.

1.5 Acknowledgments

Chapter 1 is largely adapted from the material as it appears in Kandel, R.R., and Neal, S.E., The role of rhomboid superfamily members in protein homeostasis: Mechanistic insight and physiological implications, *Biochimica et Biophysica Acta – Molecular Cell Research* (2020), https://doi.org/10.1016/j.bbamcr.2020.118793. The dissertation author was the first author of this manuscript.

1.6 References

Avci, D., Fuchs, S., Schrul, B., Fukumori, A., Breker, M., Frumkin, I., Chen, C., Biniossek, M., Kremmer, E., Schilling, O., Steiner, H., Schuldiner, M., & Lemberg, M. (2014). The Yeast ER-Intramembrane Protease Ypf1 Refines Nutrient Sensing by Regulating Transporter Abundance. *Molecular Cell*, *56*(5), 630–640. https://doi.org/10.1016/j.molcel.2014.10.012

Avci, D., & Lemberg, M. K. (2018). Membrane Protein Dislocation by the Rhomboid Pseudoprotease Dfm1: No Pore Needed? In *Molecular Cell* (Vol. 69, Issue 2, pp. 161–162). Cell Press. https://doi.org/10.1016/j.molcel.2017.12.031

Balchin, D., Hayer-Hartl, M., & Hartl, F. U. (2016). In vivo aspects of protein folding and quality control. *Science (New York, N.Y.)*, *353*(6294), aac4354. https://doi.org/10.1126/science.aac4354

Began, J., Cordier, B., Březinová, J., Delisle, J., Hexnerová, R., Srb, P., Rampírová, P., Kožíšek, M., Baudet, M., Couté, Y., Galinier, A., Veverka, V., Doan, T., & Strisovsky, K. (2020). Rhomboid intramembrane protease YqgP licenses bacterial membrane protein quality control as adaptor of FtsH AAA protease . *The EMBO Journal*, e102935. https://doi.org/10.15252/embj.2019102935

Bergbold, N., & Lemberg, M. K. (2013). Emerging role of rhomboid family proteins in mammalian biology and disease. In *Biochimica et Biophysica Acta - Biomembranes* (Vol. 1828, Issue 12, pp. 2840–2848). https://doi.org/10.1016/j.bbamem.2013.03.025

Bodnar, N. O., & Rapoport, T. A. (2017). Molecular Mechanism of Substrate Processing by the Cdc48 ATPase Complex. *Cell*, *169*(4), 722-735.e9. https://doi.org/10.1016/j.cell.2017.04.020

Bondar, A. N., del Val, C., & White, S. H. (2009). Rhomboid Protease Dynamics and Lipid Interactions. *Structure*, *17*(3), 395–405. https://doi.org/10.1016/j.str.2008.12.017

Bordallo, J., Plemper, R. K., Finger, A., & Wolf, D. H. (1998). Der3p/Hrd1p is required for endoplasmic reticulum-associated degradation of misfolded lumenal and integral membrane proteins. *Molecular Biology of the Cell*, *9*(1), 209–222. https://doi.org/10.1091/mbc.9.1.209

Brooks, C. L., & Lemieux, M. J. (2013). Untangling structure-function relationships in the rhomboid family of intramembrane proteases. In *Biochimica et Biophysica Acta - Biomembranes* (Vol. 1828, Issue 12, pp. 2862–2872). https://doi.org/10.1016/j.bbamem.2013.05.003

Burr, R., Ribbens, D., Raychaudhuri, S., Stewart, E. V., Ho, J., & Espenshade, P. J. (2017). Dsc E3 ligase localization to the Golgi requires the ATPase Cdc48 and cofactor Ufd1 for activation of sterol regulatory element-binding protein in fission yeast. *Journal of Biological Chemistry*, *292*(39), 16333–16350. https://doi.org/10.1074/jbc.M117.802025

Chen, B., Retzlaff, M., Roos, T., & Frydman, J. (2011). Cellular strategies of protein quality control. *Cold Spring Harbor Perspectives in Biology*, *3*(8), a004374. https://doi.org/10.1101/cshperspect.a004374

Christianson, J. C., Olzmann, J. A., Shaler, T. A., Sowa, M. E., Bennett, E. J., Richter, C. M., Tyler, R. E., Greenblatt, E. J., Wade Harper, J., & Kopito, R. R. (2012). Defining human ERAD networks through an integrative mapping strategy. *Nature Cell Biology*, *14*(1), 93–105. https://doi.org/10.1038/ncb2383

Clarke, H. J., Chambers, J. E., Liniker, E., & Marciniak, S. J. (2014). Endoplasmic Reticulum Stress in Malignancy. In *Cancer Cell* (Vol. 25, Issue 5, pp. 563–573). Cell Press. https://doi.org/10.1016/j.ccr.2014.03.015

Corazzari, M., Gagliardi, M., Fimia, G. M., & Piacentini, M. (2017). Endoplasmic Reticulum Stress, Unfolded Protein Response, and Cancer Cell Fate. *Frontiers in Oncology*, *7*, 78. https://doi.org/10.3389/fonc.2017.00078

Dong, Q., Fu, L., Zhao, Y., Tan, S., Wang, E., Dong, Q., Fu, L., Zhao, Y., Tan, S., Wang, E. (2017). Derlin-1 overexpression confers poor prognosis in muscle invasive bladder cancer and contributes to chemoresistance and invasion through PI3K/AKT and ERK/MMP signaling. *Oncotarget*, *8*(10), 17059–17069. https://doi.org/10.18632/oncotarget.15001

Dougan, S. K., Hu, C.-C. A., Paquet, M.-E., Greenblatt, M. B., Kim, J., Lilley, B. N., Watson, N., & Ploegh, H. L. (2011). Derlin-2-Deficient Mice Reveal an Essential Role for Protein Dislocation in Chondrocytes. *Molecular and Cellular Biology*, *31*(6), 1145–1159. https://doi.org/10.1128/mcb.00967-10

Dulloo, I., Muliyil, S., & Freeman, M. (2019). The molecular, cellular and pathophysiological roles of irhom pseudoproteases. In *Open Biology* (Vol. 9, Issue 3). Royal Society Publishing. https://doi.org/10.1098/rsob.190003

Düsterhöft, S., Künzel, U., & Freeman, M. (2017). Rhomboid proteases in human disease: Mechanisms and future prospects. In *Biochimica et Biophysica Acta - Molecular Cell Research* (Vol. 1864, Issue 11, pp. 2200–2209). Elsevier B.V. https://doi.org/10.1016/j.bbamcr.2017.04.016

Eftekharzadeh, B., Hyman, B. T., & Wegmann, S. (2016). Structural studies on the mechanism of protein aggregation in age related neurodegenerative diseases. *Mechanisms of Ageing and Development*, *156*, 1–13. https://doi.org/10.1016/j.mad.2016.03.001

Erez, E., & Bibi, E. (2009). Cleavage of a multispanning membrane protein by an intramembrane serine protease. *Biochemistry*, *48*(51), 12314–12322. https://doi.org/10.1021/bi901648g

Eura, Y., Yanamoto, H., Arai, Y., Okuda, T., Miyata, T., & Kokame, K. (2012). Derlin-1 Deficiency Is Embryonic Lethal, Derlin-3 Deficiency Appears Normal, and Herp Deficiency Is Intolerant to Glucose Load and Ischemia in Mice. *PLoS ONE*, *7*(3), e34298. https://doi.org/10.1371/journal.pone.0034298

Fleig, L., Bergbold, N., Sahasrabudhe, P., Geiger, B., Kaltak, L., & Lemberg, M. K. (2012). Ubiquitin-Dependent Intramembrane Rhomboid Protease Promotes ERAD of Membrane Proteins. *Molecular Cell*, *47*(4), 558–569. https://doi.org/10.1016/j.molcel.2012.06.008

Foresti, O., Rodriguez-Vaello, V., Funaya, C., & Carvalho, P. (2014). Quality control of inner nuclear membrane proteins by the Asi complex. *Science*, *346*(6210), 751–755. https://doi.org/10.1126/science.1255638

Freeman, M. (2014). The rhomboid-like superfamily: molecular mechanisms and biological roles. *Annual Review of Cell and Developmental Biology*, *30*(1), 235–254. https://doi.org/10.1146/annurev-cellbio-100913-012944

Goder, V., Carvalho, P., & Rapoport, T. a. (2008). The ER-associated degradation component Der1p and its homolog Dfm1p are contained in complexes with distinct cofactors of the ATPase Cdc48p. *FEBS Letters*, *582*(11), 1575–1580. https://doi.org/10.1016/j.febslet.2008.03.056

Greenblatt, E. J., Olzmann, J. a, & Kopito, R. R. (2011). Derlin-1 is a rhomboid pseudoprotease required for the dislocation of mutant α-1 antitrypsin from the endoplasmic reticulum. *Nature Structural & Molecular Biology*, *18*(10), 1147–1152. https://doi.org/10.1038/nsmb.2111

Greenblatt, E. J., Olzmann, J. A., & Kopito, R. R. (2012). Making the cut: intramembrane cleavage by a rhomboid protease promotes ERAD. *Nature Structural & Molecular Biology*, *19*(10), 979–981. https://doi.org/10.1038/nsmb.2398

Hampton, R. Y. (2008). A Cholesterol Toggle Switch. In *Cell Metabolism* (Vol. 8, Issue 6, pp. 451–453). https://doi.org/10.1016/j.cmet.2008.11.006

Hampton, R. Y., & Sommer, T. (2012). Finding the will and the way of ERAD substrate retrotranslocation. *Current Opinion in Cell Biology*, *24*(4), 460–466. https://doi.org/10.1016/j.ceb.2012.05.010

Hannun, Y. A., & Obeid, L. M. (2018). Sphingolipids and their metabolism in physiology and disease. In *Nature Reviews Molecular Cell Biology* (Vol. 19, Issue 3, pp. 175–191). Nature Publishing Group. https://doi.org/10.1038/nrm.2017.107

Hartl, F. U., Bracher, A., & Hayer-Hartl, M. (2011). Molecular chaperones in protein folding and proteostasis. *Nature*, *475*(7356), 324–332. https://doi.org/10.1038/nature10317

Hirsch, C., Gauss, R., Horn, S. C., Neuber, O., & Sommer, T. (2009). The ubiquitylation machinery of the endoplasmic reticulum. *Nature*, *458*(7237), 453–460. https://doi.org/10.1038/nature07962

Hwang, J., Ribbens, D., Raychaudhuri, S., Cairns, L., Gu, H., Frost, A., Urban, S., & Espenshade, P. J. (2016). A Golgi rhomboid protease Rbd2 recruits Cdc48 to cleave yeast SREBP. *The EMBO Journal*, *35*(21), 2332–2349. https://doi.org/10.15252/embj.201693923

Inagi, R., Nangaku, M., Onogi, H., Ueyama, H., Kitao, Y., Nakazato, K., Ogawa, S., Kurokawa, K., Couser, W. G., & Miyata, T. (2005). Involvement of endoplasmic reticulum

(ER) stress in podocyte injury induced by excessive protein accumulation. In *Kidney International* (Vol. 68). https://doi.org/10.1111/j.1523-1755.2005.00736.x

Jaeger, P. A., Ornelas, L., McElfresh, C., Wong, L. R., Hampton, R. Y., & Ideker, T. (2018). Systematic Gene-to-Phenotype Arrays: A High-Throughput Technique for Molecular Phenotyping. *Molecular Cell*, *69*(2), 321-333.e3. https://doi.org/10.1016/j.molcel.2017.12.016

Jeng, W., Lee, S., Sung, N., Lee, J., & Tsai, F. T. F. (2015). Molecular chaperones: guardians of the proteome in normal and disease states. *F1000Research*, *4*. https://doi.org/10.12688/f1000research.7214.1

Kadowaki, H., Nagai, A., Maruyama, T., Takami, Y., Satrimafitrah, P., Kato, H., Honda, A., Hatta, T., Natsume, T., Sato, T., Kai, H., Ichijo, H., & Nishitoh, H. (2015). Pre-emptive Quality Control Protects the ER from Protein Overload via the Proximity of ERAD Components and SRP. *Cell Reports*, *13*(5), 944–956. https://doi.org/10.1016/j.celrep.2015.09.047

Kadowaki, H., Satrimafitrah, P., Takami, Y., & Nishitoh, H. (2018). Molecular mechanism of ER stress-induced pre-emptive quality control involving association of the translocon, Derlin-1, and HRD1. *Scientific Reports*, *8*(1). https://doi.org/10.1038/s41598-018-25724-x

Khmelinskii, A., Blaszczak, E., Pantazopoulou, M., Fischer, B., Omnus, D. J., Dez, G. Le, Brossard, A., Gunnarsson, A., Barry, J. D., Meurer, M., Kirrmaier, D., Boone, C., Huber, W., Rabut, G., Ljungdahl, P. O., & Knop, M. (2014). Protein quality control at the inner nuclear membrane. *Nature*, *516*(7531), 410–413. https://doi.org/10.1038/nature14096

Knop, M., Finger, A., Braun, T., Hellmuth, K., & Wolf, D. H. (1996). Der1, a novel protein specifically required for endoplasmic reticulum degradation in yeast. *The EMBO Journal*, *15*(4), 753–763. https://doi.org/10.1002/j.1460-2075.1996.tb00411.x

Knopf, J. D., Landscheidt, N., Pegg, C. L., Schulz, B. L., Kühnle, N., Chao, C.-W., Huck, S., & Lemberg, M. K. (2020). Intramembrane protease RHBDL4 cleaves oligosaccharyltransferase subunits to target them for ER-associated degradation. *Journal of Cell Science*, jcs.243790. https://doi.org/10.1242/jcs.243790

Kreutzberger, A. J. B., Ji, M., Aaron, J., Mihaljević, L., & Urban, S. (2019). Rhomboid distorts lipids to break the viscosity-imposed speed limit of membrane diffusion. *Science*, *363*(6426). https://doi.org/10.1126/science.aao0076

Kühnle, N., Bock, J., Knopf, J. D., Landscheidt, N., Lee, J.-G., Ye, Y., & Lemberg, M. K. (2019). Intramembrane protease RHBDL4 interacts with erlin complex to target unstable soluble proteins for degradation. *BioRxiv*, 848754. https://doi.org/10.1101/848754

Lee, W., Kim, Y., Park, J., Shim, S., Lee, J., Hong, S. H., Ahn, H. H., Lee, H., & Jung, Y. K. (2015). IRhom1 regulates proteasome activity via PAC1/2 under ER stress. *Scientific Reports*, *5*. https://doi.org/10.1038/srep11559

Lemberg, M. K. (2013). Sampling the membrane: function of rhomboid-family proteins. *Trends in Cell Biology*, *23*(5), 210–217. https://doi.org/10.1016/j.tcb.2013.01.002

Lemberg, M. K., & Adrain, C. (2016). Inactive rhomboid proteins: New mechanisms with implications in health and disease. *Seminars in Cell & Developmental Biology*, *60*, 29–37. https://doi.org/10.1016/J.SEMCDB.2016.06.022

Lemberg, M. K., & Freeman, M. (2007). Functional and evolutionary implications of enhanced genomic analysis of rhomboid intramembrane proteases. *Genome Research*, *17*(11), 1634–1646. https://doi.org/10.1101/gr.6425307

Lemieux, M. J., Fischer, S. J., Cherney, M. M., Bateman, K. S., & James, M. N. G. (2007). The crystal structure of the rhomboid peptidase from Haemophilus influenzae provides insight into intramembrane porteolysis. *Proceedings of the National Academy of Sciences of the United States of America*, *104*(3), 750–754. https://doi.org/10.1073/pnas.0609981104

Liberti, M. V., & Locasale, J. W. (2016). The Warburg Effect: How Does it Benefit Cancer Cells? In *Trends in Biochemical Sciences* (Vol. 41, Issue 3, pp. 211–218). Elsevier Ltd. https://doi.org/10.1016/j.tibs.2015.12.001

Lilley, B. N., & Ploegh, H. L. (2004). A membrane protein required for dislocation of misfolded proteins from the ER. *Nature*, *429*(6994), 834–840. https://doi.org/10.1038/nature02592

Lim, J. J., Lee, Y., Ly, T. T., Kang, J. Y., Lee, J. G., An, J. Y., Youn, H. S., Park, K. R., Kim, T. G., Yang, J. K., Jun, Y., & Eom, S. H. (2016). Structural insights into the interaction of p97 N-Terminus domain and VBM in rhomboid protease, RHBDL4. *Biochemical Journal*, *473*(18), 2863–2880. https://doi.org/10.1042/BCJ20160237

Lloyd, S. J. A., Raychaudhuri, S., & Espenshade, P. J. (2013). Subunit architecture of the golgi dsc e3 ligase required for sterol regulatory element-binding protein (SREBP) cleavage in fission yeast. *Journal of Biological Chemistry*, *288*(29), 21043–21054. https://doi.org/10.1074/jbc.M113.468215

Lopez-Serra, P., Marcilla, M., Villanueva, A., Ramos-Fernandez, A., Palau, A., Leal, L., Wahi, J. E., Setien-Baranda, F., Szczesna, K., Moutinho, C., Martinez-Cardus, A., Heyn, H., Sandoval, J., Puertas, S., Vidal, A., Sanjuan, X., Martinez-Balibrea, E., Viñals, F., Perales, J. C., … Esteller, M. (2014). A DERL3-associated defect in the degradation of SLC2A1 mediates the Warburg effect. *Nature Communications*, *5*(1), 3608. https://doi.org/10.1038/ncomms4608

Maegawa, S., Koide, K., Ito, K., & Akiyama, Y. (2007). The intramembrane active site of GlpG, an E. coli rhomboid protease, is accessible to water and hydrolyses an extramembrane peptide bond of substrates. *Molecular Microbiology*, *64*(2), 435–447. https://doi.org/10.1111/j.1365-2958.2007.05679.x

Mehnert, M., Sommer, T., & Jarosch, E. (2013). Der1 promotes movement of misfolded proteins through the endoplasmic reticulum membrane. *Nature Cell Biology*, *16*(1), 77–86. https://doi.org/10.1038/ncb2882

Mehrtash, A. B., & Hochstrasser, M. (2019). Ubiquitin-dependent protein degradation at the endoplasmic reticulum and nuclear envelope. In *Seminars in Cell and Developmental Biology* (Vol. 93, pp. 111–124). Elsevier Ltd. https://doi.org/10.1016/j.semcdb.2018.09.013

Miao, F., Zhang, M., Zhao, Y., Li, X., Yao, R., Wu, F., Huang, R., Li, K., Miao, S., Ma, C., Ju, H., Song, W., & Wang, L. (2017). RHBDD1 upregulates EGFR via the AP-1 pathway in colorectal cancer. *Oncotarget*, *8*(15), 25251–25260. https://doi.org/10.18632/oncotarget.15694

Moin, S. M., & Urban, S. (2012). Membrane immersion allows rhomboid proteases to achieve specificity by reading transmembrane segment dynamics. *ELife*, *2012*(1), e00173. https://doi.org/10.7554/eLife.00173

Morimoto, R. I. (2011). The heat shock response: systems biology of proteotoxic stress in aging and disease. *Cold Spring Harbor Symposia on Quantitative Biology*, *76*, 91–99. https://doi.org/10.1101/sqb.2012.76.010637

Neal, S., Jaeger, P. A., Duttke, S. H., Benner, C. K., Glass, C., Ideker, T., & Hampton, R. (2018). The Dfm1 Derlin Is Required for ERAD Retrotranslocation of Integral Membrane Proteins. *Molecular Cell*, *69*(2). https://doi.org/10.1016/j.molcel.2017.12.012

Neal, S., Mak, R., Bennett, E. J., & Hampton, R. (2017). A Cdc48 'retrochaperone' function is required for the solubility of retrotranslocated, integral membrane Endoplasmic Reticulum-associated Degradation (ERAD-M) substrates. *Journal of Biological Chemistry*, *292*(8). https://doi.org/10.1074/jbc.M116.770610

Needham, P. G., & Brodsky, J. L. (2013). How early studies on secreted and membrane protein quality control gave rise to the ER associated degradation (ERAD) pathway: the early history of ERAD. *Biochimica et Biophysica Acta*, *1833*(11), 2447–2457. https://doi.org/10.1016/j.bbamcr.2013.03.018

Olzmann, J. A., Richter, C. M., & Kopito, R. R. (2013). Spatial regulation of UBXD8 and p97/VCP controls ATGL-mediated lipid droplet turnover. *Proceedings of the National Academy of Sciences of the United States of America*, *110*(4), 1345–1350. https://doi.org/10.1073/pnas.1213738110

Paschkowsky, S., Hamzé, M., Oestereich, F., & Munter, L. M. (2016). Alternative processing of the amyloid precursor protein family by rhomboid protease RHBDL4. *Journal of Biological Chemistry*, *291*(42), 21903–21912. https://doi.org/10.1074/jbc.M116.753582

Peterson, B. G., Glaser, M. L., Rapoport, T. A., & Baldridge, R. D. (2019). Cycles of autoubiquitination and deubiquitination regulate the erad ubiquitin ligase hrd1. *ELife*, *8*. https://doi.org/10.7554/eLife.50903

Radhakrishnan, A., Goldstein, J. L., McDonald, J. G., & Brown, M. S. (2008). Switch-like Control of SREBP-2 Transport Triggered by Small Changes in ER Cholesterol: A Delicate Balance. *Cell Metabolism*, *8*(6), 512–521. https://doi.org/10.1016/j.cmet.2008.10.008

Recinto, S. J., Paschkowsky, S., & Munter, L. M. (2018). An alternative processing pathway of APP reveals two distinct cleavage modes for rhomboid protease RHBDL4. *Biol. Chem*, *399*(12), 1399–1408. https://doi.org/10.1515/hsz-2018-0259

Ren, G., Tardi, N. J., Matsuda, F., Koh, K. H., Ruiz, P., Wei, C., Altintas, M. M., Ploegh, H., & Reiser, J. (2018). Podocytes exhibit a specialized protein quality control employing derlin-2 in

kidney disease. *American Journal of Physiology - Renal Physiology*, *314*(3), F471–F482. https://doi.org/10.1152/ajprenal.00691.2016

Sato, B. K., & Hampton, R. Y. (2006). Yeast Derlin Dfm I interacts with Cdc48 and functions in ER homeostasis. *Yeast*, *23*(14–15), 1053–1064. https://doi.org/10.1002/yea.1407

Schmidt, O., Weyer, Y., Baumann, V., Widerin, M. A., Eising, S., Angelova, M., Schleiffer, A., Kremser, L., Lindner, H., Peter, M., Fröhlich, F., & Teis, D. (2019). Endosome and Golgi-associated degradation (EGAD) of membrane proteins regulates sphingolipid metabolism . *The EMBO Journal*, *38*(15), 1–23. https://doi.org/10.15252/embj.2018101433

Schoebel, S., Mi, W., Stein, A., Ovchinnikov, S., Pavlovicz, R., DiMaio, F., Baker, D., Chambers, M. G., Su, H., Li, D., Rapoport, T. A., & Liao, M. (2017). Cryo-EM structure of the protein-conducting ERAD channel Hrd1 in complex with Hrd3. *Nature*, *548*(7667), 352–355. https://doi.org/10.1038/nature23314

Shibata, M., Kanda, M., Tanaka, H., Umeda, S., Miwa, T., Shimizu, D., Hayashi, M., Inaishi, T., Miyajima, N., Adachi, Y., Takano, Y., Nakanishi, K., Takeuchi, D., Noda, S., Kodera, Y., & Kikumori, T. (2017). Overexpression of Derlin 3 is associated with malignant phenotype of breast cancer cells. *Oncology Reports*. https://doi.org/10.3892/or.2017.5800

Shokhen, M., & Albeck, A. (2017). How does the exosite of rhomboid protease affect substrate processing and inhibition? *Protein Science : A Publication of the Protein Society*, *26*(12), 2355–2366. https://doi.org/10.1002/pro.3294

Sicari, D., Igbaria, A., & Chevet, E. (2019). Control of Protein Homeostasis in the Early Secretory Pathway: Current Status and Challenges. *Cells*, *8*. https://doi.org/10.3390/cells8111347

Song, W., Liu, W., Zhao, H., Li, S., Guan, X., Ying, J., Zhang, Y., Miao, F., Zhang, M., Ren, X., Li, X., Wu, F., Zhao, Y., Tian, Y., Wu, W., Fu, J., Liang, J., Wu, W., Liu, C., … Wang, L. (2015). Rhomboid domain containing 1 promotes colorectal cancer growth through activation of the EGFR signalling pathway. *Nature Communications*, *6*, 8022. https://doi.org/10.1038/ncomms9022

Sontag, E. M., Samant, R. S., & Frydman, J. (2017). Mechanisms and Functions of Spatial Protein Quality Control. *Annual Review of Biochemistry*, *86*(1), 97–122. https://doi.org/10.1146/annurev-biochem-060815-014616

Stein, A., Ruggiano, A., Carvalho, P., & Rapoport, T. a. (2014). Key steps in ERAD of luminal ER proteins reconstituted with purified components. *Cell*, *158*(6), 1375–1388. https://doi.org/10.1016/j.cell.2014.07.050

Stewart, E. V., Lloyd, S. J. A., Burg, J. S., Nwosu, C. C., Lintner, R. E., Daza, R., Russ, C., Ponchner, K., Nusbaum, C., & Espenshade, P. J. (2012). Yeast sterol regulatory element-binding protein (SREBP) cleavage requires cdc48 and dsc5, a ubiquitin regulatory X domain-containing subunit of the golgi dsc E3 ligase. *Journal of Biological Chemistry*, *287*(1), 672–681. https://doi.org/10.1074/jbc.M111.317370

Stolz, A., Schweizer, R. S., Schäfer, A., & Wolf, D. H. (2010). Dfm1 forms distinct complexes with Cdc48 and the ER ubiquitin ligases and is required for ERAD. *Traffic (Copenhagen, Denmark)*, *11*(10), 1363–1369. https://doi.org/10.1111/j.1600-0854.2010.01093.x

Strisovsky, K., Sharpe, H. J., & Freeman, M. (2009). Sequence-Specific Intramembrane Proteolysis: Identification of a Recognition Motif in Rhomboid Substrates. *Molecular Cell*, *36*(6), 1048–1059. https://doi.org/10.1016/j.molcel.2009.11.006

Sun, F., Zhang, R., Gong, X., Geng, X., Drain, P. F., & Frizzell, R. A. (2006). Derlin-1 Promotes the Efficient Degradation of the Cystic Fibrosis Transmembrane Conductance Regulator (CFTR) and CFTR Folding Mutants. *Journal of Biological Chemistry*, *281*(48), 36856–36863. https://doi.org/10.1074/jbc.M607085200

Sun, Z., & Brodsky, J. L. (2019). Protein quality control in the secretory pathway. In *Journal of Cell Biology* (Vol. 218, Issue 10, pp. 3171–3187). Rockefeller University Press. https://doi.org/10.1083/jcb.201906047

Suzuki, M., Otsuka, T., Ohsaki, Y., Cheng, J., Taniguchi, T., Hashimoto, H., Taniguchi, H., & Fujimoto, T. (2012). Derlin-1 and UBXD8 are engaged in dislocation and degradation of lipidated ApoB-100 at lipid droplets. *Molecular Biology of the Cell*, *23*(5), 800–810. https://doi.org/10.1091/mbc.E11-11-0950

Tan, X., He, X., Jiang, Z., Wang, X., Ma, L., Liu, L., Wang, X., Fan, Z., & Su, D. (2015). Derlin-1 is overexpressed in human colon cancer and promotes cancer cell proliferation. *Molecular and Cellular Biochemistry*, *408*(1–2), 205–213. https://doi.org/10.1007/s11010-015-2496-x

Taniguchi, M., & Yoshida, H. (2015). Endoplasmic reticulum stress in kidney function and disease. In *Current Opinion in Nephrology and Hypertension* (Vol. 24, Issue 4, pp. 345–350). Lippincott Williams and Wilkins. https://doi.org/10.1097/MNH.0000000000000141

Tichá, A., Collis, B., & Strisovsky, K. (2018). The Rhomboid Superfamily: Structural Mechanisms and Chemical Biology Opportunities. In *Trends in Biochemical Sciences* (Vol. 43, Issue 9, pp. 726–739). Elsevier Ltd. https://doi.org/10.1016/j.tibs.2018.06.009

Tsai, Y. C., & Weissman, A. M. (2012). A Ubiquitin-Binding Rhomboid Protease Aimed at ERADication. In *Developmental Cell* (Vol. 23, Issue 3, pp. 454–456). https://doi.org/10.1016/j.devcel.2012.08.015

Urban, S., & Freeman, M. (2003). Substrate specificity of rhomboid intramembrane proteases is governed by helix-breaking residues in the substrate transmembrane domain. *Molecular Cell*, *11*(6), 1425–1434. https://doi.org/10.1016/s1097-2765(03)00181-3

Urban, S., Lee, J. R., & Freeman, M. (2001). Drosophila Rhomboid-1 defines a family of putative intramembrane serine proteases. *Cell*, *107*(2), 173–182. https://doi.org/10.1016/S0092-8674(01)00525-6

Uritsky, N., Shokhen, M., & Albeck, A. (2016). Stepwise Versus Concerted Mechanisms in General-Base Catalysis by Serine Proteases. *Angewandte Chemie (International Ed. in English)*, *55*(5), 1680–1684. https://doi.org/10.1002/anie.201507772

Vasic, V., Denkert, N., Schmidt, C. C., Riedel, D., Stein, A., & Meinecke, M. (2020). Hrd1 forms the retrotranslocation pore regulated by auto-ubiquitination and binding of misfolded proteins. *Nature Cell Biology*, 1–8. https://doi.org/10.1038/s41556-020-0473-4

Volpi, V. G., Ferri, C., Fregno, I., Del Carro, U., Bianchi, F., Scapin, C., Pettinato, E., Solda, T., Feltri, M. L., Molinari, M., Wrabetz, L., & D'Antonio, M. (2019). Schwann cells ER-associated degradation contributes to myelin maintenance in adult nerves and limits demyelination in CMT1B mice. *PLOS Genetics*, *15*(4), e1008069. https://doi.org/10.1371/journal.pgen.1008069

Wang, J., Hua, H., Ran, Y., Zhang, H., Liu, W., Yang, Z., & Jiang, Y. (2008). Derlin-1 is overexpressed in human breast carcinoma and protects cancer cells from endoplasmic reticulum stress-induced apoptosis. *Breast Cancer Research*, *10*(1). https://doi.org/10.1186/bcr1849

Wang, Y., Guan, X., Fok, K. L., Li, S., Zhang, X., Miao, S., Zong, S., Koide, S. S., Chan, H. C., & Wang, L. (2008). A novel member of the Rhomboid family, RHBDD1, regulates BIK-mediated apoptosis. *Cellular and Molecular Life Sciences : CMLS*, *65*(23), 3822–3829. https://doi.org/10.1007/s00018-008-8452-0

Wang, Y., Zhang, Y., & Ha, Y. (2006). Crystal structure of a rhomboid family intramembrane protease. *Nature*, *444*(7116), 179–183. https://doi.org/10.1038/nature05255

Wangeline, M. A., & Hampton, R. Y. (2018). "Mallostery"—ligand-dependent protein misfolding enables physiological regulation by ERAD. *Journal of Biological Chemistry*, *293*(38), 14937–14950. https://doi.org/10.1074/jbc.RA118.001808

Wei, X., Lv, T., Chen, D., & Guan, J. (2014). Lentiviral vector mediated delivery of RHBDD1 shRNA down regulated the proliferation of human glioblastoma cells. *Technology in Cancer Research & Treatment*, *13*(1), 87–93. https://doi.org/10.7785/tcrt.2012.500362

Wu, X., Siggel, M., Ovchinnikov, S., Mi, W., Svetlov, V., Nudler, E., Liao, M., Hummer, G., & Rapoport, T. A. (2020). Structural basis of ER-associated protein degradation mediated by the Hrd1 ubiquitin ligase complex. *Science*, *368*(6489), 1–13. https://doi.org/10.1126/SCIENCE.AAZ2449

Yamazoe, K., Meguro, A., Takeuchi, M., Shibuya, E., Ohno, S., & Mizuki, N. (2017). Comprehensive analysis of the association between UBAC2 polymorphisms and Behçet's disease in a Japanese population. *Scientific Reports*, *7*(1). https://doi.org/10.1038/s41598-017-00877-3

Yang, T., Espenshade, P. J., Wright, M. E., Yabe, D., Gong, Y., Aebersold, R., Goldstein, J. L., & Brown, M. S. (2002). Crucial Step in Cholesterol Homeostasis. *Cell*, *110*(4), 489–500. https://doi.org/10.1016/S0092-8674(02)00872-3

Ye, Y., Meyer, H. H., & Rapoport, T. A. (2003). Function of the p97-Ufd1-Npl4 complex in retrotranslocation from the ER to the cytosol: dual recognition of nonubiquitinated polypeptide segments and polyubiquitin chains. *The Journal of Cell Biology*, *162*(1), 71–84. https://doi.org/10.1083/jcb.200302169

Ye, Y., Shibata, Y., Yun, C., Ron, D., & Rapoport, T. A. (2004). A membrane protein complex mediates retro-translocation from the ER lumen into the cytosol. *Nature*, *429*(6994), 841–847. https://doi.org/10.1038/nature02656

You, H., Ge, Y., Zhang, J., Cao, Y., Xing, J., Su, D., Huang, Y., Li, M., Qu, S., Sun, F., & Liang, X. (2017). Derlin-1 promotes ubiquitylation and degradation of the epithelial Na+ channel, ENaC. *Journal of Cell Science*, *130*(6).

Zettl, M., Adrain, C., Strisovsky, K., Lastun, V., & Freeman, M. (2011). Rhomboid family pseudoproteases use the ER quality control machinery to regulate intercellular signaling. *Cell*, *145*(1), 79–91. https://doi.org/10.1016/j.cell.2011.02.047

Zhang, M., Miao, F., Huang, R., Liu, W., Zhao, Y., Jiao, T., Lu, Y., Wu, F., Wang, X., Wang, H., Zhao, H., Ju, H., Miao, S., Wang, L., & Song, W. (2018). RHBDD1 promotes colorectal cancer metastasis through the Wnt signaling pathway and its downstream target ZEB1. *Journal of Experimental and Clinical Cancer Research*, *37*(1), 22. https://doi.org/10.1186/s13046-018-0687-5

Zhou, Y., Moin, S. M., Urban, S., & Zhang, Y. (2012). An internal water-retention site in the rhomboid intramembrane protease GlpG ensures catalytic efficiency. *Structure*, *20*(7), 1255–1263. https://doi.org/10.1016/j.str.2012.04.022

Zhou, Z., Liu, F., Zhang, Z.-S., Shu, F., Zheng, Y., Fu, L., & Li, L.-Y. (2014). Human rhomboid family-1 suppresses oxygen-independent degradation of hypoxia-inducible factor-1α in breast cancer. *Cancer Research*, *74*(10), 2719–2730. https://doi.org/10.1158/0008-5472.CAN-13-1027

Figure 1.2.1 Cellular localization of rhomboids

(A-F) depicts rhomboid pseudoproteases and G–H depicts rhomboid proteases. Rhomboids depicted in A and C are found in S. cerevisiae, E is found in S. pombe, G is found in B. subtilis, and B, D, F, and H are found in mammals

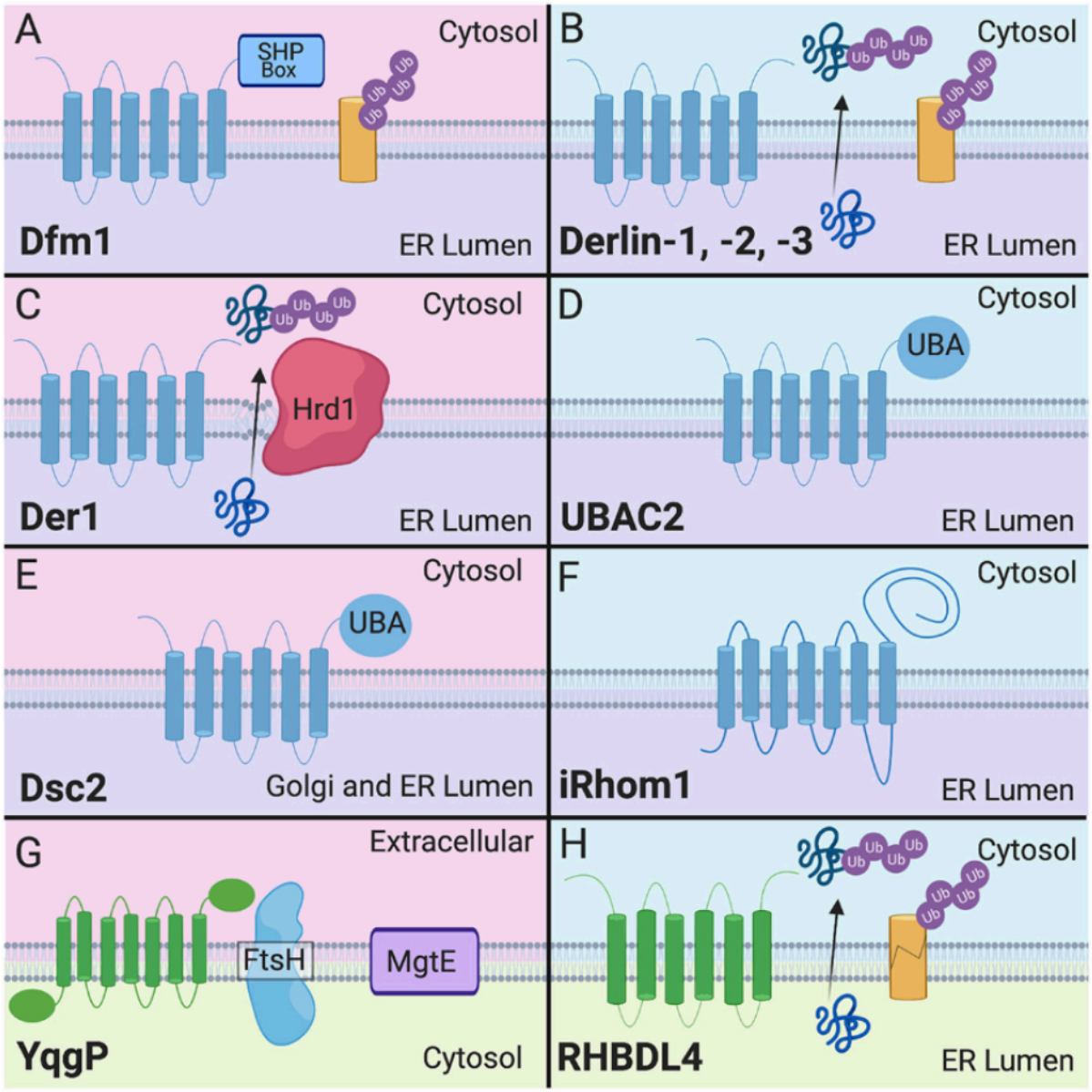
A
Cytosol
SHP Box
Ub
Dfm1
ER Lumen
B
Cytosol
Derlin-1, -2, -3
ER Lumen
C
Cytosol
Hrd1
Der1
ER Lumen
D
Cytosol
UBA
UBAC2
ER Lumen
E
Cytosol
UBA
Dsc2
Golgi and ER Lumen
F
Cytosol
iRhom1
ER Lumen
G
Extracellular
FtsH
MgtE
YqgP
Cytosol
H
Cytosol
RHBDL4
ER Lumen

Table 1.2.1 Rhomboid Member Knockout Mice

Rhomboid member knockout mice.

Mice knockout	Phenotype	Substrates
global *Derl1* −/−	Die in utero at E7-E8.	Not identified
global *Derl3* −/−	Mice were born and grew normally. Also exhibited decreased levels of Derlin-1 and Derlin-2 in the pancreas.	Not identified
global *Derl2* −/−	Pups are born at normal Mendelian ratios, but majority dies within 24 h after birth due to inability to feed. Few surviving mice developed skeletal dysplasia and exhibited dilated ER due to defects in collagen matrix protein secretion by chondrocytes. Also, all tissues were unaffected, but had upregulated levels of ER chaperones and exhibited chronic UPR.	*Derl2* −/− chondrocytes show ER retention of collagen matrix proteins.
B cells *Derl2* −/−	Der2 deficiency does not affect B cell development and antibody secretion.	Not identified
Hepatocytes *Derl2* −/−	Cells have ongoing UPR, but does not affect liver function.	Not identified
Schwann cells *Derl2* −/−	Impairment of ERAD in nerves, but no effect on developmental myelination or remyelination after nerve injury. Aged mice develop demyelinating neuropathy in which UPR fails to activate.	OS9 chaperone is stabilized and ER retention of Charcot-Marie-Tooth-associated myelin protein zero (P0-S63del).
Podocytes *Derl2* −/−	Mice were normal in appearance and behavior and exhibited negligible difference in kidney histology. These mice are susceptible to ADR-induced glomerular injury and death. This is accompanied by compromised ERAD and ER stress.	Not identified
global *iRhom1* −/−	Die by 6 weeks of age.	TACE is retained in the ER in several tissue types.
global *iRhom2* −/−	Appear normal, but have impaired immune response.	TACE is retained in the ER in macrophages.

Table 1.2.2 Rhomboid Member's Association with Diseases

Rhomboid member's association with diseases.

Rhomboid member	Disease	Disease link
Derlin-1	Colon cancer	Derlin-1 silencing led to growth inhibition and promoted apoptosis in colon cancer cells. Derlin-1 overexpression correlates with tumor differentiation, invasion, and metastasis.
Derlin-1	Breast cancer	High expression of Derlin-1 correlated with tumor grade and metastasis. Derlin-1 silencing sensitized breast cancer cells to ER stress-induced apoptosis.
Derlin-3	Breast cancer	Inhibiting Derlin-3 expression decreased BC proliferation and high DERL3 expression in patients experienced poorer prognosis.
Ubac2	Behçet disease	Two risk alleles, rs9517723 and rs7999348, significantly correlates with enhanced UBAC2 expression, which contributes to CNS lesions in patients. However, one risk allele, rs3825427, is correlated with downregulated UBAC2.
Rhbdl4	Colorectal cancer	High expression of Rhbdl4 is associated with metastatic colorectal cancer. Its role in colorectal cancer has been proposed to be through the Wnt and EGFR signaling pathways.
Rhbdl4	Glioblastoma	Knockdown of Rhbdl4 resulted in an increase in apoptosis in a glioblastoma derived cell line.
iRhom1	Breast cancer	Elevated expression of iRhom1 was found to be correlated with breast cancers with a faster progression. Possible mechanism is by promoting stability of transcription factor Hif1α, thus promoting cellular adaptation to hypoxia.

Chapter 2: Derlin Dfm1 Employs a Chaperone-Like Function to Resolve Misfolded Membrane Protein Stress

2.1 Introduction

While misfolded proteins are recognized as a source of cellular stress, the mechanisms by which cells prevent this stress and how this stress impacts cells is not fully understood. Eukaryotic cells are equipped with protein quality control pathways for preventing the accumulation of aggregation-prone misfolded proteins. The endoplasmic reticulum (ER) is responsible for folding both secretory and membrane proteins and is well equipped with quality control pathways for refolding or eliminating misfolded proteins. One of the major pathways of protein quality control at the endoplasmic reticulum (ER) is ER associated degradation (ERAD)(Hampton, 2002). ERAD utilizes the ubiquitin proteasome system (UPS) to selectively target and degrade misfolded or unassembled proteins at the ER(Werner et al., 1996).

ERAD is a well conserved process from yeast to mammals. ERAD of membrane proteins requires four universal steps: 1) substrate recognition (Bhamidipati et al., 2005; Nakatsukasa et al., n.d.; Sato et al., 2009; Stanley et al., 2011), 2) substrate ubiquitination(Bays et al., 2001), 3) retrotranslocation of substrate from the ER to the cytosol (Baldridge & Rapoport, 2016; Neal et al., 2018; Wahlman et al., 2007), and 4) degradation by the cytosolic proteasome (Farinha & Amaral, 2005; Hampton et al., 1996; Werner et al., 1996). A hexameric cytosolic ATPase, Cdc48 in yeast and p97 in mammals, is required for retrotranslocation of all ERAD substrates (Rabinovich et al., 2002; Twomey et al., 2019; Ye et al., 2001). In the context of this paper, substrate refers to a protein that is targeted by the ERAD pathway.

In yeast, ER membrane substrates can be targeted by the DOA (degradation of alpha2) pathway or the HRD pathway (hydroxymethyl glutaryl-coenzyme A reductase degradation), utilizing the E3 ligases Doa10 and Hrd1, respectively. Additionally, the yeast derlin Dfm1 is specifically required for the retrotranslocation of misfolded membrane substrates, in both the HRD and DOA pathways (Neal et al., 2018). Dfm1 facilitates retrotranslocation of membrane proteins through several mechanisms including 1) recognition and binding to misfolded membrane proteins, 2) thinning the lipid bilayer to reduce the thermodynamic barrier to extraction, 3) and recruiting the ATPase Cdc48 to the ER.

Dfm1 is a member of the derlin subclass of rhomboid proteins. Rhomboid proteins are a widely conserved family of proteins, found in all domains of life (Began et al., 2020; Freeman, 2014; Liu et al., 2020; Tichá et al., 2018). There are two major categories of rhomboid proteins: active rhomboid proteases and inactive rhomboid pseudoproteases. While the inactive rhomboid pseudoproteases lack a catalytic site, they have been implicated in a wide variety of biological processes, including protein quality control, protein trafficking, and cell signaling (Adrain & Cavadas, 2020; Greenblatt et al., 2011; Kandel & Neal, 2020; X. Wu et al., 2020; Zettl et al., 2011). Derlin proteins, including Dfm1, are rhomboid pseudoproteases that are critical for ERAD of a wide variety of substrates, both in yeast and mammalian cells (Hoelen, Zaldumbide, van Leeuwen, et al., 2015; Knop et al., 1996b; Neal et al., 2018; Oda et al., 2006; F. Sun et al., 2006).

We have previously observed that in *dfm1Δ* cells, when a misfolded membrane protein is strongly expressed, the cells show a severe growth defect (Neal et al., 2020). This

is seen specifically in the absence of Dfm1, and this growth defect is not observed in the absence of other ERAD components, indicating a specific function for Dfm1 in sensing and/or adapting cells to misfolded membrane protein stress (Fig. 1) (Neal et al., 2020). This is in line with a previous study linking Dfm1 to ER homeostasis (Sato & Hampton, 2006).

In the present study, we determine that Dfm1 prevents membrane protein toxicity because of a previously unidentified chaperone-like function that is independent of Cdc48 recruitment. This function is distinct from Dfm1's role in protein retrotranslocation, while also relying on many of the same functions deployed by Dfm1to promote retrotranslocation. We further determined that human homologs of Dfm1 have also retained this ability. This study is the first to demonstrate chaperone-like activity for any rhomboid protein. Many rhomboid proteins use similar functions to Dfm1 to promote retrotranslocation and the rhomboid protease RHBDL4 has recently been characterized as acting on aggregation-prone substrates (Bock et al., 2022; Engberg et al., 2022; Fleig et al., 2012; Nejatfard et al., 2021; X. Wu et al., 2020). It will be an interesting and important further line of inquiry to determine if a chaperone-like activity is a common ability of rhomboid proteins, both for the pseudoproteases and proteases.

As a complement to our work on the function of Dfm1 in relieving misfolded membrane protein toxicity, we also sought to determine how misfolded membrane proteins cause toxicity. We determine that misfolded membrane proteins, but not other types of misfolded proteins, impact proteasome and ubiquitin homeostasis. We also identified several proteins that promote cellular health upon misfolded membrane protein by resolving the proteasome and ubiquitin stress that misfolded membrane proteins trigger. Intriguingly, we

also find that not all protein aggregates are toxic. The combination required for toxicity appears to be both i) aggregated misfolded membrane proteins and ii) ubiquitinated misfolded membrane proteins. Either of these features alone is not sufficient for toxicity.

We propose a model in which upon accumulation of ubiquitinated misfolded membrane proteins in the absence of Dfm1, misfolded membrane proteins form toxic aggregates. In the presence of Dfm1, this toxicity is prevented by Dfm1's ability to solubilize membrane proteins, independent of its ability to retrotranslocate proteins.

2.2 Results

2.2.1 Absence of Dfm1 and Expression of Integral Misfolded Membrane Proteins Causes Growth Stress

Previous research from the Neal lab has revealed that accumulation of a misfolded membrane protein in the absence of Dfm1 causes a severe growth defect in the substrate-toxicity assay (Neal et al., 2020). In the substrate-toxicity assay, yeast strains with a misfolded protein under the control of a galactose inducible promoter are plated in a spot assay onto selection plates with either 2% galactose or 2% dextrose as a carbon source (Fig. 1) (Bhaduri & Neal, 2021). This allows for comparison of growth of yeast strains with different genetic perturbations with expression of misfolded substrates. This growth defect can be seen with strong expression of three misfolded membrane proteins in *dfm1Δ* cells: Hmg2, Pdr5*, and Ste6* (Fig. 1A-C). We have previously shown that this growth defect is specific to misfolded membrane proteins at the ER, as expression of a luminal ERAD substrate, CPY*, in *dfm1Δ* cells elicits no growth defect (Neal et al., 2020). Interestingly, this growth defect is not seen when membrane proteins accumulate in the absence other ERAD components,

such as the E3 ligases Hrd1 and Doa10 (Fig.1A-C). In the case of *dfm1Δ*, *hrd1Δ,* and *doa10Δ* cells, misfolded membrane proteins accumulate at the ER due to defects in ERAD, but only in the case of *dfm1Δ* cells is a growth defect observed with misfolded membrane protein expression. Altogether, we surmise that this growth defect triggered by the absence of Dfm1 along with expression of misfolded membrane protein is due to cellular stress caused by misfolded membrane protein toxicity.

By utilizing the substrate-toxicity assay, we observed a growth defect in *dfm1Δ* cells and normal growth in *hrd1Δ* and *doa10Δ* cells upon expression of ERAD membrane substrates (Fig. 1A-C). The cell biological difference amongst these ERAD knockout strains is that membrane substrates are ubiquitinated in *dfm1Δ* cells but not ubiquitinated in *hrd1Δ* and *doa10Δ* cells, due to the absence of the ER E3 ligases, as determined through western blot for ubiquitin (Fig. 7B). One possibility is that the growth stress is not specific to *dfm1Δ* cells and is solely dependent on the accumulation of ubiquitinated membrane substrates. To rule out this possibility, we utilized a temperature sensitive Cdc48 allele strain, *cdc48-2,* which, like *dfm1Δ* cells, results in accumulation of ubiquitinated ERAD membrane substrates (Neal et al., 2018). While we used *cdc48-2* cells at the permissive temperature of 30°C, ERAD is still comprised for Hmg2, as previously reported, and we validated using a cycloheximide chase that Pdr5* and Ste6* degradation is also impaired at 30°C in *cdc48-2* cells (Fig. S1A&B) (Neal et al., 2017, 2018). The substrate- toxicity assay was employed on *cdc48-2* strains expressing membrane substrates Hmg2, Pdr5*, and Ste6* (Fig. 1D-F). These strains showed a growth defect while growing on galactose plates due to inherent slow growth of *cdc48-2* strains, but this was not worsened by expression of misfolded integral membrane proteins, despite the E3 ligases that ubiquitinate these proteins still being

present. These results indicate that Dfm1 plays a specific role in the alleviation of misfolded membrane protein stress.

2.2.2 Disease-Associated Membrane Proteins Cause Growth Stress

Since a wide variety of misfolded membrane proteins elicit growth stress in *dfm1Δ* cells, we hypothesized that growth stress would also be observed with expression of clinically relevant human misfolded membrane proteins. We tested expression of WT cystic fibrosis transmembrane receptor (CFTR), CFTRΔF508, the most common disease-causing variant of CFTR, and the Z variant of alpha-1 proteinase inhibitor (A1PiZ), a protein variant that results in alpha-1 antitrypsin deficiency (AATD). CFTR and CFTRΔF508 are ERAD-M substrates when expressed in yeast, while A1PiZ is a soluble misfolded protein targeted by ERAD-L in yeast(Palmer et al., 2003; Zhang et al., 2001). When these proteins were expressed in *dfm1Δ* cells, both CFTR and CFTRΔF508 resulted in a growth defect, while none was observed with expression on A1PiZ (Fig. 1G). Expression of any of the proteins in WT yeast cells resulted in no growth defect (Fig. 1G). It was not wholly surprising that WT CFTR also elicited growth stress in *dfm1Δ* cells. Previous studies have shown that while virtually all CFTRΔF508 is targeted to ERAD, about 80% of WT CFTR is degraded via ERAD in yeast and mammals (Cheng et al., 1990; Gnann et al., 2004; Zhang et al., 2001).

2.2.3 Dfm1 has a Dual Role in ER Protein Stress and ERAD Retrotranslocation

Previous work from the Hampton lab establishing a role for Dfm1 in misfolded membrane protein retrotranslocation also identified several motifs of Dfm1 that are essential for its retrotranslocation function(Neal et al., 2018). Additionally, by employing an unbiased genetic screen, our lab recently identified five residues of Dfm1 that are required for

retrotranslocation(Nejatfard et al., 2021). Here, we tested whether these residues, critical for Dfm1's retrotranslocation function, are required for alleviating the growth stress in *dfm1Δ* cells expressing Hmg2.

Figure 2A shows a schematic of Dfm1, with the regions of the protein important for retrotranslocation function highlighted, and a list of specific motifs and residues that are retrotranlocation listed in a table (Neal et al., 2018; Nejatfard et al., 2021). Dfm1 contains two motifs that are well conserved amongst the rhomboid superfamily, the WR motif in Loop 1 and the GxxxG (Gx3G) motif in transmembrane domain (TMD) 6 (Greenblatt et al., 2011; Neal et al., 2018). Both of these motifs are required for Dfm1-mediated retrotranslocation(Neal et al., 2018; Nejatfard et al., 2021). We first tested the requirement of the conserved rhomboid motif mutants by expressing Hmg2 with WR mutants (WA and AR) and Gx3G mutants (Ax3G and Gx3A) and observed no restoration in growth (Fig. 2B). Our previous work determined that Loop 1 mutants (F58S, L64V, and K67E) obliterated Dfm1's ability to bind misfolded membrane substrates, and TMD 2 mutants (Q101R and F107S) reduce the lipid thinning ability of Dfm1, a function which aids in Dfm1's retrotranslocation function (Nejatfard et al., 2021). Accordingly, we utilized these mutants in our growth assay and did not observe a rescue of the growth defect (Fig. 2C). We have previously shown that alteration of the five signature residues of the Dfm1 SHP box to alanine (Dfm1-5Ashp) ablates its ability to recruit Cdc48 (Fig. 2D). We also established, Dfm1's Cdc48 recruitment function is required for Dfm1's retrotranslocation function, whereas the Dfm1-5Ashp mutant impairs its retrotranslocation function(Neal et al., 2018). Notably, in contrast to the other mutants tested, Dfm1-5Ashp was still able to alleviate the growth defect like WT Dfm1 (Fig. 2E). These results suggest that Dfm1's substrate engagement and lipid thinning function is

required for alleviating membrane substrate-induced stress whereas Dfm1's Cdc48 recruitment function is dispensable for alleviating the growth stress. We validated that expression of WT Dfm1 and all Dfm1 mutants were comparable using western blot (Fig. S1C)

2.2.4 Human Derlins Relieve Growth Stress

Dfm1 is a rhomboid pseudoprotease, and a member of the derlin subclass of rhomboid proteins (Nejatfard et al., 2021). The human genome encodes three derlins, Derlin-1, Derlin-2, and Derlin-3. Yeast Dfm1 is the closest homolog of the mammalian derlins(Greenblatt et al., 2011). All three are ER localized proteins that are implicated in ERAD and adaptation to ER stress (Hoelen, Zaldumbide, Van Leeuwen, et al., 2015; Lilley & Ploegh, 2004, 2005; Oda et al., 2006; Ren et al., 2018; Ye et al., 2004). We expressed human Derlin-1 and Derlin-2 in *dfm1Δ*+Hmg2 cells. We opted to only test Derlin-1 and Derlin-2 have been much more thoroughly researched than Derlin-3. Both human derlins were able to rescue growth in these cells in the substrate-toxicity assay (Fig. 2F). This was surprising, as we had previously found that mammalian derlins cannot complement the retrotranslocation function of Dfm1 in yeast cells for self-ubiquitinating substrate (SUS)-GFP, a similar substrate to Hmg2 (Nejatfard et al., 2021).

2.2.5 Dfm1 Solubilizes Misfolded Membrane Protein Aggregates Independent of Cdc48 Recruitment

The above studies show that Dfm1 residues critical for retrotranslocation —through substrate binding and its lipid thinning function— are also important for alleviating membrane substrate-induced stress. Conversely, addback of a Dfm1 Shp box mutant (Dfm1-5Ashp)

(Fig. 2D), that does not recruit Cdc48 and cannot retrotranslocate proteins, is able to restore growth in the substrate-toxicity assay. We surmise that Dfm1's actions —independent of its Cdc48 recruitment function— may be directly acting on misfolded membrane substrates to prevent growth stress. One possibility is that Dfm1 may directly act on misfolded membrane substrates by functioning as a chaperone-like protein to prevent misfolded membrane protein toxicity. We hypothesize that Dfm1 acts as either a holdase, preventing the aggregation of misfolded membrane substrates, or as a disaggregase, separating proteins in existing protein aggregates. To address this hypothesis, we employed a detergent solubility assay in *dfm1Δ*+Hmg2 cells with addback of WT DFM1 or DFM1 mutants. ER microsomes were isolated and incubated in 1% dodecyl maltoside (DDM) and subjected to centrifugation to separate aggregated substrate (pellet fraction) from solubilized substrate (supernatant fraction). As shown in Figure 3A, nearly all Hmg2-GFP in *dfm1Δ* cells was aggregated. Conversely, with Dfm1 and Dfm1-5Ashp add back cells, nearly all Hmg2-GFP was soluble. This striking all-or-nothing phenotype in Hmg2 aggregation demonstrates an important role for Dfm1 in influencing membrane protein aggregation. As a control for these studies, we examined Hmg2 in both WT, *hrd1Δ* cells, and *hrd1Δ*+Hrd1 cells. Nearly all protein was soluble in all three strains (Fig. 4A). We also tested a properly folded ER membrane protein, Sec61-GFP in *dfm1Δ* cells. In contrast to Hmg2-GFP, majority of Sec61-GFP was in the detergent-solubilized supernatant fraction and there was no change in Sec61-GFP detergent solubility with Dfm1 or Dfm1-5Ashp addback in *dfm1Δ* cells (Fig. 4B).

It appears Dfm1—independent of its Cdc48 recruitment function—functions as a chaperone-like protein to influence the aggregation of misfolded membrane proteins. We next explored additional Dfm1 residues that are required for solubilizing membrane

substrates. Accordingly, mutants in the conserved rhomboid motifs (AR and Ax3G) were employed in the detergent solubility assay. DFM1-AR and DFM1-Ax3G addback resulted in aggregated HMG2 (Fig. 3A). Similarly, retrotranslocation defective Dfm1 mutants in Loop 1 (F58S, L64V, and K67E) and TMD 2 mutants (Q101R and F107S) in the detergent solubility assay were not capable of solubilizing Hmg2 (Fig. 3B). This all-or-nothing effect that Dfm1's presence has on aggregation led us to determine whether Dfm1 binds to Hmg2 even after solubilization in with DDM. Indeed, using co-immunoprecipitation, we found that Dfm1 physically interacts with solubilized Hmg2 (Fig. 3C). Altogether, with all criteria examined, Dfm1 is critical in influencing the solubility of its ERAD membrane substrate (Fig. 3D). Although the ability to recruit Cdc48 is vital for Dfm1's retrotranslocation function, it is not required for this newly established chaperone-like function.

The chaperone-like function of Dfm1 is generalizable to other misfolded membrane proteins but not non-membrane misfolded proteins. We tested other membrane ERAD substrates targeted by the HRD (Pdr5*) or DOA (Ste6*) pathways, and they were both completely solubilized in the presence of Dfm1 in the detergent solubility assay (Fig. 4C and D). In contrast, solubility of a misfolded ER luminal protein, CPY*, was not altered in the presence of absence of Dfm1 (Fig. 4E). Notably, we also observed that Derlin-1 and Derlin-2 were able to prevent aggregation of Hmg2 in *dfm1Δ* cells, indicating that other derlin proteins have a conserved chaperone-like function (Fig. 4F).

While we also investigated whether more Hmg2-GFP appeared in puncta in *dfm1Δ* cells through confocal microscopy we found no significant difference between the percentage of GFP in puncta or the number of puncta with addback of WT DFM1 or any of the DFM1

mutants (Fig. S1D-F). This is in line with the view of some in the field that toxic aggregates are generally below the visible detection limit for confocal microscopy and that puncta identified through microscopy tend to be representative of sequestrosomes, a cellular adaptation to the accumulation of aggregation prone proteins (Mogk et al., 2018).

2.2.6 Misfolded Membrane Proteins do not Activate the Unfolded Protein Response

The canonical ER stress pathway triggered by the accumulation of misfolded proteins is the unfolded protein response (UPR) (Hwang & Qi, 2018). The UPR is known to be induced by the accumulation of misfolded soluble proteins within the ER lumen. To test if misfolded membrane protein accumulation at the ER activates UPR, we used a fluorescence-based flow cytometry assay. In this assay, yeast cells encoding both a galactose inducible misfolded protein or empty vector (EV)and UPR reporter 4xUPRE-GFP were treated with or without 0.2% galactose and 2 µg/mL of the ER stress inducing drug tunicamycin or DMSO as the vehicle control. GFP expression was measured by flow cytometry for 5 hours following galactose treatment. We found that GFP expression did not increase by 5 hours post-galactose addition in *dfm1Δ* cells compared to *pdr5Δ* cells expressing any of the following substrates tested: Hmg2, Ste6*, or EV (Fig. 5A-D & 5G&H). *Dfm1Δ* cells are able to activate UPR, as addition of tunicamycin to these cells allowed them to activate the UPR at similar levels as *pdr5Δ* cells (Fig. 5A-H). As expected, expression of the ER luminal substrate CPY* activated the UPR in *dfm1Δ* cells and *pdr5Δ* cells (Fig. 5E&F).

Our findings from flow cytometry experiments were further corroborated by measuring Hac1 splicing via polymerase chain reaction (PCR) (Fig. S2A&B). When the UPR is active,

the mRNA of the transcription factor Hac1 is spliced to create a transcript 252bp shorter than the full length transcript (Cox & Walter, 1996). Samples with a band for both spliced and unspliced Hac1 indicated UPR activation, while a single band of the unspliced variant indicated no UPR activation. The results from these experiments were in agreement with the flow cytometry-based assay; we found no HAC1 splicing with misfolded membrane protein overexpression in *dfm1*Δ cells (Fig. S5A&B).

2.2.7 Accumulation of Misfolded Membrane Proteins Upregulates Proteasome Components

After determining the UPR is not activated in *dfm1Δ* cells expressing Hmg2, we next sought to determine the transcriptional changes that occur with misfolded membrane protein stress. To address this question, we utilized RNA sequencing (RNA-seq). We prepared and sequenced cDNA libraries from mRNA extracted from *pdr5Δ* cells*, hrd1Δpdr5Δ* cells*,* and *dfm1Δ pdr5Δ* cells expressing Hmg2 or EV. These yeast strains were generated from a yeast knockout collection with the BY4742 strain background, and *pdr5Δ* cells are commonly used as the wildtype background for the knockout collection. We validated using the substrate-toxicity assay that *dfm1Δ pdr5Δ* +Hmg2 strains in this background also display a growth defect (Fig. S3A). We used principal component analysis (PCA) to determine genes that were upregulated and downregulated most in *dfm1Δ* cells expressing Hmg2 versus the control strains; WT+EV, WT+Hmg2, *hrd1Δ*+EV, *hrd1Δ*+Hmg2, and *dfm1Δ*+EV (Data S1). Principal component 1 (PC1) value of all replicate strains except for *dfm1Δ* + Hmg2 cells clustered closer to each other than they did to either replicate of the *dfm1Δ* + Hmg2 cells, indicating that these strains were transcriptionally distinct from the others sequenced (Fig. S3B). Additionally, the *dfm1Δ* + Hmg2 replicates were fairly distinct from each other, so while

there were genes upregulated in both replicates, there were also variable transcriptional changes (Fig. S3B). This variability is likely representative of biological variability in these strains rather than experimental variability as it was only observed between these replicates and not replicates of the other strains tested.

Upregulated (+ PC1 values) and downregulated (-PC1 values) genes in *dfm1Δ*+Hmg2 cells were used for gene ontology (GO) analysis. The most overrepresented group of upregulated genes were those classified as being involved in “Proteasomal Ubiquitin-Independent Protein Catabolic Processes”, “Regulation of Endopeptidase Activity”, and “Proteasome Regulatory Particle Assembly” (Fig. S3D). Several proteasome subunits were represented in this list of upregulated genes. The most overrepresented group of downregulated genes in this dataset were those classified as being involved in “rRNA Export from Nucleus”, “rRNA Transport”, and “Translational Termination” (Fig. S3E). Because a downregulation of the mRNA for genes encoding ribosomal proteins is a general feature of stressed yeast cells(Gasch et al., 2000), we focused on the upregulation of proteasome components. Plotting the PC1 and PC2 values for *dfm1Δ*+Hmg2 cells for the highest PC1 value genes, we observed a large overlap between genes in this dataset and those that are targets of the transcription factor Rpn4 (Fig. S3C, *highlighted in red*).

2.2.8 The Transcription Factor Rpn4 is Involved in Misfolded Membrane Protein Stress

Rpn4 is a transcription factor that upregulates genes with a proteasome-associated control element (PACE) in their promoters(Mannhaupt et al., 1999). From our RNA-seq data, there was a remarkably high overlap between the genes that were observed to be upregulated in *dfm1Δ* cells expressing Hmg2 and those that are known Rpn4 targets

(Mannhaupt et al., 1999). We reasoned that Rpn4 may be involved in adapting cells to misfolded membrane protein stress and predicted *rpn4Δ* cells should phenocopy *dfm1Δ* cells by exhibiting a growth defect induced by ERAD membrane substrates. Using the substrate-toxicity assay, we found expression of misfolded membrane proteins in *rpn4Δ* cells resulted in a growth defect equivalent to that seen in *dfm1Δ* cells (Fig. 6A & Fig. S4A), indicating that Rpn4 is also required for alleviating misfolded membrane protein stress. As with *dfm1Δ* cells, this effect was specific to membrane protein expression, as expression of CPY* in *rpn4Δ* cells did not result in a growth defect (Fig. S4B). This is in line with previous research demonstrating Rpn4 is activated in response to misfolded membrane protein accumulation and that misfolded membrane protein expression can result in proteasome impairment, even in WT cells (Boyle Metzger & Michaelis, 2008; Burns et al., 2021). Finally, we tested a transcription factor that can regulate Rpn4 and has many overlapping transcriptional targets with Rpn4, Pdr1 (Owsianik et al., 2002), and did not observe any growth defect in *pdr1Δ* + Hmg2 cells (Fig. S4C).

As a readout for Rpn4 activity, we measured the abundance of a GFP-tagged version of the proteasome component Pre6-GFP in *dfm1Δ*+Hmg2 cells 0- and 5-hours after galactose induction through flow cytometry. Pre6 is a component of the 20S core of the proteasome that can be transcriptionally upregulated by Rpn4 and Pre6-GFP has been used by others as a marker for the proteasome (Enenkel et al., 1998; Xie & Varshavsky, 2001). In comparison to WT control strains and other substrates tested, *dfm1Δ*+Hmg2 had a significant increase in Pre6-GFP after 5 hours (Fig. 6B&C).

2.2.9 Misfolded Membrane Protein Stress in dfm1Δ Cells Leads to Proteasome

Impairment

Because Rpn4 appears to be active in membrane protein-stressed *dfm1Δ* cells, we hypothesized that proteasome function is impacted in *dfm1Δ* cells expressing an integral membrane protein. We tested this using an MG132 sensitivity assay developed by the Michaelis lab(Boyle Metzger & Michaelis, 2008). MG132 is a drug that reversibly inhibits proteasome function(D. H. Lee & Goldberg, 1998). For this assay, cells in liquid culture were treated with MG132, plated, and counted the number of colony forming units (CFUs) resulting from each strain. Due to the risk of the retrotranslocation defect being suppressed in *dfm1Δ* cells with constitutive expression of a misfolded membrane protein, and thus possibly artificially increasing the number of CFUs resulting from treatment of *dfm1Δ* cells with MG132, we opted to instead test *dfm1Δ hrd1Δpdr5Δ* cells. These cells are unable to suppress the retrotranslocation defect of *dfm1Δ* cells, due to the absence of Hrd1, which has been characterized to function as an alternative retrotranslocon for membrane substrates when Dfm1 is absent(Neal et al., 2020). We utilized the engineered misfolded membrane protein SUS (self-ubiquitinating substrate)-GFP as the substrate for these experiments. SUS-GFP contains the RING domain of Hrd1 and catalyzes its own ubiquitination, thus still causing the stress that is elicited by ubiquitinated misfolded membrane proteins in *dfm1Δ* cells(Garza et al., 2009). We predicted that cells with compromised proteasome function would be more sensitive to MG132 treatment, resulting in fewer CFUs. Strikingly, no CFUs resulted from MG132 treated *dfm1Δhrd1Δpdr5Δ* cells constitutively expressing SUS-GFP (Fig. 6F). All others strains and treatments tested did not show as dramatic of a change in the number of CFUs, either with MG132 or DMSO treatment (Fig. 6D-F). These results demonstrate that proteasome function is impacted in *dfm1Δ* cells with misfolded membrane protein accumulation.

2.2.10 Misfolded Membrane Protein Stress Does Not Cause Proteasome Sequesteration

One hypothesis that we explored to understand the mechanism by which proteasomes are impaired with misfolded membrane proteins stress was direct sequestration of proteasomes at the ER. Using *dfm1Δ* cells expressing EV or Hmg2, we used western blotting to detect ER recruitment of Pre6, a proteasome component (Fig. 6G). Proteasome recruitment was similar between both strains. We also tested aggregation versus solubility of Pre6 at the ER in both strains and this was also not affected in either strain (Fig. 6G). These results indicate an indirect mechanism for proteasome impairment in membrane protein stressed cells.

2.2.11 Growth Defect in dfm1Δ Cells is Ubiquitination Dependent

The observation that a growth defect triggered by misfolded membrane proteins is only seen in the absence of Dfm1, and not in cells lacking either of the ER E3 ligases Hrd1 and Doa10, led us to hypothesize that this growth defect is dependent upon ubiquitination of the misfolded membrane proteins. The substrate-toxicity assay results using *cdc48-2* cells indicate that the growth defect is not solely due to defective ERAD or the accumulation of ubiquitinated misfolded membrane proteins. Nonetheless, we still explored the possibility that misfolded membrane protein-induced toxicity is dependent on substrate ubiquitination.

We examined whether growth defects were seen in either *dfm1Δhrd1Δ*or *dfm1Δdoa10Δ* cells expressing either Hmg2 (a Hrd1 target) or Ste6* (a Doa10 target), respectively (Fig. 7A). These results showed no growth defect in the double mutants for which the membrane protein expressed was not ubiquitinated by the absent E3 ligase:

dfm1Δhrd1Δ cells expressing Hmg2 and *dfm1Δdoa10Δ* cells expressing Ste6* (Fig. 7A). We validated that substrates were indeed not ubiquitinated in E3 ligase knockouts via western blot for ubiquitin (Fig. 7B). In contrast, a growth defect was observed in the double mutants for which the absent E3 ligase did not participate in ubiquitination of the expressed membrane protein: *dfm1Δhrd1Δ* expressing Ste6* and *dfm1Δdoa10Δ* expressing Hmg2. This indicates that growth stress in *dfm1Δ* cells is dependent upon ubiquitination of the accumulated misfolded membrane protein.

As an alternative approach to determine if membrane proteins must be ubiquitinated to cause toxicity in the absence of Dfm1, we tested the expression of well-characterized, stabilized Hmg2 mutants. These mutants, Hmg2 (K6R), Hmg2 (K357R), and Hmg2 (K6R, K357R), were previously identified by the Hampton lab in a genetic screen for stabilized Hmg2 mutants (Gardner & Hampton, 1999). Both KàR stabilized mutations disrupt Hmg2 ubiquitination, and these sites are hypothesized to be Hmg2 ubiquitination sites. While the Hampton lab has shown that ubiquitination levels of both substrates are nearly undetectable with western blot, they also showed that the K6R mutant is not further stabilized in an ERAD deficient background, while the K357R mutant is slightly more stable in an ERAD deficient background than in a WT background(Gardner & Hampton, 1999). We propose that because of this slight level of degradation in the K357R mutant, some fraction of this mutant must be ubiquitinated and targeted to the Hrd1 ERAD pathway. Our model predicts that toxicity of misfolded membrane proteins is ubiquitination dependent. Thus, we would expect that the fully stabilized Hmg2-K6R with negligible ubiquitination should not elicit a growth defect whereas Hmg2-K357R, which is a poor ERAD substrate but still can still be targeted for degradation, should elicit a growth defect in *dfm1Δ* cells. Indeed, we observed no growth

defect in *dfm1Δ* cells expressing the K6R mutant, while the K357R mutant still showed a growth defect. Moreover, the growth defect is still observed in the double mutant Hmg2-(K6R, K357R), which phenocopies Hmg2-K6R, in that it is completely stabilized, consistent with the model that growth stress in the absence of Dfm1 is dependent on the accumulation of ubiquitinated membrane substrates (Fig. 7C).

2.2.12 Ubiquitin Homeostasis is Disrupted with Misfolded Membrane Protein Accumulation

There is increasing evidence that suggests ubiquitin homeostasis and maintenance of the free ubiquitin pool is critical for cellular survival under normal and stress conditions (Anderson et al., 2005; Cartier et al., 2009; Hanna et al., 2007; H. Wu et al., 2020). Because we observed that growth defect in *dfm1Δ* cells is dependent on ubiquitination of membrane substrates, we hypothesized that ubiquitin conjugation to accumulating membrane proteins reduces the availability of free ubiquitin, impacting cell viability.

One hypothesis that would explain substrate ubiquitination dependency of the growth defect in *dfm1Δ* cells is that the pool of monomeric ubiquitin is depleted by accumulation of misfolded membrane proteins. If this hypothesis is correct, exogenous ubiquitin should rescue the growth defect seen from substrate-induced stress in *dfm1Δ* cells. To that end, *dfm1Δ* + Hmg2 cells harboring a plasmid containing ubiquitin under the control of the copper inducible promoter CUP1(Koller et al., 2000) were tested in the substrate-toxicity assay. These cells were plated on 2% galactose and 50uM copper to induce expression of Hmg2 and ubiquitin in *dfm1Δ* cells, respectively. Notably, supplementation of ubiquitin restored the growth defect (Fig. 7D). We blotted for monomeric ubiquitin to determine whether this pool is

depleted in *dfm1Δ* + Hmg2 cells and found that it was reduced compared to WT and *hrd1Δ* strains with Hmg2 (Fig. 7E&F). In contrast, *dfm1Δ* without overexpressed Hmg2 do not show a decrease in monomeric ubiquitin (Fig. S5A&B).

2.2.13 Deubiquitinases Prevent or Resolve Misfolded Membrane Protein Stress

The deubiquitinase (DUB) Ubp6 is a peripheral subunit of the proteasome and recycles ubiquitin from substrates prior to proteasome degradation(Hanna et al., 2007). Accordingly, *ubp6Δ* cells were employed in the substrate-toxicity assay to determine whether this protein is involved in alleviating misfolded membrane protein stress by replenishing the free ubiquitin pool. By utilizing the substrate-toxicity assay, we found Hmg2 or Ste6* expression causes a growth defect in *ubp6Δ* cells (Fig. 7F, Fig. S5C). Like *dfm1Δ* and *rpn4Δ* cells, this growth defect was specific to misfolded membrane proteins and was not observed with CPY* (Fig. S6D). To confirm whether this effect was specific to Ubp6, we also tested DUB Doa4, another regulator of free ubiquitin, in the substrate-toxicity assay. Unexpectedly, we found that *doa4Δ* cells phenocopy *ubp6Δ* cells with Hmg2 expression (Fig. S6A). From this observation, we tested a collection of DUB KOs in the substrate-toxicity assay. Of the fourteen yeast DUBs tested (out of twenty-two DUBs total), we observed a growth defect with both *ubp9Δ* and *ubp14Δ* cells (Fig. 7H, Fig. S6B). Interestingly, Ubp6, Doa4, and Ubp14 have all previously been implicated in ubiquitin homeostasis and, to date, no research has been conducted into the specific role of Ubp9186.

2.2.14 Absence of Deubiquitinases and RPN4 in Combination with DFM1 do not Exacerbate Toxicity

We tested double knockouts of *dfm1Δrpn4Δ, dfm1Δ ubp6 Δ,* and *rpn4 Δubp6Δ* cells expressing Hmg2 in the substrate-toxicity assay to determine whether these genetic backgrounds display the same or different growth defect than either of the single knockouts. Expression of either Hmg2 or Ste6* in either *dfm1Δrpn4Δ* or *dfm1Δubp6Δ* cells resulted in a growth defect that phenocopied that observed in any of the single knockouts (Fig. S7A&B), whereas expression of CPY* showed no growth defect (Fig. S7C). In contrast, *rpn4Δubp6Δ* cells showed a growth defect in the absence of substrates whereas *rpn4Δ* and *ubp6Δ* displayed normal growth. Moreover, *rpn4Δubp6Δ* cells along with expression of Hmg2 or Ste6* resulted in synthetic lethality (Fig. S7A-C). This indicates that there is an exacerbation of stress in *rpn4Δubp6Δ* background, whereas there is no increase in toxicity when RPN4 or UBP6 are knocked out in combination with DFM1. It is likely that there are several parallel pathways contributing to preventing stress from misfolded membrane proteins and resolving this stress, and Dfm1 appears to be one of the major mediators of misfolded membrane stress prevention.

We also tested expression of previously described Hmg2 mutants K6R and K357R in *rpn4Δ* and *ubp6Δ* cells (Fig. S7D). As with *dfm1Δ* cells expressing these mutants, expression of Hmg2-K6R does not cause toxicity while Hmg2-K357R does cause toxicity in both *rpn4Δ* and *ubp6Δ.* Thus, ubiquitination of misfolded membrane proteins influences toxicity in *dfm1Δ, rpn4Δ,* and *ubp6Δ* cells.

2.2.15 Misfolded Protein Aggregation Toxicity Requires Protein Ubiquitination

We originally hypothesize that ubiquitination of membrane proteins was promoting those proteins to become aggregated. To test this hypothesis, we measured aggregation

versus solubility of Hmg2-K6R in *dfm1Δ* cells in the detergent solubility assay (Fig. 7I). Surprisingly, Hmg2-K6R phenocopied Hmg2 in *dfm1Δ* cells, with virtually all of the protein being in the aggregated fraction. This demonstrates ubiquitin does not influence aggregation and not all misfolded membrane protein aggregates are toxic.

2.2.16 Increased Expression of Dfm1 Relieves Misfolded Membrane Protein Stress in rpn4Δ and ubp6Δ Cells

Using the substrate-toxicity assay, we examined whether increasing expression of Dfm1 could relieve growth stress in *rpn4Δ* and *ubp6Δ* cells expressing Hmg2. We utilized the substrate-toxicity assay with the addition of galactose inducible Dfm1 to address this question. Increasing Dfm1 in both *rpn4Δ*+Hmg2 and *ubp6Δ*+Hmg2 cells restored normal growth (Fig. S7E). Importantly, endogenous Dfm1 is already present in these cells, but increasing expression level relieves toxicity caused by misfolded membrane proteins.

2.3 Discussion

Proper protein folding and efficient elimination of misfolded proteins is imperative for maintaining cellular health. Accumulation of misfolded proteins, which is a widespread phenomenon in aging and diseased cells, is deleterious to cells and can impact cellular function. Despite membrane proteins accounting for one-quarter of proteins in the cell, there is a dearth of research into the mechanisms cells use to prevent misfolded membrane protein toxicity. In this study, we sought to understand how cells prevent toxicity from misfolded proteins and how they are impacted by misfolded membrane protein stress. By employing our genetically tractable substrate-toxicity assay, we found that the source of cell

toxicity was from aggregation of ubiquitinated misfolded membrane proteins and Dfm1's rhomboid motifs, lipid thinning function, and substrate engagement function are required for solubilizing aggregation-prone substrates. We propose a model in which ubiquitinated misfolded membrane proteins in *dfm1Δ* cells form aggregates, resulting in compromised proteasome function and a reduction in monomeric ubiquitin. Overall, our studies unveil a new role for rhomboid pseudoproteases in mitigating the stress state caused by ERAD membrane substrates, a function that is independent of their retrotranslocation function.

Our results above (Fig. 2B-D) indicate differential requirements for Dfm1's role in membrane substrate retrotranslocation, versus its role in stress alleviation. These results are fascinating, because of all the retrotranslocation-deficient mutants tested, we were able to identify a mutant that was still able to rescue the growth defect observed in *dfm1Δ*+Hmg2 cell. This indicates a bifurcated role of Dfm1 in retrotranslocation and membrane protein stress alleviation. The retrotranslocation defective mutants that did not restore growth were mutations of conserved rhomboid protein motifs (WR and Gx3G), mutants that obliterate substrate engagement (Loop 1 mutants: F58S, L64V, and K67E), and mutants that reduce the ability of Dfm1 to distort the ER membrane (TMD 2 mutants: Q101R and F107S). This indicates the substrate binding and lipid distortion roles of Dfm1 that are imperative for retrotranslocation are also imperative for alleviation of misfolded membrane protein stress. In contrast, the SHP box mutant, which prevents Cdc48 binding to Dfm1, restores growth in *dfm1Δ* + Hmg2 cells (Fig. 2D). While Cdc48 binding to Dfm1 is critical for retrotranslocation, this is not a requirement for Dfm1's role in preventing membrane proteotoxicity. Previous work from our lab indicates transient interactions between membrane substrates and Dfm1 still occurs even when Dfm1's Cdc48 recruitment activity is impaired (Nejatfard et al., 2021).

This suggests that this level of physical interaction is sufficient for Dfm1 to directly act on substrates to prevent membrane substrate-induced stress.

Our results from both this study and previous work from the lab on Dfm1's function indicate Dfm1 acts directly on misfolded membrane proteins to promote their solubility(Nejatfard et al., 2021). Firstly, all of the L1 mutants of Dfm1, which have previously been shown to ablate binding of Dfm1 to misfolded membrane proteins, such as Hmg2, are not able to promote solubility of Hmg2. Secondly, we demonstrate here that DDM solubilized Hmg2 still interacts with Dfm1, as shown through co-immunoprecipitation (Fig. 3C). Lastly, both human Derlin-1 and Derlin-2 are able to restore solubility of Hmg2 in *dfm1Δ* cells (Fig. 4F). It seems unlikely that if Dfm1 was influencing solubility of Hmg2 through an indirect route that mammalian derlins, which have diverged significantly from Dfm1, would still influence solubility.

We previously demonstrated that expression of integral membrane ERAD substrate induces toxicity in yeast cells when Dfm1 function is impaired. Remarkably, this strong growth defect phenotype is unique to *dfm1Δ* strains: other equally strong ERAD deficient mutants, both upstream or downstream of Dfm1 (*hrd1*△ or *cdc48-2),* show no growth stress upon similar elevation of ERAD integral membrane substrates. Thus, the growth effects above suggest the intriguing possibility that Dfm1 has a unique role in this novel ER stress.

Our data on the ability of Dfm1 to influence misfolded membrane protein solubility provides evidence that this is the mechanism by which Dfm1 prevents misfolded membrane

protein toxicity. We find that both WT Dfm1 and Dfm1-5Ashp promote solubility of Hmg2 (Fig. 3A-B). In contrast, the retrotranslocation defective Dfm1 rhomboid motif mutants, L1 mutants, and TMD2 mutants are not able to promote Hmg2-GFP solubility. This is in agreement with our observation that both WT Dfm1 and Dfm1-5Ashp can restore normal growth in *dfm1Δ* cells in the S-T assay, but the rhomboid motifs mutants cannot (Fig. 2B&D). The exact mechanism by which Dfm1 influences Hmg2 solubility is unclear. We propose two possible models that will be important to distinguish between in future works. In one model, Dfm1 functions as a disaggregase to physically separate misfolded membrane proteins from existing protein aggregates. In another model, Dfm1 functions as a holdase to promote solubility of misfolded membrane proteins and limit their ability to aggregate. We believe present data indicates a holdase function is more likely, as Dfm1 interacts with solubilized Hmg2 (Fig. 3C), potentially preventing it from forming aggregates, but this hypothesis will need to be tested more mechanistically in future studies. While the ability of Dfm1-5Ashp to increase Hmg2 solubility in *dfm1Δ* cells indicates that Dfm1's chaperone-like ability is ATP-independent, we cannot exclude the possibility that Dfm1 recruits another ATPase besides Cdc48, independent of the SHP box motif. Another possibility is that Dfm1 itself can bind and hydrolyze ATP. There are a growing number of identified ATP-independent disaggregases(Huang et al., 2021), including one membrane protein dissagregase identified in plants(Jaru-Ampornpan et al., 2010). Understanding how Dfm1 influences the solubility of membrane substrates will be an important future line of inquiry.

By analyzing the transcriptome upon triggering this unique membrane substrate-induced stress state, we find that many proteasomal subunits are upregulated. Interestingly, Rpn4 – a transcription factor known to induce proteasome subunit expression – upregulates

many of the proteasomal subunits upregulated in our transcriptome analysis. One interpretation of our data is that accumulation of integral membrane proteins results in reduced proteasome efficiency, which triggers Rpn4-mediated upregulation of proteasome subunits. Indeed, we and others have shown that *rpn4Δ* cells phenocopy *dfm1Δ* cells by exhibiting a growth defect upon expression of ER integral substrates, and not ERAD-L substrates (Metzger, M.B. and Michaelis, S., 2009) This was also supported by our above studies showing ERAD membrane substrates exacerbate cellular growth defects when proteasome function is compromised with treatment of proteasome inhibitor, MG132 (Fig. 6D-F). These data indicate that cells require optimal proteasome activity to avoid the proteotoxicity associated with integral membrane ERAD substrates.

The facile and genetically tractable substrate-toxicity assay allowed us to ascertain how membrane substrates cause the growth defect phenotype when Dfm1 is absent. Intriguingly, no growth defect was observed in *dfm1Δ* cells expressing the K6R Hmg2 mutant (with negligible ubiquitination), while the K357R Hmg2 mutant (with slight ubiquitination) still showed a growth defect, suggesting the source of Dfm1-mitigated stress is ubiquitination of the substrates. We reasoned that accumulation of ubiquitinated ERAD membrane substrates disrupts the ubiquitin pool through excessive ubiquitination of substrates and concomitant reduction of the ubiquitin pool. Indeed, a collection of DUB mutants (*ubp6*Δ, *doa4*Δ, *ubp14*Δ) –known for their role in replenishing the ubiquitin pool through their deubiquitinating function – is unable to mitigate the proteotoxic effect of integral membrane substrates and proteotoxic stress is rescued with exogenous addition of ubiquitin molecules in *dfm1Δ*+Hmg2 cells (Fig. 7D & 7G-H). This observation is extended in mammalian studies in which a mouse line with a loss-of-function mutation in Usp14, the mammalian homolog of Ubp6, reduction in the pool of

free ubiquitin in neurons results in ataxia that can be rescued with exogenous ubiquitin expression (Anderson et al., 2005). The reduction we observed in monomeric ubiquitin in *dfm1Δ* +Hmg2 cells was approximately half of that observed in WT+Hmg2 cells (Fig. 6E). The hypothesis that this reduction is enough to contribute to toxicity in these cells is supported both by our experiment demonstrating the exogenous ubiquitin restores growth in the substrate-toxicity assay (Fig. 7D) and by the observation that ataxic Usp14-deficient mice only show about a 25% reduction in monomeric ubiquitin in most tissues(Anderson et al., 2005). Perhaps what is most fascinating is that the stress state is only induced by excessive ubiquitination of integral membrane substrates and not soluble proteins residing in the cytosol, suggesting the source of stress is due to excessive ubiquitination of substrates at the ER membrane.

There is an emerging body of evidence that protein aggregation is not inherently toxic (De Groot et al., 2012; J. Li et al., 2012; Z. F. Li et al., 2008). We propose a model in which two conditions need to be met for misfolded membrane protein accumulation to become toxic; i) the misfolded membrane proteins must become aggregated and ii) the misfolded membrane proteins must be ubiquitinated (Fig. 8). If only one of these conditions is met, there is no toxicity observed in the substrate-toxicity assay. For example, Dfm1-5Ashp restores growth and solubility of Hmg2, even without restoring retrotranslocation (Fig. 2E & 3A). These accumulated membrane proteins would still be expected to be ubiquitinated, but no toxicity is observed without aggregated Hmg2 in this circumstance. Conversely, the nonubiquitinated Hmg2-K6R does not cause toxicity, even though virtually all the protein is aggregated in *dfm1Δ* cells (Fig. 7I). Additionally, the ability to influence the solubility of misfolded membrane proteins appears specific to Dfm1 among ERAD machinery, as *cdc48-2*

cells with an overexpressed misfolded membrane protein do not display growth stress, and nearly all Hmg2 is soluble in *hrd1Δ* cells in the detergent solubility assay (Fig. 1E&F, Fig. 4A).

Molecular chaperones have long been identified for their role in protein quality control systems, including ERAD, for their ability to triage terminally misfolded proteins to degradation machinery. In recent years, more studies have shown a dual function of protein quality control machinery in directly controlling degradation and being chaperones(Neal et al., 2017b; Wang et al., 2011). We have now provided evidence for rhomboid pseudoproteases, a subclass of proteins widely recognized as involved in protein quality control, having chaperone-like function. This raises the question of whether chaperone ability is more widespread among other protein quality control components, specifically those known to bind to membrane proteins. Previous work from the Brodsky lab demonstrated that aggregation-prone ER proteins are more likely to be targeted by ERAD and are disaggregated by the ATP-dependent cytoplasmic disaggregase Hsp104, which aids in retrotranslocation(Preston et al., 2018). Our results demonstrate that a component of membrane protein retrotranslocation machinery, Dfm1, also has a chaperone-like function to aid in retrotranslocation. The Carvalho group has demonstrated that the Asi complex involved in inner nuclear membrane protein quality control in yeast and the mammalian ERAD factor membralin are able to recognize transmembrane domains of misfolded proteins(Natarajan et al., 2020; van de Weijer et al., 2020). It is possible that chaperone function has arisen more than once evolutionarily among proteins involved in membrane protein quality control.

Rhomboid pseudoproteases have been recognized for over a decade as being involved in a diverse array of cellular process, from protein quality control to cell signaling to adaptations to cellular stress (Christova et al., 2013; W. Lee et al., 2015; Lilley & Ploegh, 2004; Oda et al., 2006; Zettl et al., 2011). Our lab and others have made progress towards understanding how these proteins are able to function is such diverse cellular process without an enzymatic function. With the knowledge that several derlin proteins are chaperone-like proteins, it will be of extreme interest to determine if this function is conserved among all rhomboid pseudoproteases, and even among the active rhomboid proteases. Two specific areas of interest include determining the conservation of this chaperone-like function and identifying the repertoire of substrates that can be solubilized by rhomboid pseudoproteases. There are two subclasses of rhomboid pseudoproteases, iRhoms and derlins. Both of these classes are evolutionarily distinct and it will be of interest to determine if chaperone-like ability is only specific to derlins, and not to iRhoms (Lemberg & Freeman, 2007). Derlins are known to function in retrotranslocation of a wide variety of substrates, including disease-associated membrane substrates. In this study, we observed accumulation of both WT and the disease causing CFTRΔF508 caused growth stress in *dfm1Δ* cells (Greenblatt et al., 2011; Knop et al., 1996; Lilley & Ploegh, 2004; Ye et al., 2004). Surprisingly, we found that heterologous expression of both human Derlin-1 and Derlin-2 restores growth in yeast *dfm1Δ*+Hmg2 cell and promotes solubility of Hmg2, implying the solubility function is a conserved feature amongst all derlin rhomboid pseudoproteases. Moreover, research from our lab demonstrated that Derlin-1 and Derlin-2 do not support ERAD-M retrotranslocation in *dfm1Δ* cells(Nejatfard et al., 2021). This indicates that Derlin-1 and Derlin-2 relieve toxicity in *dfm1Δ* + Hmg2 cells, without restoring retrotranslocation, through a conserved chaperone-like function.

Our studies provide the first evidence that the derlin subclass of rhomboid pseudoproteases function as chaperone-like proteins by influencing the solubilization of misfolded membrane substrates. Findings gleaned from our studies hold great promise for foundational and translational arenas of cell biology, since fundamental understanding of a membrane protein chaperone will aid in understanding a plethora of diseases associated with misfolded membrane proteins such as cystic fibrosis, retinal degeneration, and neurodegenerative diseases.

2.4 Materials and Methods

Plasmids and Strains

Plasmids used in this study are listed in Table S1. Plasmids for this work were generated using standard molecular biological cloning techniques via polymerase chain reaction (PCR) of genes from yeast genomic DNA or plasmid followed by ligation into a specific restricted digested site within a construct and verified by sequencing (Eton Bioscience, Inc.). Primer information is available upon request.

A complete list of yeast strains and their corresponding genotypes are listed in Table S2. All strains used in this work were derived from S288C or Resgen. Yeast strains were transformed with DNA or PCR fragments using the standard LiOAc method in which null alleles were generated by using PCR to amplify a selection marker flanked by 30 base pairs of the 5’ and 3’ regions, which are immediately adjacent to the coding region of the gene to be deleted. The selectable markers used for making null alleles were genes encoding resistance to G418 or CloNat/nourseothricin or ability to synthesize histidine. After transformation, strains with drug markers were plated onto YPD followed by replica-plating

onto YPD plates containing (500 µg/mL G418 or 200 µg/mL nourseothricin) or minimal media (-His) plates. All gene deletions were confirmed by PCR.

Galactose Induction

For strains with plasmids containing galactose inducible promoters, protein expression was achieved by growing proteins overnight in appropriate selection media containing 2% raffinose as carbon source. The following day, samples were diluted between 0.10-0.20OD at 600nm (diluted absorbance was assay dependent). Cells in log phase were induced by adding 0.2% galactose to media. Minimum time requirement for robust protein expression was determined for strains using flow cytometry and was 2 or 3 hours for every strain used.

Flow Cytometry

Yeast were grown in minimal medium with 2% raffinose and 0.2% galactose and appropriate amino acids into log phase (OD600 < 0.2). The BD Biosciences FACS Calibur flow cytometer measured the individual fluorescence of 10,000 cells. Experiments were analyzed using Prism8 (GraphPad).

Unfolded Protein Response Activation Assay

Strains were inoculated overnight in minimal media (-His) with 2% raffinose. The following day, samples were diluted to 0.20OD in of minimal media (-His) and allowed to grow to log phase. Samples were then diluted to 0.30OD before adding 20% galactose to a

final concentration of 0.2% galactose (+ GAL) or an equal volume of dH2O (-GAL). Timer was started after galactose addition and samples were measured using flow cytometry, as described above, every hour, starting from the 0-hour mark and ending at the 5-hour mark. At the 1-hour time point, samples were treated with either 2ug/mL tunicamycin or an equal volume of DMSO.

Hac1 Splicing PCR

Strains were prepared the same as for the unfolded protein response activation assay, except they were grown in minimal media (-Ura -His) with 2% raffinose. After 5 hours of incubation with 0.2% galactose and 2ug/mL tunicamycin, samples were pelleted and washed with dH2O. RNA from samples was extracted using Qiagen RNeasy Mini Kit. Samples were ethanol precipitated by adding 1uL of Glycoblue (Thermo Fisher), 50uL of 7.5M ammonium acetate, and 700uL of chilled 100% ethanol. Tubes were then stored at -80°C for between three hours to overnight. Samples were then centrifuged at 13,000xg for 30 minutes at 4°C and supernatant was removed. Pellets were washed twice with 75% ethanol and centrifuged at room temperature at 13,000xg for 30 seconds. After drying the pellet, it was resuspended in 15uL of molecular grade water. 250ng of RNA from each sample was used to generate cDNA using a standard protocol for ProtoscriptII Reverse Transcriptase (NEB), except with 1uL of Oligo $(dT)_{12-18}$ (Thermo Fisher Scientific) used for primer. Wizard SV Gel and PCR Clean-Up System (ProMega) was used on cDNA samples. Hac1 mRNA was amplified using forward primer 5'ACTTGGCTATCCCTACCAACT 3' and reverse primer 5'ATGAATTCAAACCTGACTGC 3'. PCR products were resolved on a 2% agarose gel.

MG132 Sensitivity Assay

MG132 sensitivity assay was performed using a protocol adapted from (Metzger, M.B. and Michaelis, S., 2009)(Boyle Metzger & Michaelis, 2008). In brief, cultures grown minimal media (-his) 2% dextrose. Cultures in log phase were split and treated with either 50uM MG132 in DMSO or an equal volume of DMSO alone and incubated for 8h at3 0°C. Cultures were diluted 1:500 and 100uL of sample was plated onto minimal media (-His) plates and grown at 30°C for 3 days. Two technical replicates and three biological replicates were done for each strain. Colony forming units (CFUs) were counted for DMSO- and MG132-treated cells using the ProMega Colony Counter application for iPhone.

Spot dilution assay (Substrate-Toxicity Assay)

Yeast strains were grown in minimal selection media (-His) supplemented with 2% dextrose to log phase (OD600 0.2-0.3) at 30°C. 0.10 OD cells were pelleted and resuspended in 1mL dH2O. 250 µL of each sample was transferred to a 96-well plate where a five-fold serial dilution in dH2O of each sample was performed to obtain a gradient of 0.1-0.0000064 OD cells. The 8x6 pinning apparatus was used to pin cells onto synthetic complete (-His) agar plates supplemented with 2% dextrose or 2% galactose. Plates were incubated at 30°C and removed from the incubator for imaging after 3 days and again after 7 days. All experiments were done in biological triplicates with technical replicates.

RNA Sequencing

RNA was isolated using a Qiagen RNeasy kit using standard protocol for yeast. Samples were eluted twice with 30uL of molecular grade water. To cleanup samples, 1uL of

DNase was added to each sample and was incubated at 37°C for 25 minutes. 6uL of DNase inactivation buffer was added to samples and was incubated for 2 minutes. Samples were spun down at 10,000xg for 1.5 minutes and supernatant was transferred to a new microfuge tube. Samples were ethanol precipitated by adding 1uL of Glycoblue (Thermo Fisher), 50uL of 7.5M ammonium acetate, and 700uL of chilled 100% ethanol. Tubes were then stored at -80°C for between three hours to overnight. Samples were then centrifuged at 13,000xg for 30 minutes at 4°C and supernatant was removed. Pellets were washed twice with 75% ethanol and centrifuged at room temperature at 13,000xg for 30 seconds. After drying the pellet, it was resuspended in 15uL of molecular grade water. Samples were measured for RNA concentration and an equal concentration of each sample was measured out into a total of 50uL of molecular grade water and RNA-seq was performed as previously described (Link et al., 2018) or as follows. Poly A enriched mRNA was fragmented, in 2x Superscript III Mg2+ containing first-strand buffer with 10mM DTT (Invitrogen), by incubation at 94°C for 9 minutes, then immediately chilled on ice before the next step. The 10 µL of fragmented mRNA, 0.5 µL of Random primer (Invitrogen), 0.5 µL of Oligo dT primer (Invitrogen), 0.5 µL of SUPERase-In (Ambion), 1 µL of dNTPs (10 mM) and 1 µL of DTT (10 mM) were heated at 50°C for three minutes. At the end of incubation, 5.8 µL of water, 1 µL of DTT (100 mM), 0.1 µL Actinomycin D (2 µg/µL), 0.2 µL of 1% Tween-20 (Sigma) and 0.2 µL of Superscript III (Invitrogen) were added and incubated in a PCR machine using the following conditions: 25°C for 10 minutes, 50°C for 50 minutes, and a 4°C hold. The product was then purified with Agentcourt RNAClean XP beads (Beckman Coulter) according to manufacturer's instruction and eluted with 10 µL nuclease-free water. The RNA/cDNA double-stranded hybrid was then added to 1.5 µL of Blue Buffer (Enzymatics), 1.1 µL of dUTP mix (10 mM dATP, dCTP, dGTP and 20 mM dUTP), 0.2 µL of RNAse H (5 U/µL), 1.05 µL of water, 1 µL of DNA polymerase I (Enzymatics) and 0.15 µL of 1% Tween-20. The

mixture was incubated at 16°C for 1 hour. The resulting dUTP-marked dsDNA was purified using 28 µL of Sera-Mag Speedbeads (Thermo Fisher Scientific), diluted with 20% PEG8000, 2.5M NaCl to final of 13% PEG, eluted with 40 µL EB buffer (10 mM Tris-Cl, pH 8.5) and frozen −80°C. The purified dsDNA (40 µL) underwent end repair by blunting, A-tailing and adapter ligation using barcoded adapters (NextFlex, Bioo Scientific). Libraries were PCR-amplified for 9–14 cycles, size selected by gel extraction, quantified by Qubit dsDNA HS Assay Kit (Thermo Fisher Scientific) and sequenced on a NextSeq 500.

RNA Sequencing Data Analysis

Data was analyzed by normalizing reads per million and using principal components analysis to determine genes with the highest PC1 (+) scores and lowest PC1 (-) scores between *dfm1*Δ +GAL_{pr}-Hmg2-GFP and every other strain tested. From this list, we used the top 100 genes with the highest (+) and lowest (-) PCA1 values, and cross referenced those to the normalized transcript per million reads value for each gene and removed genes that were not expressed at either a higher (for + PCA1 values) or lower (for - PCA1 values) reads per million level than all other conditions that were sequenced. Then, this list of upregulated and downregulated genes was used for gene ontology (GO) analysis using http://geneontology.org/.

Fluorescence Microscopy

To prepare cells, overnight cultures were diluted to ~0.20 OD in minimal media lacking uracil (-URA). After growing ~3 hours, samples were pelleted and washed with dH2O before being resuspended in 80uL of media to be used for imaging. Fluorescence

microscopy was accomplished using a CSU-X1 Spinning Disk (Yokogawa) confocal microscope at the Nikon Imaging Center on the UCSD campus. Samples were analyzed to measure the fraction of GFP in puncta.

Microscopy Quantification and Analysis

Microscopy images (16-bit) were analyzed using the Fiji distribution of ImageJ2 (Schindelin et al. 2012) and data was compiled in the RStudio integrated development environment of R (RStudio Team 2020). Briefly, cell outlines were segmented by uploading brightfield images of each field of view to the online YeastSpotter tool (Lu et al. 2019; available at http://yeastspotter.csb.utoronto.ca/). Then, fluorescent micrographs from the 488 channel were maximum-projected for all z-slices. To identify Hmg2 puncta in the 488 channel, a 20-pixel median filter was subtracted from each max-Z projected image. Then, any fluorescent Hmg2 signal above a gray value of 750 was thresholded as a "puncta". This threshold value was applied to all fields of view, regardless of replicate number or genotype, and was determined after manually comparing the puncta calls for representative images of each genotype using different threshold values. The fraction of Hmg2 in these bright puncta relative to total Hmg2 in the cell was quantified by summing the integrated density of all puncta in a cell and dividing by the total integrated density of the cell. All ImageJ macros and Rscripts used in this analysis, as well as more detailed methods, are available in a GitHub repository from 3-March-2022 (https://github.com/LiviaSongster/yeast-fluor-percent-puncta). All statistical analysis was performed using GraphPad Prism version 8.0.

Detergent Solubility Assay

ER microsomes were isolated by centrifuging and pelleting 15OD of yeast in log phase growth. Pellets were resuspended in MF buffer with protease inhibitors and 0.5mM lysis beads were added to each sample. Samples were vortexed six times in 1-minute intervals, with 1-minute on ice in between. Lysed cells were transferred to new microcentrifuge tube and samples were clarified by spinning at 1,500x for 5 minutes at 4°C. Microsomes were separated by centrifuging clarified lysate at 14,000 × *g* for 1 minute. Fractions were incubated on ice in the presence or absence of 1% DDM for 1 hour. The mixture was then centrifuged at 14,000 × *g* for 30 min at 4°C, and the detergent soluble fraction (i.e., the supernatant) was precipitated with 20% TCA on ice for 30 minutes and then centrifuged at 14,000 × *g* for 30 min to get a pellet of the soluble protein. Proteins from both the soluble and insoluble fractions were resuspended in sample buffer and resolved by SDS-PAGE.

Co-Immunoprecipitation

Yeasts were grown to mid log phase in minimal media, and 15 OD equivalents were pelleted, washed in water, and resuspended in 240 µl lysis buffer (0.24 M sorbitol, 1 mM EDTA, 20 mM KH2PO4/K2HPO4, pH 7.5) with PIs (2 mM phenylmethylsulfonyl fluoride and 142 mM tosylphenylalanyl chloromethyl ketone). Acid-washed glass beads were added up to the meniscus. Cells were lysed on a multivortexer at 4ºC for six to eight 1-min intervals with 1 min on ice in between each lysis step. The lysates were transferred to a new tube, and lysates cleared with 5-s pulses of centrifugation. Microsomes were pelleted from cleared lysates by centrifugation at 14,000 x g for 5 min. Microsome pellets were washed once in XL buffer (1.2 M sorbitol, 5 mM EDTA, 0.1 M KH2PO4/K2HPO4, pH 7.5) and resuspended in XL buffer.

Samples were then solubilized by the addition of detergent solution at 10x the desired final concentration in XL buffer (final concentration or 1% DDM). Preparations with detergent were incubated at 4 °C for 1 h with rocking and then repeatedly pipetted up and down. Finally, samples were cleared by centrifugation in a benchtop microcentrifuge for 15 min at 16,000g. The supernatants were then separated by ultracentrifugation at 89,000 RPM for 15 min, and the supernatant was incubated overnight with 10 µL of equilibrated GFP-Trap agarose (ChromoTek Inc., Hauppauge, NY) at 4°C. The next day, the GFP-Trap® agarose beads were combined to one tube, washed once with non-detergent IP buffer, washed once more with IP wash buffer and resuspended in 100 µL of 2xUSB. Samples were resolved on 8% SDS-PAGE and immunoblotted for Hmg2-GFP with α-GFP, Dfm1-HA with α-HA, and α-Sec61 antibody.

Cycloheximide-Chase Assay

Cycloheximide chase assays were performed as previously described (Sato et al., 2009). Cells were grown to log-phase (OD_{600} 0.2-.03) and cycloheximide was added to a final concentration of 50 µg/mL. At each time point, a constant volume of culture was removed and lysed. Lysis was initiated with addition of 100 µl SUME with protease inhibitors (PIs) and glass beads, followed by vortexing for 4 min. 100 µl of 2xUSB was added followed by incubation at 55°C for 10 min. Samples were clarified by centrifugation and analyzed by SDS-PAGE and immunoblotting.

in vivo ubiquitination assay

Cells were grown to log phase (OD_{600} 0.3-0.6) and 15 ODs of cells were pelleted. Cells were resuspended in H_20, centrifuged and lysed with the addition of 0.5 mM glass beads and 400 µL of XL buffer (1.2 M sorbitol, 5 mM EDTA, 0.1 M KH_2PO_4, final pH 7.5) with PIs, followed by vortexing in 1minute intervals for 6-8 min at 4°C. Lysates were combined and clarified by centrifugation at 2,500 g for 5 min. 100 µL clarified lysate was resuspended in 100 µL SUME (1% SDS, 8 M Urea, 10 mM MOPS, pH 6.8, 10 mM EDTA) with PIs and 5 mM N-ethyl maleimide (NEM, Sigma) followed by addition of 600 µL immunoprecipitation buffer (IPB) with PIs and NEM. 15 µL of rabbit polyclonal anti-GFP antisera (C. Zuker, University of California, San Diego) was added to the samples for immunoprecipitation (IP) of Hmg2-GFP. Samples were incubated on ice for 5 minutes, clarified at 14,000 g for 5 min and removed to a new eppendorf tube and incubated overnight at 4°C. 100 µL of equilibrated Protein A-Sepharose in IPB (50% w/v) (Amersham Biosciences) was added and incubated for 2 hr at 4°C. Proteins A beads were washed twice with IPB and washed once more with IP wash buffer (50 mM NaCl, 10 mM Tris), aspirated to dryness, resuspended in 2x Urea sample buffer (8 M urea, 4% SDS, 1mM DTT, 125 mM Tris, pH 6.8), and incubated at 55°C for 10 min. IPs were resolved by 8% SDS-PAGE, transferred to nitrocellulose, and immunoblotted with monoclonal anti-ubiquitin (Fred Hutchinson Cancer Center, Seattle) and anti-GFP (Clontech, Mountain View, CA). Goat anti-mouse (Jackson ImmunoResearch, West Grove, PA) and goat anti-rabbit (Bio-Rad) conjugated with horseradish peroxidase (HRP) recognized the primary antibodies. Western Lightning Plus (Perkin Elmer, Watham, MA) chemiluminescence reagents were used for immunodetection.

Western Blot Quantification

Western blot images were quantified using ImageJ/Fiji. Band intensities were measured from high resolution TIF files of western blot images acquired from a BioRad Chemidoc Imager. Data analysis was done using Prism8 (GraphPad).

2.5 Acknowledgments

Chapter 2 is currently under revision for publication for the working citation: Kandel, R., Jung, J., Syau, D., Kuo, T., Songster, L., Horn, C., Chapman, C., Aguayo, A., Duttke, S., Benner, C., Neal, S., Derlin Dfm1 Employs a Chaperone-Like Function to Resolve Misfolded Membrane Protein Stress. The dissertation author was a primary investigator and the first author of this material. The authors would like to thank Tom Rapoport (Harvard Medical School), Davis Ng (National University of Singapore), Randy Schekman (University of California, Berkeley), Susan Michaelis (John Hopkins University), and Jeff Brodsky (University of Pittsburgh) for providing plasmids and antibodies. We also thank the Neal lab members for their positive reinforcement, in depth discussions and technical assistance. These studies were supported by NIH grant 1R35GM133565-01, Pew Biomedical Award, and NSF CAREER grant to S.E.N. S.H.D is supported by NIH grant R00GM135515 to S.H.D.

2.6 References

Adrain, C., & Cavadas, M. (n.d.). *The complex life of rhomboid pseudoproteases*. https://doi.org/10.1111/febs.15548

Anderson, C., Crimmins, S., Wilson, J. A., Korbel, G. A., Ploegh, H. L., & Wilson, S. M. (2005). Loss of Usp14 results in reduced levels of ubiquitin in ataxia mice. *Journal of Neurochemistry*, *95*(3), 724–731. https://doi.org/10.1111/j.1471-4159.2005.03409.x

Baldridge, R. D., & Rapoport, T. A. (2016). Autoubiquitination of the Hrd1 Ligase Triggers Protein Retrotranslocation in ERAD. *Cell*, *166*(2), 394–407. https://doi.org/10.1016/J.CELL.2016.05.048

Bays, N. W., Gardner, R. G., Seelig, L. P., Joazeiro, C. A., & Hampton, R. Y. (2001). Hrd1p/Der3p is a membrane-anchored ubiquitin ligase required for ER-associated degradation. *Nature Cell Biology*, *3*(1), 24–29. https://doi.org/10.1038/35050524

Began, J., Cordier, B., Březinová, J., Delisle, J., Hexnerová, R., Srb, P., Rampírová, P., Kožíšek, M., Baudet, M., Couté, Y., Galinier, A., Veverka, V., Doan, T., & Strisovsky, K. (2020). Rhomboid intramembrane protease YqgP licenses bacterial membrane protein quality control as adaptor of FtsH AAA protease . *The EMBO Journal*, e102935. https://doi.org/10.15252/embj.2019102935

Bhaduri, S., & Neal, S. E. (2021). Assays for studying normal versus suppressive ERAD-associated retrotranslocation pathways in yeast. *STAR Protocols*, *2*(3), 100640. https://doi.org/10.1016/j.xpro.2021.100640

Bhamidipati, A., Denic, V., Quan, E. M., & Weissman, J. S. (2005). Exploration of the topological requirements of ERAD identifies Yos9p as a lectin sensor of misfolded glycoproteins in the ER lumen. *Molecular Cell*, *19*(6), 741–751. https://doi.org/10.1016/J.MOLCEL.2005.07.027

Bock, J., Kühnle, N., Knopf, J. D., Landscheidt, N., Lee, J. G., Ye, Y., & Lemberg, M. K. (2022). Rhomboid protease RHBDL4 promotes retrotranslocation of aggregation-prone proteins for degradation. *Cell Reports*, *40*(6), 111175. https://doi.org/10.1016/J.CELREP.2022.111175

Boyle Metzger, M., & Michaelis, S. (2008). Analysis of Quality Control Substrates in Distinct Cellular Compartments Reveals a Unique Role for Rpn4p in Tolerating Misfolded Membrane Proteins. *Molecular Biology of the Cell*, *20*(1006–1019).

Burns, G. D., Hilal, O. E., Sun, Z., Reutter, K. R., Preston, G. M., Augustine, A. A., Brodsky, J. L., & Guerriero, C. J. (2021). Distinct classes of misfolded proteins differentially affect the growth of yeast compromised for proteasome function. *FEBS Letters*, *595*(18), 2383–2394. https://doi.org/10.1002/1873-3468.14172

Cartier, A. E., Djakovic, S. N., Salehi, A., Wilson, S. M., Masliah, E., & Patrick, G. N. (2009). Regulation of synaptic structure by ubiquitin C-terminal hydrolase L1. *Journal of Neuroscience*, *29*(24), 7857–7868. https://doi.org/10.1523/JNEUROSCI.1817-09.2009

Cheng, S. H., Gregory, R. J., Marshall, J., Paul, S., Souza, D. W., White, G. A., O'Riordan, C. R., & Smith, A. E. (1990). Defective intracellular transport and processing of CFTR is the molecular basis of most cystic fibrosis. *Cell*, *63*(4), 827–834. https://doi.org/10.1016/0092-8674(90)90148-8

Christova, Y., Adrain, C., Bambrough, P., Ibrahim, A., & Freeman, M. (2013). Mammalian iRhoms have distinct physiological functions including an essential role in TACE regulation. *EMBO Reports*, *14*(10), 884–890. https://doi.org/10.1038/embor.2013.128

Cox, J. S., & Walter, P. (1996). A Novel Mechanism for Regulating Activity of a Transcription Factor That Controls the Unfolded Protein Response. *Cell*, *87*(3), 391–404. https://doi.org/10.1016/S0092-8674(00)81360-4

De Groot, N. S., Torrent, M., Villar-Piqué, A., Lang, B., Ventura, S., Gsponer, J., & Babu, M. M. (2012). Evolutionary selection for protein aggregation. *Biochemical Society Transactions*, *40*(5), 1032–1037. https://doi.org/10.1042/BST20120160

Enenkel, C., Lehmann, A., & Kloetzel, P. M. (1998). Subcellular distribution of proteasomes implicates a major location of protein degradation in the nuclear envelope-ER network in yeast. *The EMBO Journal*, *17*(21), 6144. https://doi.org/10.1093/EMBOJ/17.21.6144

Engberg, O., Ulbricht, D., Döbel, V., Siebert, V., Frie, C., Penk, A., Lemberg, M. K., & Huster, D. (2022). Rhomboid-catalyzed intramembrane proteolysis requires hydrophobic matching with the surrounding lipid bilayer. *Science Advances*, *8*(38), eabq8303. https://doi.org/10.1126/SCIADV.ABQ8303/SUPPL_FILE/SCIADV.ABQ8303_SM.PDF

Farinha, C. M., & Amaral, M. D. (2005). Most F508del-CFTR Is Targeted to Degradation at an Early Folding Checkpoint and Independently of Calnexin. *Molecular and Cellular Biology*, *25*(12), 5242–5252. https://doi.org/10.1128/MCB.25.12.5242-5252.2005/ASSET/2C5A297B-2994-4706-95BB-76C171C07C02/ASSETS/GRAPHIC/ZMB0120550950009.JPEG

Fleig, L., Bergbold, N., Sahasrabudhe, P., Geiger, B., Kaltak, L., & Lemberg, M. K. (2012). Ubiquitin-Dependent Intramembrane Rhomboid Protease Promotes ERAD of Membrane Proteins. *Molecular Cell*, *47*(4), 558–569. https://doi.org/10.1016/j.molcel.2012.06.008

Freeman, M. (2014). The rhomboid-like superfamily: molecular mechanisms and biological roles. *Annual Review of Cell and Developmental Biology*, *30*(1), 235–254. https://doi.org/10.1146/annurev-cellbio-100913-012944

Gardner, R. G., & Hampton, R. Y. (1999). A "distributed degron" allows regulated entry into the ER degradation pathway. *EMBO Journal*, *18*(21), 5994–6004. https://doi.org/10.1093/emboj/18.21.5994

Garza, R. M., Sato, B. K., & Hampton, R. Y. (2009). In vitro analysis of Hrd1p-mediated retrotranslocation of its multispanning membrane substrate 3-hydroxy-3-methylglutaryl (HMG)-CoA reductase. *The Journal of Biological Chemistry*, *284*(22), 14710–14722. https://doi.org/10.1074/jbc.M809607200

Gasch, A. P., Spellman, P. T., Kao, C. M., Carmel-Harel, O., Eisen, M. B., Storz, G., Botstein, D., & Brown, P. O. (2000). Genomic Expression Programs in the Response of

Yeast Cells to Environmental Changes. *Molecular Biology of the Cell*, *11*, 4241–4257. https://doi.org/https://doi.org/10.1091/mbc.11.12.4241

Gnann, A., Riordan, J. R., & Wolf, D. H. (2004). Cystic Fibrosis Transmembrane Conductance Regulator Degradation Depends on the Lectins Htm1p/EDEM and the Cdc48 Protein Complex in Yeast. *Mol Biol Cell*, *15*(September), 4125–4135. https://doi.org/10.1091/mbc.E04

Greenblatt, E. J., Olzmann, J. a, & Kopito, R. R. (2011). Derlin-1 is a rhomboid pseudoprotease required for the dislocation of mutant α-1 antitrypsin from the endoplasmic reticulum. *Nature Structural & Molecular Biology*, *18*(10), 1147–1152. https://doi.org/10.1038/nsmb.2111

Hampton, R. Y. (2002). ER-associated degradation in protein quality control andcellular regulation. *Current Opinion in Cell Biology*, *14*, 476–482.

Hampton, R. Y., & Bhakta, H. (1997). Ubiquitin-mediated regulation of 3-hydroxy-3-methylglutaryl-CoA reductase. *Proceedings of the National Academy of Sciences of the United States of America*, *94*(24), 12944–12948. https://doi.org/10.1073/PNAS.94.24.12944/ASSET/9FCCF2C8-649B-4B42-8C6B-B1827811DE12/ASSETS/GRAPHIC/PQ2473110004.JPEG

Hampton, R. Y., Gardner, R. G., & Rine, J. (1996). Role of 26S proteasome and HRD genes in the degradation of 3-hydroxy-3-methylglutaryl-CoA reductase, an integral endoplasmic reticulum membrane protein. *Molecular Biology of the Cell*, *7*(12), 2029. https://doi.org/10.1091/MBC.7.12.2029

Hanna, J., Meides, A., Zhang, D. P., & Finley, D. (2007). A Ubiquitin Stress Response Induces Altered Proteasome Composition. *Cell*, *129*(4), 747–759. https://doi.org/10.1016/j.cell.2007.03.042

Hoelen, H., Zaldumbide, A., van Leeuwen, W. F., Torfs, E. C. W., Engelse, M. A., Hassan, C., Lebbink, R. J., de Koning, E. J., Resssing, M. E., de Ru, A. H., van Veelen, P. A., Hoeben, R. C., Roep, B. O., & Wiertz, E. J. H. J. (2015). Proteasomal Degradation of Proinsulin Requires Derlin-2, HRD1 and p97. *PLOS ONE*, *10*(6), e0128206. https://doi.org/10.1371/JOURNAL.PONE.0128206

Huang, L., Agrawal, T., Zhu, G., Yu, S., Tao, L., Lin, J. B., Marmorstein, R., Shorter, J., & Yang, X. (2021). DAXX represents a new type of protein-folding enabler. *Nature*, *597*(7874), 132–137. https://doi.org/10.1038/s41586-021-03824-5

Hwang, J., & Qi, L. (2018). Quality Control in the Endoplasmic Reticulum: Crosstalk between ERAD and UPR pathways. *Trends in Biochemical Sciences*, *43*(8), 593–605. https://doi.org/10.1016/j.tibs.2018.06.005

Jaru-Ampornpan, P., Shen, K., Lam, V. Q., Ali, M., Doniach, S., Jia, T. Z., & Shan, S. O. (2010). ATP-independent reversal of a membrane protein aggregate by a chloroplast SRP subunit. *Nature Structural and Molecular Biology*, *17*(6), 696–702. https://doi.org/10.1038/nsmb.1836

Kandel, R. R., & Neal, S. E. (2020). The role of rhomboid superfamily members in protein homeostasis: Mechanistic insight and physiological implications. In *Biochimica et Biophysica Acta - Molecular Cell Research* (Vol. 1867, Issue 10, p. 118793). Elsevier B.V. https://doi.org/10.1016/j.bbamcr.2020.118793

Knop, M., Finger, A., Braun, T., Hellmuth, K., & Wolf, D. H. (1996). Der1, a novel protein specifically required for endoplasmic reticulum degradation in yeast. *The EMBO Journal*, *15*(4), 753–763. https://doi.org/10.1002/j.1460-2075.1996.tb00411.x

Koller, A., Valesco, J., & Subramani, S. (2000). The CUP1 promoter of Saccharomyces cerevisiae is inducible by copper in Pichia pastoris. *Yeast*, *16*(7), 651–656. https://doi.org/10.1002/(SICI)1097-0061(200005)16:7<651::AID-YEA580>3.0.CO;2-F

Lee, D. H., & Goldberg, A. L. (1998). Proteasome Inhibitors Cause Induction of Heat Shock Proteins and Trehalose, Which Together Confer Thermotolerance in Saccharomyces cerevisiae . *Molecular and Cellular Biology*, *18*(1), 30–38. https://doi.org/10.1128/mcb.18.1.30

Lee, W., Kim, Y., Park, J., Shim, S., Lee, J., Hong, S. H., Ahn, H. H., Lee, H., & Jung, Y. K. (2015). IRhom1 regulates proteasome activity via PAC1/2 under ER stress. *Scientific Reports*, *5*. https://doi.org/10.1038/srep11559

Lemberg, M. K., & Freeman, M. (2007). Functional and evolutionary implications of enhanced genomic analysis of rhomboid intramembrane proteases. *Genome Research*, *17*(11), 1634–1646. https://doi.org/10.1101/gr.6425307

Li, J., McQuade, T., Siemer, A. B., Napetschnig, J., Moriwaki, K., Hsiao, Y. S., Damko, E., Moquin, D., Walz, T., McDermott, A., Chan, F. K. M., & Wu, H. (2012). The RIP1/RIP3 necrosome forms a functional amyloid signaling complex required for programmed necrosis. *Cell*, *150*(2), 339–350. https://doi.org/10.1016/j.cell.2012.06.019

Li, Z. F., Wu, X., Jiang, Y., Liu, J., Wu, C., Inagaki, M., Izawa, I., Mizisin, A. P., Engvall, E., & Shelton, G. D. (2008). Non-pathogenic protein aggregates in skeletal muscle in MLF1 transgenic mice. *Journal of the Neurological Sciences*, *264*(1–2), 77–86. https://doi.org/10.1016/j.jns.2007.07.027

Lilley, B. N., & Ploegh, H. L. (2004). A membrane protein required for dislocation of misfolded proteins from the ER. *Nature*, *429*(6994), 834–840. https://doi.org/10.1038/nature02592

Lilley, B. N., & Ploegh, H. L. (2005). Multiprotein complexes that link dislocation, ubiquitination, and extraction of misfolded proteins from the endoplasmic reticulum membrane. *Proceedings of the National Academy of Sciences of the United States of America*, *102*(40), 14296–14301. https://doi.org/10.1073/pnas.0505014102

Link, V. M., Duttke, S. H., Chun, H. B., Holtman, I. R., Westin, E., Hoeksema, M. A., Abe, Y., Skola, D., Romanoski, C. E., Tao, J., Fonseca, G. J., Troutman, T. D., Spann, N. J., Strid, T., Sakai, M., Yu, M., Hu, R., Fang, R., Metzler, D., … Glass, C. K. (2018). Analysis of Genetically Diverse Macrophages Reveals Local and Domain-wide Mechanisms that Control Transcription Factor Binding and Function. *Cell*, *173*(7), 1796-1809.e17. https://doi.org/10.1016/j.cell.2018.04.018

Liu, G., Beaton, S. E., Grieve, A. G., Evans, R., Rogers, M., Strisovsky, K., Armstrong, F. A., Freeman, M., Exley, R. M., & Tang, C. M. (2020). Bacterial rhomboid proteases mediate quality control of orphan membrane proteins. *The EMBO Journal*, *39*(10), e102922. https://doi.org/10.15252/EMBJ.2019102922

Mannhaupt, G., Schnall, R., Karpov, V., Vetter, I., & Feldmann, H. (1999). Rpn4p acts as a transcription factor by binding to PACE, a nonamer box found upstream of 26S proteasomal and other genes in yeast. *FEBS Letters*, *450*(1–2), 27–34. https://doi.org/10.1016/S0014-5793(99)00467-6

Mogk, A., Bukau, B., & Kampinga, H. H. (2018). Cellular Handling of Protein Aggregates by Disaggregation Machines. *Molecular Cell*, *69*(2), 214–226. https://doi.org/10.1016/j.molcel.2018.01.004

Nakatsukasa, K., Brodsky, J. L., & Kamura, T. (n.d.). *A stalled retrotranslocation complex reveals physical linkage between substrate recognition and proteasomal degradation during ER-associated degradation*. https://doi.org/10.1091/mbc.E12-12-0907

Natarajan, N., Foresti, O., Wendrich, K., Stein, A., & Carvalho, P. (2020). Quality Control of Protein Complex Assembly by a Transmembrane Recognition Factor. *Molecular Cell*, *77*(1), 108-119.e9. https://doi.org/10.1016/j.molcel.2019.10.003

Neal, S., Jaeger, P. A., Duttke, S. H., Benner, C. K., Glass, C., Ideker, T., & Hampton, R. (2018). The Dfm1 Derlin Is Required for ERAD Retrotranslocation of Integral Membrane Proteins. *Molecular Cell*, *69*(2). https://doi.org/10.1016/j.molcel.2017.12.012

Neal, S., Mak, R., Bennett, E. J., & Hampton, R. (2017). A Cdc48 “retrochaperone” function is required for the solubility of retrotranslocated, integral membrane Endoplasmic Reticulum-associated Degradation (ERAD-M) substrates. *Journal of Biological Chemistry*, *292*(8). https://doi.org/10.1074/jbc.M116.770610

Neal, S., Syau, D., Nejatfard, A., Nadeau, S., & Hampton, R. Y. (2020). HRD Complex Self-Remodeling Enables a Novel Route of Membrane Protein Retrotranslocation. *IScience*, *23*(9). https://doi.org/10.1016/j.isci.2020.101493

Nejatfard, A., Wauer, N., Bhaduri, S., Conn, A., Gourkanti, S., Singh, N., Kuo, T., Kandel, R., Amaro, R. E., & Neal, S. E. (2021). Derlin rhomboid pseudoproteases employ substrate engagement and lipid distortion to enable the retrotranslocation of ERAD membrane substrates. *Cell Reports*, *37*(3), 109840. https://doi.org/10.1016/j.celrep.2021.109840

Oda, Y., Okada, T., Yoshida, H., Kaufman, R. J., Nagata, K., & Mori, K. (2006). Derlin-2 and Derlin-3 are regulated by the mammalian unfolded protein response and are required for ER-associated degradation. *Journal of Cell Biology*, *172*(3), 383–393. https://doi.org/10.1083/JCB.200507057

Owsianik, G., Balzi, L., & Ghislain, M. (2002). Control of 26S proteasome expression by transcription factors regulating multidrug resistance in Saccharomyces cerevisiae. *Molecular Microbiology*, *43*(5), 1295–1308. https://doi.org/10.1046/j.1365-2958.2002.02823.x

Palmer, E. A., Kruse, K. B., Fewell, S. W., Buchanan, S. M., Brodsky, J. L., & McCracken, A. A. (2003). Differential requirements of novel A1PiZ degradation deficient (ADD) genes in ER-

associated protein degradation. *Journal of Cell Science*, *116*(11), 2361–2373. https://doi.org/10.1242/jcs.00439

Preston, G. M., Guerriero, C. J., Metzger, M. B., Michaelis, S., & Brodsky, J. L. (2018). Substrate Insolubility Dictates Hsp104-Dependent Endoplasmic-Reticulum-Associated Degradation. *Molecular Cell*, *70*(2), 242-253.e6. https://doi.org/10.1016/j.molcel.2018.03.016

Rabinovich, E., Kerem, A., Fröhlich, K.-U., Diamant, N., & Bar-Nun, S. (2002). AAA-ATPase p97/Cdc48p, a cytosolic chaperone required for endoplasmic reticulum-associated protein degradation. *Molecular and Cellular Biology*, *22*(2), 626–634. http://www.pubmedcentral.nih.gov/articlerender.fcgi?artid=139744&tool=pmcentrez&rendertype=abstract

Ren, G., Tardi, N. J., Matsuda, F., Koh, K. H., Ruiz, P., Wei, C., Altintas, M. M., Ploegh, H., & Reiser, J. (2018). Podocytes exhibit a specialized protein quality control employing derlin-2 in kidney disease. *American Journal of Physiology - Renal Physiology*, *314*(3), F471–F482. https://doi.org/10.1152/ajprenal.00691.2016

Sato, B. K., & Hampton, R. Y. (2006). Yeast Derlin Dfm I interacts with Cdc48 and functions in ER homeostasis. *Yeast*, *23*(14–15), 1053–1064. https://doi.org/10.1002/yea.1407

Sato, B. K., Schulz, D., Do, P. H., & Hampton, R. Y. (2009). Misfolded Membrane Proteins Are Specifically Recognized by the Transmembrane Domain of the Hrd1p Ubiquitin Ligase. *Molecular Cell*, *34*(2), 212–222. https://doi.org/10.1016/j.molcel.2009.03.010

Stanley, A. M., Carvalho, P., & Rapoport, T. (2011). Recognition of an ERAD-L substrate analyzed by site-specific in vivo photocrosslinking. *FEBS Letters*, *585*(9), 1281–1286. https://doi.org/10.1016/J.FEBSLET.2011.04.009

Sun, F., Zhang, R., Gong, X., Geng, X., Drain, P. F., & Frizzell, R. A. (2006). Derlin-1 promotes the efficient degradation of the cystic fibrosis transmembrane conductance regulator (CFTR) and CFTR folding mutants. *Journal of Biological Chemistry*, *281*(48), 36856–36863. https://doi.org/10.1074/jbc.M607085200

Sun, Z., Guerriero, C. J., & Brodsky, J. L. (2021). Substrate ubiquitination retains misfolded membrane proteins in the endoplasmic reticulum for degradation. *Cell Reports*, *36*(12), 109717. https://doi.org/10.1016/J.CELREP.2021.109717

Suresh, H. G., Pascoe, N., & Andrews, B. (2020). The structure and function of deubiquitinases: Lessons from budding yeast: Mechanism and function of DUBs. *Open Biology*, *10*(10). https://doi.org/10.1098/rsob.200279rsob200279

Swanson, R., Locher, M., & Hochstrasser, M. (2001). A conserved ubiquitin ligase of the nuclear envelope/endoplasmic reticulum that functions in both ER-associated and Matα2 repressor degradation. *Genes & Development*, *15*(20), 2660–2674. https://doi.org/10.1101/GAD.933301

Tichá, A., Collis, B., & Strisovsky, K. (2018). The Rhomboid Superfamily: Structural Mechanisms and Chemical Biology Opportunities. In *Trends in Biochemical Sciences* (Vol. 43, Issue 9, pp. 726–739). Elsevier Ltd. https://doi.org/10.1016/j.tibs.2018.06.009

Twomey, E. C., Ji, Z., Wales, T. E., Bodnar, N. O., Ficarro, S. B., Marto, J. A., Engen, J. R., & Rapoport, T. A. (2019). *Substrate processing by the Cdc48 ATPase complex is initiated by ubiquitin unfolding*. https://doi.org/10.1126/science.aax1033

van de Weijer, M. L., Krshnan, L., Liberatori, S., Guerrero, E. N., Robson-Tull, J., Hahn, L., Lebbink, R. J., Wiertz, E. J. H. J., Fischer, R., Ebner, D., & Carvalho, P. (2020). Quality Control of ER Membrane Proteins by the RNF185/Membralin Ubiquitin Ligase Complex. *Molecular Cell*, *79*(5), 768-781.e7. https://doi.org/10.1016/j.molcel.2020.07.009

Wahlman, J., DeMartino, G. N., Skach, W. R., Bulleid, N. J., Brodsky, J. L., & Johnson, A. E. E. (2007). Real-Time Fluorescence Detection of ERAD Substrate Retrotranslocation in a Mammalian In Vitro System. *Cell*, *129*(5), 943–955. https://doi.org/10.1016/J.CELL.2007.03.046

Wang, Q., Liu, Y., Soetandyo, N., Baek, K., Hegde, R., & Ye, Y. (2011). A Ubiquitin Ligase-Associated Chaperone Holdase Maintains Polypeptides in Soluble States for Proteasome Degradation. *Molecular Cell*, *42*(6), 758–770. https://doi.org/10.1016/j.molcel.2011.05.010

Werner, E. D., Brodsky, J. L., & McCracken, A. A. (1996). Proteasome-dependent endoplasmic reticulum-associated protein degradation: An unconventional route to a familiar fate. *Proceedings of the National Academy of Sciences of the United States of America*, *93*(24), 13797–13801. https://doi.org/10.1073/pnas.93.24.13797

Wu, H., Ng, D. T. W., Cheong, I., & Matsudaira, P. (2020). The degradation-promoting roles of deubiquitinases Ubp6 and Ubp3 in cytosolic and ER protein quality control. *PLoS ONE*, *15*(5), 1–37. https://doi.org/10.1371/journal.pone.0232755

Wu, X., Siggel, M., Ovchinnikov, S., Mi, W., Svetlov, V., Nudler, E., Liao, M., Hummer, G., & Rapoport, T. A. (2020). Structural basis of ER-associated protein degradation mediated by the Hrd1 ubiquitin ligase complex. *Science*, *368*(6489), 1–13. https://doi.org/10.1126/SCIENCE.AAZ2449

Xie, Y., & Varshavsky, A. (2001). RPN4 is a ligand, substrate, and transcriptional regulator of the 26S proteasome: A negative feedback circuit. *Proceedings of the National Academy of Sciences of the United States of America*, *98*(6), 3056–3061. https://doi.org/10.1073/PNAS.071022298/ASSET/90604D55-2029-41EA-853B-728FBABABC48/ASSETS/GRAPHIC/PQ0710222004.JPEG

Ye, Y., Meyer, H. H., & Rapoport, T. A. (2001). The AAA ATPase Cdc48/p97 and its partners transport proteins from the ER into the cytosol. *Nature*, *414*(6864), 652–656. https://doi.org/10.1038/414652a

Ye, Y., Shibata, Y., Yun, C., Ron, D., & Rapoport, T. A. (2004). A membrane protein complex mediates retro-translocation from the ER lumen into the cytosol. *Nature*, *429*(6994), 841–847. https://doi.org/10.1038/nature02656

Zettl, M., Adrain, C., Strisovsky, K., Lastun, V., & Freeman, M. (2011). Rhomboid Family Pseudoproteases Use the ER Quality Control Machinery to Regulate Intercellular Signaling. *Cell*, *145*(1), 79–91. https://doi.org/10.1016/J.CELL.2011.02.047

Zhang, Y., Nijbroek, G., Sullivan, M. L., McCracken, A. A., Watkins, S. C., Michaelis, S., & Brodsky, J. L. (2001). Hsp70 molecular chaperone facilitates endoplasmic reticulum-associated protein degradation of cystic fibrosis transmembrane conductance regulator in yeast. *Molecular Biology of the Cell*, *12*(5), 1303–1314.

Figure 2.2.1 Integral Membrane Protein Overexpression Causes a Growth Defect in *dfm1Δ* Cells in an ERAD Independent Manner

(A) WT, *dfm1*Δ, and *hrd1*Δ cells containing either GAL_{pr}-HMG2-GFP or EV were compared for growth by dilution assay. Each strain was spotted 5-fold dilutions on glucose or galactose-containing plates to drive HMG2-GFP overexpression, and plates were incubated at 30°C. **(B)** Dilution assay as described in (A) except using WT, *dfm1*Δ, and *doa10*Δ cells containing either GAL_{pr}-STE6*-GFP or EV. **(C)** Dilution assay as described in (A) except using WT, *dfm1*Δ, and *hrd1*Δ cells containing either GAL_{pr}-PDR5*-HA or EV. **(D)** Dilution assay as described in (A) except using WT, *dfm1*Δ, and *cdc48-2* cells. **(E)** Dilution assay as described in (B) except using WT, *dfm1*Δ, and *cdc48-2* cells. **(F)** Dilution assay as described in (C) except using WT, *dfm1*Δ, and *cdc48-2* cells. **(G)** Dilution assay as described in (B) except using WT or *dfm1*Δ cells expressing human CFTR, CFTRΔF508, or A1PiZ. All dilution growth assays were performed in 3 biological and 2 technical replicates (N=3).

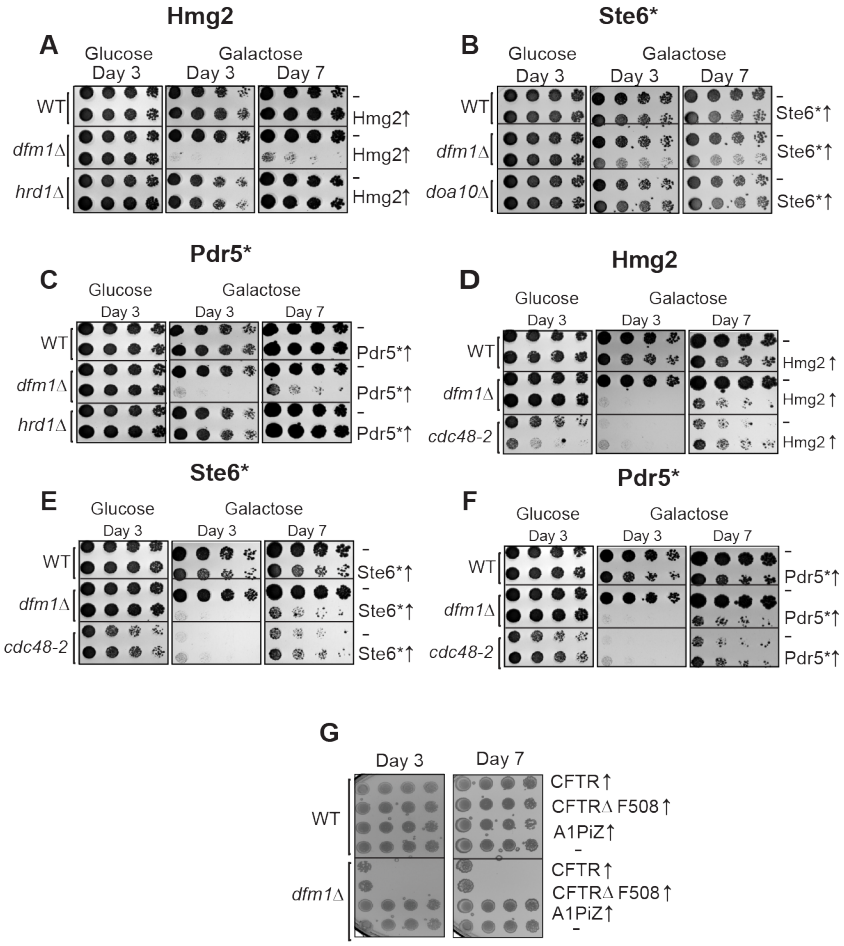
Hmg2
A
Glucose
Day 3
Galactose
Day 3
Day 7
WT
dfm1Δ
hrd1Δ
-
Hmg2↑
-
Hmg2↑
-
Hmg2↑
Ste6*
B
Glucose
Day 3
Galactose
Day 3
Day 7
WT
dfm1Δ
doa10Δ
-
Ste6*↑
-
Ste6*↑
-
Ste6*↑
Pdr5*
C
Glucose
Day 3
Galactose
Day 3
Day 7
WT
dfm1Δ
hrd1Δ
-
Pdr5*↑
-
Pdr5*↑
-
Pdr5*↑
Hmg2
D
Glucose
Day 3
Galactose
Day 3
Day 7
WT
dfm1Δ
cdc48-2
-
Hmg2↑
-
Hmg2↑
-
Hmg2↑
Ste6*
E
Glucose
Day 3
Galactose
Day 3
Day 7
WT
dfm1Δ
cdc48-2
-
Ste6*↑
-
Ste6*↑
-
Ste6*↑
Pdr5*
F
Glucose
Day 3
Galactose
Day 3
Day 7
WT
dfm1Δ
cdc48-2
-
Pdr5*↑
-
Pdr5*↑
-
Pdr5*↑
G
Day 3
Day 7
WT
dfm1Δ
CFTR↑
CFTRΔF508↑
A1PiZ↑
-
CFTR↑
CFTRΔF508↑
A1PiZ↑
-

Figure 2.2.2 Dfm1 Retrotranslocation Defective Mutants Show Differing Abilities to Restore Growth

(A) Depiction of Dfm1, which highlights L1, TM2, TM6, and its SHP box domain. The table indicates the Dfm1 region, amino acid mutation, and the corresponding function that is specifically impaired. All mutants have been previously identified as being required for retrotranslocation and that when mutated did not restore growth in *dfm1*Δ cells expressing an integral membrane protein (GAL_{pr}-HMG2-GFP). **(B)** *dfm1*Δ cells with an add-back of either WT DFM1-HA, EV, DFM1-WA-HA, DFM1-AR-HA, DFM1-Ax3G-HA, or DFM1-Gx3A-HA containing either GAL_{pr}-HMG2-GFP or EV were compared for growth by dilution assay. Each strain was spotted 5-fold dilutions on glucose or galactose-containing plates to drive Hmg2-GFP overexpression, and plates were incubated at 30°C. **(C)** Dilution assay as described in (B) except using an add-back of either WT Dfm1-HA, EV, Dfm1-F57S-HA, Dfm1-L64V-HA, Dfm1-K67E-HA, Dfm1-Q101R-HA, or Dfm1-F107S-HA. **(D)** Depiction of Dfm1 and Dfm1-5Ashp. Dfm1 is an ER-localized membrane proteins with six transmembrane domains. Both versions of Dfm1 have a cytoplasmic shp box, but the 5Ashp mutant is unable to recruit the cytosolic ATPase Cdc48. **(E)** Dilution assay as described in (B) except using add-back of either EV, WT DFM1-HA, or DFM1-5Ashp-HA mutant. **(F)** Dilution Assay as described in (B) except with add-back of human Derlin-1-Myc or Derlin-2-Myc. All dilution growth assays were performed in 3 biological replicates and 2 technical replicates (N=3).

A

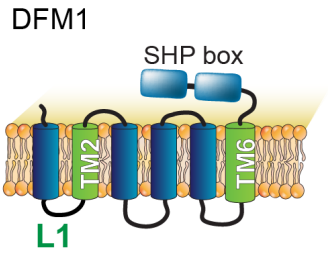

Dfm1 region	mutation	function impacted
L1: WR motif	W63A/R64A	substrate binding
L1	F58S	substrate binding
L1	L64V	substrate binding
L1	K67E	substrate binding
TM2	Q101R/F107S	lipid thinning
TM6:Gx3G motif	G206A/G210A	structural integrity

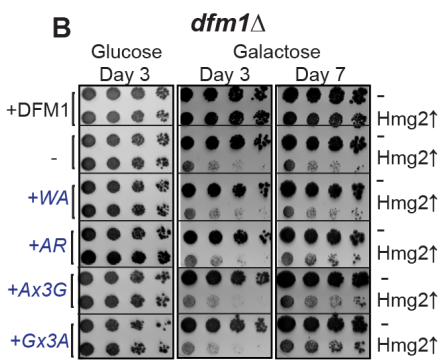

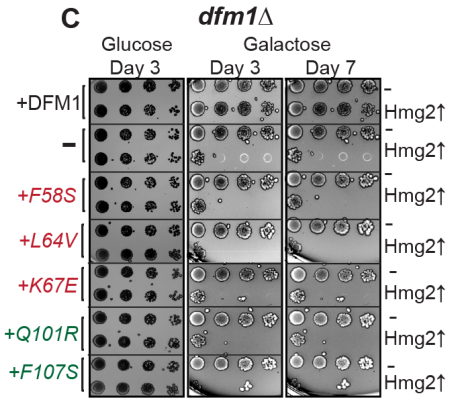

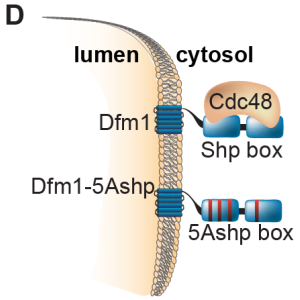

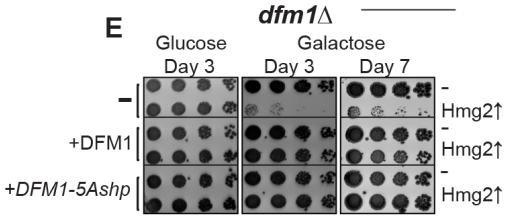

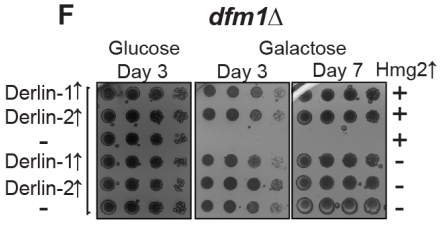

Figure 2.2.3 Dfm1 Reduces Misfolded Membrane Protein Toxicity Through a Chaperone-Like Activity

(A) Western blot of aggregated versus soluble membrane proteins at the ER. Lysates from *dfm1*Δ cells containing HMG2-GFP, with either add-back of WT DFM1-HA, EV, DFM1-5Ashp-HA, DFM1-AR-HA and DFM1-AxxxG-HA were blotted using anti-GFP to detect Hmg2. Top: Total fraction. Middle: ER aggregated fraction. Bottom: ER soluble fraction. **(B)** Western blot of aggregated versus soluble membrane proteins at the ER as in (A) but with add-back of either WT DFM1-HA, EV, DFM1-F58S-HA, DFM1-L64V-HA, DFM1-K67E-HA, DFM1-Q101R-HA, and DFM1-F107S-HA. **(C)** Hmg2-GFP binding to Dfm1-HA was analyzed by Co-IP. As negative control, cells not expressing Hmg2-GFP was used. Also, Sec61 was analyzed as another negative control for non-specific binding (3 biological replicates, N=3). **(D)** Model depicting integrated model of Dfm1's function in misfolded membrane protein stress. Top: Misfolded membrane proteins in the absence of Dfm1 forming aggregates within the ER membrane. Bottom: Cells with WT Dfm1 or 5Ashp-Dfm1 disaggregating misfolded membrane proteins and preventing cellular toxicity. All solubility assays were performed with 3 biological replicates (N=3).

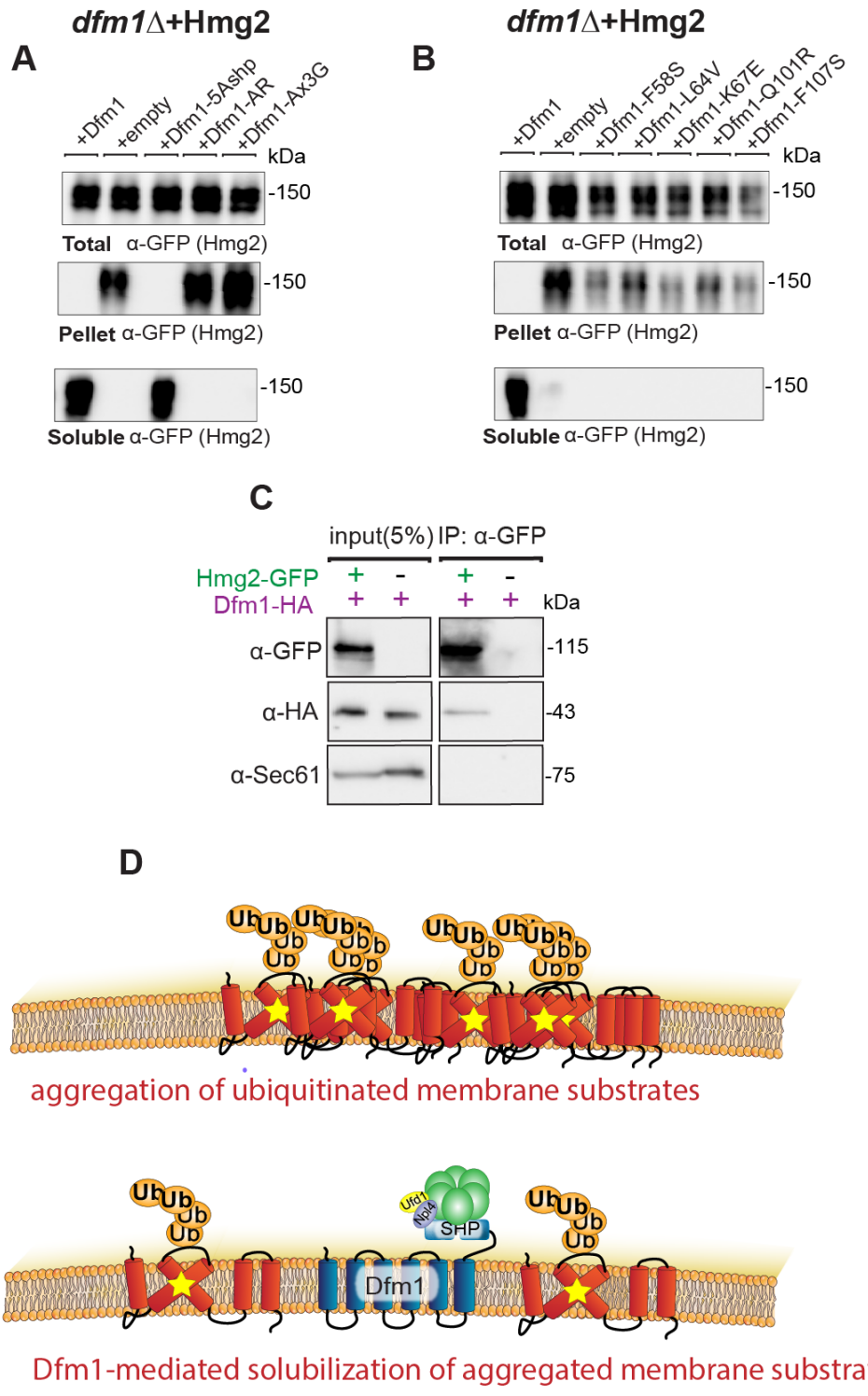
dfm1Δ+Hmg2
A
+Dfm1
+empty
+Dfm1-5Ashp
+Dfm1-AR
+Dfm1-Ax3G
kDa
-150
Total α-GFP (Hmg2)
-150
Pellet α-GFP (Hmg2)
-150
Soluble α-GFP (Hmg2)
dfm1Δ+Hmg2
B
+Dfm1
+empty
+Dfm1-F58S
+Dfm1-L64V
+Dfm1-K67E
+Dfm1-Q101R
+Dfm1-F107S
kDa
-150
Total α-GFP (Hmg2)
-150
Pellet α-GFP (Hmg2)
-150
Soluble α-GFP (Hmg2)
C
input(5%)
IP: α-GFP
Hmg2-GFP
Dfm1-HA
kDa
α-GFP
-115
α-HA
-43
α-Sec61
-75
D
aggregation of ubiquitinated membrane substrates
Ufd1
Npl4
SHP
Dfm1
Dfm1-mediated solubilization of aggregated membrane substrates

Figure 2.2.4 Dfm1 Specifically Influences Solubility of Misfolded Membrane Proteins

(A) Western blot of aggregated versus soluble membrane proteins at the ER. Lysates from WT, *hrd1*Δ, or *hrd1*Δ+HRD1 cells containing HMG2-GFP were blotted using anti-GFP to detect Hmg2. T is total protein, P is ER aggregated fraction, and S is ER soluble fraction. **(B)** Western blot of aggregated versus soluble membrane proteins at the ER as in (A) except with *dfm1*Δ cells containing SEC61-GFP with add-back of EV, WT DFM1-HA, or DFM1-5Ashp-HA. Anti-GFP was used to detect SEC61-GFP. **(C)** Western blot of aggregated versus soluble membrane proteins at the ER as in (A) except with *dfm1*Δ cells containing PDR5*-HA with add-back of WT DFM1-HA or EV. Anti-HA was used to detect PDR5*-HA. **(D)** Western blot of aggregated versus soluble membrane proteins at the ER as in (A) except with *dfm1*Δ cells containing STE6*-GFP with add-back of WT DFM1-HA or EV. Anti-GFP was used to detect STE6*-GFP. **(E)** Western blot of aggregated versus soluble membrane proteins at the ER as in (A) except with *dfm1*Δ cells containing CPY*-GFP with add-back of EV or WT DFM1-HA. Anti-GFP was used to detect CPY*-GFP. **(F)** Western blot of aggregated versus soluble membrane proteins at the ER as in (A) except with *dfm1*Δ cells containing HMG2-GFP with add-back of EV, DERLIN-1-Myc, and DERLIN-2-Myc. Anti-Myc was used to detect DERLIN-1-Myc and DERLIN-2-Myc. Data information: All solubility assays were performed with 3 biological replicates (N=3).

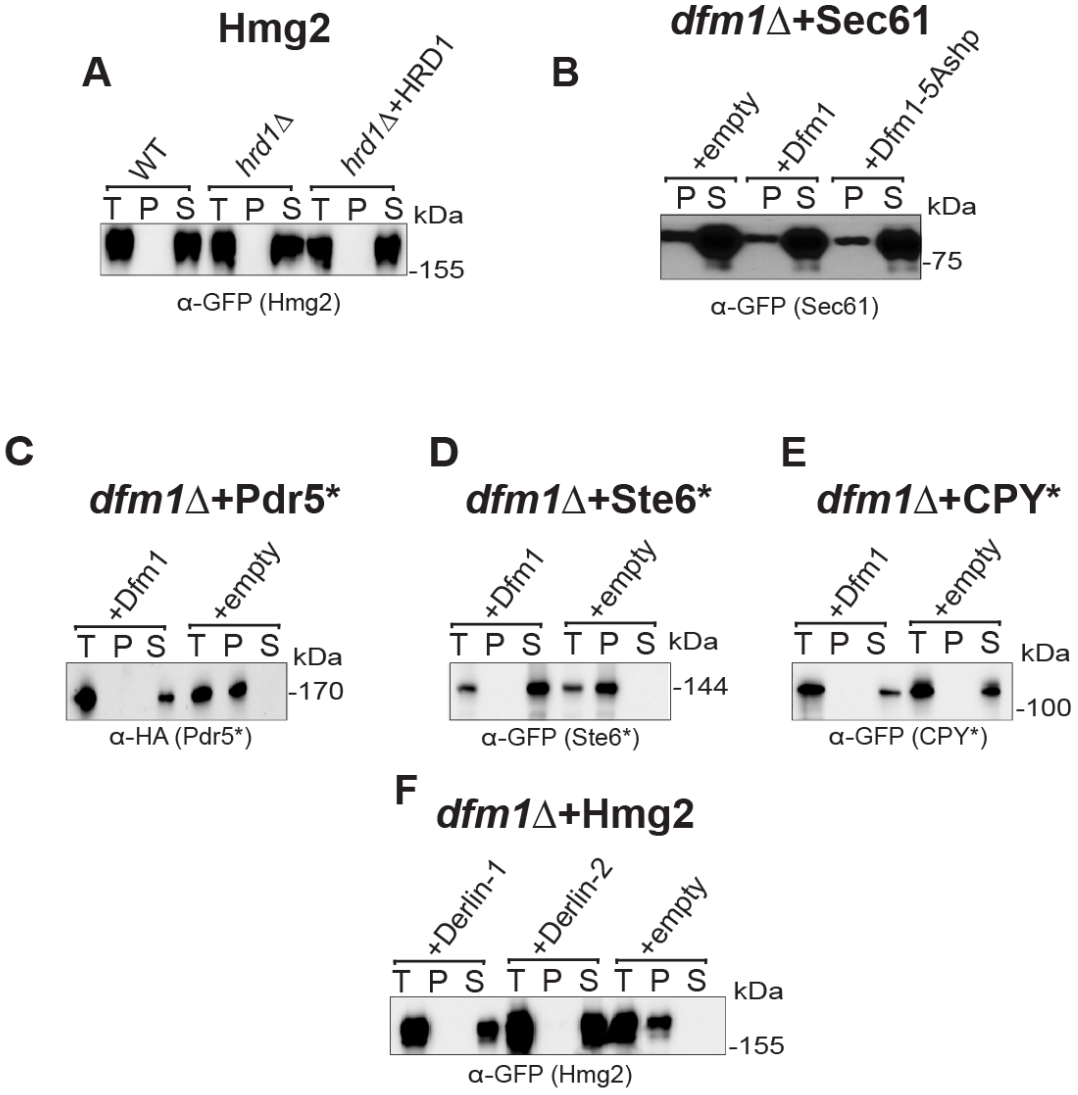
A
Hmg2
WT
hrd1Δ
hrd1Δ+HRD1
T P S T P S T P S kDa
-155
α-GFP (Hmg2)
B
dfm1Δ+Sec61
+empty
+Dfm1
+Dfm1-5Ashp
P S P S P S kDa
-75
α-GFP (Sec61)
C
dfm1Δ+Pdr5*
+Dfm1
+empty
T P S T P S kDa
-170
α-HA (Pdr5*)
D
dfm1Δ+Ste6*
+Dfm1
+empty
T P S T P S kDa
-144
α-GFP (Ste6*)
E
dfm1Δ+CPY*
+Dfm1
+empty
T P S T P S kDa
-100
α-GFP (CPY*)
F
dfm1Δ+Hmg2
+Derlin-1
+Derlin-2
+empty
T P S T P S T P S kDa
-155
α-GFP (Hmg2)

Figure 2.2.5 Misfolded Membrane Protein Stress in *dfm1Δ* Cells Does Not Activate the Unfolded Protein Response

(A) UPR activation for indicated strains with overexpression of a misfolded integral membrane protein. *pdr5*Δ cells containing GAL_{pr}-Hmg2-6MYC and 4xUPRE-GFP (a reporter that expresses GFP with activation of the UPR) were measured for GFP expression using flow cytometry every hour for 5 hours starting at the point of galactose induction and tunicamycin or equivalent volume of DMSO was added at the 1-hour timepoint. Figure depicts the GFP fluorescence in arbitrary units (A.U.) for indicated conditions 5 hours post-galactose addition. In figure legend, “Gal” indicates addition of 0.2% galactose to cultures and “Raf” indicates addition of 0.2% raffinose to culture, and “Tm" indicates tunicamycin presence (+) or absence (-) of 2ug/mL tunicamycin **(B)** Flow cytometry based UPR activation assay as described in (A) except using *dfm1*Δ cells. **(C) (E)** and **(G)** Flow cytometry based UPR activation assay as described in (A) except using cells containing GAL_{pr}-Ste6*-GFP, GAL_{pr}-CPY*-HA, or EV, respectively. **(D) (F)** and **(H)** Flow cytometry based UPR activation assay as described in (B) except using cells containing GAL_{pr}-Ste6*-GFP, GAL_{pr}-CPY*-HA, or EV, respectively. Data information: All data are measured mean ± SEM; N=3 biological replicates.

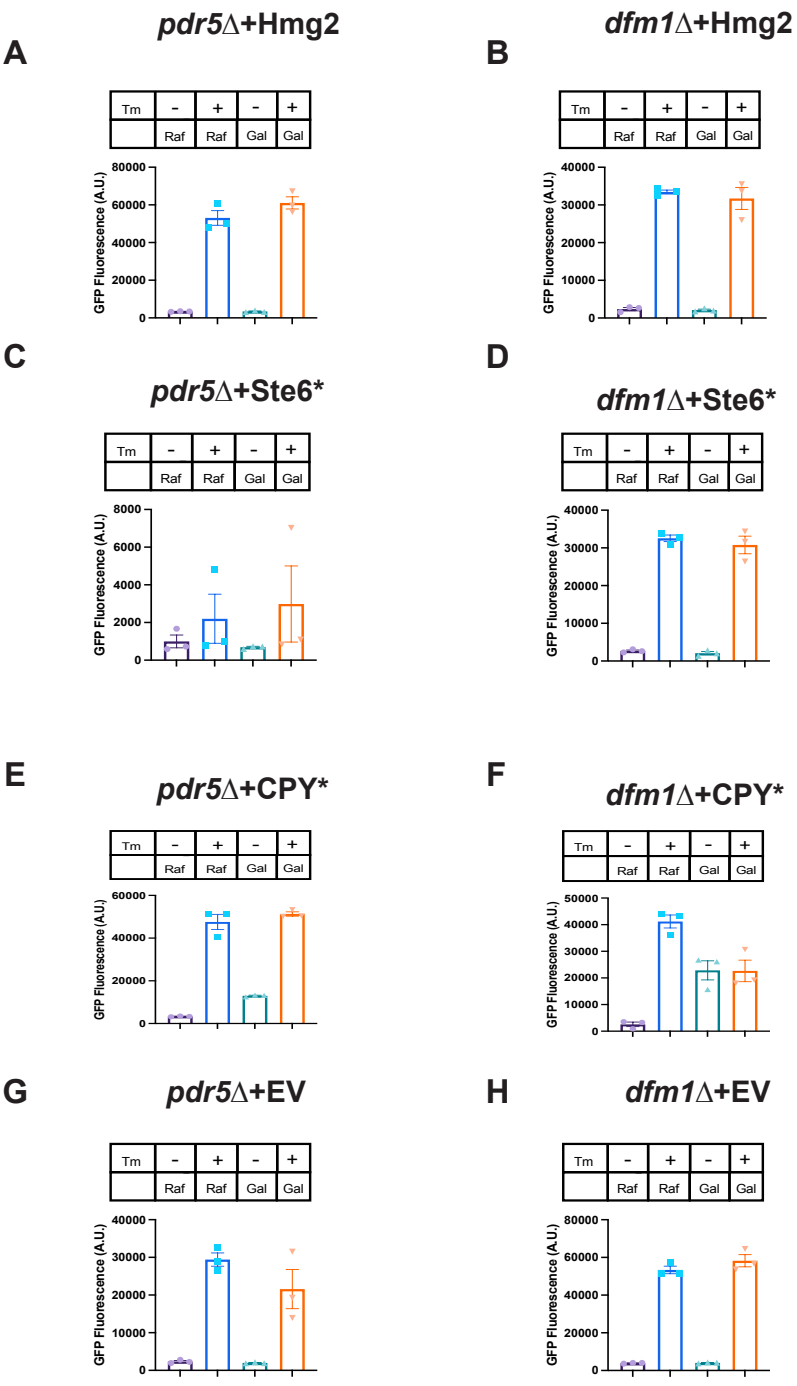
A
pdr5Δ+Hmg2
Tm - + - +
Raf Raf Gal Gal
GFP Fluorescence (A.U.)
80000
60000
40000
20000
0
B
dfm1Δ+Hmg2
Tm - + - +
Raf Raf Gal Gal
GFP Fluorescence (A.U.)
40000
30000
20000
10000
0
C
pdr5Δ+Ste6*
Tm - + - +
Raf Raf Gal Gal
GFP Fluorescence (A.U.)
8000
6000
4000
2000
0
D
dfm1Δ+Ste6*
Tm - + - +
Raf Raf Gal Gal
GFP Fluorescence (A.U.)
40000
30000
20000
10000
0
E
pdr5Δ+CPY*
Tm - + - +
Raf Raf Gal Gal
GFP Fluorescence (A.U.)
60000
40000
20000
0
F
dfm1Δ+CPY*
Tm - + - +
Raf Raf Gal Gal
GFP Fluorescence (A.U.)
50000
40000
30000
20000
10000
0
G
pdr5Δ+EV
Tm - + - +
Raf Raf Gal Gal
GFP Fluorescence (A.U.)
40000
30000
20000
10000
0
H
dfm1Δ+EV
Tm - + - +
Raf Raf Gal Gal
GFP Fluorescence (A.U.)
80000
60000
40000
20000
0

Figure 2.2.6 Misfolded Membrane Protein Toxicity Results in Proteasome Impairment

(A) WT, *dfm1*Δ, and *rpn4Δ* cells containing either GAL_{pr}-HMG2-GFP or EV were compared for growth by dilution assay. Each strain was spotted 5-fold dilutions on glucose or galactose-containing plates to drive Hmg2-GFP overexpression, and plates were incubated at 30°C. 3 biological replicates and 2 technical replicates (N=3) **(B)** PRE6-GFP levels as measured by flow cytometry at 0 versus 5 hours post-galactose induction in WT cells containing either EV, GAL_{pr}-CPY*-HA, orGAL_{pr}-HMG2-GFP. **(C)** Pre6-GFP levels as in (B) except in *dfm1*Δ cells. **(D)** Quantification of colony forming units (CFUs) formed on appropriate selection plates from proteasome sensitivity inhibition assay. *pdr5*Δ cells containing SUS-GFP or EV in log phase were treated with 25uM of proteasome inhibitor MG132 or equivalent volume of DMSO for 8 hours and samples were diluted 1:500 and 50uL of each sample was plated. **(E)** Proteasome sensitivity assay as in (D) except using *hrd1*Δ*pdr5*Δ cells. **(F)** Proteasome sensitivity assay as in (D) except using *dfm1*Δ*hrd1*Δ*pdr5*Δ cells. Data information: For (B) and (C), all data are mean ± SEM, with 7 biological replicates (N=7). For (D), (E), and (F), all data are mean ± SEM, 3 biological replicates and 2 technical replicates (N=3); statistical significance is displayed as two-tailed unpaired t test, *$P<0.05$, ns, not significant.

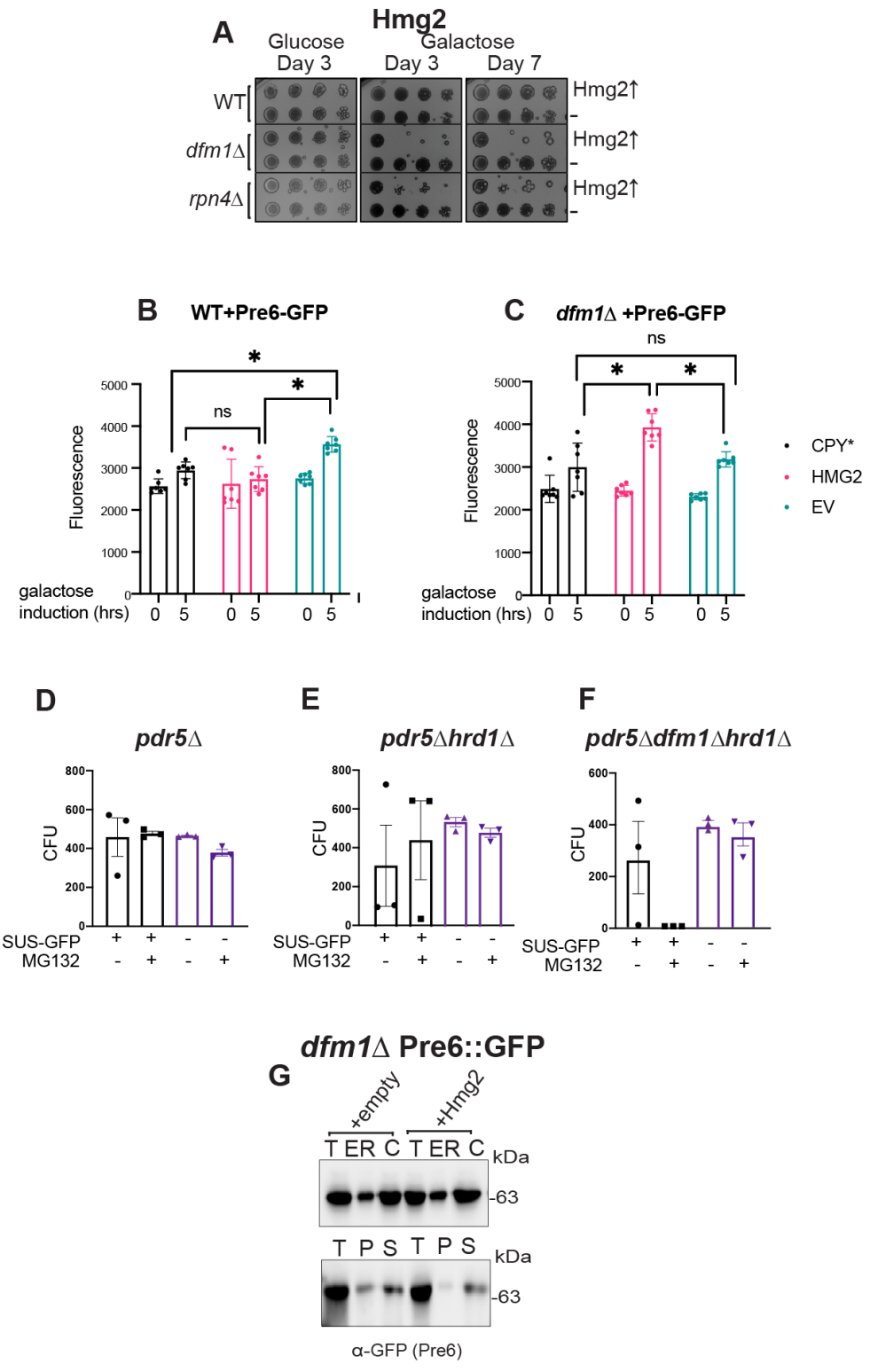
A
Hmg2
Glucose
Day 3
Galactose
Day 3
Day 7
WT
dfm1Δ
rpn4Δ
Hmg2↑
-
B
WT+Pre6-GFP
C
dfm1Δ +Pre6-GFP
Fluorescence
galactose
induction (hrs)
ns
CPY*
HMG2
EV
D
pdr5Δ
E
pdr5Δhrd1Δ
F
pdr5Δdfm1Δhrd1Δ
CFU
SUS-GFP
MG132
G
dfm1Δ Pre6::GFP
+empty
+Hmg2
T ER C T ER C
kDa
-63
T P S T P S
α-GFP (Pre6)

Figure 2.2.7 Ubiquitin Stress Contributes to Misfolded Membrane Protein Toxicity

(A) WT, *dfm1*Δ, *dfm1*Δ*hrd1*Δ and *dfm1*Δ*doa10*Δ cells containing either GAL_{pr}-Hmg2-GFP, GAL_{pr}-STE6*-GFP, or EV. were compared for growth by dilution assay. Each strain was spotted 5-fold dilutions on glucose or galactose-containing plates to drive Hmg2-GFP overexpression, and plates were incubated at 30°C. **(B)** Indicated strains expressing either Hmg2-GFP or Ste6*-GFP were grown to log-phase, lysed, and microsomes were collected and immunoprecipitated with α-GFP conjugated to agarose beads. Sample were then subjected to SDS-PAGE and immunoblot by α-Ubiquitin and α-GFP. 3 biological replicates (N=3). **(C)** Dilution assay as described in (A) except using WT and *dfm1*Δ cells containing either GAL_{pr}-Hmg2-GFP, GAL_{pr}-Hmg2-K6R-GFP, GAL_{pr}-Hmg2-K357R-GFP, GAL_{pr}-Hmg2-(K6R and K357R)-GFP or EV. **(D)** WT and *dfm1*Δ cells containing either $CUP1_{pr}$-Ub or EV and GAL_{pr}-HMG2-GFP or EV were compared for growth by dilution assay. Each strain was spotted 5-fold dilutions on glucose or galactose-containing plates to drive Hmg2-GFP overexpression, and plates were incubated at 30°C. Galactose plates containing 50uM Cu2+ were used to allow expression of Ub driven by the CUP1 promoter. **(E)** Western blot of monomeric ubiquitin in WT, *dfm1*Δ, and *hrd1*Δ expressing HMG2-GFP. Anti-ubiquitin was used to blot for ubiquitin and anti-PGK1 was used to blot for PGK1 as a loading control. **(F)** Quantification of western blots from (E). Each strain was normalized to PGK1 and the monomeric ubiquitin quantification of WT+HMG2-GFP was used to normalize all strains. **(G)** Dilution assay as described in (A) *dfm1*Δ, *ubp9Δ, ubp14Δ,* and *doa4Δ* cells. **(H)** Dilution assay as described in (A) except using WT, *dfm1*Δ, and *ubp6Δ* cells containing either GAL_{pr}-HMG2-GFP or EV. **(H)** Western blot of aggregated versus soluble membrane proteins at the ER. Lysates from *dfm1*Δ cells containing HMG2-GFP or HMG2-K6R-GFP with EV or DFM1-HA were blotted using anti-GFP to detect Hmg2. T is total fraction, P is ER aggregated fraction, and S is ER soluble fraction. Data information: All dilution growth assays were performed in 3 biological replicates and 2 technical replicates (N=3). For (F), all data are mean ± SEM, 3 biological replicates (N=3); statistical significance is displayed as two-tailed unpaired t test, *$P<0.05$, ns, not significant. Solubility assay in (H) was performed with 3 biological replicates (N=3).

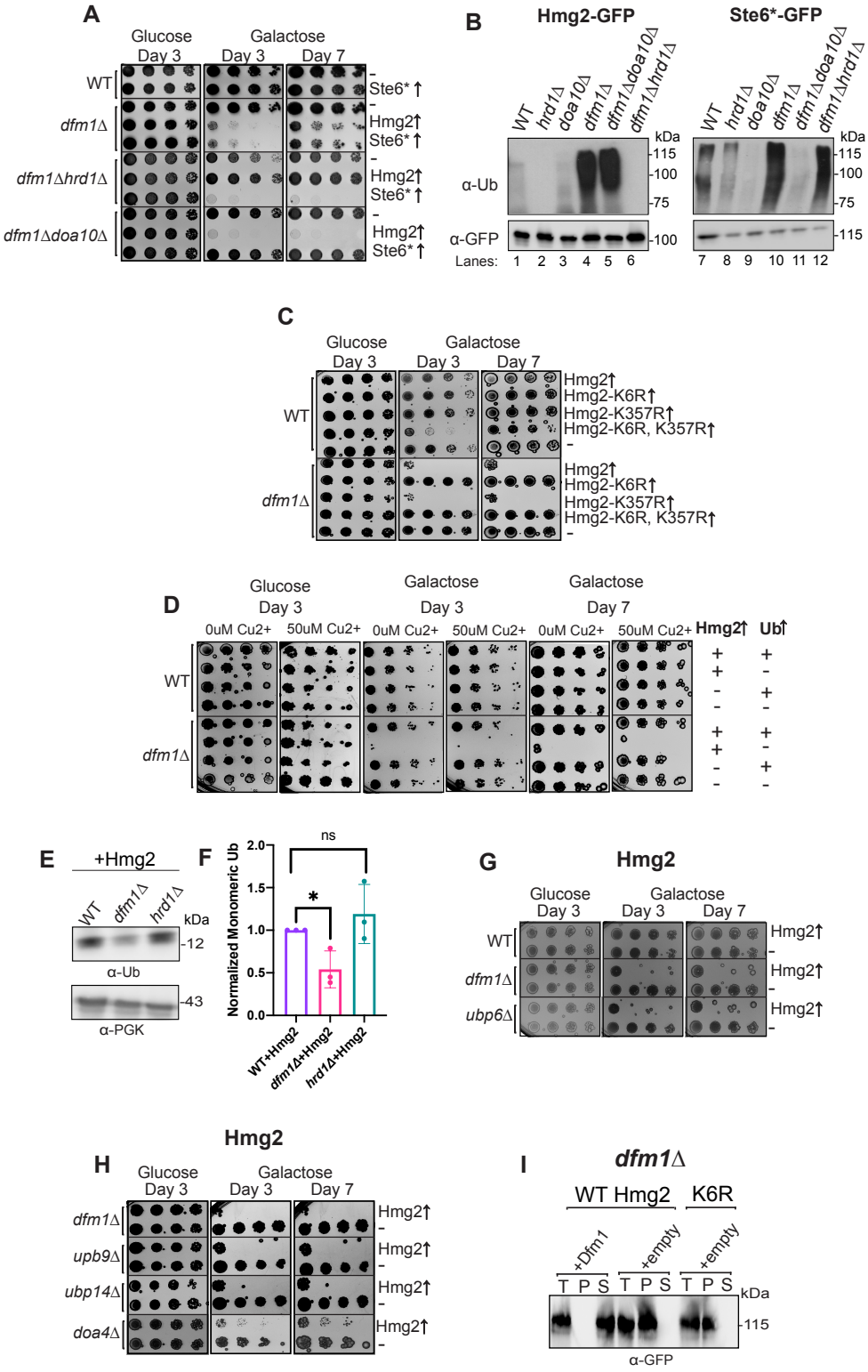
A
Glucose
Day 3
Galactose
Day 3
Day 7
WT
dfm1Δ
dfm1Δhrd1Δ
dfm1Δdoa10Δ
Ste6*↑
Hmg2↑
Ste6*↑
B
Hmg2-GFP
Ste6*-GFP
WT
hrd1Δ
doa10Δ
dfm1Δ
dfm1Δdoa10Δ
dfm1Δhrd1Δ
kDa
115
100
75
α-Ub
α-GFP
100
115
Lanes: 1 2 3 4 5 6 7 8 9 10 11 12
C
Glucose
Day 3
Galactose
Day 3
Day 7
WT
dfm1Δ
Hmg2↑
Hmg2-K6R↑
Hmg2-K357R↑
Hmg2-K6R, K357R↑
D
Glucose
Day 3
Galactose
Day 3
Galactose
Day 7
0uM Cu2+
50uM Cu2+
Hmg2↑
Ub↑
E
+Hmg2
WT
dfm1Δ
hrd1Δ
kDa
12
α-Ub
43
α-PGK
F
Normalized Monomeric Ub
ns
*
WT+Hmg2
dfm1Δ+Hmg2
hrd1Δ+Hmg2
G
Hmg2
Glucose
Day 3
Galactose
Day 3
Day 7
WT
dfm1Δ
ubp6Δ
Hmg2↑
H
Hmg2
Glucose
Day 3
Galactose
Day 3
Day 7
dfm1Δ
upb9Δ
ubp14Δ
doa4Δ
Hmg2↑
I
dfm1Δ
WT Hmg2
K6R
+Dfm1
+empty
+empty
T P S T P S T P S
kDa
115
α-GFP

Figure 2.2.8 Model for misfolded membrane protein-induced toxicity

A model depicting how accumulation of ER-resident misfolded membrane proteins would induce growth toxicity. 1) No growth toxicity is observed when misfolded membrane proteins aggregate but are not ubiquitinated. 2) No growth toxicity is observed when misfolded membrane proteins are ubiquitinated, but not aggregated. 3) Growth toxicity is observed when misfolded membrane proteins are both ubiquitinated and aggregated.

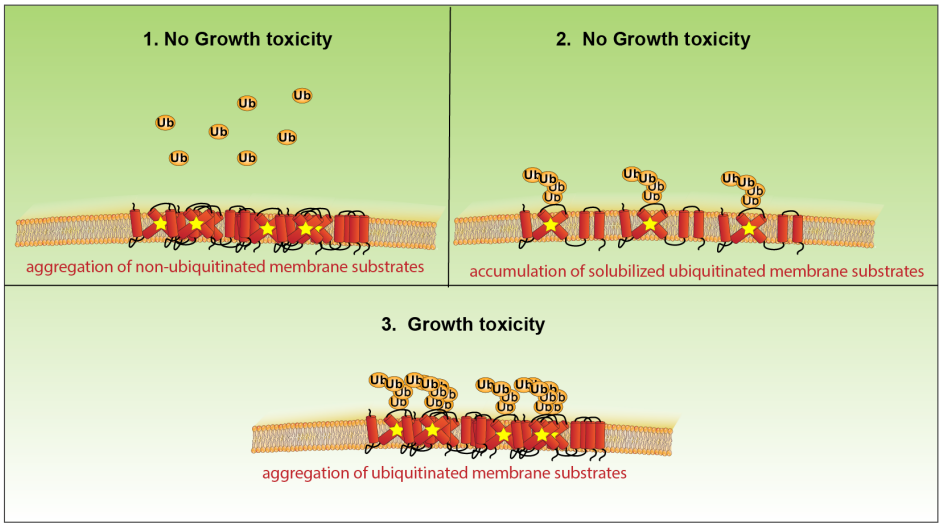
1. No Growth toxicity
Ub
aggregation of non-ubiquitinated membrane substrates
2. No Growth toxicity
accumulation of solubilized ubiquitinated membrane substrates
3. Growth toxicity
aggregation of ubiquitinated membrane substrates

Supplemental Figure 2.2.1 Hmg2-GFP Microscopy Puncta are Unaffected by Dfm1

(A) & (B) WT and *cdc48-2* strains were grown into log-phase at 30ºC and degradation was measured by cycloheximide chase (CHX). After CHX addition, cells were lysed at the indicated times, and analyzed by SDS-PAGE and immunoblotted for Pdr5*-HA with α-HA and Ste6*-GFP with α-GFP. 3 biological replicates (N=3). **(C)** Steady-state levels of Dfm1 and corresponding Dfm1 mutants from *dfm1*Δ cells containing GAL_{pr}-HMG2-GFP that were used for growth assays in Figure 2. Cells were analyzed by SDS-PAGE and immunoblotted with α-HA. 3 biological replicates (N=3). **(D)** Representative confocal microscopy images of Hmg2-GFP in *dfm1*Δ cells with add-back of EV, WT DFM1, and DFM1-5Ashp. Five biological replicates were imaged, and three images were taken of each strain (N=5). **(E)** Fraction of Hmg2-GFP in puncta for *dfm1*Δ cells with add-back of WT DFM1, EV, and DFM1-5Ashp. Each dot represents an individual cell. **(F)** Number of puncta per cell for *dfm1*Δ cells with add-back of WT DFM1, EV, and DFM1-5Ashp. Each dot represents an individual cell.

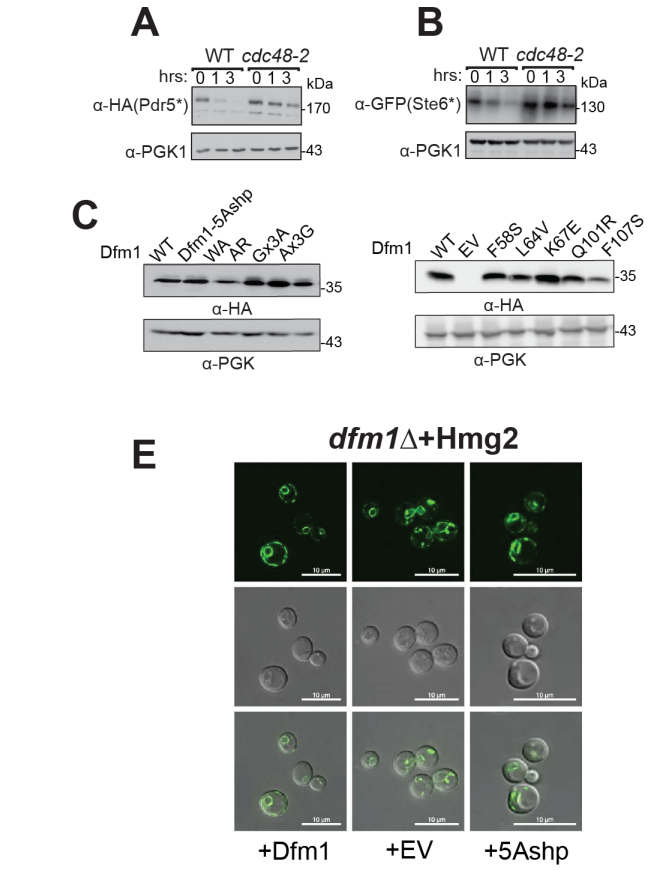
A
WT cdc48-2
hrs: 0 1 3 0 1 3
kDa
α-HA(Pdr5*)
170
α-PGK1
43
B
WT cdc48-2
hrs: 0 1 3 0 1 3
kDa
α-GFP(Ste6*)
130
α-PGK1
43
C
Dfm1 WT Dfm1-5Ashp WA AR Gx3A Ax3G
35
α-HA
43
α-PGK
Dfm1 WT EV F58S L64V K67E Q101R F107S
35
α-HA
43
α-PGK
E
dfm1Δ+Hmg2
+Dfm1
+EV
+5Ashp
E
Fraction Fluorescence in Puncta
1.0
0.5
0.0
+EV
+Dfm1
+Dfm1-5Ashp1
F
Number of Puncta
50
40
30
20
10
0
+EV
+Dfm1
+Dfm1-5Ashp1

Supplemental Figure 2.2.2 Transcriptional Changes in Membrane Protein Stressed *dfm1Δ* Cells

(A) *pdr5*Δ, *pdr5*Δ*dfm1*Δ, and *pdr5*Δ*hrd1*Δ cells containing either GAL_{pr}-HMG2-GFP or EV were compared for growth by dilution assay. Each strain was spotted 5-fold dilutions on glucose or galactose-containing plates to drive HMG2-GFP overexpression, and plates were incubated at 30°C. 3 biological replicates and 2 technical replicates (N=3). **(B)** Principal component 1 (PC1) and principal component 2 (PC2) values of each of the 2 biological replicates (N=2) of RNA-seq samples for *pdr5Δ, dfm1Δpdr5Δ*, and *hrd1Δpdr5Δ* cells containing either GAL_{pr}-HMG2-GFP or EV. **(C)** PC1 and PC2 of sorted top 100 highest PC1 value genes from both replicates of *dfm1Δpdr5Δ* cells containing GAL_{pr}-HMG2-GFP. Red dots indicate Rpn4 target genes. Table indicates upregulated genes that are targeted by Rpn4. **(D)** Top 10 gene ontology (GO) terms and their enrichment factor for the set of 100 upregulated genes with the highest PC1 scores. (**E)** Top 10 gene ontology (GO) terms and their enrichment factor for the set of 100 downregulated genes with the lowest PC1 scores.

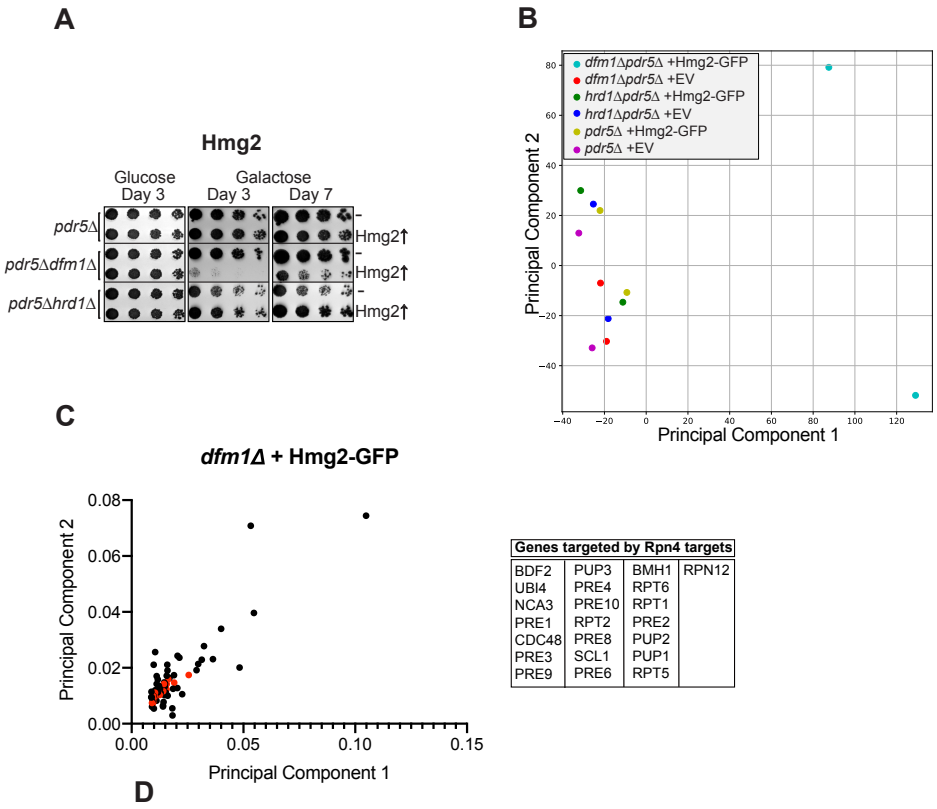
A
Hmg2
Glucose
Day 3
Galactose
Day 3
Day 7
pdr5Δ
pdr5Δdfm1Δ
pdr5Δhrd1Δ
-
Hmg2↑
B
dfm1Δpdr5Δ +Hmg2-GFP
dfm1Δpdr5Δ +EV
hrd1Δpdr5Δ +Hmg2-GFP
hrd1Δpdr5Δ +EV
pdr5Δ +Hmg2-GFP
pdr5Δ +EV
Principal Component 2
Principal Component 1
C
dfm1Δ + Hmg2-GFP
Principal Component 2
Principal Component 1
Genes targeted by Rpn4 targets
BDF2 PUP3 BMH1 RPN12
UBI4 PRE4 RPT6
NCA3 PRE10 RPT1
PRE1 RPT2 PRE2
CDC48 PRE8 PUP2
PRE3 SCL1 PUP1
PRE9 PRE6 RPT5
D
Top 10 upregulated GO terms
Proteasomal Ubiquitin-Independent Protein Catabolic Process
Regulation of Endopeptidase Activity
Proteasome Regulatory Particle Assembly
Proteasome Assembly
Regulation of Peptidase Activity
Positive Regulation of Proteolysis
Protein Refolding
'De Novo' Protein Folding
Proteasome-Mediated Ubiquitin-Dependent Protein Catabolic Proccess
Regulation of Proteolysis
Fold Enrichment
E
Top 10 downregulated GO terms
rRNA Export from Nucleus
rRNA Transport
Translational Termination
Cellular Protein Complex DIsassembly
Cytoplasmic Translation
Protein Containing Complex Disassembly
ncRNA Export from Nucleus
Cellular Componenent Dissassembly
Ribosomal Small Subunit Biogenesis
Translation
Fold Enrichment

Supplemental Figure 2.2.3 Misfolded Membrane Protein Stress in *dfm1Δ* Cells Does Not Affect Hac1 Splicing

(A) PCR products of spliced and unspliced Hac1 transcripts. *pdr5*Δ cells containing GAL_{pr}-Hmg2-6MYC, GAL_{pr}-Ste6*-GFP, GAL_{pr}-CPY*-HA, or EV were treated with 0.2% galactose and 2ug/mL tunicamycin (+) or an equivalent volume of DMSO. RNA was extracted from cells and cDNA was generated and used as a template for PCR. uHac1 represents unspliced Hac1 transcripts and sHac1 represents spliced Hac1. **(B)** Hac1 splicing assay as in (A) except using *dfm1*Δ cells. 3 biological replicates (N=3).

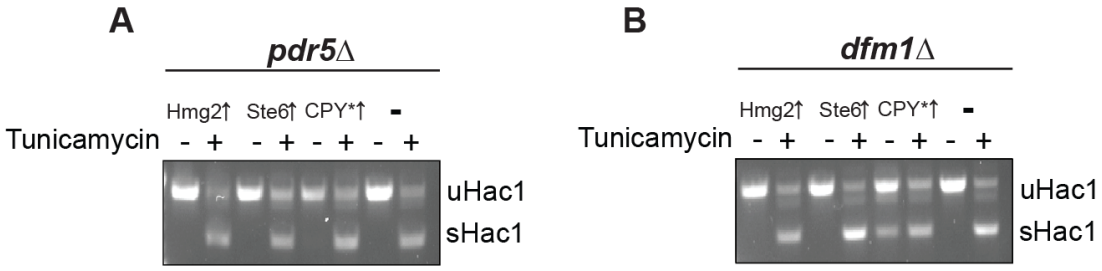
A
pdr5Δ
Hmg2↑ Ste6↑ CPY*↑ -
Tunicamycin - + - + - + - +
uHac1
sHac1
B
dfm1Δ
Hmg2↑ Ste6↑ CPY*↑ -
Tunicamycin - + - + - + - +
uHac1
sHac1

Supplemental Figure 2.2.4 *Rpn4Δ* Toxicity is Specific to Misfolded Membrane Proteins

(A) WT, *dfm1*Δ, and *rpn4Δ* cells containing either GAL_{pr}-STE6*-GFP or EV were compared for growth by dilution assay. Each strain was spotted 5-fold dilutions on glucose or galactose-containing plates to drive Ste6*-GFP overexpression, and plates were incubated at 30°C. **(B)** Dilution assay as depicted in (A) except using cells containing GAL_{pr}-CPY*-HA or EV. **(C)** Dilution assay as described in (A) except using WT, *dfm1*Δ, and *pdr1Δ* cells containing either GAL_{pr}-HMG2-GFP or EV. Data information: All dilution growth assays were performed in 3 biological and 2 technical replicates (N=3).

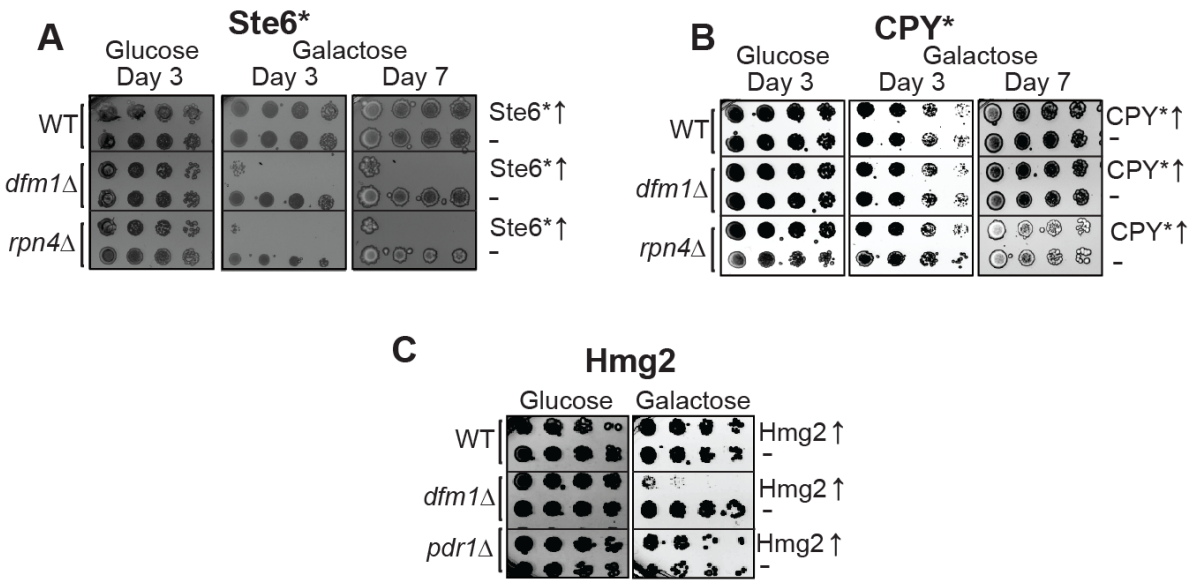
A
Ste6*
Glucose
Day 3
Galactose
Day 3
Day 7
WT
dfm1Δ
rpn4Δ
Ste6*↑
-
Ste6*↑
-
Ste6*↑
-
B
CPY*
Glucose
Day 3
Galactose
Day 3
Day 7
WT
dfm1Δ
rpn4Δ
CPY*↑
-
CPY*↑
-
CPY*↑
-
C
Hmg2
Glucose
Galactose
WT
dfm1Δ
pdr1Δ
Hmg2↑
-
Hmg2↑
-
Hmg2↑
-

Supplemental Figure 2.2.5 *Ubp6Δ* Toxicity is Specific to Misfolded Membrane Proteins

(A) Western blot of monomeric ubiquitin in WT, *dfm1*Δ, and *hrd1*Δ cells. Anti-ubiquitin was used to blot for ubiquitin and anti-PGK1 was used to blot for PGK1 as a loading control. **(B)** Quantification of western blots from (A). Each strain was normalized to PGK1 and the monomeric ubiquitin quantification of WT was used to normalize all strains. **(C)** WT, *dfm1*Δ, and *ubp6Δ* cells containing either GAL_{pr}-STE6*-GFP or EV were compared for growth by dilution assay. Each strain was spotted 5-fold dilutions on glucose or galactose-containing plates to drive Ste6*-GFP overexpression, and plates were incubated at 30°C. **(D)** Dilution assay as depicted in (C) except using cells containing GAL_{pr}-CPY*-HA or EV. All dilution growth assays were performed in 3 biological and 2 technical replicates (N=3). For (B), all data are mean ± SEM, 3 biological replicates (N=3); statistical significance is displayed as two-tailed unpaired t test, ns, not significant.

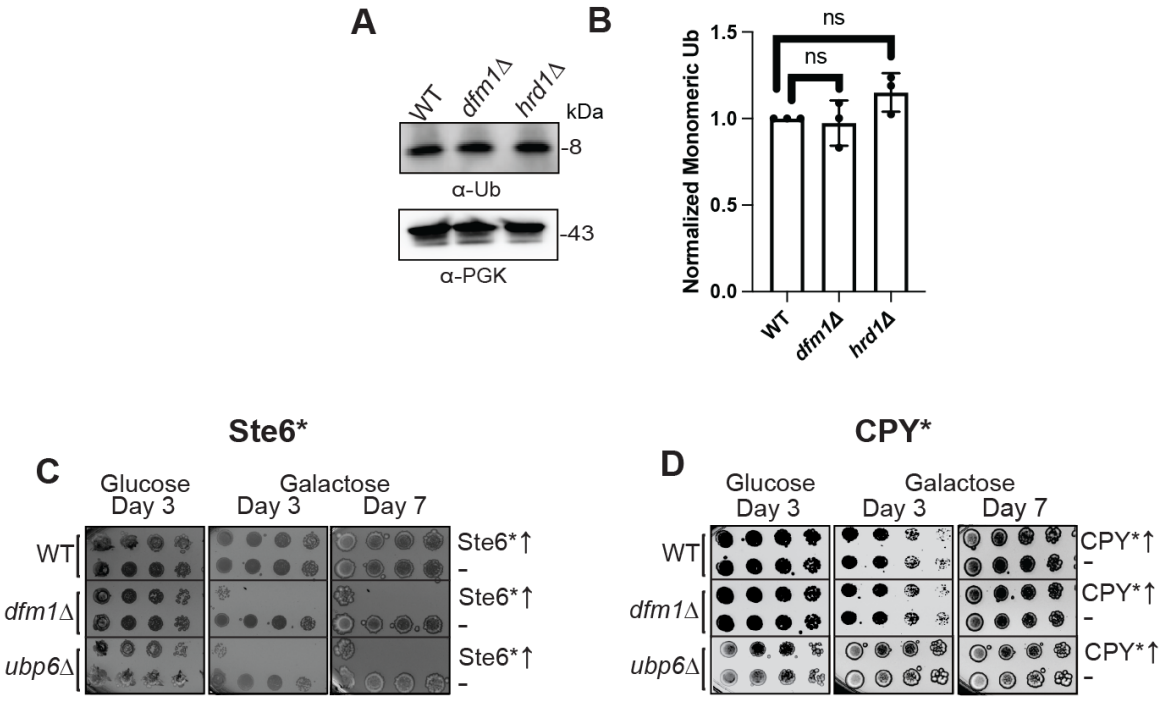
A
B
WT
dfm1Δ
hrd1Δ
kDa
-8
α-Ub
-43
α-PGK
ns
ns
Normalized Monomeric Ub
1.5
1.0
0.5
0.0
WT
dfm1Δ
hrd1Δ
Ste6*
CPY*
C
D
Glucose
Day 3
Galactose
Day 3
Day 7
WT
dfm1Δ
ubp6Δ
Ste6*↑
-
CPY*↑

Supplemental Figure 2.2.6 Not All Deubiquitinates Mediate Misfolded Membrane Toxicity and Toxicity is Specific to Misfolded Membrane Proteins

(A) WT, *dfm1*Δ, and *doa4Δ* cells containing either GAL_{pr}-HMG2-GFP or EV were compared for growth by dilution assay. Each strain was spotted 5-fold dilutions on glucose or galactose-containing plates to drive Hmg2-GFP overexpression, and plates were incubated at 30°C. **(B)** Dilution assay as in **(A)** except in *dfm1*Δ, *ubp2*Δ, *ubp5*Δ, *miy1*Δ, *ubp8*Δ, *miy2*Δ, *otu2*Δ, *ubp1*Δ, *ubp11*Δ, *ubp7*Δ, and *ubp3*Δ cells. **(C)** WT, *dfm1*Δ, *ubp6Δ, doa4Δ, ubp9Δ,* and *ubp14Δ* cells containing either GAL_{pr}- ΔssCPY*-MYC or EV were compared for growth by dilution assay. Each strain was spotted 5-fold dilutions on glucose or galactose-containing plates to drive Hmg2-GFP overexpression, and plates were incubated at 30°C. All dilution growth assays were performed in 3 biological and 2 technical replicates (N=3).

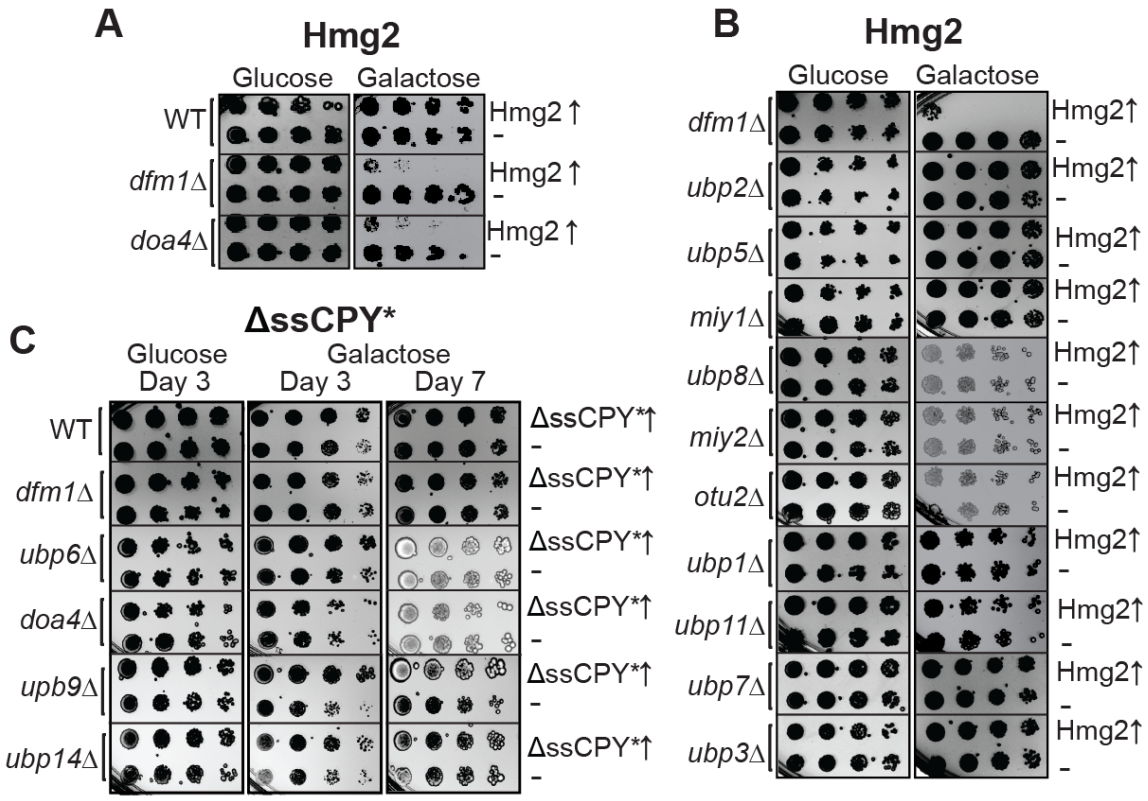
A
Hmg2
Glucose
Galactose
WT
dfm1Δ
doa4Δ
Hmg2↑
-
B
Hmg2
Glucose
Galactose
dfm1Δ
ubp2Δ
ubp5Δ
miy1Δ
ubp8Δ
miy2Δ
otu2Δ
ubp1Δ
ubp11Δ
ubp7Δ
ubp3Δ
Hmg2↑
-
C
ΔssCPY*
Glucose
Day 3
Galactose
Day 3
Day 7
WT
dfm1Δ
ubp6Δ
doa4Δ
upb9Δ
ubp14Δ
ΔssCPY*↑
-

Supplemental Figure 2.2.7 Genetic Interactions Between Dfm1, Rpn4, and Ubp6 in Resolving Misfolded Membrane Protein Toxicity

(A) *dfm1*Δ, *dfm1*Δ*rpn4Δ*, *dfm1*Δ*ubp6Δ,* and *rpn4Δubp6Δ* cells containing either GAL_{pr}-HMG2-GFP or EV were compared for growth by dilution assay. Each strain was spotted 5-fold dilutions on glucose or galactose-containing plates to drive Hmg2-GFP overexpression, and plates were incubated at 30°C. **(B)** Dilution Assays as depicted in **(A)** except using cells containing GAL_{pr}-STE6*-GFP. **(C)** Dilution Assays as depicted in (A) except using cells containing GAL_{pr}-CPY*. **(D)** *dfm1*Δ, *rpn4Δ*, and *ubp6Δ* cells containing either GAL_{pr}-Hmg2-GFP or EV and GAL_{pr}-Dfm1-10xHis or EV were compared for growth by dilution assay. Each strain was spotted 5-fold dilutions on glucose or galactose-containing plates to drive Hmg2-GFP and Dfm1-10xHis overexpression, and plates were incubated at 30°C. **(E)** Dilution assay as described in **(A)** except using *rpn4*Δ and *ubp6*Δ cells containing either GAL_{pr}-Hmg2-GFP, GAL_{pr}-Hmg2 (K6R)-GFP, GAL_{pr}-Hmg2 (K357R)-GFP, GAL_{pr}-Hmg2 (K6R and K357R)-GFP or EV. All dilution growth assays were performed in 3 biological and 2 technical replicates (N=3).

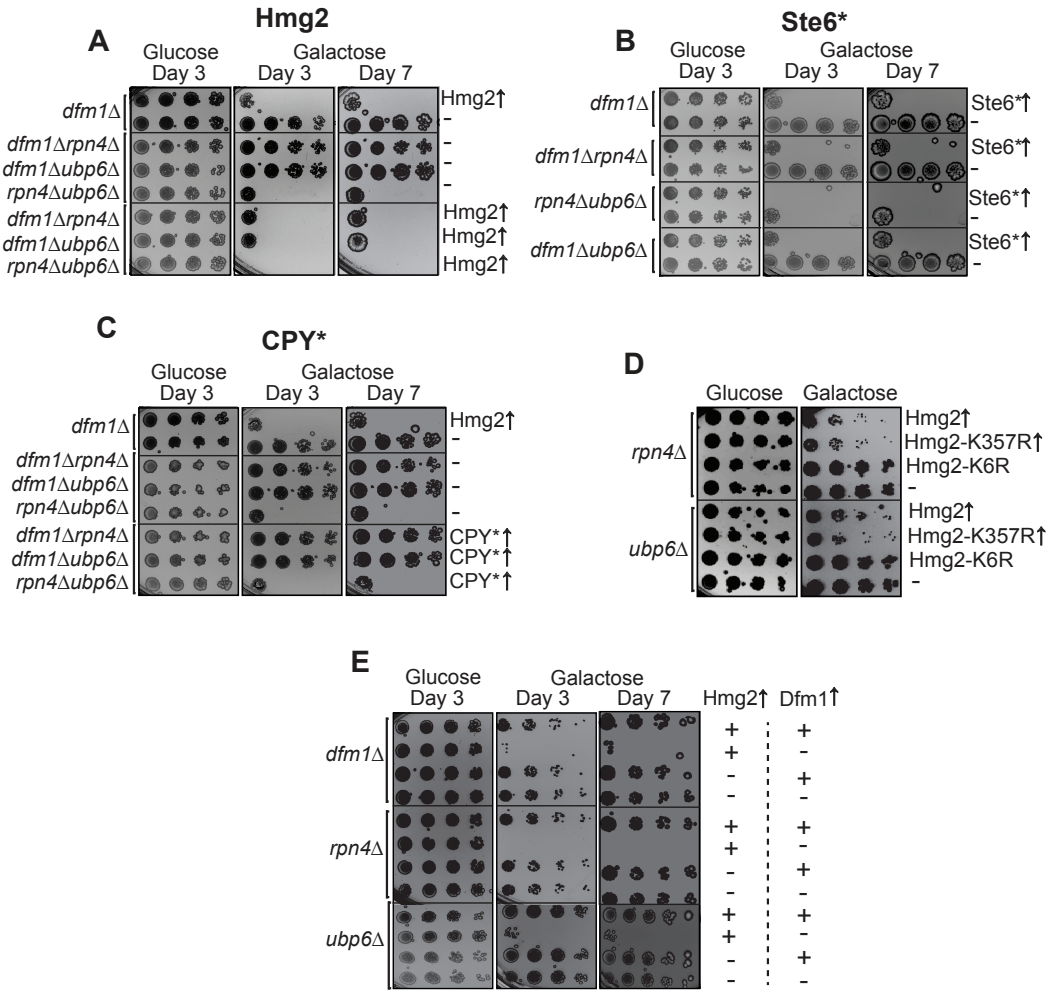
A
Hmg2
Glucose
Day 3
Galactose
Day 3
Day 7
dfm1Δ
dfm1Δrpn4Δ
dfm1Δubp6Δ
rpn4Δubp6Δ
dfm1Δrpn4Δ
dfm1Δubp6Δ
rpn4Δubp6Δ
Hmg2↑
-
-
-
-
Hmg2↑
Hmg2↑
Hmg2↑
B
Ste6*
Glucose
Day 3
Galactose
Day 3
Day 7
dfm1Δ
dfm1Δrpn4Δ
rpn4Δubp6Δ
dfm1Δubp6Δ
Ste6*↑
-
Ste6*↑
-
Ste6*↑
-
Ste6*↑
-
C
CPY*
Glucose
Day 3
Galactose
Day 3
Day 7
dfm1Δ
dfm1Δrpn4Δ
dfm1Δubp6Δ
rpn4Δubp6Δ
dfm1Δrpn4Δ
dfm1Δubp6Δ
rpn4Δubp6Δ
Hmg2↑
-
-
-
-
CPY*↑
CPY*↑
CPY*↑
D
Glucose
Galactose
rpn4Δ
ubp6Δ
Hmg2↑
Hmg2-K357R↑
Hmg2-K6R
-
Hmg2↑
Hmg2-K357R↑
Hmg2-K6R
-
E
Glucose
Day 3
Galactose
Day 3
Day 7
Hmg2↑
Dfm1↑
dfm1Δ
rpn4Δ
ubp6Δ
+ +
+ -
- +
- -
+ +
+ -
- +
- -
+ +
+ -
- +
- -

Supplemental Table 2.4.1 Plasmid List

Plasmid	Gene		
pRH1120	YCp	URA3	pGAL1-HMG2-GFP
pRH3113	YCp	URA3	pGAL1-PDR5*-HA
pRH3112	YCp	URA3	pGAL1-CPY*-HA
pRH3144	YCp	URA3	pGAL1- Ste6-166p-3HA-GFP
pRH317	YCp	URA3	
pRH316	YCp	LEU2	
pRH1945	Ylp	ADE2 URA3	4xUPRE-GFP
pRH2890	YCp	LEU2	pDFM1-DFM1-3HA-5aShp
pRH1997	YCp	LEU2	pDFM1-DFM1-3HA
pRH2812	YCp	LEU2	pDFM1-DFM1-3HA-AxxxG
pRH2813	YCp	LEU2	pDFM1-DFM1-3HA-GxxxA
pRH2826	YCp	LEU2	pDFM1-DFM1-3HA-WA
pRH2827	YCp	LEU2	pDFM1-DFM1-3HA-AR

Supplemental Table 2.4.1 Plasmid List (Continued)

Plasmid	Gene		
pRH2013	YCp	LEU2	pDFM1-DFM1-3HA
pSN12	YIp	ADE2 HIS3	
pSN11	YCp	URA3	
pSN103	YIp	ADE2 HIS3	pGAL1-HMG2-GFP-K357R
pSN104	YIp	ADE2 HIS3	pGAL1-HMG2-GFP-K6R
pSN105	YIp	ADE2 HIS3	pGAL1-HMG2-GFP
pSN59	YCp	LEU2	pDFM1-DFM1-3HA-F107S
pSN60	YCp	LEU2	pDFM1-DFM1-3HA-L64V
pSN93	YCp	LEU2	pDFM1-DFM1-3HA-K67E
pSN94	YCp	LEU2	pDFM1-DFM1-3HA-Q101R
pSN95	YCp	LEU2	pDFM1-DFM1-3HA-F57S
pSN168	YCp	ADE2 HIS3	pGAL1-HMG2-GFP-K6R-K357R
pSN86	YIp	ADE2 HIS3	pGAL1-STE6-166p-3HA-GFP
pSN88	YIp	ADE2 HIS3	pGAL1-HMG2-6MYC

Supplemental Table 2.4.1 Plasmid List (Continued)

Plasmid	Gene		
pSN100	YIp	ADE2 HIS3	pGAL1-CPY*-HA
pSN195	YCp	URA3	CFTR-HA
pSN196	YCp	URA3	CFTR-HA-ΔF508
pSN197	YCp	URA3	A1PiZ
pSN199	YCp	URA3	pGAL1-DFM1-6HIS
pSN5	YCp	URA3	
pSN193	YIp	ADE2 LEU2	pADH1-Derlin-1-MYC
pSN194	YIp	ADE2 LEU2	pADH1-Derlin-2-MYC
pSN39	YIp	ADE2 LEU2	
pSN190	YCp	URA3	pCUP1-HBT-Ubiquitin
pRH613	YIp	ADE2	pTDH3-HMG2-GFP
pRH2312	YCp	HIS3	pPGK1-PDR5*-HA
pRH2058	YCp	URA3	pPGK1-STE6-166p-3HA-GFP
pRH311	YIp	TRP1	

Supplemental Table 2.4.1 Plasmid List (Continued)

Plasmid	Gene		
pRH1862	YIp	ADE2 URA3	pTDH3-HMG2-GFP-K6R
pRH469	YIp	URA3	HMG2-GFP
pSN177	YCp	URA3	CPY*-GFP
pRH2513	YIp	TRP1	pHRD1-Hrd1-5MYC
pSN189	YCp	URA3	pGAL-ΔssCPY-MYC
pRH2880	YIp	TRP1	pTDH3-SEC61-GFP

Supplemental Table 2.4.2 Yeast Strain Used in this Study

Strain	Genotype	Reference
RHY10520	Mata *ADE2 met15Δ0 LYS2(LYS+) ura3Δ0 TRP1 leu2Δ0 his3Δ1 pdr5Δ::KanMX* *CEN::URA3*	This study
RHY10519	*Mata ADE2 met15Δ0 LYS2(LYS+) ura3Δ0 TRP1 leu2Δ0 his3Δ1 pdr5Δ::KanMX* *CEN::URA3::GAL1pr-HMG2-GFP*	This study
RHY10518	*Mata ADE2 met15Δ0 LYS2(LYS+) ura3Δ0 TRP1 leu2Δ0 his3Δ1 dfm1Δ::KanMX* *CEN::URA3*	This study
RHY10517	*Mata ADE2 met15Δ0 LYS2(LYS+) ura3Δ0 TRP1 leu2Δ0 his3Δ1* *dfm1Δ::KanMX* *CEN::URA3::GAL1pr-HMG2-GFP*	This study
RHY10655	*Mata ADE2 met15Δ0 LYS2(LYS+) ura3Δ0 TRP1 leu2Δ0 his3Δ1hrd1Δ::KanMX* *CEN::URA3*	This study
RHY10654	*Mata ADE2 met15Δ0 LYS2(LYS+) ura3Δ0 TRP1 leu2Δ0 his3Δ1 hrd1Δ::KanMX* *CEN::URA3::GAL1pr-HMG2-GFP*	This study
RHY11580	*Mata ADE2 met15Δ0 LYS2(LYS+) ura3Δ0 TRP1 leu2Δ0 his3Δ1 pdr5Δ::KanMX* *CEN::URA3::GAL1pr-PDR5*-HA*	This study
RHY11581	*Mata ADE2 met15Δ0 LYS2(LYS+) ura3Δ0 TRP1 leu2Δ0 his3Δ1 dfm1Δ::KanMX* *CEN::URA3::GAL1pr-PDR5*-HA*	This study
RHY11583	*Mata ADE2 met15Δ0 LYS2(LYS+) ura3Δ0 TRP1 leu2Δ0 his3Δ1 hrd1Δ::KanMX* *CEN::URA3::GAL1pr-PDR5*-HA*	This study

Supplemental Table 2.4.2 Yeast Strain Used in this Study (Continued)

Strain	Genotype	Reference
RHY11576	*Mata ADE2 met15Δ0 LYS2(LYS+) ura3Δ0 TRP1 leu2Δ0 his3Δ1 pdr5Δ::KanMX* *CEN::URA3::GAL1pr-CPY*-HA*	This study
RHY11577	*Mata ADE2 met15Δ0 LYS2(LYS+) ura3Δ0 TRP1 leu2Δ0 his3Δ1 dfm1Δ::KanMX* *CEN::URA3::GAL1pr-CPY*-HA*	Neal et al., 2020
RHY11579	*Mata ADE2 met15Δ0 LYS2(LYS+) ura3Δ0 TRP1 leu2Δ0 his3Δ1 hrd1Δ::KanMX* *CEN::URA3::GAL1pr-CPY*-HA*	Neal et al., 2020
RHY11817	*Mata ADE2 MET2 lys2-801 ura3Δ0 TRP1 leu2Δ0 his3Δ200* *dfm1Δ::KanMX hrd1Δ::CloNAT* *CEN::URA3*	Neal et al., 2020
RHY11818	*Mata ADE2 MET2 lys2-801 ura3Δ0 TRP1 leu2Δ0 his3Δ200* *dfm1Δ::KanMX hrd1Δ::CloNAT* *CEN::URA3::GAL1pr-HMG2-GFP*	This study
RHY 11867	*Mata ADE2 met15Δ0 LYS2(LYS+) ura3Δ0 TRP1 leu2Δ0 his3Δ1 pdr5Δ::KanMX* *CEN::URA3::GAL1pr-STE6-166p-3HA-GFP*	Neal et al., 2018
RHY 11868	*Mata ADE2 met15Δ0 LYS2(LYS+) ura3Δ0 TRP1 leu2Δ0 his3Δ1 dfm1Δ::KanMX* *CEN::URA3::GAL1pr-STE6-166p-3HA-GFP*	Neal et al., 2018
RHY 11869	*Mata ADE2 met15Δ0 LYS2(LYS+) ura3Δ0 TRP1 leu2Δ0 his3Δ1 hrd1Δ::KanMX* *CEN::URA3::GAL1pr-STE6-166p-3HA-GFP*	Neal et al., 2020
RHY 11826	*Mata ADE2 MET2 lys2-801 ura3Δ0 TRP1 leu2Δ0 his3Δ200* *dfm1Δ::KanMX hrd1Δ::CloNAT* *CEN::URA3::GAL1pr-STE6-166p-3HA-GFP*	This study

Supplemental Table 2.4.2 Yeast Strain Used in this Study (Continued)

Strain	Genotype	Reference
RHY 11873	*Mata ADE2 met15Δ0 LYS2(LYS+) ura3-52 trp1::hisG leu2Δ his3Δ1 dfm1Δ::CloNAT doa10Δ::HphMx* *CEN::URA3::GAL1pr-STE6-166p-3HA-GFP*	This study
RHY 11908	*Mata ADE2 met15Δ0 LYS2(LYS+) ura3-52 trp1::hisG leu2Δ his3Δ1 doa10Δ::HphMx* *CEN::URA3::GAL1pr-STE6-166p-3HA-GFP*	This study
RHY 11906	*Mata ADE2 met15Δ0 LYS2(LYS+) ura3-52 trp1::hisG leu2Δ his3Δ1 doa10Δ::HphMx* *CEN::URA3*	Neal et al., 2020
RHY 11907	*Mata ADE2 met15Δ0 LYS2(LYS+) ura3-52 trp1::hisG leu2Δ his3Δ1 doa10Δ::HphMx* *CEN::URA3::GAL1pr-HMG2-GFP*	Neal et al., 2020
RHY 11914	*Mata ADE2 met15Δ0 LYS2(LYS+) ura3-52 trp1::hisG leu2Δ his3Δ1 dfm1Δ::CloNAT doa10Δ::HphMx* *CEN::URA3*	This study
RHY 11915	*Mata ADE2 met15Δ0 LYS2(LYS+) ura3-52 trp1::hisG leu2Δ his3Δ1 dfm1Δ::CloNAT doa10Δ::HphMx* *CEN::URA3::GAL1pr-HMG2-GFP*	This study
RHY 11226	*Mata ADE2 met15Δ0 LYS2(LYS+) ura3Δ0 TRP1 leu2Δ0 his3Δ1 dfm1Δ::KanMX* *CEN::URA3 CEN::LEU2::pDFM1-DFM1-3HA*	Neal et al., 2018
RHY 11227	*Mata ADE2 met15Δ0 LYS2(LYS+) ura3Δ0 TRP1 leu2Δ0 his3Δ1 dfm1Δ::KanMX* *CEN::URA3:: GAL1pr-HMG2-GFP CEN::LEU2::pDFM1-DFM1-3HA*	Neal et al., 2018
RHY 11216	*Mata ADE2 met15Δ0 LYS2(LYS+) ura3Δ0 TRP1 leu2Δ0 his3Δ1 dfm1Δ::KanMX* *CEN::URA3 CEN::LEU2*	Neal et al., 2018

Supplemental Table 2.4.2 Yeast Strain Used in this Study (Continued)

Strain	Genotype	Reference
RHY12217	*Mata ADE2 met15Δ0 LYS2(LYS+) ura3Δ0 TRP1 leu2Δ0 his3Δ1 dfm1Δ::KanMX* *CEN::URA3:: GAL1pr-HMG2-GFP CEN::LEU2*	Neal et al., 2018
RHY11222	*Mata ADE2 met15Δ0 LYS2(LYS+) ura3Δ0 TRP1 leu2Δ0 his3Δ1 dfm1Δ::KanMX* *CEN::URA3 CEN::LEU2::pDFM1-DFM1-3HA-WA*	Neal et al., 2018
RHY11223	*Mata ADE2 met15Δ0 LYS2(LYS+) ura3Δ0 TRP1 leu2Δ0 his3Δ1 dfm1Δ::KanMX* *CEN::URA3:: GAL1pr-HMG2-GFP CEN::LEU2::pDFM1-DFM1-3HA-WA*	Neal et al., 2018
RHY11224	*Mata ADE2 met15Δ0 LYS2(LYS+) ura3Δ0 TRP1 leu2Δ0 his3Δ1 dfm1Δ::KanMX* *CEN::URA3 CEN::LEU2::pDFM1-DFM1-3HA-AR*	Neal et al., 2018
RHY11225	*Mata ADE2 met15Δ0 LYS2(LYS+) ura3Δ0 TRP1 leu2Δ0 his3Δ1 dfm1Δ::KanMX* *CEN::URA3:: GAL1pr-HMG2-GFP CEN::LEU2::pDFM1-DFM1-3HA-AR*	Neal et al., 2018
RHY11218	*Mata ADE2 met15Δ0 LYS2(LYS+) ura3Δ0 TRP1 leu2Δ0 his3Δ1 dfm1Δ::KanMX* *CEN::URA3 CEN::LEU2::pDFM1-DFM1-3HA-AxxxG*	Neal et al., 2018
RHY11219	*Mata ADE2 met15Δ0 LYS2(LYS+) ura3Δ0 TRP1 leu2Δ0 his3Δ1 dfm1Δ::KanMX* *CEN::URA3:: GAL1pr-HMG2-GFP CEN::LEU2::pDFM1-DFM1-3HA-AxxxG*	Neal et al., 2018
RHY11220	*Mata ADE2 met15Δ0 LYS2(LYS+) ura3Δ0 TRP1 leu2Δ0 his3Δ1 dfm1Δ::KanMX* *CEN::URA3 CEN::LEU2::pDFM1-DFM1-3HA-GxxxA*	Neal et al., 2018
RHY11221	*Mata ADE2 met15Δ0 LYS2(LYS+) ura3Δ0 TRP1 leu2Δ0 his3Δ1 dfm1Δ::KanMX* *CEN::URA3:: GAL1pr-HMG2-GFP CEN::LEU2::pDFM1-DFM1-3HA-GxxxA*	Neal et al., 2018

Supplemental Table 2.4.2 Yeast Strain Used in this Study (Continued)

Strain	Genotype	Reference
RHY11073	*Mata ADE2 met15Δ0 LYS2(LYS+) ura3Δ0 TRP1 leu2Δ0 his3Δ1 dfm1Δ::KanMX* *CEN::URA3 CEN::LEU2::pDFM1-DFM1-3HA-5aShp*	Neal et al., 2018
RHY11074	*Mata ADE2 met15Δ0 LYS2(LYS+) ura3Δ0 TRP1 leu2Δ0 his3Δ1 dfm1Δ::KanMX* *CEN::URA3:: GAL1pr-HMG2-GFP CEN::LEU2::pDFM1-DFM1-3HA-5aShp*	Neal et al., 2018
SEN141	Mata *ade2::ADE2::HIS3::pGAL1::Hmg2-GFP met2 lys2-801 ura3-52 trp1::hisG leu2Δ his3Δ200*	This study
SEN142	Mata *ade2::ADE2::HIS3 met2 lys2-801 ura3-5, trp1::hisG leu2Δ his3Δ200*	This study
SEN149	Mata *ade2::ADE2::HIS3 met2 lys2-801 ura3-52 trp1::hisG leu2Δ his3Δ200 dfm1Δ::KanMX*	This study
SEN165	Mata *ade2::ADE2::HIS3::pGAL1::Hmg2-GFP met2 lys2-801 ura3-52, trp1::hisG leu2Δ his3Δ200 dfm1Δ::KanMX*	This study
SEN407	Mata *ade2-101 met2 lys2-801 ura3-5, trp1::hisG leu2Δ his3Δ200* *CEN::ADE2::HIS3::pGAL1-Hmg2-GFP-K6R-K357R*	This study
SEN408	Mata *ade2-101 met2 lys2-801 ura3-5, trp1::hisG leu2Δ his3Δ200 dfm1Δ::KanMX* *CEN::ADE2::HIS3::pGAL1-Hmg2-GFP-K6R-K357R*	This study
SEN139	Mata *ade2::ADE2::HIS3::pGAL1::Hmg2-GFP-K357R met2 lys2-801 ura3-52 trp1::hisG leu2Δ his3Δ200*	This study
SEN147	Mata *ade2::ADE2::HIS3::pGAL1::Hmg2-GFP-K357R met2 lys2-801 ura3-52 trp1::hisG leu2Δ his3Δ200 dfm1Δ::KanMX*	This study
SEN140	Mata *ade2::ADE2::HIS3::pGAL1::Hmg2-GFP-K6R met2 lys2-801 ura3-52 trp1::hisG leu2Δ his3Δ200*	This study
SEN148	Mata *ade2::ADE2::HIS3::pGAL1::Hmg2-GFP-K6R met2 lys2-801 ura3-52 trp1::hisG leu2Δ his3Δ200 dfm1Δ::KanMX*	This study

Supplemental Table 2.4.2 Yeast Strain Used in this Study (Continued)

Strain	Genotype	Reference
SEN182	Mata *ade2::ADE2::HIS3 met2 lys2-801 ura3-52 trp1::hisG leu2Δ his3Δ200 dfm1Δ::KanMX* *CEN::LEU2::pDFM1-DFM1-3HA*	This study
SEN183	Mata *ade2::ADE2::HIS3 met2 lys2-801 ura3-52 trp1::hisG leu2Δ his3Δ200 dfm1Δ::KanMX* *CEN::LEU2*	This study
SEN192	Mata *ade2::ADE2::HIS3::pGAL1::Hmg2-GFP met2 lys2-801 ura3-52, trp1::hisG leu2Δ his3Δ200 dfm1Δ::KanMX* *CEN::LEU2::pDFM1-DFM1-3HA*	This study
SEN193	Mata *ade2::ADE2::HIS3::pGAL1::Hmg2-GFP met2 lys2-801 ura3-52, trp1::hisG leu2Δ his3Δ200 dfm1Δ::KanMX* *CEN::LEU2*	This study
SEN250	Mata *ade2::ADE2::HIS3 met2 lys2-801 ura3-52 trp1::hisG leu2Δ his3Δ200 dfm1Δ::KanMX* *CEN::LEU2::pDFM1-DFM1-3HA-F107S*	This study
SEN251	Mata *ade2::ADE2::HIS3 met2 lys2-801 ura3-52 trp1::hisG leu2Δ his3Δ200 dfm1Δ::KanMX* *CEN::LEU2::pDFM1-DFM1-3HA-L64V*	This study
SEN252	Mata *ade2::ADE2::HIS3 met2 lys2-801 ura3-52 trp1::hisG leu2Δ his3Δ200 dfm1Δ::KanMX* *CEN::LEU2::pDFM1-DFM1-3HA-K67E*	This study
SEN253	Mata *ade2::ADE2::HIS3 met2 lys2-801 ura3-52 trp1::hisG leu2Δ his3Δ200 dfm1Δ::KanMX* *CEN::LEU2::pDFM1-DFM1-3HA-Q101R*	This study
SEN254	Mata *ade2::ADE2::HIS3 met2 lys2-801 ura3-52 trp1::hisG leu2Δ his3Δ200 dfm1Δ::KanMX* *CEN::LEU2::pDFM1-DFM1-3HA-F58S*	This study
SEN256	Mata *ade2::ADE2::HIS3::pGAL1::Hmg2-GFP met2 lys2-801 ura3-52, trp1::hisG leu2Δ his3Δ200 dfm1Δ::KanMX* *CEN::LEU2::pDFM1-DFM1-3HA-F107S*	This study

Supplemental Table 2.4.2 Yeast Strain Used in this Study (Continued)

Strain	Genotype	Reference
SEN257	Mata *ade2::ADE2::HIS3::pGAL1::Hmg2-GFP met2 lys2-801 ura3-52, trp1::hisG leu2Δ his3Δ200 dfm1Δ::KanMX* *CEN::LEU2::pDFM1-DFM1-3HA-L64V*	This study
SEN258	Mata *ade2::ADE2::HIS3::pGAL1::Hmg2-GFP met2 lys2-801 ura3-52, trp1::hisG leu2Δ his3Δ200 dfm1Δ::KanMX* *CEN::LEU2::pDFM1-DFM1-3HA-K67E*	This study
SEN259	Mata *ade2::ADE2::HIS3::pGAL1::Hmg2-GFP met2 lys2-801 ura3-52, trp1::hisG leu2Δ his3Δ200 dfm1Δ::KanMX* *CEN::LEU2::pDFM1-DFM1-3HA-Q101R*	This study
SEN260	Mata *ade2::ADE2::HIS3::pGAL1::Hmg2-GFP met2 lys2-801 ura3-52, trp1::hisG leu2Δ his3Δ200 dfm1Δ::KanMX* *CEN::LEU2::pDFM1-DFM1-3HA-F58S*	This study
SEN103	Mata *ade2::ADE2::URA3::4xUPRE-GFP met15Δ0 LYS2 (LYS+) ura3Δ0 TRP1 leu2Δ0 his3Δ1 pdr5Δ::KanMX* *pGAL1::CPY*-HA*	This study
SEN111	Mata *ade2::ADE2::URA3::4xUPRE-GFP met15Δ0 LYS2 (LYS+) ura3Δ0 TRP1 leu2Δ0 his3Δ1 dfm1Δ:: KanMX* *pGAL1::CPY*-HA*	This study
SEN73	Mata *ade2::ADE2::URA3::4xUPRE-GFP met15Δ0 LYS2 (LYS+) ura3Δ0 TRP1 leu2Δ0 his3Δ1 pdr5Δ::KanMX* *pGAL1::STE6-166p-3HA-GFP*	This study
SEN75	Mata *ade2::ADE2::URA3::4xUPRE-GFP met15Δ0 LYS2 (LYS+) ura3Δ0 TRP1 leu2Δ0 his3Δ1 dfm1Δ:: KanMX* *pGAL1::STE6-166p-3HA-GFP*	This study
SEN76	Mata *ade2::ADE2::URA3::4xUPRE-GFP met15Δ0 LYS2 (LYS+) ura3Δ0 TRP1 leu2Δ0 his3Δ1 ADE2::HIS3 pdr5Δ::KanMX*	This study
SEN68	Mata *ade2::ADE2::URA3::4xUPRE-GFP met15Δ0 LYS2 (LYS+) ura3Δ0 TRP1 leu2Δ0 his3Δ1 ADE2::HIS3 dfm1Δ::KanMX*	This study

Supplemental Table 2.4.2 Yeast Strain Used in this Study (Continued)

Strain	Genotype	Reference
SEN70	Mata *ade2::ADE2::URA3::4xUPRE-GFP met15Δ0 LYS2 (LYS+) ura3Δ0 TRP1 leu2Δ0 his3Δ1 dfm1Δ::KanMX pGAL1::HMG2-6MYC*	This study
SEN71	Mata *ade2::ADE2::URA3::4xUPRE-GFP met15Δ0 LYS2 (LYS+) ura3Δ0 TRP1 leu2Δ0 his3Δ1 ADE2::HIS3 dfm1Δ::KanMX*	This study
SEN155	Mata *ADE2::HIS3 met15Δ0 LYS2 (LYS+) ura3Δ0 TRP1 leu2Δ0 his3Δ1 rpn4Δ::KanMX*	This study
SEN166	Mata *ADE2::HIS3::pGAL::Hmg2-GFP met15Δ0 LYS2 (LYS+) ura3Δ0 TRP1 leu2Δ0 his3Δ1 rpn4Δ::KanMX*	This study
SEN196	Mata *ADE2::HIS3 met15Δ0 LYS2 (LYS+) ura3Δ0 TRP1 leu2Δ0 his3Δ1 ubp6Δ::KanMX*	This study
SEN197	Mata *ADE2::HIS3::pGAL1::Hmg2-GFP met15Δ0 LYS2 (LYS+) ura3Δ0 TRP1 leu2Δ0 his3Δ1 ubp6Δ::KanMX*	This study
SEN411	Mata *ade2::ADE2::HIS3::pGAL1::STE6-166-3HA-GFP met2 lys2-801 ura3-52 trp1::hisG leu2Δ his3Δ200*	This study
SEN412	Mata *ADE2::HIS3::pGAL1::STE6-166p-3HA-GFP met15Δ0 LYS2 (LYS+) ura3Δ0 TRP1 leu2Δ0 his3Δ1 rpn4Δ::KanMX*	This study
SEN413	Mata *ade2::ADE2::HIS3:: pGAL1::STE6-166p-3HA-GFP met2 lys2-801 ura3-52 trp1::hisG leu2Δ his3Δ200 dfm1Δ::KanMX*	This study
SEN414	Mata *ADE2::HIS3::pGAL1::STE6-166p-3HA-GFP met15Δ0 LYS2 (LYS+) ura3Δ0 TRP1 leu2Δ0 his3Δ1 ubp6Δ::KanMX*	This study
SEN269	Mata *ADE2::HIS3::pGAL1::CPY*-HA met15Δ0 LYS2 (LYS+) ura3Δ0 TRP1 leu2Δ0 his3Δ1 ubp6Δ::KanMX*	This study
SEN415	Mata *ade2::ADE2::HIS3::pGAL1::CPY*-HA met2 lys2-801 ura3-52 trp1::hisG leu2Δ his3Δ200*	This study
SEN416	Mata *ADE2::HIS3::pGAL1::CPY*-HA met15Δ0 LYS2 (LYS+) ura3Δ0 TRP1 leu2Δ0 his3Δ1 rpn4Δ::KanMX*	This study
SEN417	Mata *ade2::ADE2::HIS3:: pGAL1::CPY*-HA met2 lys2-801 ura3-52 trp1::hisG leu2Δ his3Δ200 dfm1Δ::KanMX*	This study

Supplemental Table 2.4.2 Yeast Strain Used in this Study (Continued)

Strain	Genotype	Reference
SEN270	Mata *ADE2::HIS3::pGAL1::CPY*-HA met15Δ0 LYS2 (LYS+) ura3Δ0 TRP1 leu2Δ0 his3Δ1 rpn4Δ::KanMX dfm1Δ::CloNAT*	This study
SEN271	Mata *ADE2::HIS3::pGAL1::CPY*-HA met15Δ0 LYS2 (LYS+) ura3Δ0 TRP1 leu2Δ0 his3Δ1 rpn4Δ::KanMX ubp6Δ::CloNAT*	This study
SEN272	Mata *ADE2::HIS3::pGAL1::CPY*-HA met15Δ0 LYS2 (LYS+) ura3Δ0 TRP1 leu2Δ0 his3Δ1 ubp6Δ::KanMX dfm1Δ::CloNAT*	This study
SEN499	Mata *ADE2::HIS3::pGAL1::STE6-166p-3HA-GFP met15Δ0 LYS2 (LYS+) ura3Δ0 TRP1 leu2Δ0 his3Δ1 rpn4Δ::KanMX dfm1Δ::CloNAT*	This study
SEN500	Mata *ADE2::HIS3::pGAL1::STE6-166p-3HA-GFP met15Δ0 LYS2 (LYS+) ura3Δ0 TRP1 leu2Δ0 his3Δ1 rpn4Δ::KanMX ubp6Δ::CloNAT*	This study
SEN501	Mata *ADE2::HIS3::pGAL1::STE6-166p-3HA-GFP met15Δ0 LYS2 (LYS+) ura3Δ0 TRP1 leu2Δ0 his3Δ1 ubp6Δ::KanMX dfm1Δ::CloNAT*	This study
SEN273	Mata *ADE2::HIS3::pGAL1::HMG2-GFP met15Δ0 LYS2 (LYS+) ura3Δ0 TRP1 leu2Δ0 his3Δ1 rpn4Δ::KanMX dfm1Δ::CloNAT*	This study
SEN276	Mata *ADE2::HIS3 met15Δ0 LYS2 (LYS+) ura3Δ0 TRP1 leu2Δ0 his3Δ1 rpn4Δ::KanMX dfm1Δ::CloNAT*	This study
SEN274	Mata *ADE2::HIS3::pGAL1::HMG2-GFP met15Δ0 LYS2 (LYS+) ura3Δ0 TRP1 leu2Δ0 his3Δ1 rpn4Δ::KanMX ubp6Δ::CloNAT*	This study
SEN277	Mata *ADE2::HIS3 met15Δ0 LYS2 (LYS+) ura3Δ0 TRP1 leu2Δ0 his3Δ1 rpn4Δ::KanMX ubp6Δ::CloNAT*	This study
SEN275	Mata *ADE2::HIS3::pGAL1::HMG2-GFP met15Δ0 LYS2 (LYS+) ura3Δ0 TRP1 leu2Δ0 his3Δ1 ubp6Δ::KanMX dfm1Δ::CloNAT*	This study
SEN278	Mata *ADE2::HIS3 met15Δ0 LYS2 (LYS+) ura3Δ0 TRP1 leu2Δ0 his3Δ1 ubp6Δ::KanMX dfm1Δ::CloNAT*	This study

Supplemental Table 2.4.2 Yeast Strain Used in this Study (Continued)

Strain	Genotype	Reference
SEN487	Mata *ade2::ADE2::HIS3::pGAL1::Hmg2-GFP met2 lys2-801 ura3-52, trp1::hisG leu2Δ his3Δ200 dfm1Δ::KanMX* *CEN::URA3::pGAL1::DFM1-6HIS*	This study
SEN488	Mata *ade2::ADE2::HIS3::pGAL1::Hmg2-GFP met2 lys2-801 ura3-52, trp1::hisG leu2Δ his3Δ200 dfm1Δ::KanMX* *CEN::URA3*	This study
SEN489	Mata *ade2::ADE2::HIS3 met2 lys2-801 ura3-52, trp1::hisG leu2Δ his3Δ200 dfm1Δ::KanMX* *CEN::URA3::pGAL1::DFM1-6HIS*	This study
SEN490	Mata *ade2::ADE2::HIS3 met2 lys2-801 ura3-52, trp1::hisG leu2Δ his3Δ200 dfm1Δ::KanMX* *CEN::URA3*	This study
SEN491	Mata *ADE2::HIS3::pGAL::Hmg2-GFP met15Δ0 LYS2 (LYS+) ura3Δ0 TRP1 leu2Δ0 his3Δ1 rpn4Δ::KanMX* *CEN::URA3::pGAL1::DFM1-6HIS*	This study
SEN492	Mata *ADE2::HIS3::pGAL::Hmg2-GFP met15Δ0 LYS2 (LYS+) ura3Δ0 TRP1 leu2Δ0 his3Δ1 rpn4Δ::KanMX* *CEN::URA3*	This study
SEN493	Mata *ADE2::HIS3 met15Δ0 LYS2 (LYS+) ura3Δ0 TRP1 leu2Δ0 his3Δ1 rpn4Δ::KanMX* *CEN::URA3::pGAL1::DFM1-6HIS*	This study
SEN494	Mata *ADE2::HIS3 met15Δ0 LYS2 (LYS+) ura3Δ0 TRP1 leu2Δ0 his3Δ1 rpn4Δ::KanMX* *CEN::URA3*	This study
SEN517	Mata *ADE2::HIS3::pGAL::Hmg2-GFP met15Δ0 LYS2 (LYS+) ura3Δ0 TRP1 leu2Δ0 his3Δ1 ubp6Δ::KanMX* *CEN::URA3::pGAL1::DFM1-6HIS*	This study
SEN518	Mata *ADE2::HIS3::pGAL::Hmg2-GFP met15Δ0 LYS2 (LYS+) ura3Δ0 TRP1 leu2Δ0 his3Δ1 ubp6Δ::KanMX* *CEN::URA3*	This study

Supplemental Table 2.4.2 Yeast Strain Used in this Study (Continued)

Strain	Genotype	Reference
SEN519	Mata *ADE2::HIS3 met15Δ0 LYS2 (LYS+) ura3Δ0 TRP1 leu2Δ0 his3Δ1 ubp6Δ::KanMX* *CEN::URA3::pGAL1::DFM1-6HIS*	This study
SEN520	Mata *ADE2::HIS3 met15Δ0 LYS2 (LYS+) ura3Δ0 TRP1 leu2Δ0 his3Δ1 ubp6Δ::KanMX* *CEN::URA3*	This study
SEN249	Mata *ade2-101 met2 lys2-801 ura3-52 trp1::hisG::TRP1:: pTDH3-Hmg1p-MYC-Hrd1p-3HA-GFP leu2Δ his3Δ200 hrd1Δ::KanMX dfm1Δ::CloNAT pdr5Δ::HIS3*	This study
SEN378	Mata *ade2-101 met2 lys2-801 ura3-52 trp1::hisG::TRP1 leu2Δ his3Δ200 hrd1Δ::KanMX pdr5Δ::HIS3*	This study
SEN229	Mata *ade2-101 met2 lys2-801 ura3-52 trp1::hisG::TRP1:: pTDH3-Hmg1p-MYC-Hrd1p-3HA-GFP leu2Δ his3Δ200 hrd1Δ::KanMX pdr5Δ::HIS3*	This study
SEN228	Mata *ade2-101 met2 lys2-801 ura3-52 trp1::hisG::TRP1:: pTDH3-Hmg1p-MYC-Hrd1p-3HA-GFP leu2Δ his3Δ200 pdr5Δ::HIS3*	This study
SEN377	Mata *ade2-101 met2 lys2-801 ura3-52 trp1::hisG::TRP1 leu2Δ his3Δ200 pdr5Δ::HIS3*	This study
SEN379	Mata *ade2-101 met2 lys2-801 ura3-52 trp1::hisG::TRP1 leu2Δ his3Δ200 hrd1Δ::KanMX dfm1Δ::CloNAT pdr5Δ::HIS3*	This study
SEN401	Mata *ADE2::HIS3::pGAL1::Hmg2-GFP met15Δ0 LYS2 (LYS+) ura3Δ0 TRP1 leu2Δ0 his3Δ1 ubp9Δ::KanMX*	This study
SEN424	Mata *ADE2::HIS3 met15Δ0 LYS2 (LYS+) ura3Δ0 TRP1 leu2Δ0 his3Δ1 ubp9Δ::KanMX*	This study
SEN446	Mata *ADE2 met15Δ0 LYS2 (LYS+) ura3Δ0 TRP1 leu2Δ0 his3Δ1 ubp9Δ::KanMX* *CEN::URA3:: ΔssCPY*-MYC*	This study
SEN459	Mata *ADE2 met15Δ0 LYS2 (LYS+) ura3Δ0 TRP1 leu2Δ0 his3Δ1 ubp14Δ::KanMX* *CEN::URA3*	This study

Supplemental Table 2.4.2 Yeast Strain Used in this Study (Continued)

Strain	Genotype	Reference
SEN460	Mata *ADE2 met15Δ0 LYS2 (LYS+) ura3Δ0 TRP1 leu2Δ0 his3Δ1 doa4Δ::KanMX* *CEN::URA3*	This study
SEN461	Mata *ade2-101 met2 lys2-801 ura3-52 trp1::hisG leu2Δ his3Δ200* *CEN::URA3:: ΔssCPY*-MYC*	This study
SEN463	Mata *ade2-101 met2 lys2-801 ura3-52 trp1::hisG leu2Δ his3Δ200 dfm1Δ::KanMX* *CEN::URA3:: ΔssCPY*-MYC*	This study
SEN464	Mata *ADE2 met15Δ0 LYS2 (LYS+) ura3Δ0 TRP1 leu2Δ0 his3Δ1 ubp14Δ::KanMX* *CEN::URA3:: ΔssCPY*-MYC*	This study
SEN449	Mata *ADE2 met15Δ0 LYS2 (LYS+) ura3Δ0 TRP1 leu2Δ0 his3Δ1 ubp6Δ::KanMX* *CEN::URA3*	This study
SEN450	Mata *ADE2 met15Δ0 LYS2 (LYS+) ura3Δ0 TRP1 leu2Δ0 his3Δ1 ubp14Δ::KanMX* *CEN::URA3*	This study
SEN451	Mata *ade2-101 met2 lys2-801 ura3-52 trp1::hisG leu2Δ his3Δ200 dfm1Δ::KanMX* *CEN::URA3*	This study
SEN215	*Mata ADE2::URA3::pTDH3-HMG2-GFPx met15Δ0 LYS2(LYS+) ura3Δ0 TRP1 leu2Δ0 his3Δ1 dfm1Δ::KanMX* *CEN::LEU2::pDFM1-DFM1-3HA-L64V*	Nejatfard, et al., 2021
SEN216	*Mata ADE2::URA3::pTDH3-HMG2-GFPx met15Δ0 LYS2(LYS+) ura3Δ0 TRP1 leu2Δ0 his3Δ1 dfm1Δ::KanMX* *CEN::LEU2::pDFM1-DFM1-3HA-F107S*	Nejatfard, et al., 2021
SEN217	*Mata ADE2::URA3::pTDH3-HMG2-GFPx met15Δ0 LYS2(LYS+) ura3Δ0 TRP1 leu2Δ0 his3Δ1 dfm1Δ::KanMX* *CEN::LEU2::pDFM1-DFM1-3HA-K67E*	Nejatfard, et al., 2021

Supplemental Table 2.4.2 Yeast Strain Used in this Study (Continued)

Strain	Genotype	Reference
SEN218	*Mata ADE2::URA3::pTDH3-HMG2-GFPx met15Δ0 LYS2(LYS+) ura3Δ0 TRP1 leu2Δ0 his3Δ1 dfm1Δ::KanMX* *CEN::LEU2::pDFM1-DFM1-3HA-Q101R*	Nejatfard, et al., 2021
SEN219	*Mata ADE2::URA3::pTDH3-HMG2-GFPx met15Δ0 LYS2(LYS+) ura3Δ0 TRP1 leu2Δ0 his3Δ1 dfm1Δ::KanMX* *CEN::LEU2::pDFM1-DFM1-3HA-F58S*	Nejatfard, et al., 2021
SEN529	*Mata ADE2::URA3::pTDH3-HMG2-GFPx met15Δ0 LYS2(LYS+) ura3Δ0 TRP1 leu2Δ0 his3Δ1 dfm1Δ::KanMX* *CEN::LEU2*	Nejatfard, et al., 2021
SEN530	*Mata ADE2::URA3::pTDH3-HMG2-GFPx met15Δ0 LYS2(LYS+) ura3Δ0 TRP1 leu2Δ0 his3Δ1 dfm1Δ::KanMX* *CEN::LEU2::pDFM1-DFM1-3HA-AR*	Nejatfard, et al., 2021
SEN532	*Mata ADE2::URA3::pTDH3-HMG2-GFPx met15Δ0 LYS2(LYS+) ura3Δ0 TRP1 leu2Δ0 his3Δ1 dfm1Δ::KanMX* *CEN::LEU2::pDFM1-DFM1-3HA-AxxxG*	Nejatfard, et al., 2021
SEN534	*Mata ADE2::URA3::pTDH3-HMG2-GFPx met15Δ0 LYS2(LYS+) ura3Δ0 TRP1 leu2Δ0 his3Δ1 dfm1Δ::KanMX* *CEN::LEU2::pDFM1-DFM1-3HA*	Nejatfard, et al., 2021
SEN535	*Mata ADE2::URA3::pTDH3-HMG2-GFPx met15Δ0 LYS2(LYS+) ura3Δ0 TRP1 leu2Δ0 his3Δ1 dfm1Δ::KanMX* *CEN::LEU2::pDFM1-DFM1-3HA-5aShp*	Nejatfard, et al., 2021
SEN506	Mata *ade2::ADE2::HIS3 met2 lys2-801 ura3-52, trp1::hisG leu2::LEU2::ADE2:: pADH1-Derlin-1-MYC his3Δ200 dfm1Δ::KanMX*	This study
SEN507	Mata *ade2::ADE2::HIS3 met2 lys2-801 ura3-52, trp1::hisG leu2::LEU2::ADE2:: pADH1-Derlin-1-MYC his3Δ200*	This study
SEN510	Mata *ade2::ADE2::HIS3 met2 lys2-801 ura3-52, trp1::hisG leu2::LEU2::ADE2:: pADH1-Derlin-2-MYC his3Δ200*	This study
SEN512	Mata *ade2::ADE2::HIS3::pGAL1::Hmg2-GFP met2 lys2-801 ura3-52, trp1::hisG leu2::LEU2::ADE2::pADH1-Derlin-2-MYC his3Δ200 dfm1Δ::KanMX*	This study

Supplemental Table 2.4.2 Yeast Strain Used in this Study (Continued)

Strain	Genotype	Reference
SEN515	Mata *ade2::ADE2::HIS3::pGAL1::Hmg2-GFP met2 lys2-801 ura3-52, trp1::hisG leu2::LEU2::ADE2 his3∆200 dfm1∆::KanMX*	This study
SEN516	Mata *ade2::ADE2::HIS3::pGAL1::Hmg2-GFP met2 lys2-801 ura3-52, trp1::hisG leu2::LEU2::ADE2 his3∆200*	This study
SEN470	Mata *ade2::ADE2::HIS3 met2 lys2-801 ura3-5, trp1::hisG leu2∆ his3∆200* *CEN::URA3::CFTR-HA*	This study
SEN472	Mata *ade2::ADE2::HIS3 met2 lys2-801 ura3-52, trp1::hisG leu2::LEU2::ADE2 his3∆200 dfm1∆::KanMX* *CEN::URA3::CFTR-HA*	This study
SEN474	Mata *ade2::ADE2::HIS3 met2 lys2-801 ura3-5, trp1::hisG leu2∆ his3∆200* *CEN::URA3::CFTR-HA-∆F508*	This study
SEN476	Mata *ade2::ADE2::HIS3 met2 lys2-801 ura3-52, trp1::hisG leu2::LEU2::ADE2 his3∆200 dfm1∆::KanMX* *CEN::URA3::CFTR-HA-∆F508*	This study
SEN478	Mata *ade2::ADE2::HIS3 met2 lys2-801 ura3-5, trp1::hisG leu2∆ his3∆200* *CEN::URA3::A1PiZ*	This study
SEN480	Mata *ade2::ADE2::HIS3 met2 lys2-801 ura3-52, trp1::hisG leu2::LEU2::ADE2 his3∆200 dfm1∆::KanMX* *CEN::URA3::A1PiZ*	This study
SEN452	Mata *ade2::ADE2::HIS3 met2 lys2-801 ura3-52, trp1::hisG leu2::LEU2::ADE2 his3∆200 dfm1∆::KanMX* *CEN::URA3*	This study
SEN455	Mata *ade2::ADE2::HIS3 met2 lys2-801 ura3-52, trp1::hisG leu2::LEU2::ADE2 his3∆200* *CEN::URA3*	This study

Supplemental Table 2.4.2 Yeast Strain Used in this Study (Continued)

Strain	Genotype	Reference
SEN365	ata *ADE2::HIS3::pGAL1::Hmg2-GFP met15Δ0 LYS2 (LYS+) ura3Δ0 TRP1 leu2Δ0 his3Δ1 pdr1Δ::KanMX*	This study
SEN366	Mata *ADE2::HIS3 met15Δ0 LYS2 (LYS+) ura3Δ0 TRP1 leu2Δ0 his3Δ1 pdr1Δ::KanMX*	This study
SEN395	Mata *ADE2::HIS3::pGAL1::Hmg2-GFP met15Δ0 LYS2 (LYS+) ura3Δ0 TRP1 leu2Δ0 his3Δ1 ubp8Δ::KanMX*	This study
SEN418	Mata *ADE2::HIS3 met15Δ0 LYS2 (LYS+) ura3Δ0 TRP1 leu2Δ0 his3Δ1 ubp8Δ::KanMX*	This study
SEN396	Mata *ADE2::HIS3::pGAL1::Hmg2-GFP met15Δ0 LYS2 (LYS+) ura3Δ0 TRP1 leu2Δ0 his3Δ1 miy2Δ::KanMX*	This study
SEN419	Mata *ADE2::HIS3 met15Δ0 LYS2 (LYS+) ura3Δ0 TRP1 leu2Δ0 his3Δ1 miy2Δ::KanMX*	This study
SEN397	Mata *ADE2::HIS3::pGAL1::Hmg2-GFP met15Δ0 LYS2 (LYS+) ura3Δ0 TRP1 leu2Δ0 his3Δ1 otu2Δ::KanMX*	This study
SEN420	Mata *ADE2::HIS3 met15Δ0 LYS2 (LYS+) ura3Δ0 TRP1 leu2Δ0 his3Δ1 otu2Δ::KanMX*	This study
SEN398	Mata *ADE2::HIS3::pGAL1::Hmg2-GFP met15Δ0 LYS2 (LYS+) ura3Δ0 TRP1 leu2Δ0 his3Δ1 ubp2Δ::KanMX*	This study
SEN421	Mata *ADE2::HIS3 met15Δ0 LYS2 (LYS+) ura3Δ0 TRP1 leu2Δ0 his3Δ1 ubp2Δ::KanMX*	This study
SEN399	Mata *ADE2::HIS3::pGAL1::Hmg2-GFP met15Δ0 LYS2 (LYS+) ura3Δ0 TRP1 leu2Δ0 his3Δ1 ubp5Δ::KanMX*	This study
SEN422	Mata *ADE2::HIS3 met15Δ0 LYS2 (LYS+) ura3Δ0 TRP1 leu2Δ0 his3Δ1 ubp5Δ::KanMX*	This study
SEN400	Mata *ADE2::HIS3::pGAL1::Hmg2-GFP met15Δ0 LYS2 (LYS+) ura3Δ0 TRP1 leu2Δ0 his3Δ1 miy1Δ::KanMX*	This study
SEN423	Mata *ADE2::HIS3 met15Δ0 LYS2 (LYS+) ura3Δ0 TRP1 leu2Δ0 his3Δ1 miy1Δ::KanMX*	This study
SEN402	Mata *ADE2::HIS3::pGAL1::Hmg2-GFP met15Δ0 LYS2 (LYS+) ura3Δ0 TRP1 leu2Δ0 his3Δ1 ubp1Δ::KanMX*	This study
SEN425	Mata *ADE2::HIS3 met15Δ0 LYS2 (LYS+) ura3Δ0 TRP1 leu2Δ0 his3Δ1 ubp1Δ::KanMX*	This study

Supplemental Table 2.4.2 Yeast Strain Used in this Study (Continued)

Strain	Genotype	Reference
SEN403	Mata *ADE2::HIS3::pGAL1::Hmg2-GFP met15Δ0 LYS2 (LYS+) ura3Δ0 TRP1 leu2Δ0 his3Δ1 ubp11Δ::KanMX*	This study
SEN426	Mata *ADE2::HIS3 met15Δ0 LYS2 (LYS+) ura3Δ0 TRP1 leu2Δ0 his3Δ1 ubp11Δ::KanMX*	This study
SEN405	Mata *ADE2::HIS3::pGAL1::Hmg2-GFP met15Δ0 LYS2 (LYS+) ura3Δ0 TRP1 leu2Δ0 his3Δ1 ubp7Δ::KanMX*	This study
SEN428	Mata *ADE2::HIS3 met15Δ0 LYS2 (LYS+) ura3Δ0 TRP1 leu2Δ0 his3Δ1 ubp7Δ::KanMX*	This study
SEN406	Mata *ADE2::HIS3::pGAL1::Hmg2-GFP met15Δ0 LYS2 (LYS+) ura3Δ0 TRP1 leu2Δ0 his3Δ1 ubp3Δ::KanMX*	This study
SEN429	Mata *ADE2::HIS3 met15Δ0 LYS2 (LYS+) ura3Δ0 TRP1 leu2Δ0 his3Δ1 ubp3Δ::KanMX*	This study
SEN453	Mata *ade2::ADE2::HIS3 met2 lys2-801 ura3-52, trp1::hisG leu2Δ his3Δ200* *CEN::URA3::pCUP1-HBT-Ubiquitin*	This study
SEN454	Mata *ade2::ADE2::HIS3 met2 lys2-801 ura3-52, trp1::hisG leu2Δ his3Δ200* *CEN::URA3*	This study
SEN457	Mata *ade2::ADE2::HIS3 met2 lys2-801 ura3-52, trp1::hisG leu2Δ his3Δ200* *CEN::URA3::pCUP1-HBT-Ubiquitin*	This study
SEN455	Mata *ade2::ADE2::HIS3 met2 lys2-801 ura3-52, trp1::hisG leu2Δ his3Δ200* *CEN::URA3*	This study
SEN481	Mata *ade2::ADE2::HIS3::pGAL1::Hmg2-GFP met2 lys2-801 ura3-52, trp1::hisG leu2Δ his3Δ200 dfm1Δ::KanMX* *CEN::URA3::pCUP1-HBT-Ubiquitin*	This study
SEN456	Mata *ade2::ADE2::HIS3::pGAL1::Hmg2-GFP met2 lys2-801 ura3-52, trp1::hisG leu2Δ his3Δ200 dfm1Δ::KanMX* *CEN::URA3*	This study

Supplemental Table 2.4.2 Yeast Strain Used in this Study (Continued)

Strain	Genotype	Reference
SEN482	Mata *ade2::ADE2::HIS3 met2 lys2-801 ura3-52, trp1::hisG leu2Δ his3Δ200 dfm1Δ::KanMX* *CEN::URA3::pCUP1-HBT-Ubiquitin*	This study
SEN452	Mata *ade2::ADE2::HIS3 met2 lys2-801 ura3-52, trp1::hisG leu2Δ his3Δ200 dfm1Δ::KanMX* *CEN::URA3*	This study
SEN122	*ade2::ADE2::HIS3 met2 lys2-801 ura3-52::URA3::4xUPRE::GFP TRP1 leu2Δ his3Δ200 der1Δ::CloNat*	This study
SEN123	*ade2::ADE2::HIS3::pGAL::Hmg2-6MYC met2 lys2-801 ura3-52::URA3::4xUPRE::GFP TRP1 leu2Δhis3Δ200 der1Δ::CloNat*	This study
RHY11923	Mata *ade2-101 met2 lys2-801 ura3-5, trp1::hisG::pGAL::Hmg2-GFP leu2Δ his3Δ200 pdr5Δ::HIS3*	This study
RHY11924	Mata *ade2-101 met2 lys2-801 ura3-5, trp1::hisG::pGAL::Hmg2-GFP leu2Δ his3Δ200 pdr5Δ::HIS3* *hrd1Δ::KanMX*	This study
RHY11925	Mata *ade2-101 met2 lys2-801 ura3-5, trp1::hisG::pGAL::Hmg2-GFP leu2Δ his3Δ200 pdr5Δ::HIS3* *dfm1Δ::CloNAT*	This study
RHY11916	Mata *ade2-101 met2 lys2-801 ura3-5, trp1::hisG::TRP1 leu2Δ his3Δ200 pdr5Δ::HIS3*	This study
RHY11917	Mata *ade2-101 met2 lys2-801 ura3-5, trp1::hisG::TRP1 leu2Δ his3Δ200 pdr5Δ::HIS3* *hrd1Δ::KanMX*	This study

Supplemental Table 2.4.2 Yeast Strain Used in this Study (Continued)

Strain	Genotype	Reference
RHY11918	Mata *ade2-101 met2 lys2-801 ura3-5, trp1::hisG::TRP1 leu2Δ his3Δ200 pdr5Δ::HIS3* *dfm1Δ::CloNAT*	This study
SEN409	Mata *ade2 met2 lys2-801 ura3-52 trp1::hisG leu2Δ his3Δ200 dfm1Δ::KanMX* *CEN::URA3::CPY*-GFP*	Nejatfard, et al., 2021
SEN410	Mata *ade2 met2 lys2-801 ura3-52 trp1::hisG leu2Δ his3Δ200 dfm1Δ::KanMX* *CEN::URA3::CPY*-GFP* *CEN::LEU2::pDFM1-DFM1-3HA*	Nejatfard, et al., 2021
SEN206	*Mata ADE2 met15Δ0 LYS2(LYS+) ura3Δ0 TRP1 leu2Δ0 his3Δ1 hrd1Δ::KanMX* *CEN::HIS3::PDR5*-HA* *CEN::LEU2::pDFM1-DFM1-3HA*	Nejatfard, et al., 2021
SEN264	*Mata ADE2 met15Δ0 LYS2(LYS+) ura3Δ0 TRP1 leu2Δ0 his3Δ1 hrd1Δ::KanMX* *CEN::HIS3::PDR5*-HA* *CEN::LEU2*	Nejatfard, et al., 2021
SEN554	*ade2-101 met2 lys2-801 ura3-52::URA3::HMG2-GFP trp1::hisG leu2Δ his3Δ200 pdr5Δ::KanMX*	This study
SEN555	*ade2-101 met2 lys2-801 ura3-52::URA3::HMG2-GFP trp1::hisG::TRP1 leu2Δ his3Δ200 hrd1Δ::KanMX*	This study
SEN556	*ade2-101 met2 lys2-801 ura3-52::URA3::HMG2-GFP trp1::hisG::TRP1::pHrd1::Hrd1-5MYC leu2Δ his3Δ200 hrd1Δ::KanMX*	This study
RHY10584	Mata *ADE2::ADE2::URA3::TDH3p-HMG2-GFP-K6R met15Δ0 LYS2 (LYS+) ura3Δ0 TRP1 leu2Δ0 his3Δ1 dfm1Δ::KanMX*	This study

Supplemental Table 2.4.2 Yeast Strain Used in this Study (Continued)

Strain	Genotype	Reference
RHY12239	*ade2-101 met2 lys2-801 ura3-52::URA3::HMG2-GFP trp1::hisG::TRP1 leu2Δ his3Δ200 dfm1Δ::KanMX* *CEN::LEU2*	This study
RHY12240	*ade2-101 met2 lys2-801 ura3-52 trp1::hisG::TRP1::TDH3-SEC61-GFP leu2Δ his3Δ200 dfm1Δ::KanMX* *CEN::LEU2::pDFM1-DFM1-3HA*	This study
RHY12241	*ade2-101 met2 lys2-801 ura3-52 trp1::hisG::TRP1::TDH3-SEC61-GFP leu2Δ his3Δ200 dfm1Δ::KanMX* *CEN::LEU2::pDFM1-5ASHP-3HA*	This study

Chapter 3: An ERAD-independent role for rhomboid pseudoprotease Dfm1 in mediating sphingolipid homeostasis

3.1 Introduction

Nearly one-third of nascent proteins are initially targeted to the endoplasmic reticulum (ER) where they are correctly folded and assembled before being delivered to their final cellular destinations. To prevent the accumulation of misfolded membrane proteins, ER-associated-degradation (ERAD) removes these clients from the ER membrane to the cytosol in a process known as retrotranslocation. Our previous work demonstrated that rhomboid pseudoprotease, Dfm1, is involved in the retrotranslocation of ubiquitinated integral membrane ERAD substrates. To survey for potential interaction partners of Dfm1, we performed protein-proximity labeling by BioID (proximity-dependent biotin identification) followed by mass spectrometry and identified several interacting proteins known to play a role in the sphingolipid biosynthesis pathway. Specifically, we found that Dfm1 associates with the SPOTS complex, which is composed of serine palmitoyltransferase (SPT) enzymes and accessory components and is critical for catalyzing the first rate-limiting step of the sphingolipid biosynthesis pathway. Herein, we found that Dfm1 binds directly to phosphorylated Orm2, a major antagonizer of SPT activity, to facilitate in Orm2 export from the ER and its subsequent degradation by EGAD (ER Golgi Associated Degradation). Moreover, recruitment of Cdc48 by Dfm1, which is critical for its role in ERAD retrotranslocation, is dispensable for Dfm1's role in controlling Orm2 export. Given that the accumulation of human Orm2 homologs, ORMDLs, are associated with many maladies, our study serves as a molecular foothold for understanding how dysregulation of sphingolipid metabolism leads to various diseases.

The endoplasmic reticulum (ER) carries out a vast range of functions including protein synthesis and transport, protein folding, lipid and steroid synthesis, carbohydrate

metabolism, and calcium storage. Almost all eukaryotic membrane and secreted proteins are co-translationally imported into the ER where they are subsequently folded (Sicari et al., 2019; Wang and Dehesh, 2018). Proteins frequently fail to fold or assemble properly, at which point they are eliminated by ER-Associated-Degradation (ERAD) (Mehrtash and Hochstrasser, 2019; Ruggiano et al., 2014; Sun and Brodsky, 2019).

ERAD describes a range of pathways that target and ubiquitinate a large repertoire of secretory and membrane substrates for proteasomal degradation. To date, most of the knowledge about ERAD is obtained in yeast and mammals. In yeast, ERAD substrates are classified according to the location of their lesions and are referred as ERAD-L (lesion in luminal domain), ERAD-M (lesion within the transmembrane domain), and ERAD-C (lesion in the cytosolic domain). The HMG-CoA reductase degradation (HRD) pathway utilizes the E3 ligase, Hrd1, to target ERAD-M and ERAD-L substrates, and the degradation of alpha 2 (DOA) pathway utilizes the E3 ligase, Doa10, to target ERAD-C substrates (Carvalho et al., 2006; Foresti et al., 2013; Hampton et al., 1996; Hiller et al., 1996; Laney and Hochstrasser, 2003). Moreover, unassembled ER subunits escaping to the inner nuclear membrane (INM) are targeted by the Asi complex (Foresti et al., 2014; Natarajan et al., 2020). ERAD pathways are much more diverse in mammalians cells due to the complexity of lesions or degrons within ERAD substrates (Leto et al., 2019). Although there are no Asi homologs present in mammals, there are at least 20 ER-localized ubiquitin ligases characterized that contribute to ERAD (Fenech et al.; Leto et al., 2019). A common theme for all ERAD pathways is the removal or retrotranslocation of ubiquitinated substrates from the ER membrane or INM followed by degradation by the proteasome (Hampton and Sommer, 2012). Retrotranslocation has been well-characterized in yeast, with two derlins, Der1 and

Dfm1, serving as major mediators of retrotranslocation for ERAD-L and ERAD-M substrates, respectively (Neal et al., 2018; Wu et al., 2020). Moreover, previous structural studies suggest that the multi-membrane spanning yeast E3 ligases, Hrd1 and Doa10, function as channels for the retrotranslocation of luminal and single-spanning membrane substrates, respectively (Schmidt et al., 2020; Wu et al., 2020). No analogous channel for multi-spanning membrane substrates had been determined, until Neal and colleagues identified the yeast derlin, Dfm1, as a major retrotranslocation factor for a subset of membrane substrates (Neal et al., 2018).

Dfm1 is an ER-resident multi-spanning membrane protein and is classified as a rhomboid pseudoprotease. Recently, we showed that Dfm1 utilizes its conserved rhomboid protein residues for substrate engagement and its lipid thinning properties to allow retrotranslocation of multi-spanning membrane substrates (Nejatfard et al., 2021a). To identify interacting partners of Dfm1 that may assist with retrotranslocation, we employed proximity-based labeling followed by mass spectrometry. Remarkably, we identified several proteins enriched with Dfm1, which are known to play a role in the sphingolipid biosynthesis pathway. Sphingolipids constitute a major class of lipids defined by their amino-alcohol backbone with mainly eighteen-carbon and are synthesized in the ER from non-sphingolipid precursors (Hannun and Obeid, 2018). Modification of this basic structure gives rise to the vast family of sphingolipids, which have essential roles in cell signaling and function. Serine palmitoyltransferase (SPT) is the first rate-limiting enzyme in the de novo synthesis of sphingolipids, and its sole function is to catalyze the initial step in sphingolipid biosynthesis by converting serine and palmitoyl-CoA into a sphingolipid precursor, 3-keto-sphinganine (Hanada, 2003). SPT is essential for the viability of all eukaryotic cells, and mutations of SPT

are linked to hereditary sensory neuropathy type 1 (HSAN1) and early onset amyotrophic lateral sclerosis (ALS) (Bode et al., 2015; Mohassel et al.). Accordingly, SPT serves as the key point for regulation of sphingolipid biosynthesis. SPT forms the SPOTS complex, comprised of Orm1 and Orm2 (members of the orosomucoid (ORM) gene family), Tsc3, and Sac1.The SPOTS complex is highly conserved from yeast to mammals (Breslow et al., 2010). Functionally, Orm1, Orm2, and phosphoinositide phosphatase Sac1 are evolutionarily conserved negative regulators of SPT, while Tsc3 is a positive regulator.

Previous studies have demonstrated that levels of several SPOT complex members and sphingolipid biosynthesis enzymes are regulated through protein degradation pathways in order to control sphingolipid levels. For example, the TORC2-Ypk1 signaling axis phosphorylates Orm2, triggering its export from the ER to the Golgi, where it is selectively ubiquitinated by the Dsc complex before being retrotranslocated and degraded by the cytosolic proteasome. This pathway is known as ER Golgi-Associated Degradation (EGAD)(Schmidt et al., 2019, 2020). Another study analyzing systematic turnover of proteins in yeast revealed that several enzymes and regulators involved in the de novo sphingolipid biosynthesis pathway are degraded in separate organelles, such as the Golgi and vacuole (Christiano et al., 2020). Although many enzymes and regulators associated with sphingolipid biosynthesis reside in the ER, an ER-localized regulator for sphingolipid homeostasis has not yet been identified. In this study, we report a novel role for the ER-resident Dfm1 in maintaining sphingolipid homeostasis. We find that Dfm1 physically and genetically interacts with SPOTS complex components. This includes a genetic interaction with TSC3, a positive regulator of SPT, whose function is essential for stimulating SPT activity at 37^{o}C. Specifically, loss of Dfm1 rescues the growth lethality of *tsc3*Δ cells by

increasing ceramide and complex sphingolipid levels. DFM1 also genetically interacts with ORM1, a negative regulator of SPT activity, in which *orm1*Δ*dfm1*Δ cells have an exacerbated growth defect due to increased flux in sphingolipid biosynthesis. Finally, we provide the first evidence that Dfm1 is required for Orm2 degradation, a function that is independent of Dfm1's classical ERAD-M retrotranslocation function. We confirm the independence of Dfm1's ERAD function and demonstrate that the EGAD-client, Orm2, does not require ERAD nor Inner Nuclear Membrane Associated Degradation (INMAD) pathways, which is in agreement with an earlier study (Schmidt et al., 2019). To better understand the role of Dfm1 in Orm2 degradation, we show that loss of Dfm1 results in accumulation of phosphorylated Orm2 at the ER, suggesting a novel role for Dfm1 in controlling Orm2 export from the ER and its subsequent degradation by EGAD. We further show that Dfm1 does not directly function with COPII dynamics and trafficking, but functions upstream of ER export where Dfm1 interacts with Ypk1-dependent phosphorylated Orm2. Overall, our work identifies the highly conserved derlin Dfm1 as a critical mediator of sphingolipid homeostasis and provides a new therapeutic target for maladies associated with dysregulation in sphingolipid homeostasis.

3.2 Results

3.2.1 Derlin Dfm1 interacts with members of the sphingolipid biosynthetic pathway

To identify potential Dfm-1 interacting proteins, Proximity-dependent biotin identification (BioID) was employed. Briefly, BirA-3xFLAG was fused to Dfm1 to survey for potential interacting partners (Fig. 1A). Because Dfm1 included an added BirA-3xFLAG epitope at the C-terminus, we wished to confirm that the tag did not affect the expression and function of Dfm1. To this end, tagged-DFM1 was placed under a galactose inducible promoter (GAL_{pr}) and cells expressing GAL-driven Dfm1-BirA-3xFLAG were grown in the

presence of 2% galactose. Under these conditions, induced expression of Dfm1 was observed at the expected molecular weight of ~60 kDa (Fig. 1B). BirA-3xFLAG alone expressed at both the expected size of ~25 kDa and at a larger size, which most likely represents BirA aggregates (marked by asterisks, Fig. 1B). To test whether Dfm1-BirA-3xFLAG function is still intact, we performed cycloheximide (CHX)-chase of a well-characterized Dfm1 substrate, Hmg2 (Hampton et al., 1996). We observed Hmg2-GFP degradation upon addback of Dfm1-BirA-3xFLAG while Hmg2-GFP degradation was stabilized with both empty vector and BirA-3xFLAG alone (Fig. 1C). To validate the identification of Dfm1 interactors via biotinylation, cells were treated with biotin and biotinylated proteins were enriched with streptavidin beads. As expected, the ATPase Cdc48, which has previously been shown to bind directly to Dfm1 (Neal et al., 2018; Sato and Hampton, 2006), was enriched in the biotin-treated samples, whereas neither Cdc48 nor Dfm1 were enriched in untreated or BirA-3xFLAG alone cells (Fig. 1D). Next, proteins that were enriched with streptavidin beads were digested to obtain tryptic peptides and analyzed by LC/MS/MS. Quantified proteins were mapped on volcano plots based on the significance and the ratio between biotin-treated Dfm1-BirA-3xFLAG and untreated control cells. High-confidence interacting proteins were identified using DEP and Maxquant analysis (Fig. 1E and Table S4) (Zuzow et al., 2018). By applying gene ontology (GO) enrichment analyses for the sets of Dfm1 interacting proteins identified, we found GO terms related to “Ceramide Metabolic Process” to be the most enriched (Fig. 1F). The interactions were validated by the presence of several ERAD components (Hrd1, Cdc48, proteasome subunits: Rpt2 and Pre9). Interestingly, closer analysis revealed unexpected interactions with SPOTS complex members (Orm1, Tsc3, and Lcb2). Taken together, these results suggest that our data have a high level of confidence and represent a rich source of Dfm1 interactome proteins, which include members of the sphingolipid biosynthesis pathway.

To validate the interaction of Dfm1 with SPOTS complex members, we performed co-immunoprecipitation (co-IP). Cells co-expressing Dfm1-GFP and members of the SPOTS complex (Lcb1-RFP, and Orm2-RFP) were subjected to immunoprecipitation via GFP Trap. Notably, Lcb1-RFP and Orm2-RFP co-immunoprecipitated with Dfm1-GFP, whereas no detectable association was seen in control cells without Dfm1-GFP (Fig. 2A). These interactions were also validated by fluorescence microscopy, in which the majority of Dfm1-GFP co-localized with Lcb1-RFP and Orm2-RFP at the ER (Fig. 2B).

3.2.2 DFM1 genetically interacts with TSC3

We next examined whether Dfm1 genetically interacts with SPOTS complex members. The SPOTS complex consists of the SPT enzymes, Lcb1 and Lcb2, and the smaller subunit, Tsc3, which has been required to positively regulate SPT at high temperatures (Gable et al., 2000). Furthermore, SPT activity is negatively regulated by two yeast paralogs, Orm1 and Orm2, through direct interactions, and by Sac1, which negatively regulates SPT through an unknown mechanism (Breslow et al., 2010; Han et al., 2010). To survey for gene interactions, we generated double mutant yeast strains of *dfm1*Δ along with respective SPOTS complex members and performed serial dilution growth assays to test whether double knockout cells confer any distinct growth phenotypes compared with WT and single knockouts. To test the involvement of essential enzymes Lcb1/Lcb2 and non-essential regulator Sac1, we utilized *Lcb1-DaMP*, *Lcb2-DamP*, and *sac1*Δ mutants and observed no genetic interactions, since growth of *dfm1*Δ*Lcb1-DaMP*, *dfm1*Δ*Lcb2-DaMP*, and *dfm1*Δ*sac1*Δ was similar to that of WT cells at 25^{o}C, 30^{o}C, and 37^{o}C (Fig. S1A). A small subunit of the SPT, Tsc3, directly interacts with Lcb1/Lcb2 to stimulate their activity and

increase synthesis of the sphingolipid precursor, 3-ketosphinganine. The stimulatory function of Tsc3 is essential at the higher temperature where the *tsc3*Δ temperature-sensitive phenotype is lethal due to lack of phytosphingosine (PHS) production ((Gable et al., 2000) and Fig. 3A). In line with this observation, we observed a growth defect and lethality from *tsc3*Δ cells at 30°C and 37°C, respectively (Fig. 3A, *filled triangle*), and rescue of lethality when PHS was supplied to *tsc3*Δ cells (Fig. 3B, *right panel; filled triangle*). Remarkably, removal of DFM1 in this background – *dfm1*Δ*tsc3*Δ – completely rescued the lethality at 37°C (Fig. 3A, *open circle*). Thus, removal of DFM1 suppresses *tsc3*Δ lethality at 37°C.

3.2.3 *dfm1Δtsc3Δ* cells have increased steady-state levels of ceramides and complex sphingolipids

We predicted that removal of DFM1 was able to reverse the temperature-sensitive lethality in *tsc3*Δ as a result of increased production of sphingolipid precursors. Notably, myriocin is a potent inhibitor of SPT, the first committed step in the sphingolipid biosynthesis pathway, and treatment with myriocin reduces sphingolipid levels in both *S. cerevisiae* and mammals (Breslow, 2013). Because SPT activity is essential, myriocin treatment exacerbates growth due to decreased flux in the sphingolipid biosynthesis pathway. We therefore wanted to test whether *dfm1*Δ*tsc3*Δ cells are resistant to myriocin inhibition. To this end, a sublethal dose of myriocin was used in the serial growth assay to reduce sphingolipid synthesis without impairing cell growth. As expected, *tsc3*Δ cells were sensitive to myriocin treatment at 30°C since these cells already have decreased sphingolipid levels (Fig. 3B, *left panel; filled triangle*). By contrast, the *dfm1*Δ*tsc3*Δ cells were resistant to myriocin treatment, suggesting that these cells have higher levels of sphingolipids (Fig. 3B, *left panel; open circle*). Indeed, when grown at 30°C, lipidomic analysis demonstrated that *dfm1*Δ*tsc3*Δ cells

significantly produced higher levels of ceramides (Type A, C, & D) and complex sphingolipid inositolphosphorylceramide (IPC) (Type B & C) in comparison to WT cells (Fig. 3C). Altogether, *dfm1*Δ*tsc3* cells appear to produce higher steady-state levels of ceramide and complex sphingolipids.

3.2.4 DFM1 genetically interacts with ORM1

Because removal of DFM1 leads to higher levels of ceramides and complex sphingolipids in *tsc3*Δ cells, we hypothesized that Dfm1 is antagonizing the sphingolipid biosynthesis pathway. If this hypothesis is correct, *dfm1*Δ cells should phenocopy both *orm1*Δ and *orm2*Δ cells, which are established negative regulators of the SPT enzymes, in the growth assays. To test this hypothesis, *orm1*Δ*tsc3*Δ and *orm2*Δ*tsc3*Δ cells were generated and employed in the growth assays at 25^{o}C, 30^{o}C, and 37^{o}C (Fig. 3D). Under these conditions, both *orm1*Δ and *orm2*Δ phenocopied *dfm1*Δ; both *orm1*Δ*tsc3*Δ and *orm2*Δ*tsc3*Δ cells were able to rescue the temperature-sensitive lethality displayed by *tsc3*Δ cells (Fig. 3D). Because *dfm1*Δ cells phenocopy both *orm1*Δ and *orm2*Δ cells, we next examined whether DFM1 genetically interacts with either ORM1 or ORM2. Although no growth defect was observed for *dfm1*Δ*orm2*Δ cells, we did observe a growth defect in *dfm1*Δ*orm1*Δ cells at room temperature, 30^{o}C, and 37^{o}C, suggesting that DFM1 functions with ORM1 in a parallel pathway (Fig. 4A, *filled triangle*). Furthermore, lipidomic analysis confirmed that *dfm1*Δ*orm2*Δ cells showed no increase in ceramides compared with WT cells. This was in contrast to *dfm1*Δ*orm1*Δ cells where there were significant changes in ceramides levels compared to WT cells (discussed below) (Fig. 4B & S1B). Orm1 and Orm2 have been shown to coordinate lipid homeostasis with ER protein quality control. This was demonstrated through growth sensitivity of *orm1*Δ*orm2*Δ cells to agents that increase protein

misfolding in the ER (Han et al., 2010). Because DFM1 genetically interacts with ORM1, we surmise that *dfm1*Δ*orm1*Δ cells should also exhibit growth sensitivity to ER protein misfolding agents (Fig. S1C). We performed growth assays on plates containing tunicamycin, an inhibitor of N-linked glycosylation. Growth sensitivity to tunicamycin was observed for *orm1*Δ, *orm2*Δ, and *dfm1*Δ cells whereas exasperated growth defects were observed for *dfm1*Δ*orm1*Δ and *orm1*Δ*orm2*Δ, but not *dfm1*Δ*orm2*Δ cells, further confirming that DFM1 genetically interacts with ORM1 and not ORM2. Cells lacking ORM1 and ORM2 exhibit a growth defect (Fig. 4A, *bottom panel*) due to an increased flux in de novo sphingolipid synthesis and the knockout cells were more resistant to myriocin inhibition (Breslow et al., 2010; Han et al., 2010). Given the growth defect seen in *dfm1*Δ*orm1*Δ cells, we reasoned that the flux in sphingolipid synthesis should be similarly increased. Notably, *dfm1*Δ*orm1*Δ cells were resistant to myriocin treatment (Fig. 4B, *left panel; open circle*) and sensitive to exogenously-added PHS (Fig. 4B, *right panel; open circle*), since *dfm1*Δ*orm1*Δ cells already exhibit higher levels of sphingolipids. Both dihydrosphingosine (DHS) and phytosphingosine (PHS) are early precursors of the sphingolipid biosynthesis pathway and are derivatives of long-chain bases (LCBs). Lipidomic analysis via mass spectrometry showed that C18-DHS levels were significantly higher in *dfm1*Δ*orm1*Δ cells than in WT cells. Also, C18-PHS levels were significantly higher in both *dfm1*Δ and *dfm1*Δ*orm1*Δ cells in comparison to WT cells, suggesting there is increased flux in sphingolipid biosynthesis in *dfm1*Δ*orm1*Δ cells (Fig. 4C). In contrast, the levels of ceramides and complex sphingolipids varied in *dfm1*Δ*orm1*Δ cells. There were higher levels of ceramide and complex sphingolipids (Type D) and lower levels of ceramide (Type A,B,&C) and complex sphingolipids (Type B) in *dfm1*Δ*orm1*Δ cells in comparison to WT cells (Fig. 4E). Notably, *orm1*Δ*orm2*Δ control cells also exhibited similar fluctuating levels of the varying types of ceramides and complex sphingolipids (Fig. 4E). Despite varying levels of ceramides and complex sphingolipids, *dfm1*Δ*orm1*Δ cells have

higher LCB levels and are resistant to myriocin treatment, which suggests that the major physiological effect of *dfm1*Δ*orm1*Δ cells is from increased SPT activity (Fig. 4B&C).

3.2.5 Orm2 is targeted by Dfm1 for degradation

Given the myriad biological processes carried out by sphingolipids, it is not surprising that disruptions to sphingolipid homeostasis have deleterious effects and must be tightly regulated. One possible mode of regulation is through regulated degradation of key enzymes and regulators of sphingolipid biosynthesis in a manner analogous to the regulated degradation of Orm2 by EGAD to establish sphingolipid homeostasis. We therefore tested whether key enzymes or regulators within the sphingolipid biosynthesis pathway are targeted for Dfm1-mediated degradation by performing cycloheximide (CHX)-chase assays on candidate substrates (Lcb1, Lcb2, Orm1, Orm2, Sac1, Tsc3, Ypk1 and Tsc10), which function in either SPT synthesis or regulation (Fig. S2A). Of these, Orm2 was rapidly degraded in wild-type strains and its degradation was completely prevented in *dfm1*Δ cells (Fig. 5A). The yeast paralog of Dfm1, Der1, has a strong broad role in retrotranslocating ERAD-L substrates (Wu et al., 2020). We therefore directly tested the role of Der1 in Orm2 degradation using the CHX-chase assay and found that in both WT and *der1*Δ cells, Orm2 was still degraded (Fig. 5B). These results imply that the degradation of Orm2 is specifically dependent on derlin Dfm1 and not Der1.

3.2.6 Derlin Dfm1's Cdc48 recruitment function is not required for Orm2 degradation

We have previously identified specific motifs and residues of Dfm1 that are critical for its ERAD retrotranslocation function. Accordingly, we wished to test the importance of these motifs/residues for Orm2 degradation by performing CHX-chase assays. Dfm1 possesses a

unique C-terminal SHP box motif, which recruits the ATPase, Cdc48, directly to the ER surface (Neal et al., 2018). Cdc48 functions as an energy source for membrane substrate retrotranslocation and as a retrochaperone where it acts to maintain the solubility of retrotranslocated membrane substrates prior to proteasome degradation (Neal et al., 2017). We previously demonstrated that mutations within the SHP box, Dfm1-5Ashp, ablates Cdc48 recruitment and the retrotranslocation function of Dfm1 (Fig. 5C) (Neal et al., 2018). We also demonstrated that a Der1-SHP chimera, which consists of Der1, the paralog of Dfm1, fused to the cytoplasmic SHP tail of Dfm1, supports Cdc48 recruitment via binding of Cdc48 to the chimera's SHP tail, but does not support retrotranslocation through Der1's transmembrane segment (Fig. 5C) (Neal et al., 2018). We utilized these retrotranslocation-deficient variants in our CHX-chase assay to test whether Dfm1's Cdc48 recruitment function is required for Orm2 degradation. Addback of Der1-SHP in *dfm1*Δ cells impaired Orm2 degradation whereas Dfm1-5Ashp addback still enabled Orm2 degradation (Fig. 5D). These results suggest that recruitment of Cdc48 by Dfm1 is dispensable for Orm2 degradation. In addition, the inability of Der1-SHP to facilitate degradation of Orm2 implies the involvement of additional residues within the transmembrane segments of Dfm1.

Dfm1 contains the highly conserved WR motif in loop 1 (L1) and a Gx3G motif in transmembrane 6 (TM6). Both motifs have previously been substituted for alanine residues (WA and Gx3A) and such mutants are unable to support retrotranslocation (Fig. 5E & F) (Neal et al., 2018). In addition, we have previously identified that the L1 and TM2 regions of Dfm1 are critical for its retrotranslocation function (Fig. 5E & F). Specifically, L1 mutants (F58S, L64V, and K67E) impaired membrane substrate binding to Dfm1 and TM2 mutants (R98L, S99V, S100V, and Q101L) impaired Dfm1's lipid thinning distortion function

(Nejatfard et al., 2021). The lipid distortion function of Dfm1 increases lipid permeability to aid the extraction of integral membrane substrates from the lipid bilayer. All mutants are well characterized to date where they show robust Dfm1 expression (Fig. S2B) (Neal et al., 2018; Nejatfard et al., 2021). Accordingly, the effect of these retrotranslocation-deficient mutants on Orm2 degradation was directly tested with the CHX-chase assay. All Dfm1 mutants, with the exception of Dfm1-5Ashp, completely stabilized Orm2 (Fig. 5G). Furthermore, we employed the substrate binding co-IP assay to analyze the association of Dfm1 L1 mutants with Orm2-GFP. Orm2-GFP was immunoprecipitated with GFP Trap and immunoblotted for Dfm1 with α-HA. There was no detectable association of Orm2 with Dfm1 L1 mutants, implying that all three L1 residues are required for Orm2 binding (Fig. 5H). Overall, the conserved rhomboid motifs, WR and Gx3G, the L1 region for substrate binding, and the TM2 region for lipid thinning, are all required for Orm2 degradation. We employed another functional assay for Dfm1 to test whether the retrotranslocation-deficient Dfm1 mutants can restore growth in *dfm1*Δ*orm1*Δ cells, which normally have impaired growth at 37°C due to increased flux in sphingolipid synthesis. To this end, adding back empty vector or wild-type DFM1 to *dfm1*Δ*orm1*Δ cells resulted in the expected impairment and rescue of normal growth, respectively (Fig. S2C & D). Introduction of Dfm1 mutants to *dfm1*Δ*orm1*Δ cells did not rescue growth defects, with the exception of Dfm1-5Ashp, which was able to rescue the growth defect in a manner similar to that of WT Dfm1 (Fig. S2C). Taken together, these data suggest that the substrate binding, lipid distortion function, and conserved rhomboid motifs, but not Cdc48 recruitment function, of Dfm1 are required for Orm2 degradation.

3.2.7 Orm2 degradation is dependent on EGAD, but not ERAD or INMAD

Given that the Cdc48 recruitment function of Dfm1 is dispensable for Orm2 degradation, it seems likely that Dfm1's retrotranslocation function in ERAD is not required for Orm2 degradation. Accordingly, we wished to survey for all protein degradation pathways in which Dfm1 may participate. The secretory pathway possesses several protein quality-control pathways including the INM-associated degradation (INMAD), ERAD, and EGAD, which govern both regulated and quality-control degradation of INM proteins, ER proteins, and Endosomal/Golgi proteins, respectively (Sicari et al., 2019; Sun and Brodsky, 2019). All pathways employ dedicated E3 ligases that determine substrate specificity and ubiquitination. Specifically, the Asi and Doa10 E3 ligases mediate INMAD, the Hrd1 and Doa10 E3 ligases mediate ERAD, and Tul1 E3 ligase mediates EGAD. A unifying theme for all protein degradation pathways is that they require the hexameric AAA ATPase, Cdc48, and the proteasome for retrotranslocation and degradation of all substrates. We utilized the CHX-chase assay to test the requirement for all E3 ligases, Cdc48, and the proteasome for degradation of Orm2. In line with previous studies (Schmidt et al., 2019), Orm2 was still degraded with similar kinetics to wild-type strains in *hrd1Δ, doa10Δ*, and *asi1Δ* (Fig. 6A). These results indicate that Orm2 degradation does not require either the INMAD or ERAD pathways. As expected, Orm2 degradation was completely inhibited in *tu1lΔ* cells, *cdc48-2* cells, and proteasome subunit mutant, *hrd2-1* (Fig. 6B) (Schmidt et al., 2019). These observations are in accordance with previous studies and demonstrate that Orm2 ubiquitination, extraction, and proteasome degradation is mediated solely by EGAD (Schmidt et al., 2019). To further confirm that Orm2 degradation is independent of ERAD and INMAD, we performed *in vivo* ubiquitination assays on WT, *asi1Δ*, *hrd1Δ*, *doa10Δ*, *tul1Δ*, *cdc48-2*, and *hrd2-1* strains. Strains were lysed and subjected to immunoprecipitation (IP) using anti-RFP antibodies, followed by immunoblotting (IB) with anti-ubiquitin and anti-RFP antibodies. As suggested by CHX-chase experiments conducted by our lab and others (Schmidt et al.,

2019), the degree of Orm2 ubiquitination in *asi1Δ*, *hrd1Δ*, and *doa10Δ* was similar to that seen in WT strains, demonstrating that the E3 ligases Asi, Hrd1, and Doa10 are not involved in the polyubiquitination of Orm2 (Fig. 6C, *lanes 1, 2, 3, 4*). In line with a previous study, the amount of Orm2 ubiquitination is increased in *cdc48-2* and *hrd2-1* cells, suggesting that Orm2 is on pathway for retrotranslocation and proteasome degradation (Fig. 6C, *lanes 8, 9*) (Schmidt et al., 2019).

As expected, Orm2 ubiquitination was decreased in *tul1Δ* strains, indicating that Orm2 is ubiquitinated by Tul1-dependent EGAD (Fig. 6C, lane 5). To further confirm that Orm2 degradation is independent of EGAD and INMAD, we next tested whether any of the ERAD components besides Dfm1, genetically interacted with Tsc3 and Orm1. Specifically, we examined whether any ERAD mutants phenocopy *dfm1Δtsc3Δ* cells, which rescues lethality at 37°C, or *dfm1Δorm1Δ*, which exhibits a growth defect at 37°C. To this end, double mutants were generated in which *tsc3Δ* or *orm1*Δ was knocked out, along with the following HRD and DOA pathway components: *hrd1Δ*, *hrd3*Δ, *der1*Δ, and *doa10*Δ. In all cases, the HRD and DOA pathway mutants did not phenocopy *dfm1*Δ: *hrd1Δtsc3Δ*, *hrd3Δtsc3Δ*, *der1Δtsc3Δ*, and *doa1Δtsc3Δ* were unable to rescue the temperature-sensitive lethality of *tsc3*Δ (Fig. 6D); and *hrd1Δorm1Δ, doa10Δorm1Δ, hrd2-1orm1Δ,* and *cdc48-2Δorm1Δ* did not exhibit an exacerbated growth defect at 30°C (Fig. S2E). Hence, the DOA and HRD ERAD pathways do not genetically interact with Tsc3 or Orm1. In summary, CHX-chase, genetics, and *in vivo* ubiquitination assays confirmed that Orm2 is degraded solely by the EGAD pathway and not by INMAD or ERAD.

3.2.8 Dfm1 does not function at the post-ubiquitination step of Orm2 degradation

pathway

To determine the step at which Dfm1 functions in Orm2 degradation, the ubiquitination status of Orm2 in *dfm1Δ* strains was analyzed. We have previously demonstrated that Dfm1 functions at the post-ubiquitination step of ERAD, with an increased degree of polyubiquitination of ERAD-M substrates was observed in *dfm1Δ* strains (Neal et al., 2018). This was caused by the inability of Dfm1 to retrotranslocate its substrates, resulting in build-up of polyubiquitinated membrane substrates along the ER membrane. Surprisingly, in *dfm1Δ* strains, the level of Orm2 ubiquitination was the same as in WT strains and did not phenocopy retrotranslocation-deficient strains, *cdc48-2*, or the proteasomal mutant *hrd2-1* (Fig. 6C, lanes 7,8,9). Hence, Dfm1 does not function in the post-ubiquitination step of EGAD. We also tested the requirement of Der1 for Orm2 ubiquitination and saw no change in Orm2 ubiquitination levels in *der1Δ* strains compared with WT strains (Fig. 6C, lanes 1 & 7). Taken together, these data suggest that Dfm1 does not function at the post-ubiquitination step of the Orm2 degradation pathway.

3.2.9 Dfm1 does not directly function in EGAD

Given the requirement for Dfm1 in Orm2 degradation, it is surprising that the Dfm1-dependent ERAD pathway is not involved with Orm2 degradation. It is possible that Dfm1 directly functions in EGAD. To test this hypothesis, we examined the interaction of Dfm1 with the Dsc complex (E3 ligase Tul1 and Dsc2), which mediates substrate detection and ubiquitination within the Golgi in the EGAD pathway. Dfm1-GFP was immunoprecipitated with GFP Trap antibodies followed by SDS-PAGE and immunoblotting for endogenous Tul1 and Dsc2 with anti-Tul1 and anti-Dsc2, respectively. In all cases, no association of Dfm1 with Tul1 and Dsc2 was observed, while Dfm1 was able to associate with Cdc48, as expected

(Fig. S3). Moreover, fluorescence microscopy demonstrated that Dfm1 is solely localized in the ER and does not co-localize with Golgi-associated markers (Fig. 2B). Finally, there were no significant interactions between Dfm1 and any EGAD components identified from our proteomic analysis (Fig. 1E, Table S4).

3.2.10 Dfm1 is required for Orm2 export from the ER to the Golgi

The observation that Dfm1-5Ashp can still facilitate Orm2 degradation suggest that Dfm1-mediated degradation of Orm2 is independent of its canonical retrotranslocation role in ERAD. Hence, we sought to identify the specific step at which Dfm1 functions within the Orm2 degradation pathway. EGAD-mediated degradation of Orm2 is most well characterized in yeast where it consists of five steps: 1) phosphorylation of Orm2 by Ypk1 in the ER, 2) COPII-mediated export of phosphorylated Orm2 from ER to Golgi and endosome, 3) polyubiquitination of Orm2 by the E3 ligase Dsc2, 4) retrotranslocation of substrates from the Golgi/endosome to the cytosol, and 5) degradation of the ubiquitinated substrates by the cytosolic proteasome (Schmidt et al., 2019). To determine which step was blocked in Dfm1-deficient cells, we analyzed the phosphorylation status of Orm2 in *dfm1*Δ cells. In *dfm1*Δ, Orm2 phosphorylation was increased to levels similar to those in the Dsc complex mutant *tul1*Δ, a knockout that blocks Orm2 degradation and leads to accumulation of phosphorylated Orm2 (Fig. 7A). This indicates *dfm1*Δ cells result in defective trafficking of Orm2 to the Golgi. To validate this in a cellular context, we next utilized live cell imaging fluorescence microscopy to determine the cellular compartment in which Orm2 was accumulating in *dfm1*Δ cells. In line with a previous study, Orm2 accumulated mainly in the early endosomes in *tul1*Δ cells (Schmidt et al., 2019), indicating that Orm2 was being routed to the Golgi/endosomes for degradation. By contrast, in *dfm1*Δ cells, Orm2 accumulated mainly at the ER and Orm2

co-localized with an ER, but not an endosome marker (Fig. 7B). In parallel, we utilized a phospho-mimetic Orm2 variant (Orm2-3D), which has been shown to mimic Ypk1-dependent constitutive phosphorylation and is continuously exported from the ER and degraded via EGAD. Indeed, we and others show that in WT cells, Orm2-3D is rapidly degraded (Fig. 7C) (Schmidt et al., 2019, 2020). Remarkably, by employing a CHX-chase assay, we found that Orm2-3D degradation was completely prevented in *dfm1*Δ cells (Fig. 7C). Using microscopy, we confirmed that Orm2-3D remained exclusively in the ER in *dfm1*Δ cells (Fig. 7E). By contrast, degradation of an Orm2 phosphonull variant (Orm2-3A) was completely prevented in WT cells (Fig. 7C) and we and others showed that Orm2-3A was not exported to the ER (Fig. S4)(Schmidt et al., 2019). Because *orm2*Δ cells can rescue *tsc3*Δ lethality, we wanted to test whether Orm2-3D or Orm2-3A elicits the same effect. To test this, either phosphonull Orm2-3A or phosphomimetic Orm2-3D were added to *tsc3*Δ*orm2*Δ cells and the growth assay was employed. As controls, Orm2-3A alone and Orm2-3D cells grew similarly as WT cells whereas *tsc3*Δ cells exhibited the expected growth lethality at 37°C. Notably, *tsc3*Δ*orm2*Δ cells containing Orm2-3D alleviated *tsc3*Δ lethality whereas *tsc3*Δ*orm2*Δ cells containing Orm2-3A did not rescue *tsc3*Δ lethality (Fig. 7D). These results suggest that two conditions are sufficient in rescuing *tsc3*Δ lethality: 1) absence of Orm2 (*orm2*Δ) or 2) continuous phosphorylation and degradation of Orm2 via EGAD (Orm2-3D). In summary, based on CHX-chase, live image florescence microscopy, and genetic interaction assays, we demonstrate that Dfm1 is required for the export of phosphorylated Orm2 from the ER to Golgi. The physiological consequence for Dfm1 dysfunction is retention of Orm2 in the ER, which prevents its subsequent degradation.

Our data demonstrates that Dfm1-deficient cells accumulate phosphorylated Orm2 within the ER, the negative regulator of sphingolipid biosynthesis, which raises the question of why increased levels of LCBs, ceramides, and complex sphingolipids were observed in *dfm1*Δ and *dfm1*Δ*tsc3*Δ cells? Our results were in contrast to our initial expectation that accumulation of Orm2 would decrease levels of LCB and ceramides, since Orm2 antagonizes the sphingolipid biosynthesis pathway. One possibility is that in *dfm1*Δ cells, ER-localized phosphorylated Orm2 is no longer able to repress SPT activity. To test this possibility, we measured steady-state levels of PHS in WT and *dfm1*Δ cells either expressing phosphomimic Orm2-3D or phosphonull Orm3A. As expected, in both WT and *dfm1*Δ cells, Orm2-3A leads to low steady-state levels of PHS whereas in WT cells with Orm2-3D, which is constitutively degraded by EGAD, leads to significantly higher levels of PHS (Fig. 7F). Notably, *dfm1*Δ cells with Orm2-3D, which is phosphomimic Orm2 accumulating in the ER, leads to significantly higher levels of PHS (Fig. 7F). This finding suggests accumulation of phosphorylated Orm2 at the ER does indeed increase SPT activity.

3.2.11 Loss of Dfm1 does not affect COPII-mediated trafficking

Because loss of Dfm1 resulted in accumulation of Orm2 in the ER, we directly interrogated the role of Dfm1 in COPII-mediated trafficking. To test whether Dfm1 has a direct function in COPII-mediated trafficking, we analyzed the steady-state levels of COPII cargo substrate, carboxypeptidase Y (CPY), and found that in *dfm1*Δ cells, the mature form of CPY accumulated at similar levels as WT cells (*m*; Fig. S4B). As a control for a deficiency in COPII-mediated export, when *sec12-1* cells were shifted to nonpermissive growth temperature at 37^{o}C, there was the expected buildup of the premature form (*P*; Fig. S4B). Finally, we did not identify significant interactions between Dfm1 and any COPII trafficking

components from our proteomic analysis (Fig. 1C, Table S4). Taken together, our data suggests that Dfm1 does not directly function in COPII-dependent trafficking.

3.2.12 Dfm1 interacts with Ypk1-dependent phosphorylated Orm2

Because Dfm1 isn't functioning in ER exit, we hypothesize that Dfm1 is functioning directly with the SPOTs complex where it specifically interacts with phosphorylated Orm2. To interrogate this, we used co-IP to test interactions of Dfm1 with either phosphomimic Orm2-3D or phospho-null Orm2-3A. As a negative control, a strain containing empty vector (instead of Dfm1-HA) was included. We also tested the binding of Dfm1 to an ER membrane protein, Sec61, that isn't normally associated with SPOTS complex members and Dfm1. Notably, Dfm1 associated with both WT Orm2 or phosphomimic Orm2-3D and not phospho-null Orm2-3A (Fig. 8A). In strains expressing Orm2-3A, Dfm1 no longer interacted with Orm1, Lcb1, and Lcb2, which implicates that Dfm1 interacts with SPOTs complex members through binding of Orm2. We confirmed this using co-IP in *orm2*Δ cell in which Dfm1 no longer interacted with Orm1, Lcb1, and Lcb2 (Fig. 8B). In yeast, TORC2-Ypk1 signaling axis is required for Orm2 phosphorylation, which triggers Orm2 degradation by EGAD whereas TORC1-Npr1 signaling axis is required for Orm2 phosphorylation at distinct sites to stimulate synthesis of complex sphingolipids (Schmidt et al., 2020; Shimobayashi et al., 2013). We were interested in investigating the effect of Ypk1-mediated *versus* Npr1-mediated Orm2 phosphorylation on Dfm1 interaction. To address this, co-IP was performed in *ypk1*Δ and *npr1*Δ cells. In *npr1*Δ cells, the SPOTs complex remain intact where Orm2 associated with Dfm1, Lcb1, Lcb2, and Orm1 (Fig. 8C). In contrast, in *ypk1*Δ cells, Orm2 no longer associated with Dfm1, but remain associated with Lcb1, Lcb2, and Orm1 (Fig. 8C). Interestingly, in cells lacking either Npr1 or Ypk1, Orm2 still associated with other SPOTs

complex members indicating phosphorylation status of Orm2 doesn't affect its interactions with the SPOTs complex. Overall, our findings indicate that Dfm1 specifically interacts with Ypk1-dependent phosphorylated Orm2.

3.3 Discussion

In this study, we describe a novel role for the derlin rhomboid pseudoprotease, Dfm1, in maintaining sphingolipid homeostasis. The function of Dfm1 in ERAD-M retrotranslocation of misfolded membrane protein substrates has been well established in our laboratory and this study uncovers an additional biological function of Dfm1. The role of Dfm1 in maintaining sphingolipid homeostasis appears to be separate from its role in ERAD-M retrotranslocation. Our study indicates that Dfm1 is required to facilitate the export of phosphorylated Orm2 from the ER and that this function requires substrate bindingand lipid thinning activity, but not its Cdc48 recruitment function. Specifically, Dfm1 functions immediately downstream of Ypk1-dependent Orm2 phosphorylation where Dfm1 associates with the SPOTs complex through binding of phosphorylated Orm2 and not unphosphorylated Orm2 (Fig. 8D). Overall, our studies reveal a novel role for rhomboid pseudoproteases in maintaining sphingolipid homeostasis, a function that is independent of their role in ERAD.

To identify Dfm1 interacting partner proteins, we performed proximity-dependent biotinylation (BioID) coupled with mass spectrometry. Several proteins found in close proximity to Dfm1 were involved in the sphingolipid biosynthesis pathway. The first committed step of the sphingolipid biosynthetic pathway is catalyzed by the serine palmitoyl transferase (SPT) complex, which consists of Lcb1, Lcb2, and Tsc3. This step is strictly regulated by Orm1/Orm2 and Sac1, which negatively regulates SPT, and Tsc3, and enhances SPT activity 100-fold. Indeed, we confirmed a physical interaction between Dfm1

and the SPOTS complex members Orm2 and Lcb1. To further explore the relationship between Dfm1 and SPOTS complex members, we examined the genetic interactions between *dfm1*Δ and knockout of SPOTS complex members or sphingolipid biosynthetic enzymes. We exploited the *tsc3*Δ growth lethality phenotype at 37°C, which is due to Tsc3 being required for enhancing SPT activity at 37°C. Growth assays and lipidomic analyses indicated that *dfm1*Δ cells phenocopy established negative regulators of the SPT enzymes, *orm1*Δ and *orm2*Δ, where all three are able to reverse the temperature-sensitive lethality of *tsc3*Δ by increasing ceramide and complex sphingolipid levels. Therefore, we propose that Dfm1 antagonizes the sphingolipid biosynthesis pathway.

The mechanism associated with Dfm1-dependent Orm2 export from the ER remains to be elucidated. Our data suggests that Dfm1 functions at the post-phosphorylation step of Orm2 where loss of Dfm1 blocks ER export of phosphorylated Orm2. Moreover, Dfm1 does not directly function in COPII export since its absence does not abrogate export of a COPII cargo, CPY. Instead, Dfm1 directly binds to Ypk1-dependent phosphorylated Orm2, which is followed by its exit from the ER and degradation by EGAD. Our laboratory has recently identified a chaperone-like Dfm1 function where it influences the solubility of aggregate-prone misfolded membrane substrates along the ER membrane (Kandel et al., 2022). Similar to Dfm1's function as a mediator in sphingolipid homeostasis, its chaperone-like role requires Dfm1's substrate binding and lipid thinning function, but not its Cdc48 recruitment function. Based on the solubility assay, Dfm1 doesn't significantly enhance the solubility of Orm2 since majority of it remains solubilized in the presence and absence of Dfm1 (Fig. S4C). In this case, Dfm1 may not be required for influencing the solubility of Orm2, but is utilizing another chaperone-like activity to prime Orm2 for delivery to the COPII machinery for ER export (Fig.

8D). The extent to which the chaperone-like activity of Dfm1 is required for Orm2 export from the ER warrants future investigations.

Based on lipidomic analysis, *dfm1*Δ cells accumulate phosphorylated Orm2, which no longer inhibits SPT activity. This was shown through marked increase in PHS steady-state levels in *dfm1*Δ cells expressing phosphomimic Orm2-3D. This raises the question of why accumulation of a negative regulator wouldn't inhibit sphingolipid biosynthesis? A possible explanation is based from a previous study in which Orms have been found to directly regulate the localization and oligomerization state of SPT at the ER in a manner that is dependent upon their phosphorylation state. Specifically, phosphorylated Orm2 shifts SPT to the monomeric state, which contributes to sustained SPT activity (Han et al., 2019). This model is supported by our co-IP experiment, in which phosphorylated Orm2 still associated with the SPOTs complex (Fig. 8A). In this context, phosphorylated Orm2 may have a direct influence on increasing SPT activity. Investigating how phosphorylated Orm2 leads to increased SPT activity will be a fruitful line of inquiry to address in the future.

The ER hosts metabolic pathways that synthesize a variety of lipids such as phospholipids, cholesterol, and sphingolipids. Thus, it is critical for the ER to sense and respond to fluctuations in lipid composition in order to maintain cellular homeostasis (Fun and Thibault, 2020; Piña et al., 2018; Tam et al., 2018). Several pathways are employed to maintain the flux of the lipid biosynthetic pathway. One such pathway is the targeting and degradation of lipid biosynthetic enzymes through ERAD-mediated degradation. For example, cholesterol synthesis is downregulated through regulated ERAD of the rate-controlling cholesterol biosynthetic enzymes Hmg-CoA reductase and squalene monooxygenase (Wangeline et al., 2017). Maintenance of lipid homeostasis is also critical

for protein synthesis, as dysregulated lipid levels negatively impact ER protein quality-control machineries. This is supported by studies demonstrating that increased flux of sphingolipids induces UPR and sensitivity of cells to ER stress (Han et al., 2010). This is also in alignment with our observations where *dfm1*Δ*orm1*Δ cells are sensitive to ER stress due to dysregulated sphingolipid metabolism (Fig. S1A). Previous studies from our lab and others have demonstrated that lipid thinning by the ERAD machinery facilitates the removal of misfolded substrates from the ER (Neal et al., 2018; Wu et al., 2020). Because lipids play a large role in ERAD retrotranslocation, fine-tuning lipid levels is critical to ensure that ERAD remains intact and functional. Our findings implicate Dfm1 as a mediator in sphingolipid homeostasis. Interestingly, by utilizing homology modeling and bionformatic analysis, we identified sphingolipid-binding motifs on TM1 and TM6 of Dfm1, suggesting that Dfm1 may directly detect sphingolipid levels and fine-tune the control of sphingolipid production by modulating the export of Orm2 (unpublished data). Similarly, cholesterol has been shown to directly regulate levels of the E3 ligase MARCH6 levels, with increased MARCH6 levels leading to ubiquitination and degradation of the key cholesterol enzyme, squalene monoozygenase (Zelcer et al., 2014). Future studies on the lipid-sensing function of Dfm1 and how it de-represses SPT activity via Orm2 export from the ER will require additional experimentation.

The Orm family proteins are well conserved and all three human ORMDLs associate with SPT and directly regulate SPT activity. However, unlike their yeast counterparts, they do not appear to be phosphorylated since they lack the homologous N-terminal domains that are phosphorylated by Npr1, Ypk1, and Ypk2 in yeast. Instead, ORMDL protein levels are regulated directly by ceramide levels (Davis et al., 2019). Consistent with this finding, altered

protein levels of ORMDLs are associated with the pathophysiology of a range of diseases, including colorectal cancer, inflammation, obesity, and diabetes (Davis et al., 2018). Moreover, single nucleotide polymorphisms near ORMDL3, which lead to its increased expression, are associated with childhood asthma. Accordingly, our observation that yeast Dfm1 alters Orm2 protein levels and impacts sphingolipid metabolism raises the possibility that derlins have a causative role in these diseases. Defining the mechanism of Dfm1-mediated regulation of Orm2 levels should illuminate new treatment paradigms for patients with dysregulated sphingolipid metabolism.

In summary, we have performed proteomic analyses to enable the identification of Dfm1 interacting factors. These studies have demonstrated that several key regulators of sphingolipid biosynthesis are associated with Dfm1 and we report a novel function for Dfm1 in mediating sphingolipid homeostasis. Sphingolipids play diverse roles in cellular functions, which includes cell signaling, supporting cellular structure, providing energy storage, and regulating cell growth cycles. Dysregulation of sphingolipid levels has been associated with several life-threatening disorders. Overall, this study identifies derlin rhomboid pseudoproteases as key regulators of sphingolipid levels and reveals them as potential therapeutic targets for treatment of lipid disorders that are associated with the dysregulation of sphingolipid levels.

3.4 Methods

Yeast and Bacteria Growth Media

Standard yeast *Saccharomyces cerevisiae* growth media were used as previously described (Hampton and Rine, 1994), including yeast extract-peptone-dextrose (YPD)

medium and ammonia-based synthetic complete dextrose (SC) and ammonia-based synthetic minimal dextrose (SD) medium supplemented with 2% dextrose and amino acids to enable growth of auxotrophic strains at 30°C. *Escherichia coli* Top10 cells were grown in standard LB media with ampicillin at 37°C as previously described (Gardner et al., 1998). HEK293 cells were cultured in DMEM medium supplemented with 10% FBS.

Plasmids and Strains

Plasmids used in this study are listed in Table S1. Plasmids for this work were generated using standard molecular biological techniques (Sato et al., 2009) and verified by sequencing (Eton Bioscience, Inc.). Primer information is available upon request. Lcb1-RFP and Orm2-RFP plasmids were a gift from Theresa Dun (Uniformed Services University of the Health Sciences, MD). Orm2-3A-GFP and Orm2-3D-GFP plasmids were a gift from Oliver Schmidt and David Teis (Medical University of Innsbruck, Austria).

A complete list of yeast strains and their corresponding genotypes are listed in Table S2. All strains used in this work were derived from S288C or Resgen. Yeast strains were transformed with DNA or PCR fragments using the standard LiOAc method (Ito et al., 1983). Null alleles were generated by using PCR to amplify a selection marker flanked by 50 base pairs of the 5' and 3' regions, which are immediately adjacent to the coding region of the gene to be deleted. The selectable markers used for making null alleles were genes encoding resistance to G418 or CloNat/nourseothricin. After transformation, strains with drug markers were plated onto YPD followed by replica-plating onto YPD plates containing (500 µg/mL G418 or 200 µg/mL nourseothricin). All gene deletions were confirmed by PCR.

*dfm1*Δ strain handling

Due to rapid suppression nature of *dfm1*Δ null strains, freshly transformed *dfm1*Δ null cells with the respective substrates should be used in every assay. Generation of Dfm1 mutant strains and troubleshooting guidelines are found in (Bhaduri and Neal, 2021).

Proximity dependent-biotinylation (BioID)

WT cells expressing either BirA-3xFlag or Dfm1-BirA-3xFlag cells were inoculated in minimal media supplemented with 1 µM biotin and 0.2% raffinose and grown overnight at 30^{o}C. The following day, the cells were diluted to 0.2 OD_{600} and grown to log phase (0.3-0.5 OD_{600}). Once in log-phase, 0.2% galactose was added to induce the expression of BirA-3xFlag and Dfm1-BirA-3xFlag. After 1 hour of incubation, cells were pelleted and stored at -80°C overnight. The next day, cells were thawed and resuspended in lysis buffer (50 mM Tris-HCl pH 7.5, 150 mM NaCl, 1.5 mM $MgCl_2$, 1 mM EDTA, 0.1% SDS, 1% NP-40, 0.4% sodium deoxycholate, and 1 mM DTT supplemented with proteasezinhibitors: 1 m*M* phenylmethylsulfonyl fluoride, 260 µ*M* 4-(2-aminoethyl) benzenesulfonyl fluoride hydrochloride, 100 µ*M* leupeptin hemisulfate, 76 µ*M* pepstatin A, 5 m*M* aminocaproic acid, 5 m*M* benzamidine, and 142 µ*M* *N*-tosyl-l-phenylalanine chloromethyl ketone. Cells were lysed with grinding using liquid nitrogen. Crude lysate was transferred to a 1.5 mL Eppendorf tube and centrifuged for 5 min. at 2,500 x g to remove cellular debris. Clarified lysate was subjected to affinity purification with preactivated MyOne Sreptavidin C1 Magnetic Dynabeads (Invitrogen) for 4 hours at 4^{o}C using a nutator. The beads were subsequently separated from the flowthrough using a magnetic stand and

washed five times with cold PBS to separate the non-biotinylated proteins. Protein concentration was measured using a nanodrop, and samples (biotinylated proteins bound to magnetic beads) were submitted for mass-spectrometry to analyze the biotinylated interaction partners of Dfm1.

Liquid chromatography and mass spectrometry analysis

The BioID samples were in-solution digested overnight at 37 °C in 400 ng of mass spectrometry grade trypsin (Promega) enzyme. The digestion was stopped by adding formic acid to the 0.5% final concentration. The digested peptides were desalted by using C18 StageTips and were transferred to a fresh tubes and then vacuum dried. The vacuum-dried peptides were resuspended in 5% formic acid/5% acetonitrile buffer and added to the vials for mass spectrometry analysis. Samples were analyzed with duplicate or triplicate injections by LC-MS-MS using EASY-nLC 1000 liquid chromatography connected with Q-Exactive mass spectrometer (Thermo Scientific) with the following modifications. A fused silica microcapillary column (75-µm inner diameter, 15 cm) packed with C18 reverse-phase resin (ReproSil-pur 120 C18-AQ, 1.9 µm; Dr. Maisch GmbH) using an in-line nano-flow EASY-nLC 1000 UHPLC (Thermo Scientific) was used to resolve the peptides. Peptides were eluted over a 100-min 2%–30% ACN gradient, a 5-min 30%–60% ACN gradient, and a 5-min 60%–95% ACN gradient, with a final 10-min step at 0% ACN for a total run time of 120 min at a flow rate of 250 nl/min. All gradient mobile phases contained 0.1% formic acid. MS/MS data were collected in a data-dependent fashion using a top 10 method with a full MS mass range from 400–1800 m/z, 70,000 resolutions, and an AGC target of 3e6. MS2 scans were triggered when an ion intensity threshold of 1e5 was reached with a maximum injection time of 250 ms. Peptides were fragmented using a normalized collision energy setting of 25. A

dynamic exclusion time of 40 s was used, and the peptide match setting was disabled. Singly charged ions, charge states above 8 and unassigned charge states were excluded. The MS/MS spectra were searched against the UniProt *Saccharomyces cerevisiae* reference proteome database using the Maxquant software with standard settings. Statistical analysis of interactome data was carried out using Differential Enrichment analysis of Proteomics (DEP) and Maxquant package (available online https://rdrr.io/bioc/DEP/man/DEP.html and https://www.maxquant.org/. All proteome datasets were compared to Dfm1-BioID untreated control samples. Filter cut-offs were set at $\log_2 FC \geq 2$, *p* value of $\leq .01$, and at least two quantitative peptide features. These parameters were chosen in an attempt to minimize false positives while maximizing true positives.

Spot dilution growth assay

Yeast strains were grown in YPD or minimal selection media (-Leu -Ura) supplemented with 2% dextrose to log phase (OD_{600} 0.2-0.3) at 30°C. 0.2 OD cells were pelleted and resuspended in 500 µL dH_2O. 12 µL of each sample was transferred to a 96-well plate where a five-fold serial dilution in dH_2O of each sample was performed to obtain a gradient of 0.2-0.0000128 OD cells. The 8x12 pinning apparatus was used to pin cells onto synthetic complete (-Ura) agar plates supplemented with 2% dextrose or 2% galactose. Droplets of cells were air-dried in sterile conditions, then the plates were sealed with parafilm and incubated at 30°C. Plates were removed from the incubator for imaging after 3 days and again after 7 days.

Cycloheximide-Chase Assay

Cycloheximide chase assays were performed as previously described (Sato et al., 2009). Cells were grown to log-phase (OD_{600} 0.2-.03) and cycloheximide was added to a final concentration of 50 µg/mL. At each time point, a constant volume of culture was removed and lysed. Lysis was initiated with addition of 100 µl SUME with protease inhibitors (PIs) and glass beads, followed by vortexing for 4 min. 100 µl of 2xUSB was added followed by incubation at 55°C for 10 min. Samples were clarified by centrifugation and analyzed by SDS-PAGE and immunoblotting.

Fluorescence Microscopy

To prepare cells, overnight cultures were diluted to ~0.20 OD in minimal media. After growing ~3 hours, to log-phase (OD_{600}~.3-.6) samples were pelleted and washed with dH2O. Fluorescence microscopy was accomplished using a CSU-X1 Spinning Disk (Yokogawa) confocal microscope at the Nikon Imaging Center on the UCSD campus.

Native Co-IP

Cultures from various yeast strains were grown to OD_{600} .2-.45 and 15 ODs of cells were pelleted, rinsed with H_20 and lysed with 0.5 mM glass beads in 400 µL of MF buffer supplemented with protease inhibitors. This was followed by vortexing at 1-minute intervals for 6-8 minutes at 4°C. Lysates were combined and clarified by centrifugation at 2,500 g for 5 min followed by centrifugation at 14,000 g for 15 min to obtain the microsomal pellet. The microsomal pellet was resuspended in 1 mL of Tween IP buffer (500 mM NaCl, 50 mM Tris, pH 7.5, 10 mM EDTA. 1.5% Tween-20) and incubated on ice for 30 minutes. Lysates were then centrifuged for 30 min at 14,000 x g, and the supernatant was incubated overnight with

10 µL of equilibrated GFP-Trap® agarose (ChromoTek Inc., Hauppauge, NY) at 4°C. The next day, the GFP-Trap® agarose beads were combined to one tube, washed once with non-detergent IP buffer, washed once more with IP wash buffer and resuspended in 100 µL of 2xUSB. Samples were resolved on 8% SDS-PAGE and immunoblotted for Lcb1-RFP and Orm2-RFP α-RFP and Dfm1-GFP with α-GFP.

In vivo ubiquitination assay

Western blotting to detect in vivo ubiquitination was performed as described previously (Garza et al., 2009). Briefly, yeast strains were grown to log phase (OD600 of 0.2 to 0.3). 15 OD equivalents of cells were pelleted by centrifugation and resuspended in lysis buffer (0.24 M sorbitol, 1 mM EDTA, 20 mM KH2PO4, pH 7.5) with PIs, after which 0.5 mm glass beads were added to the meniscus. The cells were lysed by vortexing in 1-min cycles at 4° C, with 1 min on ice in between, for 6 to 8 cycles. Lysates were clarified by centrifugation at 2,500 x g for 5 min. The clarified lysates were moved to fresh tubes, and 600 µL immunoprecipitation buffer (IPB; 15mM Na2HPO4, 150mM NaCl, 2% Triton X-100, 0.1% SDS, 0.5% deoxycholate, 10mM EDTA, pH 7.5) and 20 µL of GFP Trap (Chromotek) were added. Samples were incubated on ice for 5 min, clarified by centrifugation at 14,000 x g for 5 min, and moved to a fresh tube. Tubes were incubated at 4° C overnight with rocking. Beads were washed twice with IPB and then washed once with IP wash buffer (50 mM NaCl, 10 mM Tris, pH 7.5). Beads were aspirated to dryness, resuspended in 55 µL 2x USB, and incubated at 65° C for 10 minutes. Samples were resolved by SDS-PAGE on 10% gels, transferred to nitrocellulose, and immunoblotted with monoclonal anti-ubiquitin (Fred Hutchinson Cancer Research Institute) and anti-RFP (ThermoFisher) primary antibodies

followed by goat anti-mouse (Jackson ImmunoResearch Laboratories) or goat anti-rabbit (Bio-Rad) HRP conjugated secondary antibody.

Phosphorylation status of Orm2

Indicated strains were grown to log-phase at 30°C, pelleted, and lysed with 100 µl SUME with protease inhibitors (PIs) and glass beads, followed by vortexing for 4 min. 100 µl of 2xUSB was added followed by incubation at 55°C for 10 min. Samples were clarified by centrifugation, loaded onto Phos-tag precast gel (FujiFilm), and immunoblotted for Orm2 with α-GFP.

Lipid analyses

Yeast cells (1 A_{600} units) were suspended in 100 µL of extraction solution [ethanol/water/diethyl ether/pyridine/15 M ammonia (15:15:5:1:0.018, v/v)], mixed with internal standards, and incubated at 60 °C for 15 min. As internal standards, four types of ceramides containing nine deuterium atoms (d_9) [*N*-palmitoyl(d_9)-dihydrosphingosine (d_9-C16:0 Cer-A), *N*-palmitoyl(d_9)-D-*ribo*-phytosphingosine (d_9-C16:0 Cer-B), *N*-(2'-(*R*)-hydroxypalmitoyl(d_9))-D-*erythro*-sphinganine (d_9-C16:0 Cer-B'), *N*-(2'-(*R*)-hydroxypalmitoyl(d_9))-D-*ribo*-phytosphingosine (d_9-C16:0 Cer-C) (all purchased from Avanti Polar Lipids, Alabaster, AL)] were used (5 pmol each). After centrifugation (2,300 × *g*, room temperature, 2 min), the supernatant was recovered, and the pellets were suspended in 100 µL of extraction solution and incubated at 60 °C for 15 min again. After centrifugation (2,300 × *g*, room temperature, 2 min), the supernatant was recovered. The two supernatants were pooled, mixed with 700 µL of chloroform/methanol (1:2, v/v). To hydrolyze glycerolipids,

alkaline treatment was performed by adding 37.5 µL of 3 M KOH and incubating at 37 °C for 30 min. After neutralization by adding 22.5 µL of 5 M formic acid, the samples were sequentially mixed with 250 µL of chloroform and 250 µL of water and centrifuged (20,400 × *g*, room temperature, 3 min) for phase separation. The organic phase containing lipids was recovered and dried. Lipids were resuspended in 625 µL of chloroform/methanol/water (5:4:1, v/v) and subjected to liquid chromatography (LC)-coupled tandem mass spectrometry (MS/MS) using a triple quadrupole mass spectrometer Xevo TQ-S (Waters, Milford, MA, USA) via multiple reaction monitoring and positive ion modes. The settings for LC separation and electrospray ionization were as described previously (Ohno et al., 2017)and the used *m/z* values and collision energies in the MS/MS measurement were listed in Supplementary Table 3. Ceramides were quantified by calculating the ratio of the peak area of each ceramide species to that of the internal standard corresponding to each type of ceramides. D-type ceramides were quantified using C-type ceramide standard (d_9-C16:0 Cer-C).

Detergent Solubility Assay

ER microsomes were isolated by centrifuging and pelleting 15OD of yeast in log phase growth. Pellets were resuspended in MF buffer with protease inhibitors and 0.5mM lysis beads were added to each sample. Samples were vortexed six times in 1-minute intervals, with 1-minute on ice in between. Lysed cells were transferred to new microcentrifuge tube and samples were clarified by spinning at 1,500x for 5 minutes at 4°C. Microsomes were separated by centrifuging clarified lysate at 14,000 × *g* for 1 minute. Fractions were incubated on ice in the presence or absence of 1% DDM for 1 hour. The mixture was then centrifuged at 14,000 × *g* for 30 min at 4°C, and the detergent soluble fraction (i.e., the supernatant) was precipitated with 20% TCA on ice for 30 minutes and then

centrifuged at 14,000 × *g* for 30 min to get a pellet of the soluble protein. Proteins from both the soluble and insoluble fractions were resuspended in sample buffer and resolved by SDS-PAGE.

Quantification and Statistical Analysis

ImageJ (NIH) was used for all western blot quantifications. "Mean gray value" was set for band intensity measurements. In such experiments, a representative western blot was shown and band intensities were normalized to PGK1 loading control and quantified. t=0 was taken as 100% and data is represented as mean ± SEM from at least three experiments. GraphPad Prism was used for statistical analysis. Nested t-test, unpaired t-test or one-way factorial ANOVA followed by Bonferroni's post-hoc analysis was applied to compare data. Significance was indicated as follow: n.s, not significant; * $p<0.05$, ** $p<0.01$, *** $p<0.001$, **** $p<0.0001$. The investigators were blinded during data analysis.

3.5 Acknowledgments

Chapter 3 is currently accepted for publication for the working citation: Bhaduri, S., Aguayo, A., Ohno, Y., Proietto, M., Jung, J., Wang, I., Kandel, R., Singh, N., Ibrahim, I., Fulzele, A., Bennett, E., Kihara, A., Neal, S., An ERAD-independent role for rhomboid pseudoprotease Dfm1 in mediating sphingolipid homeostasis. The dissertation author was conducted experiments for this manuscript and is a co-author of this material. The authors would like to thank Peter Espenshade (Johns Hopkins Medicine), Oliver Schmidt (Medical University of Innsbruck), David Teis (Medical University of Innsbruck), Teresa Dunn (National Institutes of Health), Jim Wilhelm (University of California, San Diego), and Peter Novick (University of California, San Diego) for providing plasmids, yeast strains, antibodies. We thank Dr. Oswald Quehenberger from the UCSD Lipidomic Core Facility for performing lipidomic analysis. We also thank Dr. Maho Niwa, Dr. David Teis, Dr. Oliver Schmidt, and the Neal lab members for in depth discussions and technical assistance. These studies were supported by NIH grant 1R35GM133565-01, Pew Biomedical Award 34089, and NSF CAREER grant 2047391 (to S.E.N), NIH grants 5R01GM136994-02 and DP2GM119132 (to E.J.B), HHMI Gilliam Fellowship GT15096 (to S.E.N and A.A.), and KAKENHI grant JPSSH04986 (to A.K.).

3.6 References

Bhaduri, S., & Neal, S. E. (2021). Assays for studying normal versus suppressive ERAD-associated retrotranslocation pathways in yeast. *STAR Protocols*, *2*(3), 100640. https://doi.org/10.1016/j.xpro.2021.100640

Bode, H., Bourquin, F., Suriyanarayanan, S., Wei, Y., Alecu, I., Othman, A., Von Eckardstein, A., & Hornemann, T. (2015). *HSAN1 mutations in serine palmitoyltransferase reveal a close structure-function-phenotype relationship*. https://doi.org/10.1093/hmg/ddv611

Breslow, D. K. (n.d.). *Sphingolipid Homeostasis in the Endoplasmic Reticulum and Beyond*. https://doi.org/10.1101/cshperspect.a013326

Breslow, D. K., Collins, S. R., Bodenmiller, B., Aebersold, R., Simons, K., Shevchenko, A., Ejsing, C. S., & Weissman, J. S. (2010). Orm family proteins mediate sphingolipid homeostasis. *Nature*, *463*(7284), 1048–1053. https://doi.org/10.1038/NATURE08787

Carvalho, P., Goder, V., & Rapoport, T. A. (2006). Distinct ubiquitin-ligase complexes define convergent pathways for the degradation of ER proteins. *Cell*, *126*(2), 361–373. https://doi.org/10.1016/j.cell.2006.05.043

Christiano, R., Arlt, H., Kabatnik, S., Mejhert, N., Lai, Z. W., Farese, R. V., & Walther, T. C. (2020). A Systematic Protein Turnover Map for Decoding Protein Degradation. *Cell Reports*, *33*(6), 108378. https://doi.org/10.1016/j.celrep.2020.108378

Davis, D., Kannan, M., & Wattenberg, B. (2018). Orm/ORMDL proteins: Gate guardians and master regulators. *Advances in Biological Regulation*, *70*(August), 3–18. https://doi.org/10.1016/j.jbior.2018.08.002

Davis, D. L., Gable, K., Suemitsu, J., Dunn, T. M., & Wattenberg, B. W. (2019). The ORMDL/Orm–serine palmitoyltransferase (SPT) complex is directly regulated by ceramide: Reconstitution of SPT regulation in isolated membranes. *Journal of Biological Chemistry*, *294*(13), 5146–5156. https://doi.org/10.1074/jbc.RA118.007291

Fenech, E. J., Lari, F., Charles, P. D., Fischer, R., Laé titia-Thé zé nas, M., Bagola, K., Paton, A. W., Paton, J. C., Gyrd-Hansen, M., Kessler, B. M., & Christianson, J. C. (n.d.). *Interaction mapping of endoplasmic reticulum ubiquitin ligases identifies modulators of innate immune signalling*. https://doi.org/10.7554/eLife.57306

Foresti, O., Rodriguez-Vaello, V., Funaya, C., & Carvalho, P. (2014). Quality control of inner nuclear membrane proteins by the Asi complex. *Science*, *346*(6210), 751–755. https://doi.org/10.1126/science.1255638

Foresti, O., Ruggiano, A., Hannibal-Bach, H. K., Ejsing, C. S., & Carvalho, P. (2013). Sterol homeostasis requires regulated degradation of squalene monooxygenase by the ubiquitin ligase Doa10/Teb4. *ELife*, *2*, e00953. https://doi.org/10.7554/eLife.00953

Fun, X. H., & Thibault, G. (2020). Lipid bilayer stress and proteotoxic stress-induced unfolded protein response deploy divergent transcriptional and non-transcriptional programmes. *Biochimica et Biophysica Acta - Molecular and Cell Biology of Lipids*, *1865*(1), 158449. https://doi.org/10.1016/j.bbalip.2019.04.009

Gable, K., Slife, H., Bacikova, D., Monaghan, E., & Dunn, T. M. (2000). Tsc3p is an 80-amino acid protein associated with serine palmitoyltransferase and required for optimal enzyme activity. *Journal of Biological Chemistry*, *275*(11), 7597–7603. https://doi.org/10.1074/jbc.275.11.7597

Gardner, R., Cronin, S., Leader, B., Rine, J., Hampton, R., & Leder, B. (1998). Sequence determinants for regulated degradation of yeast 3-hydroxy-3-methylglutaryl-CoA reductase, an integral endoplasmic reticulum membrane protein. *Molecular Biology of the Cell*, *9*(9), 2611–2626.

Hampton, R. Y., Gardner, R. G., & Rine, J. (1996). Role of 26S proteasome and HRD genes in the degradation of 3-hydroxy-3-methylglutaryl-CoA reductase, an integral endoplasmic reticulum membrane protein. *Molecular Biology of the Cell*, *7*(12), 2029–2044. https://doi.org/10.1091/mbc.7.12.2029

Hampton, R. Y., & Rine, J. (1994). Regulated degradation of HMG-CoA reductase, an integral membrane protein of the endoplasmic reticulum, in yeast. *The Journal of Cell Biology*, *125*(2), 299–312.

Hampton, R. Y., & Sommer, T. (2012). Finding the will and the way of ERAD substrate retrotranslocation. *Current Opinion in Cell Biology*, *24*(4), 460–466. https://doi.org/10.1016/j.ceb.2012.05.010

Han, G., Gupta, S. D., Gable, K., Bacikova, D., Sengupta, N., Somashekarappa, N., Proia, R. L., Harmon, J. M., & Dunn, T. M. (2019). The ORMs interact with transmembrane domain 1 of Lcb1 and regulate serine palmitoyltransferase oligomerization, activity and localization. *Biochimica et Biophysica Acta - Molecular and Cell Biology of Lipids*, *1864*(3), 245–259. https://doi.org/10.1016/j.bbalip.2018.11.007

Han, S., Lone, M. A., Schneiter, R., & Chang, A. (n.d.). *Orm1 and Orm2 are conserved endoplasmic reticulum membrane proteins regulating lipid homeostasis and protein quality control*. https://doi.org/10.1073/pnas.0911617107

Hanada, K. (2003). Serine palmitoyltransferase, a key enzyme of sphingolipid metabolism. *Biochimica et Biophysica Acta - Molecular and Cell Biology of Lipids*, *1632*(1–3), 16–30. https://doi.org/10.1016/S1388-1981(03)00059-3

Hannun, Y. A., & Obeid, L. M. (2018). Sphingolipids and their metabolism in physiology and disease. In *Nature Reviews Molecular Cell Biology* (Vol. 19, Issue 3, pp. 175–191). Nature Publishing Group. https://doi.org/10.1038/nrm.2017.107

Hiller, M. M., Finger, A., Schweiger, M., & Wolf, D. H. (1996). ER degradation of a misfolded luminal protein by the cytosolic ubiquitin-proteasome pathway. *Science (New York, N.Y.)*, *273*(5282), 1725–1728.

Ito, H., Fukuda, Y., Murata, K., & Kimura, A. (1983). Transformation of intact yeast cells treated with alkali cations. *Journal of Bacteriology*, *153*(1), 163–168.

Kandel, R., Jung, J., Syau, D., Kuo, T., Songster, L., Aguayo, A., Duttke, S., Benner, C., & Neal, S. (2022). Derlin Dfm1 Employs a Chaperone Function to Resolve Misfolded Membrane Protein Stress. *BioRxiv*, 2022.01.25.477788. https://doi.org/10.1101/2022.01.25.477788

Laney, J. D., & Hochstrasser, M. (2003). Ubiquitin-dependent degradation of the yeast Matα2 repressor enables a switch in developmental state. *Genes and Development*, *17*(18), 2259–2270. https://doi.org/10.1101/gad.1115703

Leto, D. E., Morgens, D. W., Zhang, L., Walczak, C. P., Elias, J. E., Bassik, M. C., & Kopito, R. R. (2019). Genome-wide CRISPR Analysis Identifies Substrate-Specific Conjugation Modules in ER-Associated Degradation. *Molecular Cell*, *73*(2), 377-389.e11. https://doi.org/10.1016/j.molcel.2018.11.015

Mehrtash, A. B., & Hochstrasser, M. (2019). Ubiquitin-dependent protein degradation at the endoplasmic reticulum and nuclear envelope. In *Seminars in Cell and Developmental Biology* (Vol. 93, pp. 111–124). Elsevier Ltd. https://doi.org/10.1016/j.semcdb.2018.09.013

Mohassel, P., Donkervoort, S., Lone, M. A., Nalls, M., Gable, K., Gupta, S. D., Foley, A. R., Hu, Y., Alex, J., Saute, M., Moreira, A. L., Kok, F., Introna, A., Logroscino, G., Grunseich, C., Nickolls, A. R., Pourshafie, N., Neuhaus, S. B., Saade, D., … Bönnemann, C. G. (n.d.). *Childhood amyotrophic lateral sclerosis caused by excess sphingolipid synthesis*. https://doi.org/10.1038/s41591-021-01346-1

Natarajan, N., Foresti, O., Wendrich, K., Stein, A., & Carvalho, P. (2020). Quality Control of Protein Complex Assembly by a Transmembrane Recognition Factor. *Molecular Cell*, *77*(1), 108-119.e9. https://doi.org/10.1016/j.molcel.2019.10.003

Neal, S., Jaeger, P. A., Duttke, S. H., Benner, C. K., Glass, C., Ideker, T., & Hampton, R. (2018). The Dfm1 Derlin Is Required for ERAD Retrotranslocation of Integral Membrane Proteins. *Molecular Cell*, *69*(2). https://doi.org/10.1016/j.molcel.2017.12.012

Neal, S., Mak, R., Bennett, E. J., & Hampton, R. (2017). A Cdc48 ‘retrochaperone’ function is required for the solubility of retrotranslocated, integral membrane Endoplasmic Reticulum-associated Degradation (ERAD-M) substrates. *Journal of Biological Chemistry*, *292*(8). https://doi.org/10.1074/jbc.M116.770610

Nejatfard, A., Wauer, N., Bhaduri, S., Conn, A., Gourkanti, S., Singh, N., Kuo, T., Kandel, R., Amaro, R. E., & Neal, S. E. (2021). Derlin rhomboid pseudoproteases employ substrate engagement and lipid distortion to enable the retrotranslocation of ERAD membrane substrates. *Cell Reports*, *37*(3), 109840. https://doi.org/10.1016/j.celrep.2021.109840

Ohno, Y., Kamiyama, N., Nakamichi, S., & Kihara, A. (2017). PNPLA1 is a transacylase essential for the generation of the skin barrier lipid *ω*-*O*-acylceramide**.** *Nature Communications*. https://doi.org/10.1038/ncomms14610

Piña, F., Yagisawa, F., Obara, K., Gregerson, J. D., Kihara, A., & Niwa, M. (2018). Sphingolipids activate the endoplasmic reticulum stress surveillance pathway. *Journal of Cell Biology*, *217*(2), 495–505. https://doi.org/10.1083/jcb.201708068

Ruggiano, A., Foresti, O., & Carvalho, P. (2014). ER-associated degradation: Protein quality control and beyond. In *Journal of Cell Biology* (Vol. 204, Issue 6, pp. 869–879). Rockefeller University Press. https://doi.org/10.1083/jcb.201312042

Sato, B. K., & Hampton, R. Y. (2006). Yeast Derlin Dfm1 interacts with Cdc48 and functions in ER homeostasis. *Yeast*, 1053–1064. https://doi.org/10.1002/yea

Sato, B. K., Schulz, D., Do, P. H., & Hampton, R. Y. (2009). Misfolded membrane proteins are specifically recognized by the transmembrane domain of the Hrd1p ubiquitin ligase. *Molecular Cell*, *34*(2), 212–222. https://doi.org/10.1016/j.molcel.2009.03.010

Schmidt, C. C., Vasic, V., & Stein, A. (2020). Doa10 is a membrane protein retrotranslocase in er-associated protein degradation. *ELife*, *9*, 1–31. https://doi.org/10.7554/eLife.56945

Schmidt, O., Weyer, Y., Baumann, V., Widerin, M. A., Eising, S., Angelova, M., Schleiffer, A., Kremser, L., Lindner, H., Peter, M., Fröhlich, F., & Teis, D. (2019). Endosome and Golgi-associated degradation (EGAD) of membrane proteins regulates sphingolipid metabolism . *The EMBO Journal*, *38*(15), 1–23. https://doi.org/10.15252/embj.2018101433

Schmidt, O., Weyer, Y., Sprenger, S., Widerin, M. A., Eising, S., Baumann, V., Angelova, M., Loewith, R., Stefan, C. J., Hess, M. W., Fröhlich, F., & Teis, D. (2020). TOR complex 2 (TORC2) signaling and the ESCRT machinery cooperate in the protection of plasma

membrane integrity in yeast. *Journal of Biological Chemistry*, *295*(34), 12028–12044. https://doi.org/10.1074/jbc.RA120.013222

Shimobayashi, M., Oppliger, W., Moes, S., Jenö, P., & Hall, M. N. (2013). TORC1-regulated protein kinase Npr1 phosphorylates Orm to stimulate complex sphingolipid synthesis. *Molecular Biology of the Cell*, *24*(6), 870–881. https://doi.org/10.1091/mbc.E12-10-0753

Sicari, Igbaria, & Chevet. (2019). Control of Protein Homeostasis in the Early Secretory Pathway: Current Status and Challenges. *Cells*, *8*(11), 1347. https://doi.org/10.3390/cells8111347

Sun, Z., & Brodsky, J. L. (2019). Protein quality control in the secretory pathway. In *Journal of Cell Biology* (Vol. 218, Issue 10, pp. 3171–3187). Rockefeller University Press. https://doi.org/10.1083/jcb.201906047

Tam, A. B., Roberts, L. S., Chandra, V., Rivera, I. G., Nomura, D. K., Forbes, D. J., & Niwa, M. (2018). The UPR Activator ATF6 Responds to Proteotoxic and Lipotoxic Stress by Distinct Mechanisms. *Developmental Cell*, *46*(3), 327-343.e7. https://doi.org/10.1016/j.devcel.2018.04.023

Wang, J.-Z., & Dehesh, K. (2018). ER: the Silk Road of interorganellar communication. *Current Opinion in Plant Biology*, *45*(Pt A), 171–177. https://doi.org/10.1016/j.pbi.2018.07.012

Wangeline, M. A., Vashistha, N., & Hampton, R. Y. (2017). Proteostatic Tactics in the Strategy of Sterol Regulation. *Annual Review of Cell and Developmental Biology*, *33*(1), 467–489. https://doi.org/10.1146/annurev-cellbio-111315-125036

Wu, X., Siggel, M., Ovchinnikov, S., Mi, W., Svetlov, V., Nudler, E., Liao, M., Hummer, G., & Rapoport, T. A. (2020). Structural basis of ER-associated protein degradation mediated by

the Hrd1 ubiquitin ligase complex. *Science*, *368*(6489), 1–13. https://doi.org/10.1126/SCIENCE.AAZ2449

Zelcer, N., Sharpe, L. J., Loregger, A., Kristiana, I., Cook, E. C. L., Phan, L., Stevenson, J., & Brown, A. J. (2014). The E3 Ubiquitin Ligase MARCH6 Degrades Squalene Monooxygenase and Affects 3-Hydroxy-3-Methyl-Glutaryl Coenzyme A Reductase and the Cholesterol Synthesis Pathway. *Molecular and Cellular Biology*, *34*(7), 1262–1270. https://doi.org/10.1128/mcb.01140-13

Zuzow, N., Ghosh, A., Leonard, M., Liao, J., Yang, B., & Bennett, E. J. (2018). Mapping the mammalian ribosome quality control complex interactome using proximity labeling approaches. *Molecular Biology of the Cell*, *29*(10), 1258–1269. https://doi.org/10.1091/mbc.E17-12-0714

Figure 3.2.1 BioID proximity-based labeling to identify interaction partners of Dfm1

(A) Schematic of Dfm1 fused with a biotin ligase, BirA, at the C-terminus along with un-tagged Dfm1.Cartoon representation of the labeling of rhomboid pseudoprotease Dfm1 with the biotin ligase, BirA. **(B)** GALpr-Dfm1-BirA-Flag and GALpr-BirA-Flag levels were measured by western blotting with α -FLAG at 0 (uninduced) vs. 5 hours post-galactose induction (3 biological replicates; n=3). **(C)** Dfm1-BirA is still functional and able to degrade Hmg2-GFP. dfm1Δ+Hmg2-GFP strains containing DFM1-BIRA, empty vector, or BIRA only addbacks were grown to log phase and degradation was measured by CHX. After CHX addition, cells were lysed at the indicated times and analyzed by SDS-PAGE and immunoblotted for Hmg2-GFP with α-GFP. **(D)** Yeast strains expressing Dfm1-Bira and BirA only negative control were incubated with different amounts of biotin: 0, 0.1, and 1 mM. dfm1Δ+Hmg2-GFP. Microsomes were isolated from each strain and subjected to streptavidin pulldown (3 biological replicates; n=3). Flow- through and pull-down fractions were detected by western blotting for Dfm1-BirA with α-Flag and Cdc48 with α-Cdc48 antibodies. **(E)** A volcano plot showing enrichment versus significance of proteins identified in Dfm1-BirA experiments relative to control (BirA only) experiments. Components that were significantly enriched were ERAD components in blue (Hrd1, Cdc48, Pre9, and Rpt2) and sphingolipid biosynthesis in orange (Lcb2, Tsc3, and Orm1). Statistical analysis of interactome data was carried out using Differential Enrichment analysis of Proteomics (DEP). Filter cut-offs were set at log2FC>2, p value of < .01, and at least two quantitative peptide features. **(F)** Top 10 gene ontology (GO) terms and their enrichment factor for the set of genes with the highest significance and fold enrichment.

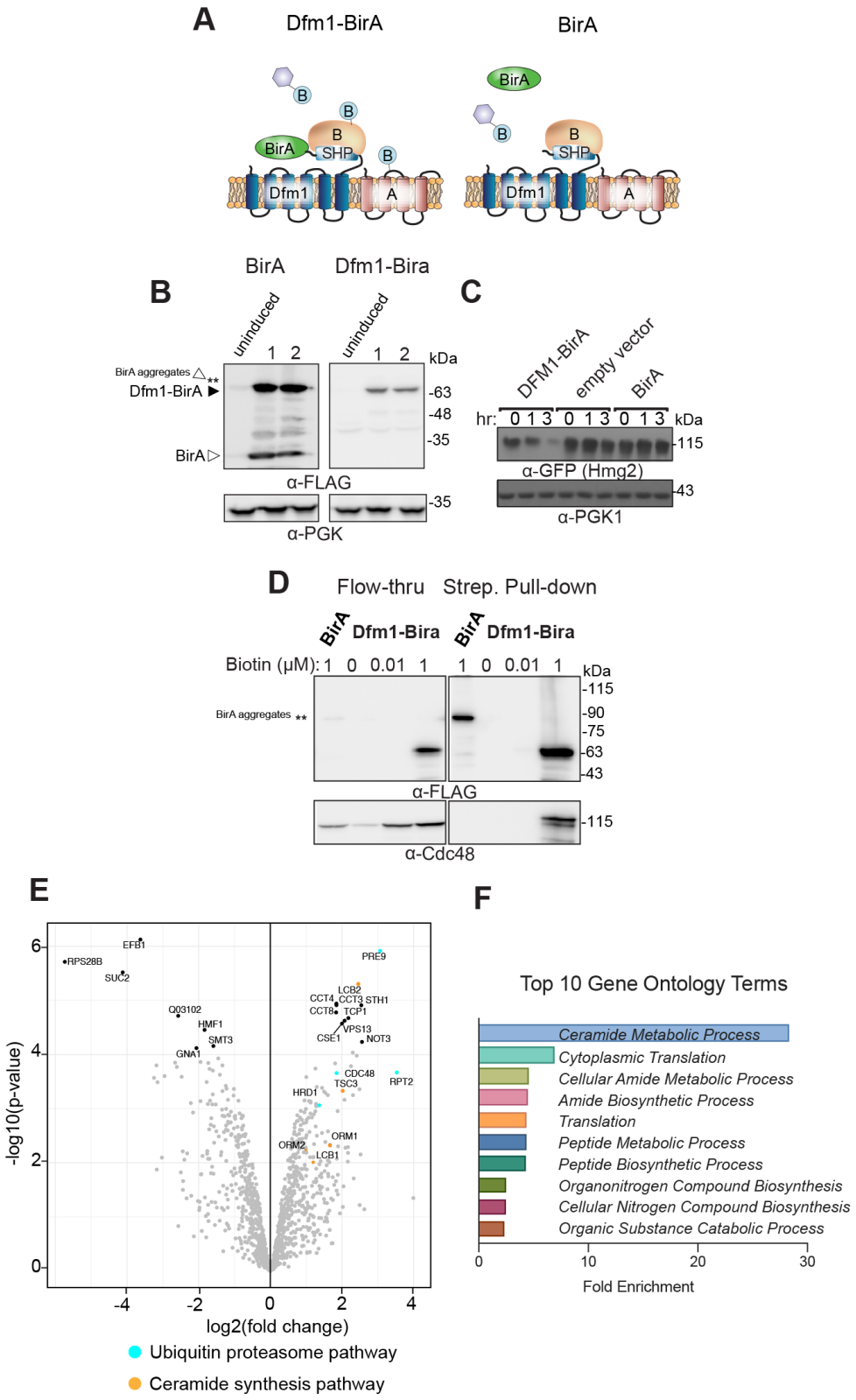
A
Dfm1-BirA
BirA
B
SHP
BirA
Dfm1
A
B
BirA
Dfm1-Bira
uninduced
1 2
kDa
BirA aggregates
Dfm1-BirA
BirA
-63
-48
-35
α-FLAG
α-PGK
C
DFM1-BirA
empty vector
BirA
hr: 0 1 3 0 1 3 0 1 3
kDa
-115
α-GFP (Hmg2)
-43
α-PGK1
D
Flow-thru
Strep. Pull-down
BirA
Dfm1-Bira
Biotin (μM): 1 0 0.01 1 1 0 0.01 1
BirA aggregates
-115
-90
-75
-63
-43
α-FLAG
α-Cdc48
E
-log10(p-value)
log2(fold change)
EFB1
RPS28B
SUC2
Q03102
HMF1
SMT3
GNA1
PRE9
LCB2
CCT4
CCT3
STH1
CCT8
TCP1
VPS13
CSE1
NOT3
CDC48
TSC3
RPT2
HRD1
ORM1
ORM2
LCB1
Ubiquitin proteasome pathway
Ceramide synthesis pathway
F
Top 10 Gene Ontology Terms
Ceramide Metabolic Process
Cytoplasmic Translation
Cellular Amide Metabolic Process
Amide Biosynthetic Process
Translation
Peptide Metabolic Process
Peptide Biosynthetic Process
Organonitrogen Compound Biosynthesis
Cellular Nitrogen Compound Biosynthesis
Organic Substance Catabolic Process
Fold Enrichment

Figure 3.2.2 Dfm1 colocalizes and binds to SPOTS complex proteins

(A) Dfm1-GFP binding to Lcb2-RFP and Orm2-RFP were analyzed by co-IP. As negative control, cells not expressing Dfm1-GFP were used (3 biological replicates; n=3). **(B)** Dfm1-GFP colocalizes with Lcb1-RFP and Orm22-RFP. Strains were grown to mid- exponential phase in minimal media GFP and RFP fluorescence was examined on an AxioImager.M2 fluorescence microscope using a 100x objective and 28HE-GFP or 20HE- rhodamine filter sets (3 biological replicates; n=3)(Zeiss). Scale bar, 5 μM.

A

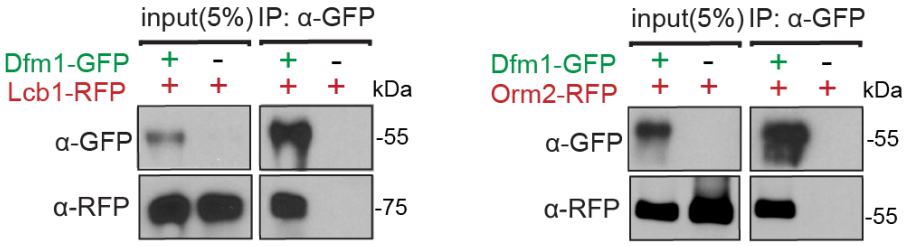
input(5%)
IP: α-GFP
Dfm1-GFP
Lcb1-RFP
kDa
α-GFP
α-RFP
-55
-75
input(5%)
IP: α-GFP
Dfm1-GFP
Orm2-RFP
kDa
α-GFP
α-RFP
-55
-55

B

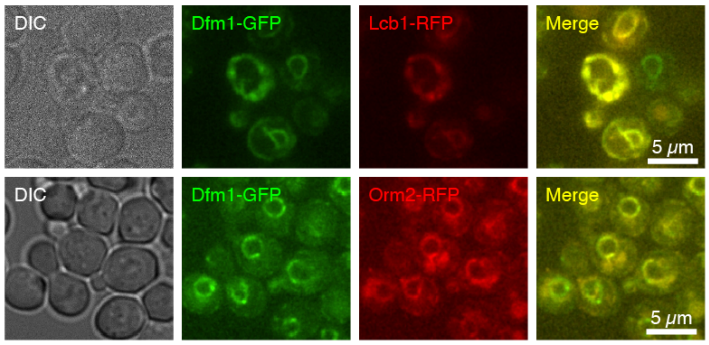
DIC
Dfm1-GFP
Lcb1-RFP
Merge
5 μm
DIC
Dfm1-GFP
Orm2-RFP
Merge
5 μm

Figure 3.2.3 Dfm1 genetically interacts with Tsc3

(A) Indicated strains were spotted 5-fold dilutions on synthetic complete (SC) plates , and plates were incubated at room temperature, 30oC, and 37oC (3 biological replicates, 2 technical replicates; n=5). WT, dfm1Δ, tsc3Δ, and dfm1Δtsc3Δ were compared for growth in the dilution assay. Arrowhead indicates growth phenotype of tsc3Δ cells; open circle indicates growth phenotype of dfm1Δtsc3Δ cells. **(B)** dfm1Δtsc3Δ confers resistance to myrocin. WT, dfm1Δ, tsc3Δ, and dfm1Δtsc3Δ strains were grown to log-phase in YPD medium, and 5-fold serial dilutions of cultures were spotted on (SC) plates containing either drug vehicle alone, 1 μM of myriocin and 10 μM of PHS (3 biological replicates, 2 technical replicates; n=5). Arrowhead indicates growth phenotype of tsc3Δ cells; open circle indicates growth phenotype of dfm1Δtsc3Δ cells. **(C)** WT, dfm1Δ, tsc3Δ, and dfm1Δtsc3Δ cells were grown to log-phase at 30oC and lipids were extracted and subjected to LC-MS/MS. A- B- C- & D-Type ceramides containing C16, C18, C20, C22, C24, and C26 fatty acid (left graph) and B- C- & D-type IPCs containing C24 and C26 fatty acid (right graph) were measured. Values represent the means±S.E.M. (3 biological replicates; n=3). Pairwise Dunnett's test followed by Bonferroni's post-hoc analysis was used to determine statistically significant differences in comparison to WT cells; *P<0.05, **P<0.01). **(D)** Indicated strains were spotted 5-fold dilutions on SC plates in 3 biological replicates and 2 technical replicates (n=5), and plates were incubated at room temperature, 30oC, and 37oC (n=3). Upper panel: WT, orm1Δ, tsc3Δ, and orm1Δtsc3Δ were compared for growth by dilution assay. Middle panel: WT, orm2Δ, tsc3Δ, and orm2Δtsc3Δ were compared for growth by dilution assay. Bottom panel: WT, orm1Δ, orm2Δ, tsc3Δ, and orm1Δorm2Δtsc3Δ, were compared for growth by dilution assay. Upper panel: arrowhead indicates growth phenotype of tsc3Δ cells; open circle indicates growth phenotype of orm1Δtsc3Δ cells. Lower panel: arrowhead indicates growth phenotype of orm2Δ cells; open circle indicates growth phenotype of orm2Δtsc3Δ cells.

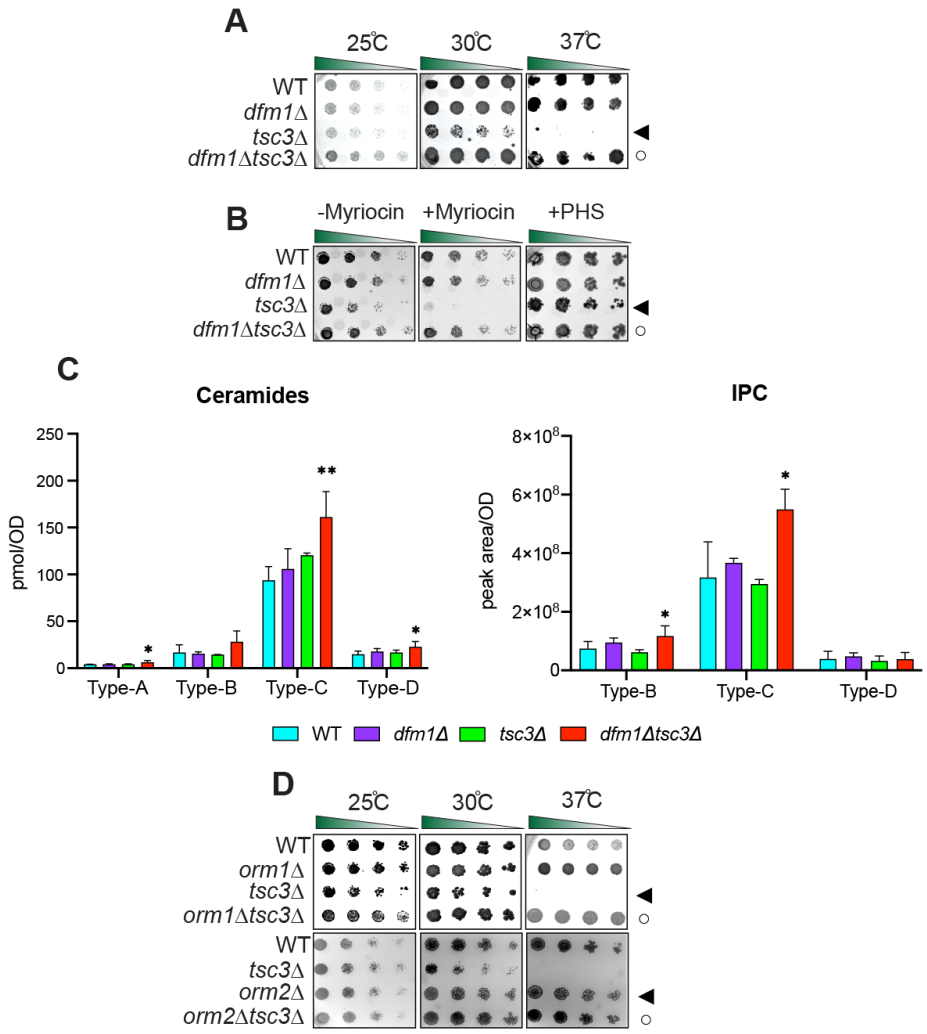
A
25℃
30℃
37℃
WT
dfm1Δ
tsc3Δ
dfm1Δtsc3Δ
B
-Myriocin
+Myriocin
+PHS
WT
dfm1Δ
tsc3Δ
dfm1Δtsc3Δ
C
Ceramides
IPC
pmol/OD
peak area/OD
Type-A
Type-B
Type-C
Type-D
WT
dfm1Δ
tsc3Δ
dfm1Δtsc3Δ
D
25℃
30℃
37℃
WT
orm1Δ
tsc3Δ
orm1Δtsc3Δ
WT
tsc3Δ
orm2Δ
orm2Δtsc3Δ

Figure 3.2.4 Dfm1 genetically interacts with Orm1

(A) Indicated strains were spotted 5-fold dilutions on SC plates in 3 biological replicates and 2 technical replicates (n=5), and plates were incubated at room temperature, 30oC, and 37oC. Upper panel: WT, dfm1Δ, orm1Δ, and dfm1Δorm1Δ were compared for growth by dilution assay. Middle panel: WT, dfm1Δ, orm2Δ, and orm2Δtsc3Δ were compared for growth by dilution assay. Bottom panel: WT, dfm1Δ, orm1Δ, orm2Δ, and orm2Δ, and orm1Δorm2Δ were compared for growth by dilution assay. Upper, middle, and lower panel: gray arrowhead depicts growth phenotype of dfm1Δorm1Δ, dfm1Δorm2Δ, and orm1Δorm2Δ respectively. **(B)** dfm1Δorm1Δ confers resistance to myriocin and sensitivity to PHS. WT, dfm1Δ, orm1Δ, and dfm1Δorm1Δ strains were grown to log-phase in SC medium, and 5-fold serial dilutions of cultures were spotted on YPD plates containing either drug vehicle alone, 1 mM of myriocin and 10 μM of PHS with each condition performed in 3 biological replicates and 2 technical replicates (n=5). Plates were incubated at room temperature and photographed after 3 days. Open circle indicates growth phenotype of dfm1Δorm1Δ cells. **(C)** WT, dfm1Δ, orm1Δ, and orm1Δdfm1Δ cells were grown to log-phase at 30oC and lipids were extracted and subjected to LC-MS/MS. C18 PHS and DHS levels were measured as described in Methods (3 biological replicates; n=3). Values represent the means±S.E.M. Statistically significant differences compared to WT cells are indicated (Pairwise Dunnett's test followed by Bonferroni's post-hoc analysis; *P<0.05, **P<0.01). **(D)** WT, dfm1Δ, orm1Δ, orm2Δ, dfm1Δorm1Δ, and orm1Δorm2Δ cells were grown to log-phase at 30oC and lipids were extracted and subjected to LC-MS/MS. A- B- C- & D-Type ceramides containing C16, C18, C20, C22, C24, and C26 fatty acid (left graph) and B- C- & D-type IPCs containing C24 and C26 fatty acid (right graph) were measured (3 biological replicates; n=3). Values represent the means±S.E.M. Statistically significant differences compared to WT cells are indicated (Pairwise Dunnett's test followed by Bonferroni's post-hoc analysis; *P<0.05, **P<0.01).

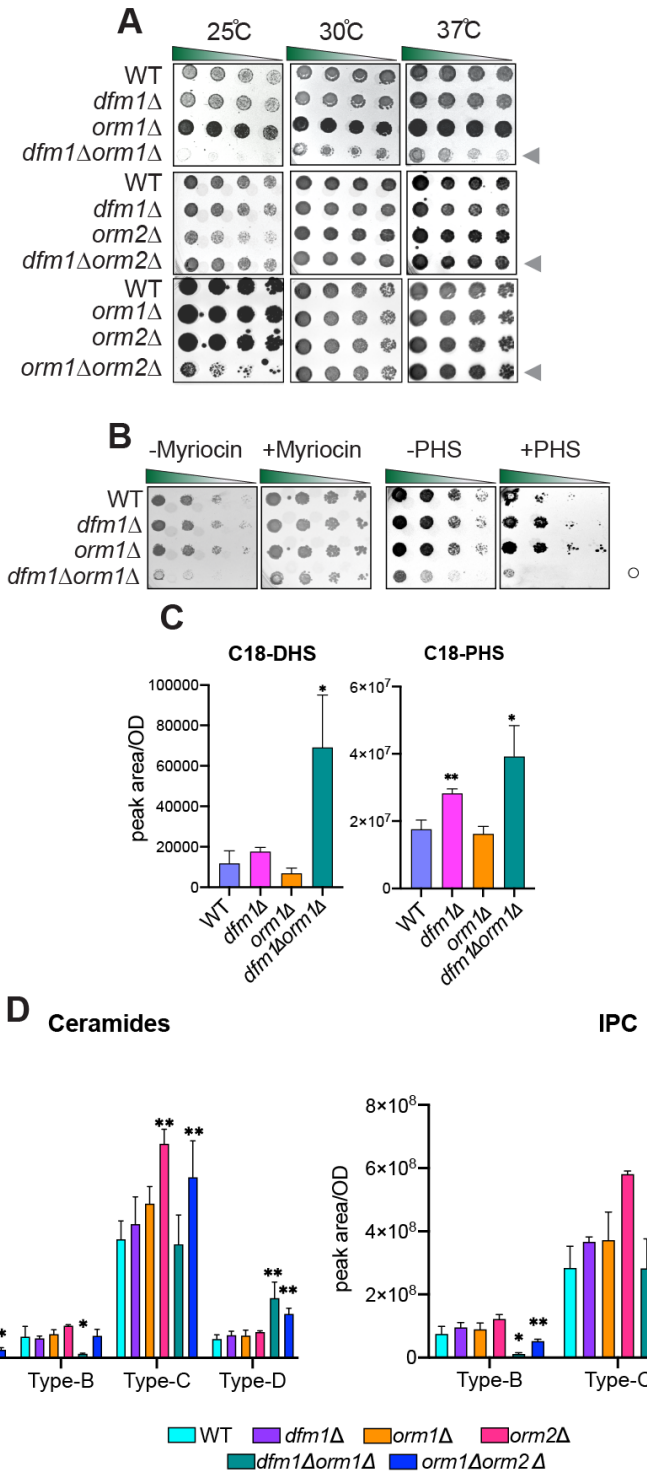
A
25℃
30℃
37℃
WT
dfm1Δ
orm1Δ
dfm1Δorm1Δ
WT
dfm1Δ
orm2Δ
dfm1Δorm2Δ
WT
orm1Δ
orm2Δ
orm1Δorm2Δ
B
-Myriocin
+Myriocin
-PHS
+PHS
WT
dfm1Δ
orm1Δ
dfm1Δorm1Δ
C
C18-DHS
C18-PHS
peak area/OD
100000
80000
60000
40000
20000
0
6×10^7
4×10^7
2×10^7
0
WT
dfm1Δ
orm1Δ
dfm1Δorm1Δ
D
Ceramides
IPC
pmol/OD
200
150
100
50
0
Type-A
Type-B
Type-C
Type-D
peak area/OD
8×10^8
6×10^8
4×10^8
2×10^8
0
Type-B
Type-C
Type-D
WT
dfm1Δ
orm1Δ
orm2Δ
dfm1Δorm1Δ
orm1Δorm2Δ

Figure 3.2.5 Dfm1 targets Orm2 for degradation

(A) Degradation of Orm2 depends on Dfm1 and not Der1. The indicated strains expressing Orm2-RFP were grown into log phase and degradation was measured by cycloheximide chase (CHX). After CHX addition, cells were lysed at the indicated times, and analyzed by SDS-PAGE and immunoblotted for Orm2-RFP with α-RFP (3 biological replicates (n=3). (B) Same as (A) except degradation of Orm2-RFP was measured in WT and der1Δ cells (3 biological replicates; n=3). (C) Depiction of Dfm1, Der1, Dfm1-5Ashp, and Der1-Shp. Dfm1 and Der1 are ER-localized membrane proteins with six transmembrane domains (Greenblatt et al., 2011). Unlike Der1, Dfm1 has an extended cytoplasmic tail containing two SHP boxes. (D) Dfm1's SHP box is not required for degradation of Orm2-RFP. In the indicated strains, degradation of Orm2-RFP was measured by CHX-chase assay. Cells were analyzed by SDS- PAGE and immunoblotted for Orm2-RFP with α-RFP (3 biological replicates; n=3). (E) Depiction of Dfm1, which highlights L1, TM2, TM6, and its SHP box domain. (F) Table indicating the location and specific function that is impaired for retrotranslocation- deficient Dfm1 mutants (Nejatfard et al., 2021). (G) Dfm1's WR motif, GxxxG motif, substrate binding and lipid thinning function are required for degradation of Orm2-RFP. In the indicated strains, degradation of Orm2-RFP was measured by CHX-chase assay. Cells were analyzed by SDS-PAGE and immunoblotted for Orm2-RFP with α-RFP (3 biological replicates; n=3). (H) Dfm1 L1 residues are required for binding to Orm2. Orm2-RFP and binding to retrotranslocation-deficient Dfm1 L1 mutants was analyzed by co-IP. The IP was analyzed for presence of Dfm1-HA. As a negative control, cells not expressing Orm2-RFP were used (3 biological replicates; n=3). Band intensities for all western blots were normalized to PGK1 loading control and quantified by ImageJ. Data information: t=0 was taken as 100% and data is represented as mean ± SEM.

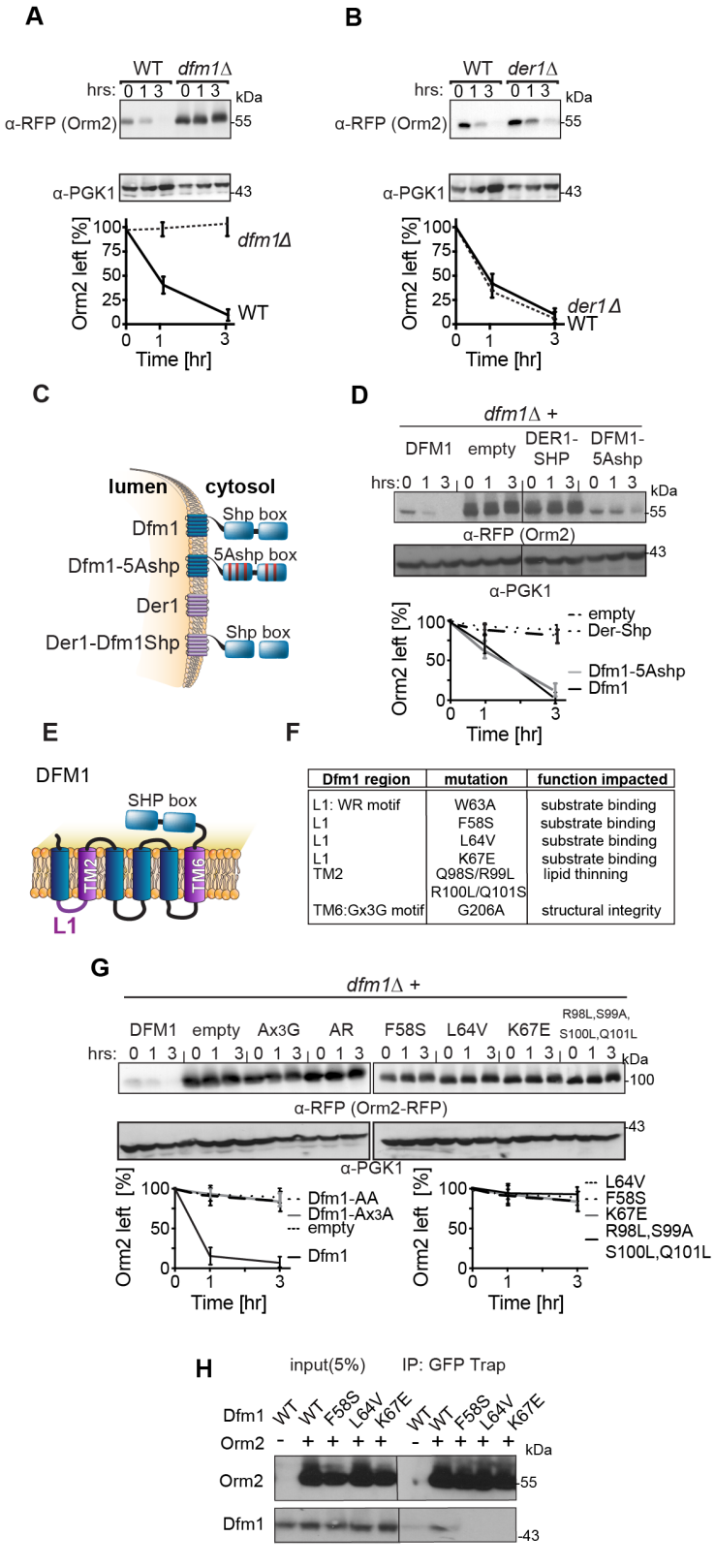
A
WT
dfm1Δ
hrs: 0 1 3 0 1 3
kDa
α-RFP (Orm2)
55
α-PGK1
43
Orm2 left [%]
100
75
50
25
0
dfm1Δ
WT
0 1 3
Time [hr]
B
WT
der1Δ
hrs: 0 1 3 0 1 3
kDa
α-RFP (Orm2)
55
α-PGK1
43
Orm2 left [%]
100
75
50
25
0
der1Δ
WT
0 1 3
Time [hr]
C
lumen
cytosol
Dfm1
Shp box
Dfm1-5Ashp
5Ashp box
Der1
Der1-Dfm1Shp
Shp box
D
dfm1Δ +
DFM1
empty
DER1-SHP
DFM1-5Ashp
hrs:0 1 3 0 1 3 0 1 3 0 1 3
kDa
55
α-RFP (Orm2)
43
α-PGK1
Orm2 left [%]
100
50
0
empty
Der-Shp
Dfm1-5Ashp
Dfm1
0 1 3
Time [hr]
E
DFM1
SHP box
TM2
TM6
L1
F
Dfm1 region | mutation | function impacted
L1: WR motif | W63A | substrate binding
L1 | F58S | substrate binding
L1 | L64V | substrate binding
L1 | K67E | substrate binding
TM2 | Q98S/R99L R100L/Q101S | lipid thinning
TM6:Gx3G motif | G206A | structural integrity
G
dfm1Δ +
DFM1
empty
Ax3G
AR
F58S
L64V
K67E
R98L,S99A, S100L,Q101L
hrs: 0 1 3 0 1 3 0 1 3 0 1 3 0 1 3 0 1 3 0 1 3 0 1 3
kDa
100
α-RFP (Orm2-RFP)
43
α-PGK1
Orm2 left [%]
100
50
0
Dfm1-AA
Dfm1-Ax3A
empty
Dfm1
0 1 3
Time [hr]
Orm2 left [%]
100
50
0
L64V
F58S
K67E
R98L,S99A
S100L,Q101L
0 1 3
Time [hr]
H
input(5%)
IP: GFP Trap
Dfm1 WT WT F58S L64V K67E WT WT F58S L64V K67E
Orm2 - + + + + - + + + +
kDa
Orm2
55
Dfm1
43

Figure 3.2.6 Orm2 degradation requires EGAD, but not ERAD or INMAD pathway

(A) E3 ligase Tul1 is required for Orm2 degradation. In the indicated strains, degradation of Orm2-RFP was measured by CHX-chase assay. Cells were analyzed by SDS-PAGE and immunoblotted for Orm2-RFP with α-RFP (3 biological replicates; n=3). t=0 was taken as 100% and data is represented as mean ± SEM. **(B)** Cdc48 and the proteasome are required for Orm2 degradation. Same as (A), except cdc48-2 and hrd2-1 were analyzed for Orm2-RFP degradation (3 biological replicates; n=3). t=0 was taken as 100% and data is represented as mean ± SEM. **(C)** Dfm1 does not function in the post-ubiquitination step of Orm2 degradation pathway. Indicated strains expressing Orm2-RFP were grown into log phase. Cells were lysed, and microsomes were collected and immunoprecipitated with α-RFP conjugated to agarose beads. Samples were then subjected to SDS-PAGE and immunoblot by α-Ubiquitin and α-RFP (3 biological replicates; n=3). **(D)** ERAD mutants do not rescue temperature-sensitive lethality of tsc3Δ. Indicated strains were grown to log-phase in SC and serially diluted cultures were plated on SC plates and incubated at 37°C and imaged at Day 2 (3 biological replicates, 2 technical replicates; n=5).

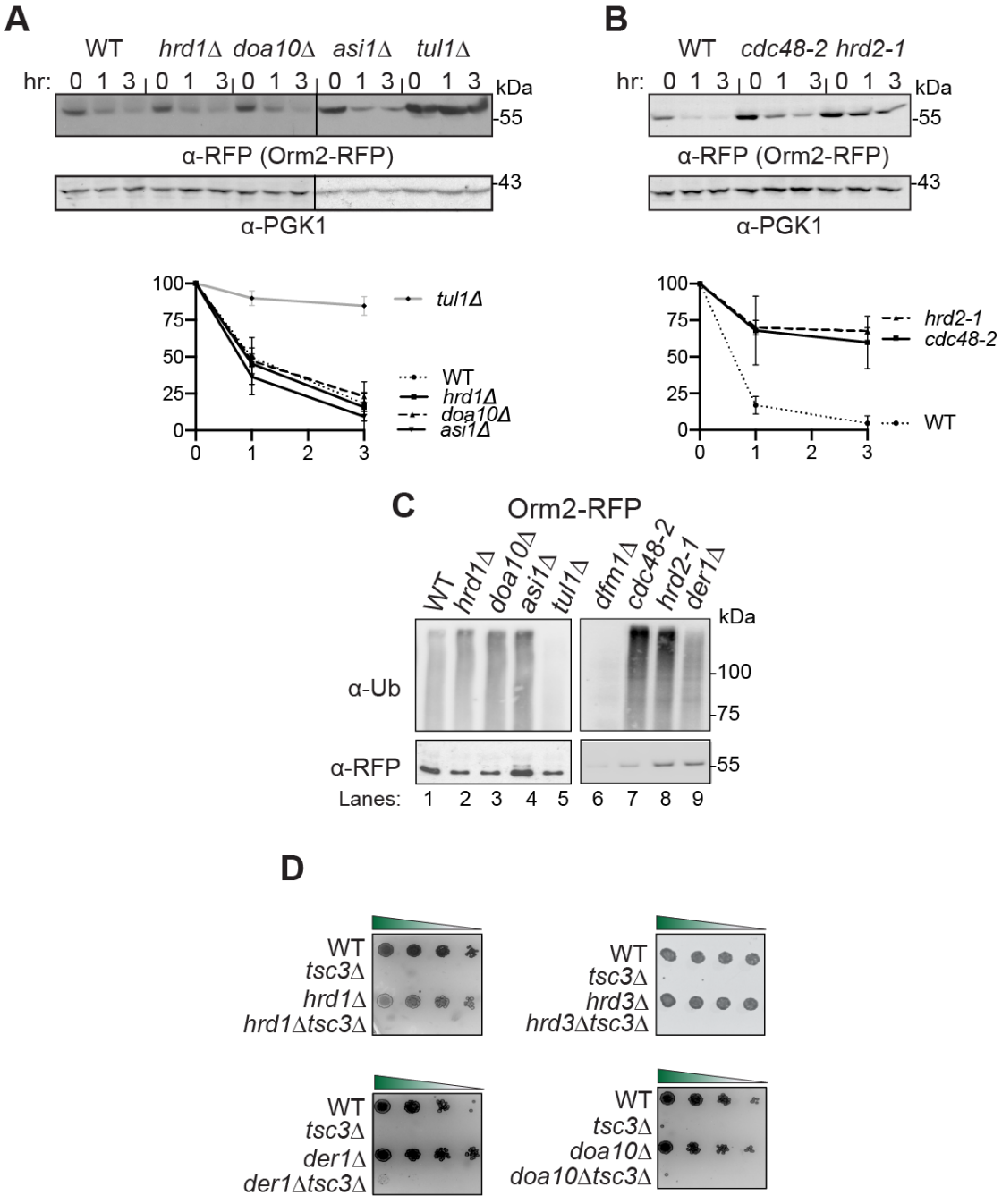
A
WT hrd1Δ doa10Δ asi1Δ tul1Δ
hr: 0 1 3 0 1 3 0 1 3 0 1 3 0 1 3
kDa
55
α-RFP (Orm2-RFP)
43
α-PGK1
100
75
50
25
0
0 1 2 3
tul1Δ
WT
hrd1Δ
doa10Δ
asi1Δ
B
WT cdc48-2 hrd2-1
hr: 0 1 3 0 1 3 0 1 3
kDa
55
α-RFP (Orm2-RFP)
43
α-PGK1
100
75
50
25
0
0 1 2 3
hrd2-1
cdc48-2
WT
C
Orm2-RFP
WT
hrd1Δ
doa10Δ
asi1Δ
tul1Δ
dfm1Δ
cdc48-2
hrd2-1
der1Δ
kDa
α-Ub
100
75
α-RFP
55
Lanes: 1 2 3 4 5 6 7 8 9
D
WT
tsc3Δ
hrd1Δ
hrd1Δtsc3Δ
WT
tsc3Δ
hrd3Δ
hrd3Δtsc3Δ
WT
tsc3Δ
der1Δ
der1Δtsc3Δ
WT
tsc3Δ
doa10Δ
doa10Δtsc3Δ

Figure 3.2.7 dfm1Δ accumulates phosphorylated Orm2 exclusively in the ER

(A) Phosphorylated Orm2 accumulates in the absence of Dfm1. Phos-tag western blot analysis shows that there is an accumulation of phosphorylated Orm2 in dfm1Δ cells. The indicated strains were grown to log phase, treated with vehicle or 1.5 μM myriocin for 1 hour and subjected to SDS-PAGE or Phos-tag western blot analysis via blotting for Orm2 with α-RFP and PGK1 with α-PGK1 antibodies (2 biological replicates; n=2). **(B)** Orm2 is retained in the ER in dfm1Δ cells. Strains were grown to mid-exponential phase in minimal media and GFP and RFP fluorescence was examined on an AxioImager.M2 fluorescence microscope using a 100x objective and 28HE-GFP or 20HE-rhodamine filter sets (Zeiss) (2 biological replicates n=2). WT, dfm1Δ, and tul1Δ cells expressing Orm2-RFP. HDEL-GFP (ER marker, green) or VPS4-GFP (endosome marker, green) were used to test for co-localization with Orm2-RFP. Arrowheads indicate Orm2 co-localizing in post-ER compartments. Scale bar, 5 μM. **(C)** dfm1Δ cells block the degradation of phosphorylated mimic of Orm2 (Orm2-3D). In the indicated strains, degradation of Orm2-3A-GFP and Orm2-3D-GFP was measured by CHX- chase assay. Cells were analyzed by SDS-PAGE and immunoblotted α-GFP (3 biological replicates; n=3). t=0 was taken as 100% and data is represented as mean ± SEM. **(D)** Accumulation of phosphorylated Orm2 within the ER is sufficient for rescuing the temperature-sensitive lethality of tsc3Δ cells. Indicated strains were spotted 5-fold dilutions on SC plates and plates were incubated at 37oC (3 biological replicates, 2 technical replicates; n=5). **(E)** dfm1Δ blocks export of phosphorylated Orm2. Fluorescence imaging was performed as in (B) except WT and dfm1Δ cells expressing Orm2-3D-GFP was used (2 biological replicates; n=2). Sec61-mCherry (ER marker, red) or CHS5-mCherry (endosome marker, red) were used to test for co-localization with Orm2-3D-GFP. Arrowheads indicate Orm2 co-localizing in post-ER compartments. Scale bar, 5 μM. **(F)** WT and dfm1Δ cells expressing either Orm2-3A-GFP or Orm2-3D-GFP were grown to log- phase at 30oC and lipids were extracted and subjected to LC-MS/MS. C18 PHS and DHS levels were measured as described in Methods in 3 biological replicates (n=3). Values represent the means±S.E.M. Statistically significant differences compared to WT cells are indicated (Pairwise Dunnett's test followed by Bonferroni's post-hoc analysis; ***P<0.0001).

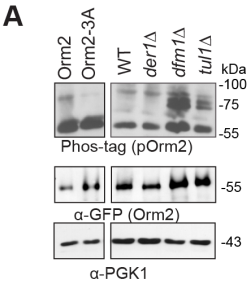
A
Orm2
Orm2-3A
WT
der1Δ
dfm1Δ
tul1Δ
kDa
-100
-75
-55
Phos-tag (pOrm2)
-55
α-GFP (Orm2)
-43
α-PGK1

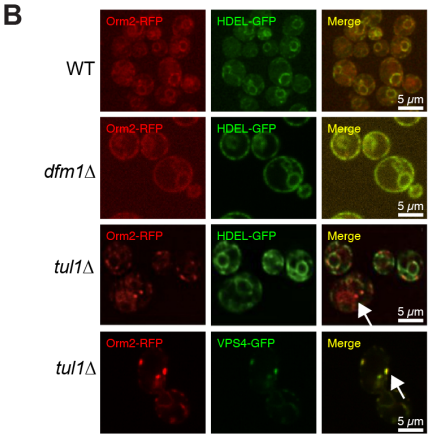
B
WT
dfm1Δ
tul1Δ
tul1Δ
Orm2-RFP
HDEL-GFP
VPS4-GFP
Merge
5 μm

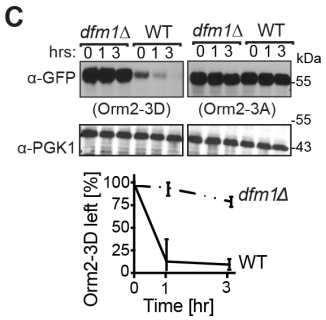
C
dfm1Δ
WT
hrs: 0 1 3 0 1 3
kDa
α-GFP
-55
(Orm2-3D)
(Orm2-3A)
-55
α-PGK1
-43
Orm2-3D left [%]
100
75
50
25
0
dfm1Δ
WT
0 1 3
Time [hr]

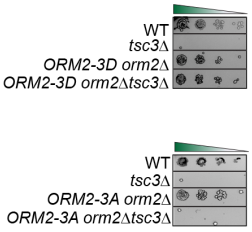
D
WT
tsc3Δ
ORM2-3D orm2Δ
ORM2-3D orm2Δtsc3Δ
WT
tsc3Δ
ORM2-3A orm2Δ
ORM2-3A orm2Δtsc3Δ

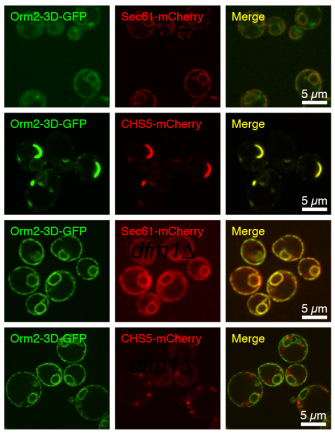
E
Orm2-3D-GFP
Sec61-mCherry
CHS5-mCherry
Merge
dfm1Δ
5 μm

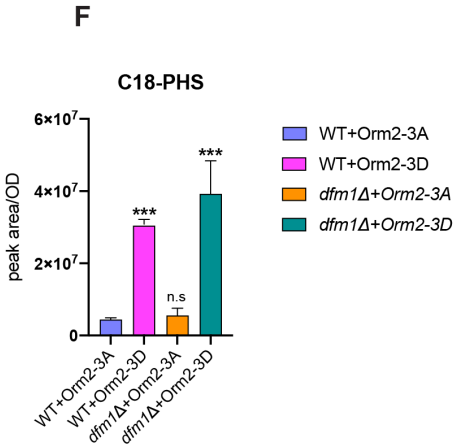
F
C18-PHS
6×10^7
4×10^7
2×10^7
0
peak area/OD
***
***
n.s
WT+Orm2-3A
WT+Orm2-3D
dfm1Δ+Orm2-3A
dfm1Δ+Orm2-3D
WT+Orm2-3A
WT+Orm2-3D
dfm1Δ+Orm2-3A
dfm1Δ+Orm2-3D

Figure 3.2.8 Dfm1 binds to phosphorylated Orm2

(A) Dfm1-HA binding to Orm2-GFP, Orm2-3A-GFP, Orm2-3D-GFP, Orm1, Lcb1, and Lcb2 were analyzed by co-IP. As negative control, cells not expressing Dfm1-HA were used. Also, Sec61 was also included to test for non-specific binding (3 biological replicates; n=3). **(B)** Same as (A), except co-IP was performed on WT and orm2Δ cells and Dfm1-HA binding to Orm1, Lcb1, and Lcb2 was analyzed (3 biological replicates; n=3). **(C)** Same as (A), except Orm2-GFP binding to Dfm1-HA, Orm1, Lcb1, and Lcb2 was analyzed by co-IP (3 biological replicates; n=3). **(D)** Schematic of Dfm1's role in Orm2 degradation. 1) Orm2 is inactivated via phosphorylation by TORC2-YPK1 signaling axis. 2) Dfm1 binds phosphorylated Orm2. 3) Phosphorylated Orm2 is delivered to COPII vesicles. 3) Phosphorylated Orm2 is routed to the Golgi and degraded via EGAD.

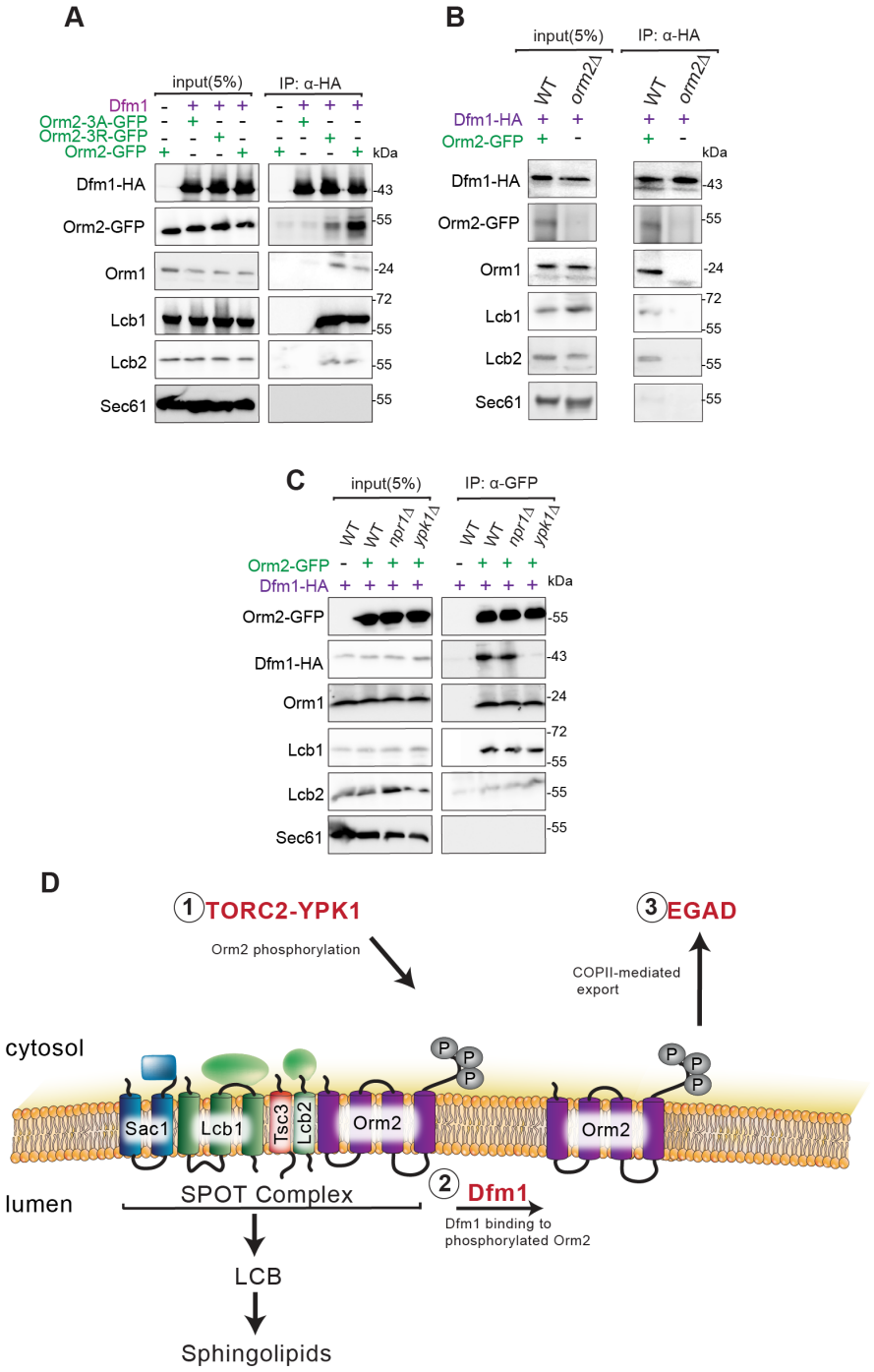
A
input(5%)
IP: α-HA
Dfm1
Orm2-3A-GFP
Orm2-3R-GFP
Orm2-GFP
kDa
Dfm1-HA
Orm2-GFP
Orm1
Lcb1
Lcb2
Sec61
B
input(5%)
IP: α-HA
WT
orm2Δ
Dfm1-HA
Orm2-GFP
C
input(5%)
IP: α-GFP
WT
npr1Δ
ypk1Δ
D
1 TORC2-YPK1
Orm2 phosphorylation
3 EGAD
COPII-mediated export
cytosol
Sac1
Lcb1
Tsc3
Lcb2
Orm2
lumen
SPOT Complex
2 Dfm1
Dfm1 binding to phosphorylated Orm2
LCB
Sphingolipids

Supplemental Figure 3.2.1 Dfm1 does not genetically interact with Lcb1, Lcb2, and Sac1

(A) Indicated strains were spotted 5-fold dilutions on SC plates in triplicates, and plates were incubated at room temperature, 30oC, and 37oC (3 biological replicates, 2 technical replicates; n=3). Upper panel: WT, dfm1Δ, Lcb1-DaMP, and dfm1ΔLcb1-DaMP were compared for growth by dilution assay. Middle panel: WT, dfm1Δ, Lcb2-DaMP, and dfm1ΔLcb2-DaMP were compared for growth by dilution assay. Bottom panel: WT, dfm1Δ, and dfm1Δ sac1Δ, were compared for growth by dilution assay. **(B)** WT, dfm1Δ, orm2Δ, and orm2Δdfm1Δ cells were grown to log-phase at 30oC and lipids were extracted and subjected to LC-MS/MS. A- B- C- & D-Type ceramides containing C16, C18, C20, C22, C24, and C26 fatty acids were measured (3 biological replicates; n=3). Values represent the means±S.E.M. Statistically significant differences compared to WT cells are indicated (Pairwise Dunnett's test followed by Bonferroni's post-hoc analysis; ns=non- significant, *P<0.05). **(C)** Serial dilution growth was performed on YPD plates in the presence or absence of 1 µg/mL tunicamycin using WT, orm1Δ, orm2Δ, dfm1Δ, dfm1Δorm1Δ, orm1Δorm2Δ, and dfm1Δorm2Δ cells (3 biological replicates, 2 technical replicates; n=3).

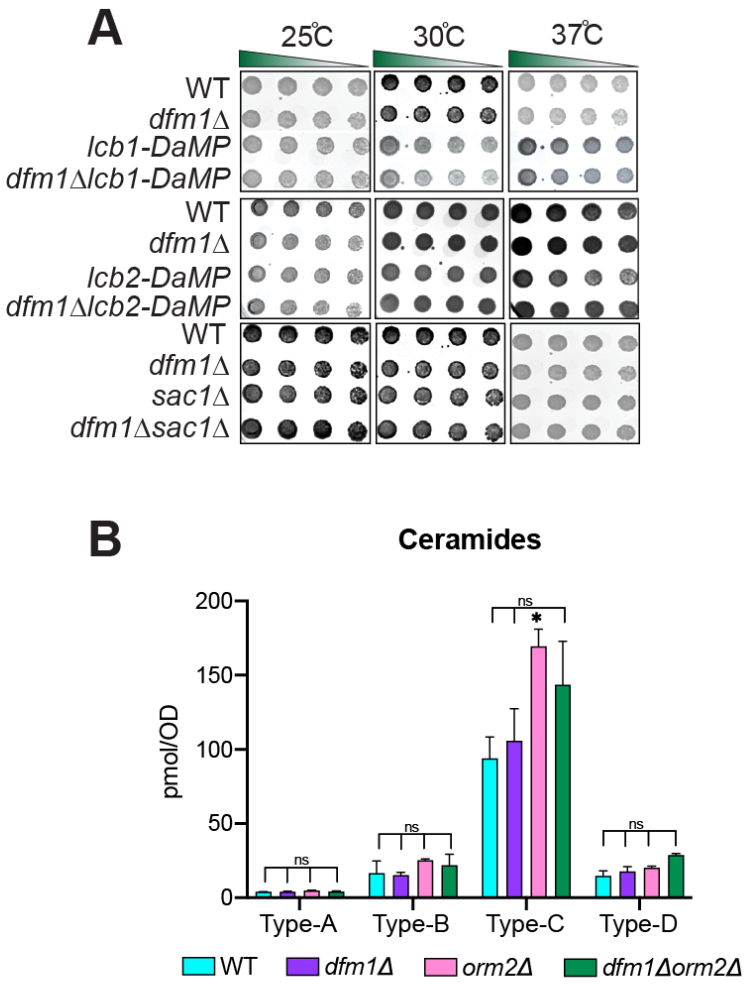
A
25°C
30°C
37°C
WT
dfm1Δ
lcb1-DaMP
dfm1Δlcb1-DaMP
WT
dfm1Δ
lcb2-DaMP
dfm1Δlcb2-DaMP
WT
dfm1Δ
sac1Δ
dfm1Δsac1Δ
B
Ceramides
pmol/OD
200
150
100
50
0
ns
*
Type-A
Type-B
Type-C
Type-D
WT
dfm1Δ
orm2Δ
dfm1Δorm2Δ
-tunicamycin
+tunicamycin
C
30°C
30°C
WT
orm1Δ
dfm1Δ
orm2Δ
dfm1Δorm2Δ
dfm1Δorm1Δ
orm1Δorm2Δ

Supplemental Figure 3.2.2 Orm2 is degraded in WT strains

(A) In the indicated WT strains, degradation of Lcb1-GFP, Lcb2-GFP, Orm2-GFP, Orm2-GFP, Sac1-GFP, Tsc3-GFP, Tsc10-GFP, and Ypk1-GFP was measured by CHX-chase assay (3 biological replicates; n=3). Cells were analyzed by SDS-PAGE and immunoblotted with α-GFP. **(B)** Steady-state levels of Dfm1 and corresponding Dfm1 mutants. Cell were analyzed by SDS- PAGE and immunoblotted with α-HA. **(C)** Serial dilution growth assay was performed on dfm1∆orm1∆ and strains with DFM1, DER1- SHP, DFM1-AA, DFM1-Ax3A, DFM1-5Ashpmtnt, and empty vector addback (3 biological replicates, 2 technical replicates; n=3). **(D)** Same as (C), except serial dilution growth assay was performed on dfm1∆orm1∆ strains with L1 mutant addback: F58S, L64V, K67E and TMD2 quad mutant addback: DFM1-R98L, S99V, S100V, Q101L. Indicated strains were grown on SC-Leu plates at room temperature, 30°C and 37°C, and imaged on Day 2 and Day 7 (3 biological replicates, 2 technical replicates; n=3). **(E)** ERAD mutants do not genetically interact with orm1∆. Indicated strains were spotted 5-fold dilutions on SC plates in triplicates, and plates were incubated at room temperature, 30oC, and 37oC (3 biological replicates, 2 technical replicates; n=3).

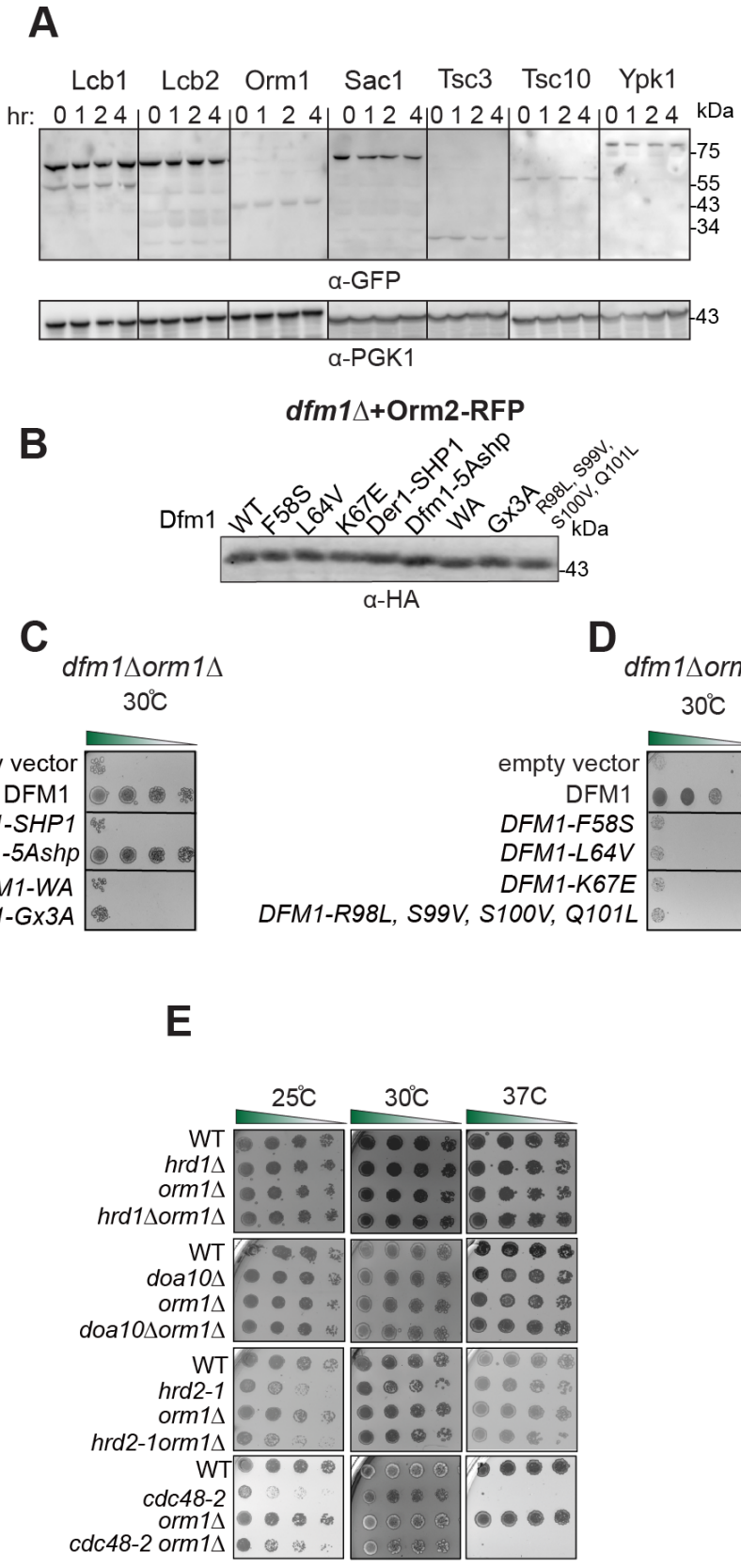
A
Lcb1
Lcb2
Orm1
Sac1
Tsc3
Tsc10
Ypk1
hr: 0 1 2 4 | 0 1 2 4 | 0 1 2 4 | 0 1 2 4 | 0 1 2 4 | 0 1 2 4 | 0 1 2 4
kDa
75
55
43
34
α-GFP
43
α-PGK1
B
dfm1Δ+Orm2-RFP
Dfm1
WT
F58S
L64V
K67E
Der1-SHP1
Dfm1-5Ashp
WA
Gx3A
R98L, S99V, S100V, Q101L
kDa
43
α-HA
C
dfm1Δorm1Δ
30℃
empty vector
DFM1
DER1-SHP1
DFM1-5Ashp
DFM1-WA
DFM1-Gx3A
D
dfm1Δorm1Δ
30℃
empty vector
DFM1
DFM1-F58S
DFM1-L64V
DFM1-K67E
DFM1-R98L, S99V, S100V, Q101L
E
25℃
30℃
37C
WT
hrd1Δ
orm1Δ
hrd1Δorm1Δ
WT
doa10Δ
orm1Δ
doa10Δorm1Δ
WT
hrd2-1
orm1Δ
hrd2-1orm1Δ
WT
cdc48-2
orm1Δ
cdc48-2 orm1Δ

Supplemental Figure 3.2.3 Dfm1 does not interact with EGAD components

Dfm1-GFP binding to EGAD members, Dsc2 and Tul1, were analyzed by co-IP. As negative control, cells not expressing Dfm1-GFP were used (2 biological replicates; n=2).

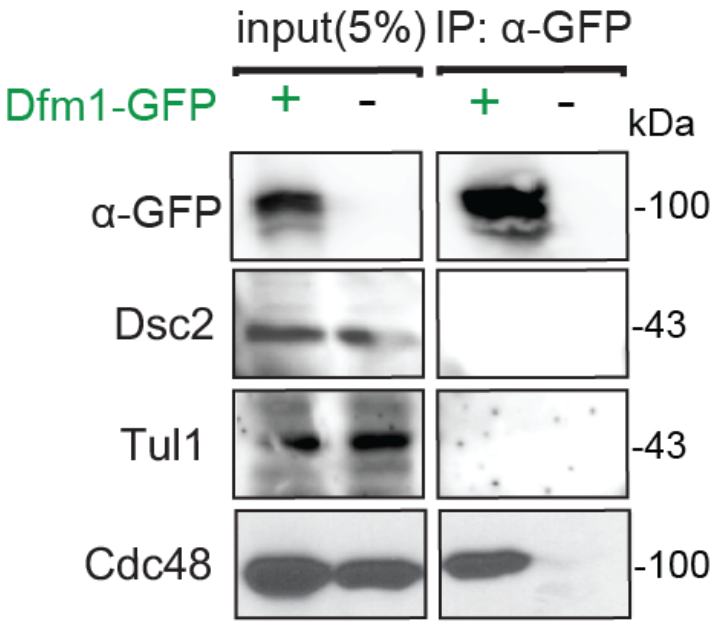
input(5%)
IP: α-GFP
Dfm1-GFP
+
-
+
-
kDa
α-GFP
-100
Dsc2
-43
Tul1
-43
Cdc48
-100

Supplemental Figure 3.2.4 Orm2-3A accumulates exclusively in the ER

(A) Fluorescence imaging was performed as in Fig. 7B except WT and dfm1Δ cells expressing Orm2-3A-GFP was used. Sec61-RFP (ER marker, red) was used to test for co-localization with Orm2-3A-GFP (2 biological replicates; n=2). Arrowheads indicate Orm2 co-localizing in post- ER compartments. Scale bar, 5 μM. **(B)** *dfm1*Δ cells do not abrogate COPII-mediated export of CPY. The indicated cells were either grown at room temperature or shifted to non-permissive growth at 37°C. Cells were analyzed by SDS-PAGE and immunoblotted for CPY with α-CPY and PGK1 with α-PGK1. **(C)** Western blot of aggregated versus soluble Orm2-GFP at the ER. Lysates from WT and *dfm1*Δ cells containing ORM2-GFP were blotted using anti-GFP to detect Orm2. P is ER aggregated fraction and S is ER soluble fraction.

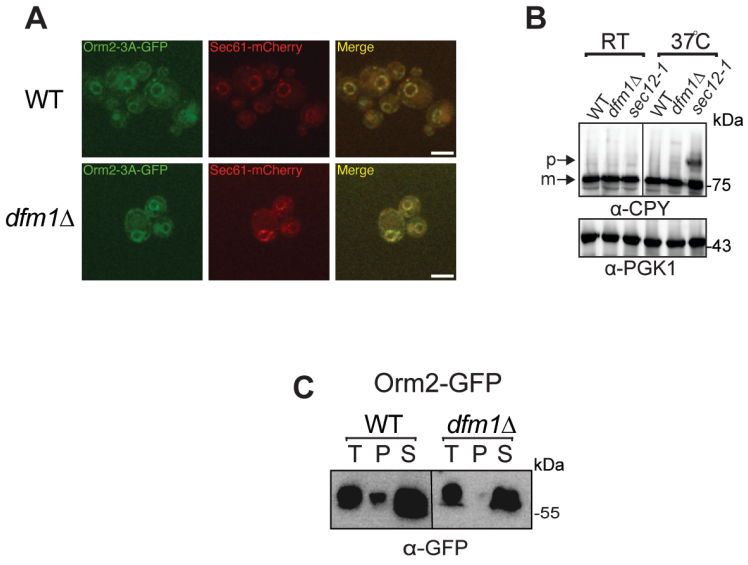
A
Orm2-3A-GFP
Sec61-mCherry
Merge
WT
dfm1Δ
B
RT
37°C
WT
dfm1Δ
sec12-1
kDa
p
m
75
α-CPY
43
α-PGK1
C
Orm2-GFP
WT
dfm1Δ
T P S T P S
kDa
55
α-GFP

Supplemental Table 3.4.1 Plasmids used in this study

Plasmid	Gene		
pSN184	YIp	ADE2/URA3	pTDH3-HMG2-GFP
pSN149	2μ	URA3	pGAL- BIRA-3xFLAG
pSN148	2μ	URA3	pGAL-DFM1-BIRA-3xFLAG
pSN246	YCp	URA3	pORM2-RFP
pSN247	YCp	LEU2	pLCB1-RFP
pSN266	YCp	URA3	pORM2-GFP
pSN267	YCp	URA3	pORM2-3D-GFP
pSN268	YCp	URA3	pORM2-3A-GFP
pSN60	YCp	LEU2	pDFM1-L64V
pSN90	YCp	LEU2	pDFM1
pSN93	YCp	LEU2	pDFM1-K67E
pSN230	YCp	LEU2	pDFM1-R98L, S99A, S100A, Q101L
pSN95	YCp	LEU2	pDFM1-F58S
pSN162	YCp	LEU2	pDFM1-5Ashp-3HA
pSN161	YCp	LEU2	pDER1-SHP-3HA
pSN164	YCp	LEU2	pDFM1-AR-3HA
pSN163	YCp	LEU2	pDFM1-Ax_3G-3HA

Supplemental Table 3.4.2 Yeast strains used in this study

Strain	Genotype	Reference
SEN 1	*Mata ade2-101 met2 lys-801 ura3-52 trp1::hisG leu2 his3Δ200*	This study
BY4741	*Mata met15Δ0 his3Δ1 leu2Δ0 ura3Δ0*	This study
SEN 322	*SEN1 2μ::URA3::GAL1pr-Dfm1-BIRA-FLAG*	This study
SEN 324	*SEN1 2μ::URA3::GAL1pr- BIRA-FLAG*	This study
SEN 167	*SEN1 dfm1Δ::KanMX ade2-101::ADE2::URA3::TDH3pr-HMG2-GFP 2μ::URA3::GAL1pr-Dfm1-BIRA-3xFLAG*	This study
SEN 168	*SEN1 dfm1Δ::KanMX ade2-101::ADE2::URA3::TDH3pr- HMG2-GFP 2μ::URA3::GAL1pr-BIRA-3xFLAG*	This study
SEN 169	*SEN1 dfm1Δ::KanMX ade2-101::ADE2::URA3::TDH3pr- HMG2-GFP 2μ::URA3*	This study
SEN 280	*BY4741 DFM1::DFM1-GFP::HIS*	This study
SEN 439	*BY4741 DFM1::DFM1-GFP::HIS CEN::URA3:: prORM2-RFP*	This study
SEN 438	*BY4741 DFM1::DFM1-GFP::HIS CEN::LEU2:: prLCB1-RFP*	This study
SEN 635	*SEN1 dfm1Δ::KanMX*	This study
SEN 637	*SEN1 tsc3Δ::NatR*	This study
SEN 638	*SEN1 dfm1Δ::KanMX tsc3Δ::NatR*	This study
SEN 640	*SEN1 orm1Δ::KanMX*	This study
SEN 641	*SEN1 orm1Δ::KanMX tsc3Δ::NatR*	This study
SEN 644	*SEN1 orm2Δ::KanMX*	This study
RHY 646	*SEN1 orm2Δ::KanMX tsc3Δ::NatR*	This study
SEN 285	*SEN1 dfm1Δ::KanMX orm1Δ::NatR*	This study
SEN 291	*SEN1 dfm1Δ::KanMX orm2Δ::NatR*	This study

Supplemental Table 3.4.2 Yeast strains used in this study (Continued)

Strain	Genotype	Reference
SEN 280	*BY4741 orm1Δ::KanMX*	This study
SEN 281	*BY4741 orm2Δ::KanMX*	This study
SEN 369	*BY4741 orm1Δ::KanMX orm2Δ::LEU2*	This study
SEN 282	*BY4741 Lcb2-DaMP*	This study
SEN 266	*BY4741 dfm1Δ::KanMX Lcb2-DaMP*	This study
SEN 392	*SEN1 sac1Δ:NatR*	This study
SEN 301	*SEN1 dfm1Δ::KanMX sac1Δ:NatR*	This study
SEN 599	*SEN1 CEN::URA3:: prORM2-RFP*	This study
SEN 659	*SEN1 dfm1Δ::KanMX CEN::URA3:: prORM2-RFP*	This study
SEN 615	*SEN1 der1Δ::KanMX CEN::URA3:: prORM2-RFP*	This study
SEN 623	*SEN1 dfm1Δ::KanMX CEN::URA3:: prORM2-RFP CEN::LEU2:: prDFM1-3xHA*	This study
SEN 624	*SEN1 dfm1Δ::KanMX CEN::URA3:: prORM2-RFP CEN::LEU2*	This study
SEN 625	*SEN1 dfm1Δ::KanMX CEN::URA3:: prORM2-RFP CEN::LEU2:: prDER1-SHP1*	This study
SEN 629	*SEN1 dfm1Δ::KanMX CEN::URA3:: prORM2-RFP CEN::LEU2:: prDFM1-5Ashp*	This study
SEN 626	*SEN1 dfm1Δ::KanMX CEN::URA3:: prORM2-RFP CEN::LEU2:: prDFM1-Ax3G*	This study
SEN 628	*SEN1 dfm1Δ::KanMX CEN::URA3:: prORM2-RFP CEN::LEU2:: prDFM1-AR*	This study
SEN 635	*SEN1 dfm1Δ::KanMX CEN::URA3:: prORM2-RFP CEN::LEU2:: prDFM1-F58S*	This study
SEN 632	*SEN1 dfm1Δ::KanMX CEN::URA3:: prORM2-RFP CEN::LEU2:: prDFM1-L64V*	This study
SEN 634	*SEN1 dfm1Δ::KanMX CEN::URA3:: prORM2-RFP CEN::LEU2:: prDFM1-K67E*	This study
SEN 630	*SEN1 dfm1Δ::KanMX CEN::URA3:: prORM2-RFP CEN::LEU2:: prDFM1-R98L, S99V, S100V, Q101L*	This study
SEN 598	*SEN1 hrd1Δ::KanMX CEN::URA3:: prORM2-RFP*	This study

Supplemental Table 3.4.2 Yeast strains used in this study (Continued)

Strain	Genotype	Reference
SEN 604	*SEN1 doa10Δ::NatR CEN::URA3:: prORM2-RFP*	This study
SEN 607	*SEN1 asi1Δ::HphMX CEN::URA3:: prORM2-RFP*	This study
SEN 622	*SEN1 tul1Δ::KanMX CEN::URA3:: prORM2-RFP*	This study
SEN 606	*SEN1 cdc48Δ::cdc48-2::NatR CEN::URA3:: prORM2-RFP*	This study
SEN 608	*SEN1 hrd2-1 CEN::URA3:: prORM2-RFP*	This study
SEN 345	*SEN1 hrd3Δ::KanMX*	This study
SEN 346	*SEN1 tsc3Δ::KanMX hrd3Δ::NatR*	This study
SEN 437	*SEN1 tsc3Δ::KanMX hrd1Δ::NatR*	This study
SEN 3	*SEN1 hrd1Δ::KanMX*	This study
SEN 652	*SEN1 doa10Δ::HphMx*	This study
SEN 654	*SEN1 doa10Δ:: HphMx tsc3Δ::KanMX*	This study
SEN 649	*SEN1 der1Δ::NatR*	This study
SEN 650	*SEN1 der1Δ::NatR tsc3Δ::KanMX*	This study
SEN 521	*BY4741 LCB1-GFP::HIS3*	This study
SEN 522	*BY4741 LCB2-GFP::HIS3*	This study
SEN 523	*BY4741 ORM1-GFP::HIS3*	This study
SEN 524	*BY4741 ORM2-GFP::HIS3*	This study
SEN 525	*BY4741 SAC1-GFP::HIS3*	This study
SEN 526	*BY4741 TSC3-GFP::HIS3*	This study
SEN 527	*BY4741 YPK1-GFP::HIS3*	This study
SEN 528	*BY4741 TSC10-GFP::HIS3*	This study

Supplemental Table 3.4.2 Yeast strains used in this study (Continued)

Strain	Genotype	Reference
SEN 662	*SEN1 dfm1Δ::KanMX orm1Δ::NatR CEN::LEU2::prDFM1-3xHA*	This study
SEN 661	*SEN1 dfm1Δ::KanMX orm1Δ::NatR CEN::LEU2*	This study
SEN 675	*SEN1 dfm1Δ::KanMX orm1Δ::NatR CEN::LEU2::prDER1-SHP*	This study
SEN 676	*SEN1 dfm1Δ::KanMX orm1Δ::NatR CEN::LEU2::prDFM1-5Ashp*	This study
SEN 677	*SEN1 dfm1Δ::KanMX orm1Δ::NatR CEN::LEU2::prDFM1-AR*	This study
SEN 678	*SEN1 dfm1Δ::KanMX orm1Δ::NatR CEN::LEU2::prDFM1-Ax3G*	This study
SEN 665	*SEN1 dfm1Δ::KanMX orm1Δ::NatR CEN::LEU2::prDFM1-L64V*	This study
SEN 664	*SEN1 dfm1Δ::KanMX orm1Δ::NatR CEN::LEU2::prDFM1-F58S*	This study
SEN 666	*SEN1 dfm1Δ::KanMX orm1Δ::NatR CEN::LEU2::prDFM1-K67E*	This study
SEN 667	*SEN1 dfm1Δ::KanMX orm1Δ::NatR CEN::LEU2::prDFM1-R98L, S99V, S100V, Q101L*	This study
SEN 552	*SEN1 orm1Δ::NatR*	This study
SEN 551	*SEN1 orm1Δ::NatR hrd1Δ::KanMX*	This study
SEN 543	*SEN1 hrd2-1*	This study
SEN 544	*SEN1 cdc48::cdc48-2::NatR*	This study
SEN 545	*SEN1 doa10Δ:: HphMx*	This study
SEN 546	*SEN1 hrd2-1 orm1Δ::NatR*	This study
SEN 547	*SEN1 cdc48::cdc48-2::NatR orm1Δ::KanMx*	This study

Supplemental Table 3.4.2 Yeast strains used in this study (Continued)

Strain	Genotype	Reference
SEN 548	*SEN1 doa10Δ:: HphMx orm1Δ::NatR*	This study
SEN 671	*SEN1 orm2Δ::KanMX tsc3Δ::NatR CEN::URA3::prORM2-3R-GFP*	This study
SEN 672	*SEN1 orm2Δ::KanMX tsc3Δ::NatR CEN::URA3::prORM2-3A-GFP*	This study
SEN 673	*BY4741 orm2Δ::KanMX CEN::URA3::prORM2-3R-GFP*	This study
SEN 674	*BY4741 orm2Δ::KanMX CEN::URA3::prORM2-3A-GFP*	This study
SEN 679	*SEN1 CEN::TRP1::ORM2-RFP CEN::URA3::HDEL-GFP*	This study
SEN 680	*SEN1 dfm1Δ::KanMX CEN::TRP1::ORM2-RFP CEN::URA3::HDEL-GFP*	This study
SEN 681	*SEN1 tul1Δ::KanMX CEN::TRP1::ORM2-RFP CEN::URA3::HDEL-GFP*	This study
SEN 682	*SEN1 tul1Δ::KanMX CEN::TRP1::ORM2-RFP CEN::URA3:VPS4-GFP*	This study
SEN 683	*SEN1 CEN::URA3::ORM2-3R-GFP CEN::LEU2::HIS3::SEC61-mCherry*	This study
SEN 684	*SEN1 CEN::URA3::ORM2-3R-GFP CEN::TRP1::CHS5-mCherry*	This study
SEN 685	*SEN1 dfm1Δ::KanMX CEN::URA3::ORM2-3R-GFP CEN::LEU2::HIS3::SEC61-mCherry*	This study
SEN 686	*SEN1 dfm1Δ::KanMX CEN::URA3::ORM2-3R-GFP CEN::TRP1::CHS5-mCherry*	This study
SEN 687	*SEN1 CEN::URA3::ORM2-3A-GFP CEN::LEU2::HIS3::SEC61-mCherry*	This study
SEN 688	*dfm1Δ::KanMX CEN::URA3::ORM2-3A-GFP CEN::LEU2::HIS3::SEC61-mCherry*	This study

Supplemental Table 3.4.3 Key Resources Table

REAGENT or RESOURCE	SOURCE	IDENTIFIER
Antibodies		
Mouse monoclonal anti-GFP	Clontech Laboratories, Inc.	Cat#632381; RRID: AB_2313808
Mouse monoclonal anti-HA	Thermo Fisher Scientific	Cat#32-6700; RRID: AB_2533092
Rabbit polyclonal anti-myc	Genscript	Cat#A00172; RRID: AB_914457
Rabbit polyclonal anti-Cdc48	Neal et al., 2016	N/A
Mouse monoclonal anti-PGK	Thermo Fisher Scientific	Cat#459250; RRID: AB_2569747
Mouse monoclonal anti-Ubiquitin	Richard Gardner: University of Washington	N/A
Bacterial and Virus Strains		
Escherichia coli DH5 alpha Competent Cells	Thermo Fisher Scientific	Cat#18265017
Biological Samples		
Chemicals, Peptides, and Recombinant Proteins		
MG132 (benzyloxycarbonyl-Leu-Leu-aldehyde)	Sigma-Aldrich	474787; CAS: 133407-82-6
Cycloheximide	Sigma-Aldrich	C7698; CAS: 66-819
Protein A Sepharose	GE Healthcare	17-0780-01
Deposited Data		
Raw Files	This study, Mendeley Data	DOI: 10.17632/py236jc9fh.1
Experimental Models: Organisms/Strains		
Saccharomyces cerevisiae BY4741	GE Dharmacon	Cat#YSC1048
Saccharomyces cerevisiae S288C	This study	N/A
Additional yeast strains used: refer to Table S2	This study	
Recombinant DNA		
Plasmids used: refer to Table S1	This study	
Software and Algorithms		
Prism 7 for Mac	GraphPad Software	https://www.graphpad.com/scientific-software/prism/
Image J	NIH	https://imagej.nih.gov/ij/
FlowJo	Vashistha et al., 2016	https://www.flowjo.com/solutions/flowjo
BD Accuri C6	BD Accuri	Cat # 653122

Chapter 4: Conclusions and Closing Remarks

4.1 Conclusions and Closing Remarks

Over the course of graduate school, I have been able to see the Neal lab grow, and with that, our collective understanding of the role of rhomboid family proteins evolve. Starting from Dr. Neal's discovery that Dfm1 is required for endoplasmic reticulum associated degradation (ERAD) of integral membrane proteins, our lab has now gained a more mechanistic understanding of how Dfm1 participates in retrotranslocation of membrane proteins. We have additionally unveiled novel roles for Dfm1 that are independent of its role in ERAD, establishing a much broader role for this pseudoprotease in maintaining ER homeostasis. Chapter 2 and Chapter 3 both describe ERAD-independent functions of Dfm1. In Chapter 2, we establish Dfm1 prevents cellular stress through a chaperone-like function for promoting solubility of membrane proteins. In Chapter 3, we establish Dfm1 is critical for trafficking Orm2 to the Golgi for degradation, and, in doing so, Dfm1 regulates sphingolipid homeostasis.

In Chapter 2, we characterize Dfm1 as having a chaperone-like function for influencing solubility of misfolded membrane proteins. This project began as interesting, albeit confusing, set of phenotypic observations. We observed that in the absence of Dfm1, misfolded membrane protein accumulation was toxic, but that this same toxicity was not observed in other ERAD defective cells. We also observed that ubiquitination of substrates was required for toxicity in the absence of Dfm1.

The path that a research project takes is usually winding and less straightforward than it might appear once it is published. I initially started this project exploring the cellular effects of misfolded membrane protein accumulation in the absence of Dfm1. Here, we uncovered that both proteasome function and ubiquitin homeostasis are disrupted in these cells. I struggled with forming hypotheses of what Dfm1's specific role could be in prevention of misfolded membrane stress. A chaperone function seemed unlikely because this stress alleviation function of Dfm1 did not require recruitment of the ATPase Cdc48. I eventually tested this hypothesis anyway and established that Dfm1 acts as a chaperone-like protein on misfolded membrane proteins. Strikingly, we found Dfm1's effect on solubility of misfolded membrane proteins to be all-or-nothing, an effect beyond anything I expected to uncover. One experiment can rapidly change the direction of a project.

While my doctoral research into Dfm1 and membrane protein stress unveiled a new function for rhomboid pseudoproteases, this research opens many additional avenues of exploration. For example, is this chaperone-like function conserved among active rhomboid proteases? Is solubilization of membrane proteins one step during Dfm1-mediated ERAD that aids in the retrotranslocation process. What type of misfolded proteins can be solubilized by derlins in human cells? What substrates does Dfm1 act on as a chaperone in wildtype cells?

Possibly the most intriguing follow-up to this work is understanding mechanistically how derlin proteins are able to act as chaperones. We determine in Chapter 2 that Dfm1 does interact with solubilized Hmg2. This indicates a likely holdase function for Dfm1, whereby Dfm1 prevents soluble membrane proteins from becoming aggregated. It will be

important to conduct structural studies of Dfm1 with Hmg2 to better understand Dfm1's chaperone function at a mechanistic level. Additionally, reconstitution of Dfm1 and Hmg2 *in vitro* will be important for determining 1) if Dfm1 does act as a holdase or has a different type of chaperone function, 2) if Dfm1 is an ATP independent chaperone, and 3) if Dfm1 requires other cellular machinery for its chaperone function.

There has been a long-held assumption in the field of proteostasis that aggregation is always deleterious to cells. Others have challenged this assumption, and our work in Chapter 2 continues to add to that emerging body of work that aggregation does not always cause toxicity. Using our substrate-toxicity assay and solubility assay, we were able to determine that two conditions must be met for misfolded proteins to become toxic; misfolded membrane proteins must be ubiquitinated and must be aggregated. Aggregation alone is not enough to cause toxicity to cells. Even outside of the context of Dfm1 as a chaperone, it is critical to continue characterizing aggregation at a biochemical level (through the solubility assay) along with toxicity at the organismal level (through the substrate-toxicity assay) to better understand the conditions and circumstances where aggregation becomes toxic.

The Neal labs recent work into derlin proteins has laid the groundwork for generating a more holistic understanding of rhomboid proteins. This family of membrane protein proteases and pseudoproteases clearly has wide ranging roles in homeostasis that are just beginning to be appreciated. While considerable progress has been made by many groups in the last two decades into the function of rhomboid proteins, there is still much that remains to be uncovered, as evidenced by the novel functions and roles of rhomboid proteins that our lab has uncovered in just the last few years. By coupling biochemistry, structural biology, and

cell biology to understand the various substrates of and mechanistic roles of different rhomboid proteins, both in yeast and mammalian cells, we will gain a better understanding of how these elusive membrane proteins promote cellular homeostasis.